Vol. 118 No. 1, July 1, 1980 ISSN 0003-2670

ANALYTICA CHIMICA ACTA

International journal devoted to all branches of analytical chemistry

ELSEVIER SCIENTIFIC PUBLISHING COMPANY

ANALYTICA CHIMICA ACTA

International journal devoted to all branches of analytical chemistry
Revue internationale consacrée à tous les domaines de la chimie analytique
Internationale Zeitschrift für alle Gebiete der analytischen Chemie

PUBLICATION SCHEDULE FOR 1980 (incorporating the section on Computer Techniques and Optimization).

	J	F	M	A	M	J	J	A	S	O	N	D
Analytica Chimica Acta	113/1 113/2	114	115	116/1	116/2	117	118/1	118/2	119/1	119/2	120	121
Section on Computer Techniques and Optimization			122/1			122/2			122/3			122/

Scope. *Analytica Chimica Acta* publishes original papers, short communications, and reviews dealing with every aspect of modern chemical analysis, both fundamental and applied. The section on *Computer Techniques and Optimization* is devoted to new developments in chemical analysis by the application of computer techniques and by interdisciplinary approaches, including statistics, systems theory and operation research. The section deals with the following topics: Computerized acquisition, processing and evaluation of data. Computerized methods for the interpretation of analytical data including chemometrics, cluster analysis, and pattern recognition. Storage and retrieval systems. Optimization procedures and their application. Automated analysis for industrial processes and quality control. Organizational problems.

Submission of Papers. Manuscripts (three copies) should be submitted as designated below for rapid and efficient handling:

Papers from the Americas to: Professor Harry L. Pardue, Department of Chemistry, Purdue University, West Lafayette, IN 47090, U.S.A.

Papers from all other countries to: Dr. A. M. G. Macdonald, Department of Chemistry, The University, P.O. Box 363, Birmingham B15 2TT, England.

For the section on *Computer Techniques and Optimization:* Dr. J. T. Clerc, Universität Bern, Pharmazeutisches Institut, Sahlistrasse 10, CH-3012 Bern, Switzerland.

American authors are recommended to send manuscripts and proofs by INTERNATIONAL AIRMAIL.

Information for Authors. Papers in English, French and German are published. There are no page charges. Manuscripts should conform in layout and style to the papers published in this Volume. Authors should consult Vol. 111, p. 343 for detailed information. Reprints of this information are available from the Editors or from: Elsevier Editorial Services Ltd., Mayfield House, 256 Banbury Road, Oxford OX2 7DE (Great Britain).

Reprints. Fifty reprints will be supplied free of charge. Additional reprints (minimum 100) can be ordered. An order form containing price quotations will be sent to the authors together with the proofs of their article.

Advertisements. Advertisement rates are available from the publisher.

Subscriptions. Subscriptions should be sent to: Elsevier Scientific Publishing Company, P.O. Box 211, 1000 AE Amsterdam, The Netherlands. The section on *Computer Techniques and Optimization* can be subscribed to separately.

Publication. *Analytica Chimica Acta* (including the section on *Computer Techniques and Optimization*) appears in 10 volumes in 1980. The subscription for 1980 (Vols. 113–122) is Dfl. 1390.00 plus Dfl. 160.00 (postage) (total approx. U.S. $795.00). The subscription for the *Computer Techniques and Optimization* section only (Vol. 122) is Dfl. 139.00 plus Dfl. 16.00 (postage) (total approx. U.S. $79.50). Journals are sent automatically by airmail to the U.S.A. and Canada at no extra cost and to Japan, Australia and New Zealand for a small additional postal charge. All earlier volumes (Vols. 1–103) except Vols. 23 and 28 are available at Dfl. 150.00 (U.S. $77.00), plus Dfl. 10.00 (U.S. $5.00) postage and handling, per volume.

Claims for issues not received should be made within three months of publication of the issue, otherwise they cannot be honoured free of charge.

Customers in the U.S.A. and Canada who wish to obtain additional bibliographic information on this and other Elsevier journals should contact Elsevier/North Holland Inc., Journal Information Center, 52 Vanderbilt Avenue, New York, NY 10017. Tel: (212) 867-9040.

Analytica Chimica Acta, 118 (1980) 191—225

Review

BIOCHEMICAL AND CLINICAL ANALYSIS BY ENTHALPIMETRIC MEASUREMENTS — A REALISTIC ALTERNATIVE APPROACH?

J. KEITH GRIME

Department of Chemistry, University of Denver, Denver, CO 80208 (U.S.A.)

(Received 21st January 1980)

SUMMARY

The contribution of enthalpimetric measurements to biochemical and clinical analysis is evaluated. After a brief discussion of instrumental considerations, non-enzymatic and enzymatic approaches to biochemical and clinical enthalpimetry are considered. The main focus of the review is on the incorporation of enzyme-catalyzed reactions with enthalpimetric measurements to provide analytical selectivity; determinations of enzyme activity, substrate concentration, inhibitor concentration and biochemical constants are discussed. Enthalpimetric devices based on immobilized enzyme technology, e.g. flow enthalpimeters and enzyme-coated thermistors and the latest technique to evolve, thermometric enzyme-linked immunoassay are treated separately. The advantages and limitations of enthalpimetry in these areas of analysis are discussed in the context of routine clinical analysis.

This review focuses on those thermoanalytical techniques generally classified as enthalpimetric methods. Until recently, this would normally have encompassed such techniques as thermometric enthalpy titrations (t.e.t.), direct injection enthalpimetry (d.i.e.), thermokinetic titrimetry and kinetic d.i.e. This nomenclature has been discussed in more detail elsewhere [1]. Historically, the distinction between enthalpimetry and adiabatic calorimetry (both titration and injection) has been made mainly on the degree of sophistication of the instrumentation based on its "adiabaticity" and, related to this, the time scale, sensitivity and ultimate application of the measurements. Accordingly, quasi-adiabatic enthalpimetric methods have been employed, for the most part, in semi-micro and macro determinations since the relatively large temperature changes involved (0.05—0.1°C) require minimal control of environmental temperature fluctuations. Indeed, many successful applications have been reported using very simple apparatus in which short-term temperature control, for reactions complete within ca. 1 min, was provided by polystyrene insulation.

The term calorimetry has traditionally been reserved for techniques associated with the compilation of precise thermodynamic and kinetic data, usually implying a much more rigorous experimental approach. The time scale of such experiments and the need for highly specialized and expensive instrumentation have precluded the routine use of classical adiabatic and isothermal calorimetry in analytical chemistry.

With the increasing demand for analytical sensitivity and the trend towards the study of rate-based enzymatic determinations, the traditional boundaries between enthalpimetry and analytical calorimetry have become vague. Enthalpimetric instrumentation has evolved to the point where the research instruments are in fact isoperibol (constant temperature environment) calorimeters. The term enthalpimetry is now more appropriately used to describe an analytical technique based on the measurement of enthalpy changes without reference to the sophistication of the apparatus. Consequently, no distinction will be made in this review between enthalpimetry and analytical calorimetry unless the use of a highly specialized approach warrants this. In the interests of consistency, the term microcalorimetry will not be restricted to describe Tian-Calvet heat-flow calorimetry, as sometimes seen in the literature, but will be used in its wider generic sense to describe the measurement of small heat changes, typically in the mJ range. Microcalorimetry and microenthalpimetry will therefore be used as synonyms. Discussion will however be biased towards pseudo-adiabatic rather than isothermal instruments, since the latter have found only limited analytical acceptance because of the time scale of such measurements. Within this framework, the review should be regarded as comprehensive.

There has been considerable dialogue in the literature addressed towards the promotion of enthalpimetry as an alternative to existing routine methods of clinical assay, although its adoption has clearly not materialized. It is the author's intention, during the course of this review, to add some perspective to the contribution that enthalpimetry has to make to contemporary biochemical and clinical assay.

THE DEVELOPMENT OF CLINICAL AND BIOCHEMICAL ENTHALPIMETRY

Prior to ca. 1974, the primary reasons cited for the use of enthalpimetry as an analytical method of choice were two-fold. First, the detection system is based on a ubiquitous property of all chemical reactions, the molar enthalpy change. Accordingly, enthalpimetric methodology simplifies many analytical procedures considerably. It precludes the search for a reagent that must not only react quickly and stoichiometrically with the analyte, but also produces, directly or indirectly, a physically measurable entity, e.g. a chromophore. The technique therefore offers almost universal applicability within its sensitivity range. Secondly, the detection system will also tolerate the presence of unreacting matrix constituents without a significant loss in precision or accuracy. Provided that a reasonably efficient heat transfer is maintained through the solution to the detector, the analyte solution may contain large amounts of insolubles that would prohibit the use of many other types of detectors. This has facilitated many applications of enthalpimetry in areas of analytical chemistry where "clean" samples are rarely encountered, e.g. in the pharmaceutical sector [2, 3]. The instrumentation, experimental constraints, and fundamental principles of enthalpimetric measurements in general have been the subjects of many reviews [1, 4—16].

The features already mentioned suggest that enthalpimetry would be an ideal measurement tool in the analysis of complex biological solutions. However, the major advantage of enthalpimetry, its universal nature, also represents its major limitation, a lack of selectivity. The practical exploitation of the technique demands selectivity which, unless fortuitously provided by the kinetic or thermodynamic parameters associated with the species in the analytical solution, must be incorporated by a suitable choice of separations, reagent or experimental variables, such as pH. For this reason, the literature prior to ca. 1974 contains few significant references to enthalpimetric clinical or biochemical determinations in which selectivity is a prerequisite.

It is only with the advent of commercially available stable and inexpensive enzymes that clinical analysis incorporating enthalpimetric measurements has become a reality. The inclusion of the inherent selectivity of enzymatic reactions into the enthalpimetric methodology produces an analytical approach of considerable potential merit, one which embodies selectivity and wide applicability. Several reviews have discussed selected aspects of clinical and biochemical enthalpimetry from a variety of viewpoints [17—33].

APPARATUS

Although the simple "enthalpimeters" mentioned earlier were successful in certain situations, their lack of sensitivity and "adiabaticity" renders them unsuitable for applications in biochemical and/or clinical analysis. In particular, they cannot be used successfully to monitor the temperature changes associated with rate-controlled processes of finite duration. There is also little doubt that the absence of versatile commercial instrumentation in recent years has slowed the widespread acceptance of enthalpimetry as a realistic alternative method of analysis. There are several commercial enthalpimeters, calorimeters and "thermometric analyzers" currently available that have, to some extent, filled this gap.

The isoperibol or "constant temperature environment" instrument is probably the commonest type of calorimeter in analytical use since it represents a compromise between the simple "enthalpimeter" and the sophisticated adiabatic and heat leak calorimeters, in terms of analysis time, sensitivity and cost. A schematic representation of a comprehensive isoperibol enthalpimeter, including optional facilities for digital data acquisition and treatment, is shown in Fig. 1. The characteristic feature of this type of instrument is that the reaction cell is thermally insulated from the surrounding thermostated bath by means of a Dewar-type vessel.

It is critically important that the reaction cell be constructed to have a fast response time (ca. 2 s) and a low heat transfer modulus if long thermal equilibration periods and ill-defined enthalpograms are to be avoided. Typically this is achieved by minimizing the thickness of the inner wall (<0.5 mm) and the quantity of glass forming the boundary between the vessel and its surroundings. The temperature transducer, housed in the reaction cell, is usually

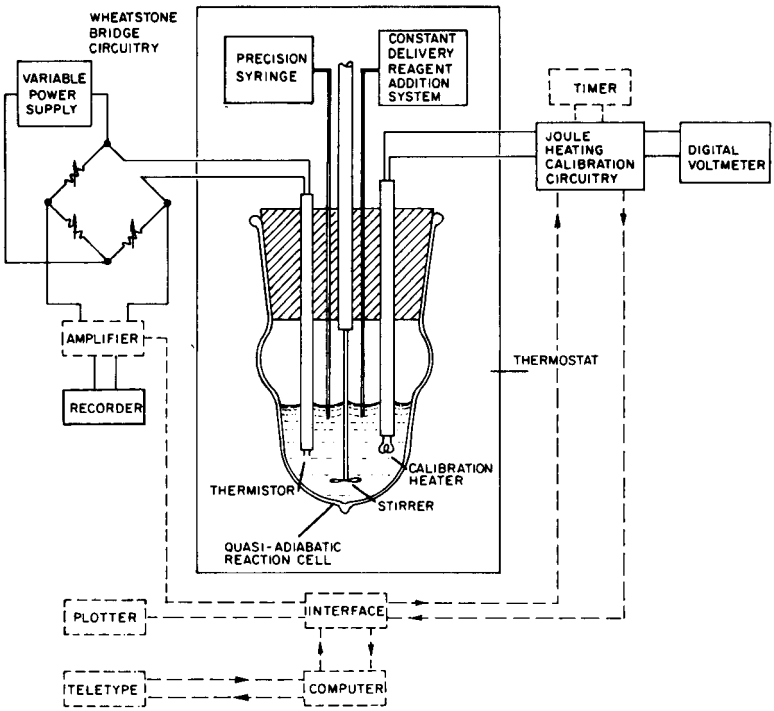

Fig. 1. Comprehensive enthalpimetric instrumentation. Dashed lines represent optional facilities.

a thermistor (ca. 10 kΩ) incorporated as one arm of a d.c. Wheatstone bridge. The thin glass envelope surrounding the sensor bead is sometimes etched to decrease the response time.

In the simplest configuration, the imbalance potential resulting from a temperature change in solution is recorded directly onto a strip-chart potentiometer. Bowers and Carr [34, 35] have discussed the optimization of d.c. bridge sensitivity. The typical range of signals that can be expected from a conventional d.c. bridge system is 0.3 mV to 2 mV for most analytical measurements.

Very low level measurements can be made by inclusion of an a.c. Wheatstone bridge, linear ramp generator and phase–lock amplification system [36].

Other essential elements of enthalpimetric instrumentation are Joule heating calibration circuitry and facilities for batch (injection or ampoule) or titration enthalpimetry.

The insulation between the cell and its environment in an isoperibol instrument is not perfect; the measurements cannot therefore be described as truly adiabatic. The inevitable heat exchange that occurs at the interface can easily be compensated for by applying Newton's law of cooling [37, 38] or for processes of short duration, by means of a graphical extrapolation pro-

cedure [39]. For slow chemical processes, arbitrarily defined as those with a duration longer than 30 min, errors associated with heat loss in an isoperibol system become unacceptable. In general, this can be considered as the maximum allowable analysis time period when using this type of instrument with cell volumes $\geqslant 10$ cm^3. Within this time frame, millidegree temperature changes can be measured with adequate precision. Ultimately, the signal-to-noise ratio of such devices is governed by the Joule heating of the thermistor itself and the heat evolved by the stirring of the solution.

Cell volumes of 10 cm^3 or more are typical for conventional enthalpimetric measurements. The reduction of cell volume increases the sensitivity of the calorimeter since the observed temperature change is inversely proportional to the reaction solution volume for a given enthalpy change and amount of reactant. However, other thermal events are induced for which a correction must be made. Since there is a practical limit to the diminution of the detection, calibration and stirring facilities in the cell, the heat loss modulus increases exponentially with diminished cell volume. In addition, heat effects from both stirring and evaporation become more significant [40]. Hansen et al. [41] have derived exact equations for the calculation of heat loss from isoperibol calorimeter reaction vessels with a volume less than 5 cm^3. These authors point out that increasing the titration time increases (non-linearly) the heat correction required and vice versa. A compromise must be made, however, since decreasing the titration time increases the error in the volume of titrant added. The latter point underlines the necessity for precise buret systems when making microcalorimetric measurements. Moreover, the significant heat losses encountered in such cells considerably reduce the acceptable analysis time.

The analytical isoperibol calorimeter is typified by the Tronac Model 450 currently used in the reviewer's laboratory. This bench-top instrument, originally developed by the Brigham Young University Thermochemical group [42–44], is adequate for most analytical measurements, including many biochemical processes.

It has recently been proposed that two simple modifications to isoperibol microcalorimeters decrease the thermal equilibration periods and can increase sensitivity by a factor of three [45]. In essence, water, preequilibrated with the thermostat bath, is pumped through a teflon tubing loop inserted into the solution in the reaction vessel prior to the experiment. Equilibration with the bath temperature is defined as the point at which no thermistor response is observed when the water pump is activated. The temperature differential between the water bath and the contents of the cell is therefore minimized and hence the need for corrections from this source. At high sensitivities evaporative cooling has a major influence on the time required for the contents of the microcell to reach equilibrium with the water bath. The simple expedient of introducing water-saturated air into the air space above the analytical solution in the cell apparently reduces this problem significantly.

LKB (Sweden) produces an excellent series of constant-temperature

environment and heat-leak calorimeters for titration, injection, and flow calorimetry. These instruments were originally designed for precise and sensitive measurements of fundamental biochemical and chemical processes; they are relatively expensive and not well suited for routine analytical purposes. Detailed discussions of these and other calorimeters and their use in analytical studies of biochemical and biological systems have been published [5, 23, 24].

Recently, there has been considerable activity directed towards the development of commercial automated and semi-automated enthalpimeters for routine analytical measurements. These instruments, produced by Technicon (U.S.A.) and MOM (Hungary), are based on the principles of injection enthalpimetry and are designed primarily with industrial inorganic applications in mind, where a market has already been established. Since no biochemical or clinical studies have been reported using these instruments, the reader is referred to the literature for further details [46—51].

Computer-interfaced data treatment and collection devices are not in routine use for enthalpimetric measurements. A "calorimeter-programmer" is available from Tronac. This accessory allows only limited computer control of the titration/calibration sequence and digital data recording at preselected time intervals; it does not have the capability for data correction or treatment.

In view of the data treatment now necessary for successful microenthalpimetric measurements, the development of an inexpensive and versatile data collection and analysis facility, possibly based on a microcomputer, would be a significant advance. This need is particularly germane to the enthalpimetric compilation of enzyme kinetic data, which will be discussed in a later section.

Little interest has been generated in the use of Curie point or positive temperature coefficient devices in enthalpimetric detection systems. The sensitive response of these devices, which can be of the order of +16% per degree [22, 52], would extend the capabilities of enthalpimetric measurements particularly with respect to biological systems, since this response represents a 4-fold increase in sensitivity over conventional thermistor transducers. The slow response of these devices (cf. thermistors) is however a significant disadvantage.

APPLICATIONS

There are several distinct areas of activity in the application of enthalpimetry to clinical and biochemical analysis which, for review purposes, will be broadly classified as non-enzymatic or enzymatic. The enzymatic methods will then be subdivided into the enthalpimetric determination of (1) enzyme activity, (2) substrate concentration, (3) inhibitor concentration and (4) biochemical kinetic constants. Enzyme immobilization technology and the devices that have evolved from it will be discussed separately. A brief account of the latest technique to evolve, thermometric enzyme-linked immunosorbent assay (t.e.l.i.s.a.), will also be presented.

NON-ENZYMATIC METHODS

Although limited in scope by selectivity and sensitivity considerations, this area of research has produced some significant data, primarily illustrating the ease with which untreated sera can be handled by enthalpimetric techniques.

There have been several enthalpimetric studies of non-enzymatic protein chemistry. Jespersen and Jordan [53] showed that the carboxyl, imidazole, and amino protons of egg albumin can be delineated by means of serial thermometric enthalpy titrations with sodium hydroxide solution. This is in contrast to a classical potentiometric titration which determines only the carboxylic protons.

The interaction between the anionic precipitant, 12-phosphotungstic acid, and bovine serum albumin has been investigated by t.e.t. [54, 55] and ultimately applied to the determination of total serum protein [56]. The viscosity of human sera affects the shape of the enthalpograms, an effect which can be minimized by adjustment of the stirring rate. The reaction stoichiometry, however, is related to both the titrant delivery rate and the protein concentration. The latter effect is related to the rate of reaction and can be minimized at low titrant delivery rates. Under the appropriate conditions, the reported precision was 0.5% (r.s.d.) and comparison with the Kjeldhal and biuret techniques was favorable. Correlation coefficients of 0.982 and 0.990, respectively, were calculated at the 95% confidence level.

Thermometric enthalpy titrations have also been used as a complementary measurement for the study of micelle formation in the interaction of block polypeptides with surfactants [57]. Other enthalpimetric investigations of fundamental protein chemistry include studies on the adsorption of proteins by membranes [58] and the reaction of metal ions or protons with proteins [59].

The serial thermometric enthalpy titration of relatively high concentrations of calcium and magnesium (2 mmol dm^{-3}) in unbuffered aqueous solution with EDTA has been known since 1957 [60]. The relative magnitudes of the formation constants and reaction enthalpies (Ca/EDTA; log K = 10.6, ΔH = −25.2 kJ mol^{-1}. Mg/EDTA; log K = 8.7, ΔH = +16.8 kJ mol^{-1}) make this an attractive approach for the serial determination of calcium and magnesium in human serum [61]. In practice, however, the characteristic exo/endothermic serial enthalpogram is not obtained. The exchange reactions are acid-catalyzed and therefore a pH of 8.0 is required to offset the slow exchange that becomes apparent at serum concentrations of calcium and magnesium. Consequently, when buffered in Tris, the overall enthalpy of both complexation reactions appears to be exothermic because of the attendant buffer protonation (−50.4 kJ mol^{-1}). This does not hinder the measurement since the slopes of the enthalpograms are sufficiently well defined to allow accurate extrapolation, even when applied to 1 cm^3 of untreated (except for dilution) human serum.

In order to obtain an acceptable signal-to-noise ratio at this concentration level (ca. 2.50×10^{-3} mol dm^{-3} Ca, 1.30×10^{-3} mol dm^{-3} Mg), a sensitive a.c. Wheatstone bridge, linear ramp generator, and phase-lock amplification system [36] were employed. A series of statistical data treatments revealed good correlation with atomic absorption measurements. The technique was also successful when applied to Versatol control sera, with the exception of the high Ca:Mg serum, Versatol-A-Alternate.

The determination of chloride ion in synthetic serum samples by means of "peak enthalpimetry" [62], a flow injection variant of d.i.e., has been reported [22]. By means of a sample loop system, 0.1-cm^3 samples were injected into a continuously flowing solvent stream and mixed with aqueous mercury(II) nitrate in a vibrating (60 Hz) reaction cell. Accuracy and precision of 2% were reported for the determination of chloride ion concentrations of clinical interest.

In a purely qualitative clinical application, the possibility of continuously recording the process of blood clot lysis with a thermometric clot detector has been evaluated [63]. Bostick and Carr [64] have also pointed out that the response of a gently vibrated self-heated thermistor is very sensitive to plasma and blood coagulation. This phenomenon was attributed to the termination of relative bulk flow around the thermistor and not to a change in the thermal conductivity or the temperature of the solution.

ENZYMATIC METHODS

The determination of enzyme activity

An enzyme does not affect the thermodynamic equilibrium position of a chemical reaction, merely its rate. Accordingly, the amount of enzyme participating in a chemical reaction can only be determined by a kinetic measurement. In this context, the data are usually reported in terms of enzyme activities, conventionally expressed as the number of moles of substrate consumed per unit time under specified conditions of pH and temperature.

The reagent concentrations necessary to perform a valid enzyme activity assay are often determined empirically. The efficient optimization of such an experiment is, in fact, based on fulfilling the requirements of the Michaelis–Menten equation

$$v = k_{+2}\,[\mathrm{E}]\,[\mathrm{S}]/(K_\mathrm{m} + [\mathrm{S}]) \qquad (1)$$

which describes the parameters governing the initial rate, v, of an enzymatic reaction. In this expression, [S] is the initial substrate concentration, [E] is the total enzyme concentration and K_m is the Michaelis constant usually defined as $(k_{-1} + k_{+2})/k_{+1}$. The term k_{+2} [E] can be simplified to V_{max}, the maximum velocity of the reaction for a given amount of enzyme (mol dm^{-3} time^{-1}). The steady-state derivation of eqn. (1) assumes the classical enzyme–substrate intermediate mechanism, $\mathrm{E} + \mathrm{S} \underset{k_{-1}}{\overset{k_{+1}}{\rightleftharpoons}} \mathrm{ES} \overset{k_{+2}}{\rightarrow} \mathrm{E} + \mathrm{P}$ is in operation, where k_{+2} is the rate constant for the breakdown of ES, the rate-determining

step. Equation (1) is the fundamental equation of enzyme kinetics, which, although derived from a simple mechanistic model, is valid for many more complex mechanisms [65] requiring more intricate definitions of K_m and V_{max}.

The graphical form of this equation is a rectangular hyperbola with asymptotes of [S] $= -K_m$ and $v = V_{max}$. At values of [S] for which [S] $\gg K_m$, v approaches V_{max} and the reaction is apparently zero order with respect to [S]; under these conditions the active sites of the enzyme are said to be "saturated" and the reaction rate depends only on enzyme concentration and not on small variations in substrate concentration. This represents the ideal situation for enzyme activity determinations and should theoretically occur only at infinite substrate concentration, since v approaches V_{max} slowly. In practice however, a substrate concentration of around 10 K_m is sufficient to permit rate measurements that are independent of [S]. Clearly, whatever the fundamental significance of K_m, its value is essential in defining the experimental conditions necessary for valid enzyme assay. There are several factors which may limit the feasible substrate concentration, e.g. solubility or substrate inhibition or, in the special case of thermal measurements, the heat of substrate dilution. Examples of the latter two phenomena will be presented in this section.

It is easily shown that when zero-order kinetics prevail, the rate of change of temperature associated with an enzymatic reaction can be represented by

$$\Delta T/\Delta t = k_{+2}[\mathrm{E}]\ V\Delta H/C_p \quad (\mathrm{deg\ time^{-1}}) \tag{2}$$

where V is the volume of solution (dm^3) and C_p is the heat capacity of the cell and its contents (J deg^{-1}). Thus, a plot of temperature change versus time will be linear with a slope of k_{+2} [E] $V\Delta H/C_p$

Since $\Delta T = \Delta q/C_p$, where Δq is the attendant heat change (J) and k_{+2} [E] V = enzyme activity under zero-order conditions, eqn. (2) can be rearranged to give the working equation of kinetic d.i.e.

$$\text{enzyme activity} = \Delta q/\Delta H\Delta t \quad (\mathrm{mol\ time^{-1}}) \tag{3}$$

Appropriate factors can be incorporated into this relationship to present the data in International Units (μmol min^{-1}) or katals, the SI equivalent (mol s^{-1}).

Methodology. Enthalpimetric enzyme assays are implemented by means of a kinetic d.i.e. experiment in which a saturating amount of pre-equilibrated substrate is injected into a buffered solution of enzyme. Precise standardization of the injected reagent is unnecessary once the minimum amount required to maintain zero-order kinetics during the measurement period has been established. The heat capacity of the cell and its contents are then determined by a Joule heating experiment. In the interest of brevity, this calibration sequence can be performed while the enzymatic reaction continues. The ongoing signal from the reaction is attenuated by a decrease in recorder sensitivity after a rate measurement period of around 3—5 min. It is essential therefore that zero-order kinetics are maintained throughout the calibration sequence if a non-linear enthalpogram is to be avoided. A typical enzyme

activity determination and calibration sequence is depicted in Fig. 2. In order to minimize errors from heat leakage, measurements of the calibrative heat effect, q_c, are standardized at $t_{c/2}$, where t_c is the activation time of the calibration heater. q_c can then be calculated from the equation

$$q_c = V_H V_S t_c / R_S \quad \text{(J)} \tag{4}$$

where V_H is the voltage measured across the calibration resistor and V_S, R_S is the voltage and resistance, respectively of a precision resistor in series with the calibration heater.

Implicit in the use of eqn. (3) is knowledge of the overall enthalpy of the enzymatic reaction, including contributions from any attendant buffer reactions. If this datum is not tabulated, as is often the case, an enthalpimetric substrate-limiting reaction will provide this information.

Applications. One of the first reports of an enthalpimetric determination of enzyme activity appeared in 1969 and discussed the potential of a flow approach for the assay of glucose oxidase, cholinesterase, alkaline phosphatase, lactate dehydrogenase and ATPase in tissue homogenate [66].

However, there have been relatively few enthalpimetric enzyme assays documented since, primarily because of sensitivity considerations. Indeed, it was not until 1975 that the use of conventional enthalpimetric instrumentation for this purpose was promoted, with the introduction of kinetic d.i.e. [67]. The reaction studied was the hexokinase-catalyzed phosphorylation of glucose at pH 8, which was shown to have a total enthalpy change of -74.9 kJ mol^{-1}; the detection limit of 8.4 nkat (0.5 IU) of hexokinase is typical for enthalpimetric enzyme assays. The endothermic temperature mismatch spike deliberately induced in the procedure by the injection of a cooler reagent

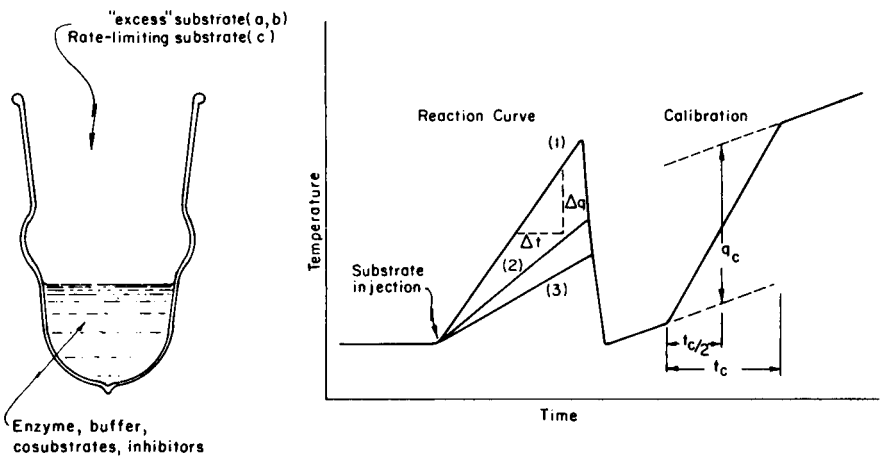

Fig. 2. Kinetic enthalpogram for the determination of (a) enzyme activity, (b) inhibitor concentration or (c) substrate concentration by the initial slope technique. Curves 1, 2, 3: (a) $EA_1 > EA_2 > EA_3$ (constant [S]); (b) $[I]_1 < [I]_2 < [I]_3$ (constant [S], [E]); (c) $[S]_1 > [S]_2 > [S]_3$ (constant [E]).

solution should be used with caution since it can cause spurious rate assignments if there is a significant heat transfer between the cell and its environment [68]. High $\Delta q/\Delta t$ values will be recorded in this event, as the cell and its contents strive to re-equilibrate with the bath temperature as it is represented by the balance point of the Wheatstone bridge. Similar problems can be caused by the endothermic dilution heats obtained on the injection of concentrated reagents.

Serum enzyme assays generally fall into the realm of microenthalpimetry. However, the level of serum cholinesterase (ChE) can be monitored by conventional enthalpimetric instrumentation [68] since it has a normal activity range of 36.7—86.8 nkat per cm^3 of human serum (2.2—5.2 IU cm^{-3}). The enzymatic hydrolysis of butyrylcholine (BuCh) in Tris buffer (pH 8.0) can be represented, thus

$$C_3H_7\overset{O}{\overset{\|}{C}}-O(CH_2)_2\overset{+}{N}(CH_3)_3I^- + H_2O \rightarrow C_3H_7\overset{O}{\overset{\|}{C}}-OH + HO(CH_2)_2\overset{+}{N}(CH_3)_3I^-$$

The heat change produced by this enzymatic hydrolysis can be amplified by the enthalpy change associated with the concurrent protonation of Tris buffer, Tris-NH_2 + H_3O^+ = Tris-NH_3^+ + H_2O. In this particular example, the "chemical amplification" of the temperature change is the key to the feasibility of the measurement, since the enthalpy of protonation, −47.7 kJ mol^{-1} [69], dominates the total enthalpy change; the small endothermic enthalpy of hydrolysis (ca. +1.3 kJ mol^{-1}) would not, by itself, allow a precise determination of ChE activity with isoperibol instrumentation. BuCh has a significant endothermic heat of dilution; the injected amount of reagent can be adjusted to maintain zero order kinetics while minimizing thermal dilution effects. The precision of the enthalpimetric results, 1.4% (r.s.d.), compared favorably with a colorimetric procedure for the assay of 1 cm^3 of reference serum.

In a study of the serum ChE-catalyzed hydrolysis of acetylcholine, using a more sensitive Tian-Calvet microcalorimeter [70], it was found that the mixing and dilution of serum contributes an endothermic response to the overall heat effect at high serum concentrations (80% v/v in buffer). Adjustment of experimental conditions to minimize this effect and the subtraction of signals from reagent blanks, produced results that correlated well with a classical spectrophotometric procedure. Similar instrumentation has been employed for the determination of acetylcholinesterase activity [71].

The determination of peroxidase activity is not of direct physiological importance per se, however, the enzyme is important analytically in that it is often used as a coupling reagent in the assay of enzymes or substrates producing hydrogen peroxide in a primary enzymatic reaction. Peroxidase-limiting rate measurements are, however, problematic since the kinetics of the reaction are complicated by a multi-step mechanism and by the fact that hydrogen peroxide exhibits substrate inhibition at high concentrations. In the event, substrate-dependent kinetics inevitably prevail. If the peroxidase

mechanism is represented simply as $E + S \underset{k_2}{\overset{k_1}{\rightleftharpoons}} ES$; $ES + AH_2 \xrightarrow{k_4} E + P$ where S is hydrogen peroxide and AH_2 the electron donor, it can be shown [72] that the relative magnitudes of the rate constants k_1 and k_4 affect the feasibility of zero-order kinetics. Clearly, this criterion dominates the choice of AH_2. If an enthalpimetric detection system is used, the options are not further limited by the ability of the donor to act as a chromophore, for example. The peroxidase-catalyzed oxidation of iodide ion by hydrogen peroxide has an enthalpy change of -123.7 kJ mol^{-1} when buffered in acetate/acetic acid at pH 3.9 [73] and can be used for a thermal peroxidase assay. 5—35 ng of horseradish peroxidase can be determined in this manner with a precision <3.1% (r.s.d.), at a specified hydrogen peroxide concentration.

The activity of lactate dehydrogenase (LDH) has been measured calorimetrically [74] by utilizing the sequence of reactions associated with the catalyzed reduction of pyruvate to lactate in the presence of reduced nicotinamide adenine dinucleotide, NADH. Buffer reaction (in this instance deprotonation) once again forms an integral part of the calorimetric measurement. Indeed, the selection of the buffer system is crucial to the sensitivity of the method. These authors state that a 3-fold enhancement of the signal can be achieved by utilizing phosphate (ΔH, -47.3 kJ mol^{-1}) instead of Tris (ΔH, -15.4 kJ mol^{-1}). The small endothermic enthalpy of deprotonation of phosphate buffer has a smaller subtractive effect on the dominant exothermic reduction of pyruvate.

An outstanding illustration of the versatility of calorimetric measurements is contained in a recent report describing the use of isothermal microcalorimetry for the evaluation of metabolic and enzyme activity in human epidermis [75]. In particular, LDH activity (0.37 nkat mg^{-1}, 22.1 mIU mg^{-1}) was determined on isolated epidermis stretched on small frames in the calorimetric cell. Adenosine-5′-triphosphatase activity at the surface of tissue cells has also been detected by microcalorimetry [76].

In another clinical analysis, the assay for serum aldolase isoenzymes was investigated by means of a Tian-Calvet conduction calorimeter [77]. In an extension of this study [78], the ratio of enzyme activities toward fructose-1,6-diphosphate and fructose-1-monophosphate was used as a measure of cancerous disease state. A distinct and unambiguous differentiation between cancerous and non-cancerous states was achieved by using this parameter.

The activity of several proteolytic enzymes, including trypsin, pepsin and pronase, has been determined by flow-microcalorimetry [79].

The utility of calorimetric methods for the determination of enzyme activity lies in the facility to measure the primary enzymatic event without recourse to coupling reactions in order to produce a measurable entity. Furthermore, determinations of enzymes in biological specimens can be done with a minimum of sample pretreatment. The propagation of errors inherent in these procedures can therefore be avoided.

The direct enthalpimetric determination of most serum enzymes is precluded by sensitivity limitations. The limit of detection for enthalpimetric

enzyme assay is about 0.5 IU whereas the activity of many serum enzymes lies between 5 mIU cm^{-3} and 100 mIU cm^{-3}. The range of serum enzymes amenable to enthalpimetric assay can be extended by use of an integral "two-point" technique [80], in which the residual substrate is determined following incubation with the enzyme for a finite time period. Preliminary experiments in this laboratory show that the limit of detection can be improved by a factor of 10 if 30-min incubation periods are used. In general, however, enthalpimetry cannot compete with spectroscopic techniques as a routine method of clinical enzyme assay.

Determination of substrates

Methodology. Enzymatic substrate determinations can be performed by either kinetic or equilibrium approaches. The kinetic measurement can be rationalized by inspection of eqn. (1). If $[S] \ll K_m$, the equation approximates to $v = [S]\ V_{max}/K_m$, i.e. the classical mathematical description of a first-order chemical process. In this case, V_{max}/K_m is analogous to the first-order rate constant. The initial rate of an enzymatic reaction under these conditions is therefore proportional to the initial concentration of substrate. In practice, this approximation is valid when $[S] < 0.1\ K_m$. Since both the enzyme and substrate concentrations are rate-determining, precise volume control of the injected solution must be maintained. Gravimetrically calibrated precision syringes are appropriate for this purpose. The resultant enthalpogram for an initial rate measurement is analogous to that shown for enzyme activity determination in Fig. 2. The initial slope will, under the conditions described, be proportional to the initial substrate concentration at constant enzyme concentration. Analytical results can be obtained by comparison of sample data with a series of calibration rates recorded with substrate standards.

The equilibrium approach is based on the measurement of the total thermal change associated with the completion of the enzyme substrate reaction. The essential features of an enthalpimetric "equilibrium" experiment are shown in Fig. 3. An excess of enzyme, that is, enough to bring the reaction to completion within an acceptable time period, is injected into a buffered solution of the substrate and co-factors, and the temperature change is monitored until the reaction comes to completion. Since the amount of enzyme injected affects only the rate at which equilibrium is achieved and not its ultimate position, precise control of the injected reagent volume or concentration is unnecessary. Knowledge of the molar enthalpy of reaction allows the calculation of the analyte concentration from the calibrated heat change, q_c, assuming the degree of completion of the reaction is known. If the enthalpy change is not tabulated, an identical experiment with a known amount of subtstrate will yield this information.

Applications. The kinetic methodology offers little advantage over the equilibrium measurement, which is not subject to the vagaries of kinetic

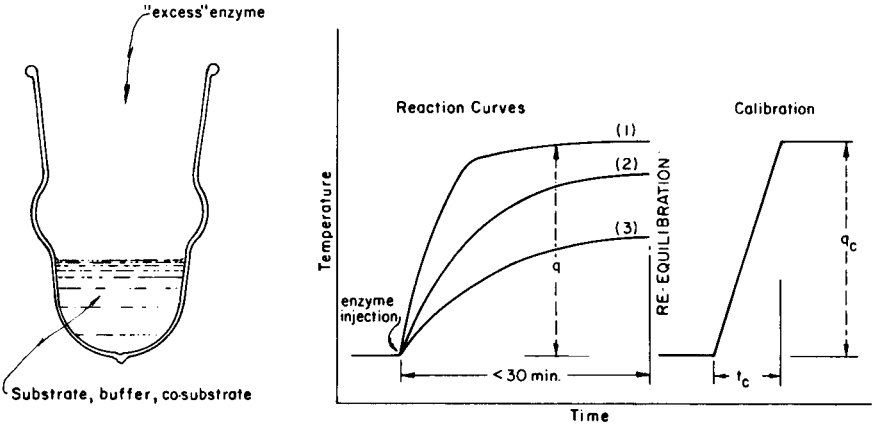

Fig. 3. Direct injection enthalpogram for the determination of (a) substrate concentration by the equilibrium method (often given the misnomer "end-point" method) and (b) biochemical constants. (Curves 1, 2, 3: $[S]_1 > [S]_2 > [S]_3$ (constant [E]).

analysis (substrate and product inhibition, enzyme stability, pH dependence), and thus it has found few applications. The ability of enthalpimetry to measure an overall process can be utilized, however, for the differentiation of two simultaneous or sequential reactions that proceed at different rates, if the enthalpy changes of the two reactions are known independently. Consequently, the use of two enzymatic reactions, one of which proceeds rapidly and the other slowly and at a rate limited by substrate concentration, allows the determination of two substrates by equilibrium and kinetic measurements, respectively. This novel concept has been used for the microcalorimetric assay of free cholesterol and cholesterol ester in serum [81] by monitoring the fast enzymatic oxidation of the former and the simultaneous, but slow, enzymatic hydrolysis of the latter. The resultant enthalpogram is simply a slowly increasing and linear temperature change (hydrolysis) superimposed on a conventional equilibrium enthalpogram (oxidation).

The post-reaction slope of the enthalpogram in fact represents the rate of the hydrolysis reaction, which is in turn proportional to the concentration of cholesterol ester.

This slope can be subtracted from the overall enthalpogram, leaving a total heat change proportional to the concentration of free cholesterol. This operation is facilitated by computer treatment of the data. The combination of kinetic and equilibrium measurements to this end is an interesting innovation which warrants further study.

The determination of serum glucose levels has been the subject of several reports. In a conventional enthalpimetric experiment, McGlothlin and Jordan [82] report the enthalpy of phosphorylation of glucose by $Mg(ATP)^{2-}$ in Tris buffer (pH 8.0) to be -74.9 kJ mol^{-1}. Subtraction of the contribution of buffer protonation leads to an enthalpy assignment of -27.6 kJ mol^{-1} for the phosphorylation process per se, glucose + $Mg(ATP)^{2-}$ → glucose-6-

phosphate + $Mg(ADP)^-$ + H^+. Equilibrium constant and entropy assignments for this reaction were subsequently calculated. The assignment of −74.9 kJ mol^{-1} for the overall process may seem at odds with a value of −61.4 kJ mol^{-1} reported by Goldberg et al. [83] in a previous microcalorimetric study. Apparently, under Goldberg's conditions (sub-stoichiometric amounts of magnesium ions), several competing equilibria between magnesium ions, ATP^{4-} and ADP^{3-} contribute to the enthalpy assignment [82]. When these reactions are taken into account, the two calculations are in excellent agreement. The experimental conditions therefore should be consistent with the operational enthalpy when this reaction is utilized. Both these studies have led to glucose determinations in serum [84, 85]. In an excellent illustration of the ability of enthalpimetry to tolerate the presence of unreactive matrix ingredients without a significant loss in precision, McGlothlin and Jordan extended their procedure to the determination of glucose in plasma and whole blood [85]. They state that up to three 500-μl whole blood samples or five serum samples can be successively injected into the same buffered reaction mixture and that adequate analytical precision is maintained. The d.i.e. procedure is quantitative over more than a 30-fold glucose concentration range, a range much greater than that for the spectrophotometric procedures listed for comparison.

The successive injection technique reduces the analysis time and the cost of enzymatic determinations in homogeneous solutions. This practice was also employed for the determination of some penicillins by monitoring the temperature change associated with the penicillinase-catalyzed hydrolysis of penicillin G, ampicillin sodium and phenoxymethylpenicillin in pure and dosage forms [86]. Accuracy and precision data were reported for 10 successive analyses although, under the conditions described, up to 20 successive analyses are feasible.

The enzymatic oxidation of cholesterol,

$$\text{cholesterol} + O_2 \xrightarrow{\text{cholesterol oxidase}} \text{4-cholesten-3-one} + H_2O_2$$

is exothermic (−52.9 kJ mol^{-1}) [81]. The single-stage microcalorimetric determination of serum cholesterol (3.9—7.2 mmol dm^{-3}) is therefore feasible. It is necessary, however, to remove hydrogen peroxide in order to avoid interfering side-reactions with other serum components. This can be achieved conveniently by the introduction of catalase into the analytical solution, since no other co-factors are required [87]. In practice, a 3-fold enhancement of signal is achieved by the additional heat generated by this reaction (−100.5 kJ mol^{-1}). A similar coupling procedure has been used for the calorimetric determination of uric acid in serum [81]. In this case, the coupling reaction is essential to bring the total heat change (−149.6 kJ mol^{-1}) within the sensitivity range of enthalpimetric measurements.

An enzymatic enthalpimetry approach can also be used to determine iodide ions in admixture with one or all of the other halides [88] since the peroxidase-catalyzed oxidation of iodide ion is unaffected by the presence of bromide and chloride. Fluoride inhibits the reaction, but this only affects the time for the reaction to come to completion and hence the curvature of

the enthalpogram. Small variations in hydrogen peroxide and peroxidase concentrations are acceptable, provided that the hydrogen peroxide is present in excess; the peroxidase concentration dictates only the rate of the enzymatic reaction. The procedure is therefore simple, with no reagent standardization or accurate replication of reagent volumes necessary because heat capacity is measured in situ for each analysis. Depending on the limiting reagent, the procedure can be used for the determination of hydrogen peroxide or iodide.

In the biochemical area, substrate determination represents the most precise and convenient calorimetric measurement which will also provide "operational" enthalpy assignments. The substrate limiting procedures can be adapted to allow relatively rapid successive measurements with the same enzyme reagent solution without entering into flow-analysis technology. The logical extension of repetitive substrate determinations in homogeneous solution is the use of enthalpimetric immobilized enzyme reactors. Discussion of the considerable activity in this area of research will be reserved for a separate section.

Determination of inhibitors

Compounds which reduce the rate of an enzyme-catalyzed reaction are called inhibitors. There are in fact several mechanisms of enzyme inhibition and many different types of inhibitors. The inhibitory effect is sometimes very sensitive; for example, nanomole amounts of some inhibitors can cause significant attenuation of the rate of certain enzyme—substrate reactions. Accordingly, the possibility exists for the determination of trace amounts of inhibitors if inhibitor concentration can be related linearly to the degree of inhibition.

"Irreversible" inhibition. Enzyme inhibition is generally classified as either "irreversible" or reversible. Most thermal measurements, at least in the analytical sector, have been concerned with "irreversible" inhibition, which is characterized by a progressive increase with time, ultimately reaching complete inhibition even with very small amounts of inhibitor, provided that the amount of inhibitor is in excess of the amount of enzyme. The effectiveness of this type of inhibitor is expressed not by an equilibrium constant, but by a rate constant which determines the fraction of enzyme inhibited in a given period of time by a certain concentration of inhibitor.

If [I] > [E] then the "irreversible" inhibition process, E + I → EI, can be treated as a pseudo first-order reaction [89, 90] whose rate can be expressed as

$$E_1 = E_0 \exp(-k_i[\mathrm{I}]\,t) \tag{5}$$

where E_1 is the enzyme concentration at the time t when the inhibition process is stopped by the addition of substrate; E_0 is the initial enzyme concentration and [I] is the inhibitor concentration. This equation can be transformed to

$$\log(\%\ \text{inhibition}) = 2 - (k_i\,[\mathrm{I}]\,t/2.303) \tag{6}$$

where % inhibition = 100 (enzyme activity at time t/enzyme activity at zero time). A plot of log (% inhibition) versus [I] is therefore linear and can be used as an analytical calibration plot. This relationship was validated in a pioneering investigation based on the flow calorimetric measurement of the inhibition of cholinesterase activity by organophosphorus pesticides [91]; the commercial pesticide Dimefox (tetramethylphosphodiamido fluoride) was used as a model. Later reports on the determination of 10^{-4} mol dm^{-3} parathion and 10^{-6} mol dm^{-3} tetraethylphosphate (TEPP) confirmed the principles of the technique [92].

"Irreversible" is a misnomer since most "irreversible" inhibitors are in fact reversible inhibitors with a very high affinity for the enzyme. In such cases, the equilibrium, E + I $\rightleftharpoons$ EI, exists, but lies far to the right. K_i, the inhibition constant, [E] [I]/[EI], typically has a value of 10^{-9} mol dm^{-3} for such interactions.

A much more important class of inhibitor from an enzyme kinetic viewpoint is that of the reversible inhibitors, which form dynamic complexes with the enzyme itself or with an enzyme—substrate complex. In contrast to "irreversible" inhibition, the reversible mechanism is characterized by a definite degree of inhibition, depending on the inhibitor concentration, which is usually reached rapidly and is thereafter independent of time, provided that the inhibitor is stable. The percentage inhibition is often much less than 100% and is dependent on the magnitude of the equilibrium constant, K_i. With some notable exceptions, it is a less sensitive effect than "irreversible" inhibition which, at least in part, accounts for its limited analytical application.

Reversible inhibition may result in an increased K_m value in the case of competitive inhibition or a reduced V_{max} in the case of pure noncompetitive inhibition. Two other mechanisms are possible, uncompetitive inhibition or some combination of these effects (mixed inhibition). The latter two options have not found analytical application and will not be discussed further.

Noncompetitive inhibition. Most elementary texts on enzyme inhibition describe noncompetitive inhibition in detail as an obvious alternative to competitive inhibition. The mechanism is based on the assumption that the inhibitor binds at a site on the enzyme that will not affect the binding of the substrate (K_m unchanged) but does attenuate the catalytic properties of the enzyme (V_{max} decreased). In fact, only small species (e.g. protons and metal ions) are likely to act in this manner and most commonly quoted examples of noncompetitive inhibition have been shown to be mixed inhibition [65]. As with the "irreversible" mechanism, noncompetitive inhibition is a special instance which is of more interest to the analytical chemist than the enzyme kineticist.

The initial rate of a noncompetitively inhibited reaction can be represented by the equation

$$v = V_{max}[S]/(K_m + [S])(1 + [I]/K_i) \qquad (7)$$

where K_i is the dissociation constant for the processes E + I ⇌ EI and EI + S ⇌ EIS. The tacit assumption is made that the value of K_i for these equilibria is the same.

If experimental conditions are controlled such that [S] ⩾ K_m and [S] ≈ constant then the rate equation simplifies to $v \approx$ constant $(1 + [I]/K_i)^{-1}$. It follows therefore that, when [I] = K_i, the reaction velocity will be half its initial value in the absence of the inhibitor. This rationale is the basis of an enthalpimetric procedure for the determination of silver ion in its capacity as an inhibitor of the urease-catalyzed hydrolysis of urea [93, 94]. Experimentally, silver solutions, containing an amount of urea to minimize substrate dilution, were titrated into a zero-order urea hydrolysis reaction already in progress. When the titration is complete, as represented by the cessation of the heat effect, the point on the enthalpogram corresponding to a slope of one-half that of the initial slope can be identified. The silver ion concentration in the titrant can then be calculated from a knowledge of K_i. The approximation that the concentration of free inhibitor is equal to the total inhibitor concentration is valid for reversible inhibitors. A careful choice of buffers must be made to avoid heavy metal precipitation or complexation. A detection limit, defined as a minimum 3% change in slope, of 1 ng cm^{-3} silver ion was quoted for this procedure.

Competitive inhibition. The most common type of inhibition, competitive inhibition, occurs when the inhibitor, by definition a substrate analog, competes with the substrate for the same active site on the enzyme. The substrate and inhibitor are therefore mutually exclusive at the site and since the EI complex (in the simplest case) is non-productive, an attenuation of the reaction rate results. The affinity of the substrate for the enzyme is unchanged.

The velocity of a competitively inhibited enzymatic reaction can be represented by the equation,

$$v = V_{max}[S]/\{[S] + K_m(1 + I/K_i)\} \quad (8)$$

The rate of a competitively inhibited reaction will therefore decrease with increasing inhibitor concentration, asymptotically approaching an equilibrium value depending on the magnitude of K_i. A plot of % inhibition versus inhibitor concentration is typically rectilinear at low inhibitor concentration [95].

The optimum substrate for serum ChE is butyrylcholine iodide; it follows therefore, that the most effective competitive inhibitors of serum ChE would contain a quaternary nitrogen atom, an ester group and would be highly methylated. A number of quaternary ammonium compounds, carbamate derivatives and alkaloids therefore inhibit ChE activity to a greater or lesser extent [96]. In a technique termed "enzymatic inhibition enthalpimetry", the analytical potential of the inhibitory action of some physiologically active alkaloids, including morphine, codeine and procaine, on the activity of serum ChE has been evaluated [97]: 0.5 cm^3 of substrate solution, at a concentration sufficient to ensure zero-order kinetics, was injected into

a previously equilibrated, buffered solution of enzyme and inhibitor. Characteristically, incubation time, beyond the minimum period required for thermal equilibration, was not a quantitative factor.

Inhibition curves were compiled by recording the rate of a zero-order reaction in the presence of different concentrations of inhibitor and determining the % inhibition:

$$\% \text{ Inhibition} = 100\,[\text{Control rate}([I] = 0) - \text{Inhibited rate}]\,/\,\text{Control rate}([I] = 0) \quad (9)$$

The nature of competitive inhibition demands that the substrate and enzyme concentrations are the same for the inhibited and uninhibited reactions. Typical inhibition data are shown in Fig. 4. Analytical calibration graphs were constructed from the linear regions of such inhibition curves. The inhibition curves can be displaced in either direction along the abscissa by changing either the substrate or enzyme concentration. Clearly, a compromise must be made between the amount of substrate needed to ensure zero-order kinetics, the amount needed to maximize the inhibitory effect and the sensitivity of the measurement. The detection limits, under the conditions described in the report ranged from 8×10^{-8} g for physostigmine, the strongest inhibitor, to 4×10^{-3} g for thiamine, the weakest. Linearity extended over a 5-fold concentration range and the precision of the measurements ranged from 0.4—2.6 % (r.s.d.).

Although predicted several years ago [15] as a development area, enzymatic inhibition enthalpimetry has never gained wide acceptance, as evidenced by the number of reports. Notwithstanding the sensitivity that inhibition analysis can provide, it lacks selectivity, whatever the measurement device, since the detector monitors a property of the substrate (or product) and not the

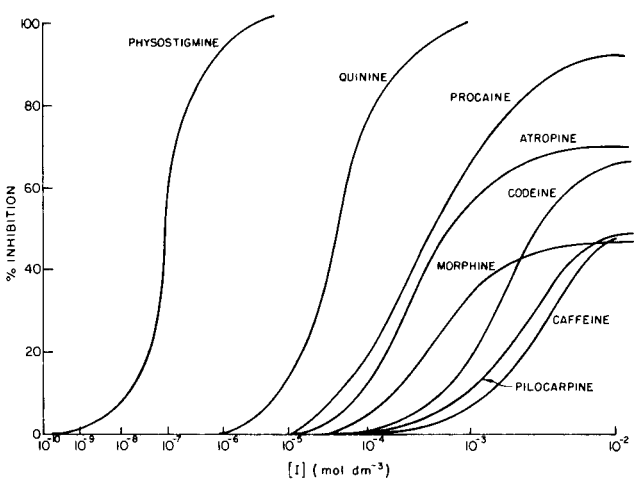

Fig. 4. Enzymatic inhibition enthalpimetry; the competitive inhibition of serum ChE by a series of alkaloids.

inhibitor. This constraint, coupled with a limited linear range, severely restricts the application of such techniques for analytical measurements in complex solutions.

It should be emphasized however that, as a measurement technique for the pharmacological compilation of comparative inhibition data, enthalpimetry offers the distinct advantage of monitoring the primary enzymatic reaction thereby simplifying the experimental variables and resultant kinetics considerably. It is in this type of measurement in which solution composition is carefully controlled, that enzymatic inhibition enthalpimetry has a significant contribution to make.

Determination of biochemical constants

The fundamental significance of K_m has been the subject of debate for many years, since its form depends on the relative magnitudes of the rate constants involved in the enzyme—substrate interaction and the subsequent formation of product. These arguments have been succinctly discussed elsewhere [65]. In spite of the dubious status that K_m may have as an intrinsic parameter of enzyme-catalyzed reactions, its value is essential in empirically defining the rate law for such a reaction, permitting the design of valid enzyme activity measurements. Furthermore, the factors that affect the velocity of enzyme-catalyzed reactions will be reflected in the magnitudes of K_m and V_{max}, respectively. In addition, V_{max}/K_m is a fundamental parameter itself since it represents the pseudo-first-order rate constant for an enzymatic reaction proceeding at low substrate concentration. Clearly, accurate and precise methods for the determination of these parameters are essential.

The determination of these constants has usually been achieved by the graphical representation of one of three well known linear transformations of the Michaelis—Menten equation [98—100]. The statistical bias inherent in all the linear transformations has been discussed at length [101]. Although shown to exhibit the greatest bias [102], the Lineweaver—Burk double-reciprocal plot of $1/v$ versus $1/[S]$ is by far the most widely used.

Kinetic d.i.e. has been used to determine discrete initial reaction rates for the urea—urease system [21] which were then incorporated into a double-reciprocal plot to obtain K_m. Treatment of the data in this fashion yielded a straight line with a regression coefficient of 0.9918.

An enthalpimetric determination of K_m for the enzymatic reduction of pyruvate to lactate has been reported in which reaction velocities, calculated by tangential extrapolation at selected points on the enthalpogram, were plotted by the Lineweaver—Burk method [103]. Although this procedure involves only one experiment per K_m assignment, the difficulties in obtaining reproducible reaction rates from points on a curve are obvious.

An alternative approach is to generate an enthalpimetric progress curve at a single substrate concentration and then apply the integrated form of eqn. (1) to the data, thus

$$-d[S]t/dt = V_{max}[S]_t/(K_m + [S]_t) \quad (10)$$

where $[S]_t$ is the substrate concentration at time t. Integrating between the limits $[S] = [S]_0$ and $[S]_t$, $t = 0$ and t gives

$$([S]_0 - [S]_t)/t = (V_{max} - K_m \ln[S]_{0/[S]_t})/t \quad (11)$$

Thus, a plot of $([S]_0 - [S]_t)/t$ versus $(1/t)\ln[S]_0/[S]_t$ will be a straight line with an ordinate intercept of V_{max} and a slope of $-K_m$.

In the absence of any extraneous heat effects, the heat output at any instant in a rate-controlled process, $q_{(t)}$, is a direct measure of the extent of the reaction as represented by $[S]_t$, the concentration of residual substrate at time t. $[S]_t$ can therefore be calculated from any point on an enthalpimetric progress curve from the relationship, $q_{(t)} = -([S]_0 - [S]_t)\ \Delta H V_c$ where V_c is the volume of the solution in dm^3.

The principle has been utilized in the enthalpimetric determination of K_m for the chymotrypsin-catalyzed hydrolysis of *N*-acetyl-L-tyrosine ethyl ester (ATEE) in Tris buffer [69]. The reported precision of these measurements, 7.6% r.s.d., compares favorably with other methods. The correction of heat losses occurring during the measurement periods is not trivial and can be achieved by the arithmetic addition of the slope of the post-reaction line to the progress curve after 0.5 t, where t is the measurement period for the entire curve. The implicit approximation that the heat losses are only significant during the latter half of the measurement period is adequate for this purpose. Data correction, compilation and computation were performed manually in this report; microcomputer control of these operations is under development in this laboratory. The treatment of enthalpimetric progress curves in this manner is a convenient, one-step procedure for the routine determination of K_m, particularly if under computer control.

An important consideration that must not be neglected when employing the integrated rate equation method is that product inhibition is not apparent from the progress curve and will invalidate the results if present and ignored. Equations have been developed to compensate for product inhibition if it is known to occur [65].

Beezer et al. have carried out a feasibility study for the determination of fundamental biochemical parameters, including K_m, by flow calorimetry [104, 105]. The urea—urease reaction was used as a model for this project.

The instrument response (I) from the flow calorimeter has been shown [18] to take the form,

$$I = I_z = \beta\ V_{max} V_c\ \Delta H \quad (12)$$

where β is an instrument calibration factor and V_c is the volume of the flow cell. When first-order kinetics prevail

$$I = \beta\ [S]_0\ (V_{max}/K_m)\ V_c\ \Delta H \exp -(V_{max}\ t/K_m) \quad (13)$$

Thus

$$I_0/[S]_0 = (\beta\ V_{max}\ V_c\ \Delta H)/K_m \quad (14)$$

where I_0 is the instrument response extrapolated to zero time. Ideally, K_m can be determined from the ratio of eqns. (12) and (14). Rearrangement of this relationship yields a familiar first-order equation

$$I_0 = I_z/K_m\ [S]_0 \quad (15)$$

Beezer points out that if the condition $K_m \gg [S]_0$, necessary for first-order behavior, is not fulfilled, a more accurate version of eqn. (15) is

$$I_0 = I_z[S]_0/(K_m + [S]_0)$$

which is analogous to the classical Michaelis—Menten equation and can be transformed into the linear equation

$$1/I_0 = (K_m/I_z[S]_0) + (1/I_z) \quad (16)$$

K_m can then be determined via the usual double-reciprocal plot. K_m values determined in this way are consistent with other data.

A flow technique has also been employed to investigate the kinetics of ribonuclease-catalyzed hydrolyses [106].

The enthalpimetric determination of biochemical kinetic parameters is clearly a realistic alternative to existing techniques. The enthalpimetric technique can be extended to the comparison of K_m values for enzymes in homogeneous and heterogeneous systems, where the facility to carry out kinetic measurements on reactions occurring at the solid—solution interface presents a considerable advantage over other methods.

Enthalpimetric devices based on immobilized enzyme technology

One of the most rapidly developing areas of scientific research over the past five years has been that of immobilization technology. In particular, enormous progress has been made in the development of methods for the immobilization of biological macromolecules, including enzymes, onto solid support systems. From an analytical chemistry viewpoint, the most obvious benefit to be gained from the use of an immobilized enzyme reagent is the removal of the two problems that have hindered the development of enzymatic methods of analysis for many years. Primarily, the exploitation of the catalytic properties of the enzyme as a re-usable reagent considerably reduces the cost of an enzymatic analysis, which in homogeneous solution can be prohibitive. Further, "stabilization" of an enzyme often occurs in an immobile form, which considerably enhances the resistance of the enzyme to environmental changes, pH, ionic strength, etc.

Description of the large number of immobilization techniques currently available is beyond the scope of this review. Four major categories can however be recognized; (a) physical adsorption onto a water-insoluble matrix; (b) covalent bonding to water-insoluble, functionalized polymers; (c) intermolecular cross-linking with a multifunctional reagent; and (d) physical

entrapment within water-insoluble gel matrices, microcapsules and fibers. All these techniques have been used to construct enthalpimetric immobilized enzyme reactors of one form or another.

Immobilized enzymes have been incorporated into enthalpimetric instrumentation in three forms: (a) immobilized enzyme flow reactors, usually in a fixed-bed configuration; (b) the so-called enzyme thermistor, a device in which the thermistor is placed in the center of a packed bed of an immobilized enzyme; and (c) enzyme-coated thermistors or thermal enzyme probes.

Enthalpimetric immobilized enzyme flow reactors (flow enthalpimeters). The activity in the field of immobilization chemistry is reflected in the volume of literature concerned specifically with the design, construction and application of analytical thermochemical devices incorporating an immobilized enzyme in a flow cell. In the interests of brevity therefore, only the relevant principles of these flow enthalpimeters will be discussed in the text followed by a tabulation of applications.

The essential elements of a thermochemical enzyme reactor, as typified by the flow enthalpimeter designed by Schifreen et al. [107], are depicted in Fig. 5. This particular design has been chosen for discussion since it was used as a definitive model to examine comprehensively the parameters affecting the performance of such a flow analyzer. The following discussion, which refers to the instrument in Fig. 5 and summarizes Schifreen's conclusions, is however, applicable to any analogous system.

A typical analytical measurement sequence is initiated by the injection of a sample plug into the pre-equilibrated buffer stream which then flows through a pre-column thermal equilibration coil, past a reference thermistor and into the adiabatic reactor column where conversion to products ensues.

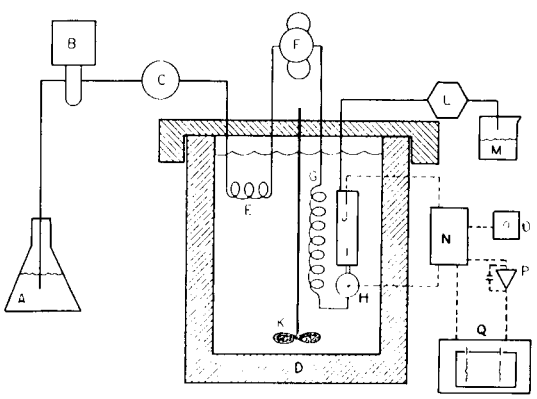

Fig. 5. Schematic drawing of the flow enthalpimeter [107]. (By courtesy of The American Chemical Society.) (a) reservoir, (b) pump, (c) pulse dampener-pressure gauge, (d) insulated water-bath, (e) pre-equilibration coil, (f) sample injection valve, (g) equilibration coil, (h) reference thermistor, (i) adiabatic column, (j) reference thermistor, (k) overhead stirrer, (l) flow meter, (m) waste receptacle, (n) a.c. phase-lock bridge amplifier, (o) oscilloscope, (p) integrator and (q) recorder.

The temperature rise associated with this reaction is monitored as the column effluent flows past a sensing thermistor in the column exit. Provision is made for flow rate measurements after the solution leaves the column. In order to maximize sample throughput, it is recommended that a non-compressible support (porous glass) and fast-response thermistors be incorporated into the apparatus. Conventional d.c. bridge, or a.c. phase-lock bridge amplifier systems for high sensitivity work, can be used for signal measurement.

The overall conclusion obtained from a study of the parameters affecting the behavior of this apparatus is that, except for the phenomenon of heat loss, it serves as a model for any immobilized enzyme reactor with a concentration sensitive detector. The pertinent points can be summarized as follows.

Dispersion. The major sources of dispersion are the thermal equilibration coil and the reactor column. The degrees of freedom here are limited by a minimum length of equilibration coil consistent with an adequate signal-to-noise ratio and a minimum reactor volume required for complete sample conversion and long lifetime. Reactor volume could be diminished by using very small particles.

Sample volume. Once a certain value of $[S]_0$ has been exceeded, peak broadening, caused by incomplete reaction, will occur. This threshold value is governed by total column activity, reactor volume, flow rate and K_m. If this value has not been exceeded, the effect of sample volume on peak height is controlled by sample dispersion and not enzyme kinetics.

Similarly, below a critical volume, sample size has no effect on peak width. However, once the sample volume becomes large relative to the intrinsic peak width, the peak width increases. There must therefore be a compromise between sensitivity and sample throughput, a fact of life for all flow systems.

Flow rate. A characteristic of a thermal flow system is a dramatic attenuation of peak height at low flow rates. This phenomenon, which is attributed to heat loss from the column, is evident in Fig. 6 which compares the effect of flow rate on peak height for a refractive index and thermal detection system. This hypothesis is given credence by the fact that peak height also decreases with increasing column volume (Fig. 6, column IV) and that a 3-fold increase in signal can be obtained by additional insulation of the column (Fig. 7).

For both detection systems, peak height decreases slowly with increasing flow rate, reflecting the increased resistance to mass transfer and hence dispersion that occurs as the mobile phase velocity increases.

It is evident that careful reactor design and optimization of experimental variables are essential for the development of an efficient and sensitive thermochemical flow reactor. This is apparent from the signal enhancement reported by Schifreen following optimization; a signal amounting to 12% of that based on a pure plug flow model was increased to 68%.

"Enzyme thermistor" or "flow enthalpimeter"? The term "enzyme thermistor" was introduced in 1974 [108], by analogy with the "enzyme electrode", to describe an alternative approach to microcalorimetry that

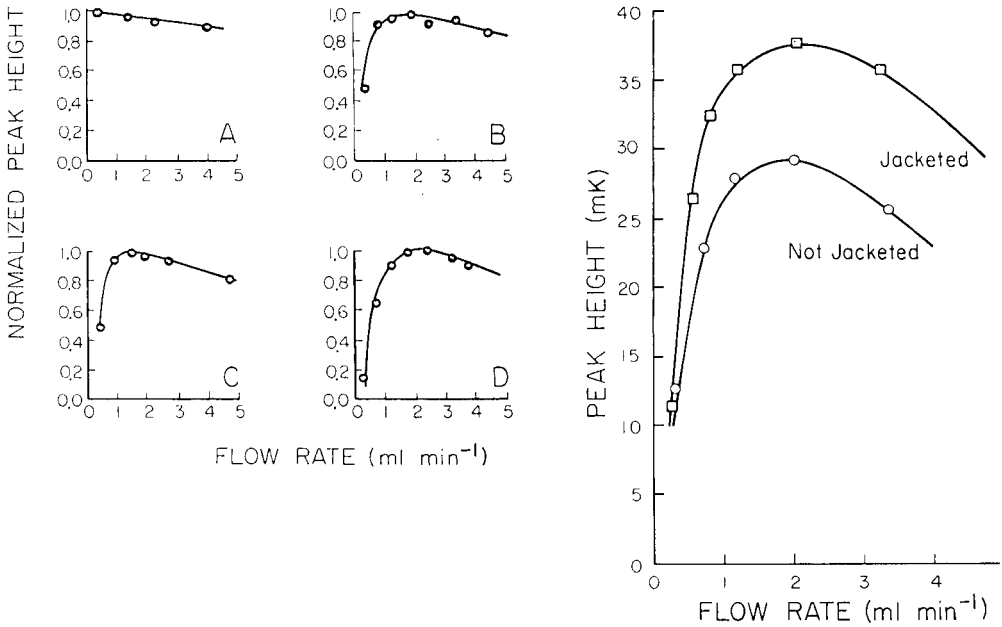

Fig. 6. Dependence of normalised peak height on flow rate [107]. (By courtesy of The American Chemical Society.) (A) column I, sample 120 μl of 20 mM urea, refractive index detector; (B) column I, sample 120 μl of 20 mM urea; (C) column II, sample 120 μl of 20 mM urea: (D) column IV, sample 120 μl of 20 mM urea. Dimensions:

Column	I	II	IV
Volume (ml)	0.42	0.67	0.85
Length (cm)	3.3	5.3	12.0
Internal diameter (mm)	4.0	3.7	3.0
Fraction active packing	1.0	1.0	1.0

Fig. 7. Effect of improved adiabaticity on peak height as a function of flow rate [107]. (By courtesy of The American Chemical Society.) Conditions: column IV, sample 120 μl of 20 mM urea. (○) Column without teflon jacket; (□) column with teflon jacket.

would allow sensitive biochemical and clinical assay that is inexpensive with regard to instrumentation and reagents [109, 110]. Although misleading, both these misnomers are in common usage. The rationale behind these devices is that the time constants normally associated with microcalorimetric measurements can be considerably reduced, and heat losses minimized, if the thermistor is placed in close proximity to the site of an immobilized-enzyme reaction. This also results in a considerable simplification of the apparatus compared with that required for microcalorimetry.

The original report [108] cited three possible configurations: (a) chemical bonding or physical adsorption of the enzyme directly onto the thermistor; (b) physical entrapment of an insolubilized enzyme around the thermistor by a semi-permeable membrane; and (c) encirclement of the thermistor by a

coil of tubing packed with a matrix-bound enzyme (thermal contact in this case is provided by paraffin oil). Configuration (c) was in fact preferred in the initial communication since it maximized enzyme activity and minimized diffusional considerations. The design of this device has now evolved to the implantation of the sensing thermistor in the center of a packed-bed microcolumn of immobilized enzyme incorporated in a conventional flow system [111]. The location of the thermistor in this manner has resulted in a highly efficient system which will record as much as one half of the total heat change as a temperature change. This is in accord with the findings of Schifreen et al. [107] that heat loss in a thermal flow column is a significant factor and has a finite effect on sensitivity as represented by the recorded peak height. There is, in principle, no essential difference between the "enzyme thermistor" and the "flow enthalpimeters" described earlier, especially if the reaction goes to completion before reaching the sensing thermistor: in view of the high enzyme loadings employed, this is likely to be the case. In the author's opinion, the term "enzyme thermistor" does not accurately describe this type of instrument since the immobilized enzyme does not form an integral part of the thermistor, nor is it physically or chemically attached to it. It is important however, to differentiate between this methodology and configurations (a) and (b), which are subject to totally different considerations. In accordance with this distinction, instruments in which the enzyme is not physically or chemically confined to the immediate microenvironment around the thermistor and which are based on flow methodology will all be classed as flow enthalpimeters for the purpose of this review.

A split-flow enthalpimeter, comprising two identical microcolumns, one of which contains an enzyme immobilized on alkylamine glass and the other just the glass support, has been developed [112]. The introduction of a reference column minimizes spurious thermal effects caused by variation in sample parameters, pH, ionic strength, viscosity, etc. The device is designed particularly for the analysis of complex solutions, e.g. milk and urine, in which such artifacts may occur.

A comprehensive listing of biochemical and clinical assays based on the principles of flow enthalpimetry is presented in Table 1.

Non-flow immobilized systems. Non-flow immobilized enzyme reactors have received little attention because of the low sample throughput associated with such devices. If analysis rate is not of paramount importance, a non-flow system has considerable merit since kinetic and thermodynamic as well as analytical information can be obtained conveniently and economically from the resultant progress curves.

Immobilized enzyme modules designed for use in a conduction-type calorimeter have been fabricated from cellulose acetate tubes and cellulose filter paper [126]. Activation of these surfaces was achieved by a cyanogen bromide procedure. Instrument response was observed to be faster when paper modules were used; this phenomenon can be attributed to reduced heat transfer and greater substrate availability in the porous paper matrix.

TABLE 1

Applications of enthalpimetric immobilized enzyme flow reactors (flow enthalpimeters) substrate/analyte

Substrate/analyte	Enzyme	Support	Coupling method	Comments	Ref.
Pyruvate/NADH, uric acid	Lactate dehydrogenase, uricase	CPG[a]	Bifunctional silane/glutaraldehyde	Comparison of kinetic properties of soluble/immobilized enzymes	113
Glucose/$MgATP^{2-}$ aqueous standards, human and reference serum	Hexokinase	CPG (Glycophase)	Direct coupling via Glycophase oxidation	Fructose, glucosamine and mannose interfere, galactose does not ca. 40 samples/h	114
Serum urea	Urease	CPG	Bifunctional silane/glutaraldehyde	Ammonia, protein, bilirubin and hemoglobin do not interfere ca. 40 samples/h	115
Urea, simulated serum	Urease	CPG	Bifunctional silane/arylation/diazotization	Signal attenuation 0.4% per day	116
Glucose and urea	Glucose oxidase catalase, urease	Porous cellulose triacetate fibers	Microcavity entrapment		117
Serum urea	Urease	CPG	Bifunctional silane/glutaraldehyde	12—15 samples/h, linear range 0.02—200 mol dm^{-3}	118
Glucose and urea	Glucose oxidase catalase, urease	Commercial immobilized enzyme gels	Entrapment in polyacrylgel or chemically bound to cellulose	Mechanical strength and high flow resistance of gels a problem	119
Gluose, penicillin G, benzoyl-L-arginine ethyl ester and urea, control sera	Glucose oxidase penicillinase, trypsin and urease	CPG	Bifunctional silane/glutaraldehyde	Very efficient heat transfer to sensor and low heat capacity give sensitive measurements	111
Cyanide in aqueous standards and blast furnace effluent	Rhodanase or injectase	CPG	Bifunctional silane/glutaraldehyde	Reactions monitored $CN^- + S_2O_3^{2-} \xrightarrow[r/ase]{} SCN^- + SO_3^{2-}$ CN^- + L-cysteine $\xrightarrow[inj/ase]{} SH^-$ + β-cyanoalanine. Pre-column ion exchange used for complex samples	120
Glucose in serum	Glucose oxidase/catalase	CPG	Bifunctional silane/glutaraldehyde	Linear range 0.01—0.09 mmol dm^{-3}, sample throughput 12/h	121
Cholesterol, oxalic acid, glucose and lactose in aqueous standards and biological samples	Cholesterol oxidase, oxalate decarboxylase, glucose oxidase, catalase, lactase	CPG	Bifunctional silane/glutaraldehyde		122
Hg(II), Cu(II) in aqueous standards	Urease	CPG	Bifunctional silane/glutaraldehyde	% inhibition of urease-catalyzed hydrolysis of urea by Hg(II) and Cu(II) monitored as attenuation of peak height. NaI, EDTA flush to regenerate column.	123
Cholesterol, glucose, lactose and uric acid in standard solutions, serum	Glucose oxidase, urate oxidase, cholesterol oxidase and lactase	CPG	Bifunctional silane/glutaraldehyde		124
Amylose, *p*-nitrophenylphosphate, urea, hydrogen peroxide	Amylase, alkaline phosphatase, urease, catalase			Immobilization not necessary for direct determination of EA. ΔT measured as function of EA in the sample	125

[a]Controlled pore glass

Such modules will undoubtedly become more widespread as enthalpimetric methods are used for the study of immobilized enzyme kinetics.

"Enzyme-coated thermistors" (thermistor enzyme probes). The essential criterion which defines a true "enzyme-coated thermistor" (ECT) is that the instrument measures the temperature change associated with an enzymatic reaction confined to a microenvironment around the thermistor sensor and catalyzed by a very small amount of enzyme. All else being equal, a smaller overall temperature change will be measured by such a device (c.f. a packed-bed) since the reaction will be diffusion-limited and will consume only a fraction of the total substrate concentration. The signal will be characterized, however, by a rapid response time; it will be limited only by the time taken for the substrate to diffuse across the unstirred layer of solution adjacent to the probe and the time constant of the probe (1—2 s). There are clearly fundamental differences between an ECT and the packed-bed devices mentioned in the previous section which warrant delineation by nomenclature. This can be achieved by careful use of the term "enzyme-coated thermistor" to describe only those devices in which the enzyme is chemically bonded, physically adsorbed or mechanically constrained to the surface or immediate proximity of the thermistor sensor bead.

A simple mathematical model can be used to estimate the expected steady-state ΔT as a function of bulk substrate concentration, and to identify the parameters affecting the design of an efficient ECT [127, 128]. It can be shown that, for a diffusion-limited reaction ($[S]_0 < K_m$),

$$\Delta T = D_s \Delta H [S]_0 / K \qquad (17)$$

where D_s is the substrate diffusivity ($cm^2\ s^{-1}$), K the thermal conductivity of the solution ($J\ s^{-1}\ cm^{-1}\ K^{-1}$) and $[S]_0$ is the bulk substrate concentration (mol cm^{-3}). When the assumptions made in the derivation of eqn. (17) hold, neither the enzyme concentration at the surface, nor the thickness of the unstirred layer around the surface, affect the steady-state ΔT. If $[S]_0 > K_m$, however, the saturation response will depend on the amount of enzyme per unit area. The model also predicts that the idealized time response is ca. 5 s for a well stirred system. ΔT will increase linearly with increasing bulk substrate concentration, until saturation kinetics are achieved. Finally, the response is inversely proportional to the thermal conductivity of the solution surrounding the probe. Substitution of typical data into eqn. (17) ($D_s = 10^{-5}$ $cm^2\ s^{-1}$, $\Delta H = 4.4 \times 10^4$ J mol^{-1}, $K = 5.6 \times 10^{-3}$ $J\ s^{-1}\ K^{-1}$) shows that a temperature change of only 1×10^{-4} K can be expected for a bulk substrate concentration of 1.25×10^{-3} mol dm^{-3}. A review of possible biomedical applications for ECT measurements has been recently published [129].

An interesting approach to the development of a thermistor enzyme probe is based on the physical adsorption of an enzyme onto a drop of mercury [130]. The mercury drop, contained in the open end of a glass U-tube which encapsulates the thermistor, acts as both support and heat conduction site. In an unstirred solution, the temperature increase at the mercury/solution

interface depends on the bulk substrate concentration and the enthalpy of reaction if diffusion control of the reaction prevails. There are two important criteria which contribute to the predominance of a microenvironment temperature effect rather than a "batch" temperature rise of the sample solution. The thermal conductivity ratio of mercury and water is ca. 13.6 : 1; the mercury drop therefore rapidly assumes the temperature of the interface (see eqn. 17). This phenomenon is aided by the low heat capacity of mercury. Rich et al. [130] calculate that even after 230 measurements, each measurement allowing 60 s for the attainment of a steady-state temperature, only a 5% reduction in concentration of a 10 mmol dm^{-3} substrate solution would result. The true enzyme-coated thermistor is effectively a non-destructive device in contrast to the packed-bed configurations described earlier. Physical adsorption of enzymes is the simplest and most convenient immobilization technique since it merely requires that the support and enzyme be brought into contact with each other. Moreover, very little activity is lost in the process. Unfortunately, adsorbed enzymes are not robust and their stability is usually dependent on many factors: pH, ionic strength, etc. This is borne out by the observation that an adsorbed urease probe remains active for only 4 measurements when applied to the repetitive determination of 10 mmol dm^{-3} of urea. Immersion of the probe in a urease solution between measurements extended its lifetime to 8 measurements. EDTA was added to all solutions to minimize urease inhibition by mercury(II).

A thermistor probe coated with a mixture of albumin and enzyme, cross-linked with glutaraldehyde has been described for the determination of hydrogen peroxide, glucose and urea [131]. Measurements were made by immersing a sensing thermistor, coated in this fashion, along with a differential reference thermistor into stirred solutions of buffered substrate. In some situations, a glass sleeve was placed around the sensor to reduce the dissipation of heat by forced convection.

Under the prevailing experimental conditions, $[S]_0 > K_m$ and immobilized enzyme loadings up to 170 μkat (10 000 IU), this type of probe will have different response characteristics to those already described. The response, ΔT, is dependent on enzyme concentration and the temperatures developed will ensure significant heat dissipation into the bulk of the solution. Indeed, the authors report that in certain situations the temperature increase is sufficient to cause irreversible destruction of the enzyme at the surface of the probe. In essence therefore this device is a non-flow enzyme reactor.

There is little doubt that the non-destructive ECT is a significant development in enthalpimetric technology and will find application in the biological sector. The small temperature change associated with this type of device does represent a significant sensitivity constraint.

Thermometric enzyme-linked immunosorbent assay (t.e.l.i.s.a.)

It was shown several years ago that thermodynamic information can be obtained from the enthalpimetric study of immunological reactions [132].

The analytical exploitation of antibody—antigen reactions is however a recent development with the introduction of enthalpimetric detection for enzyme-linked immunosorbent assay [133]. The motivation for such a combination is the wider choice of enzymes available for labeling when an enthalpy-related detector is used. Moreover, incorporation of the measurement into a flow system precludes the separation of bound and unbound species. The flow enthalpimeter consists of a thermistor implanted in the center of a glass or teflon microcolumn packed with human serum albumin (HSA) antibody immobilized onto a Sepharose gel. The experimental procedure is analogous to radioimmunoassay. A known amount of HSA antigen, coupled with a labeling enzyme, catalase, is mixed with the sample containing an unknown amount of HSA antigen; the mixture is then pumped through the column. Competitive binding of HSA antigen and HSA antigen—catalase to a limited amount of immobilized HSA antibody results. The temperature change recorded when hydrogen peroxide is subsequently passed through the column is a measure of the enzyme activity in the column and therefore inversely proportional to the amount of (uncoupled) HSA antigen in the sample. The column can be regenerated by eluting the antigen with glycine and beginning the sequence again. A detection limit of 10^{-10} mol dm^{-3} HSA antigen was quoted for this procedure.

T.e.l.i.s.a. does not have the absolute sensitivity of radioimmunoassay nor its speed. The low cost of the apparatus, coupled with the lack of health hazards, is however a significant advantage. Comparative studies of t.e.l.i.s.a. with bromocresol green, immunoturbidimetric and rocket immunoelectrophoretic methods suggest that this technique is a realistic alternative [134].

The t.e.l.i.s.a. methodology has been extended to the determination of enzyme substrates, including hydrogen peroxide, penicillin, sucrose, glucose, phenol and tyrosine [135]. The advantage of using an enzyme immobilized via an antigen—antibody interaction is that the function of the flow enthalpimeter can be changed by flowing the appropriate reagents through the column. Mattiasson [135] reports that the exchange between two different enzyme assays can be achieved in 8—10 min.

CONCLUSION

In summary, it is evident that enthalpimetric measurements have already made a significant impact on fundamental and applied areas of biochemical and clinical research. The catholic nature of enthalpic measurements will ensure that this trend continues.

It is not realistic to consider enthalpimetry as an alternative method for routine clinical determinations, except for a limited number of serum enzymes and physiological substrates. The primary limitation is sensitivity; this is borne out by the preponderance of reports concerned with the determination of analytes present in relatively large amounts in biological fluids, e.g. glucose, urea and cholinesterase. This inadequacy is particularly apparent

for the determination of diagnostically relevant enzymes. The current limit of detection for direct (derivative) enthalpimetric analysis is ca. 0.5 IU. Most serum enzymes are in the activity range 5 mIU—100 mIU. The sensitivity can of course be increased by using microcalorimetric techniques, although this approach nullifies one of the advantages of conventional enthalpimetry, the relatively low cost and simplicity of instrumentation required. Moreover, the increased thermal interferences encountered with isoperibol microcalorimetry place the technique firmly in the hands of the specialist.

In this context, analysis time is of critical importance. It has been shown that with careful design some flow enthalpimeters can assay up to 60 samples per hour. However, sample throughput decreases markedly with increased sensitivity for calorimetric measurements, as thermal equilibration procedures become more delicate. In the clinical laboratory where sample throughput is of paramount importance, the utility of enthalpimetric meaurements lies in their ability to simplify assays which may be difficult and/or time-consuming by other techniques or to form the basis of a widely applicable reference method. The capacity to execute direct enthalpimetric determinations of analytes in highly complex biological solutions, without recourse to error-generating and time-consuming separations, is a feature that must be weighed carefully before rejecting the technique solely from considerations of analysis time.

Enzymatic inhibition enthalpimetry is a useful universal technique for the characterization of enzyme inhibitors, e.g. as chemotherapeutic agents. Sample throughput, sensitivity and chemical interference are not critical factors in this type of application. Chemical interference severely restricts the scope of this methodology for quantitative analytical measurements in unknown samples.

The determination of biochemical constants (e.g. K_m, K_i) by enthalpimetric techniques has a distinct advantage in the facility to monitor the primary enzymatic reaction thereby simplifying the kinetic considerations considerably. Since such determinations are generally not sample- or time-limited, enthalpimetry offers a real alternative.

A logical extension of this work would seem to be the enthalpimetric study of functionalized surfaces and the kinetics of enzymes immobilized on these surfaces. In this area of analysis the ability of enthalpimetric measurements to monitor the progress of chemical and biochemical reactions in the presence of solid matrices is an invaluable and unusual attribute.

The author is grateful to Ms. D. Ohmes for assistance in the literature search associated with this review.

REFERENCES

1 J. Jordan, J. K. Grime, D. H. Waugh, C. D. Miller, H. M. Cullis and D. Lohr, Anal. Chem., 48 (1976) 427A.
2 L. S. Bark and J. K. Grime, Anal. Chim. Acta, 64 (1973) 276.
3 L. S. Bark and J. K. Grime, Analyst, 98 (1973) 452.

4 P. W. Carr, Crit. Rev. Anal. Chem., 3 (1972) 491.
5 J. Barthel, Thermometric Titrations, Wiley, New York, 1975.
6 L. S. Bark and S. M. Bark, Thermometric Titrimetry, Pergamon, Oxford, 1969.
7 H. J. V. Tyrrell and A. E. Beezer, Thermometric Titrimetry, Chapman and Hall, London, 1968.
8 G. A. Vaughan, Thermometric and Enthalpimetric Titrimetry, Van Nostrand Reinhold, London, 1973.
9 J. Jordan, in I. M. Kolthoff and P. J. Elving (Eds.), Treatise on Analytical Chemistry, Part 1, Vol. 8, Interscience, New York, 1968, p. 5175.
10 J. J. Christensen and R. M. Izatt, in H. A. O. Hill and P. Day (Eds.), Physical Methods in Advanced Inorganic Chemistry, Interscience, New York, 1968, p. 538.
11 L. D. Hansen, R. M. Izatt and J. J. Christensen, in J. Jordan (Ed.), Treatise on Titrimetry, Vol .2, M. Dekker, New York, 1974, p. 1.
12 L. S. Bark, P. Bate and J. K. Grime, in L. S. Bark (Ed.), Selected Annual Reviews of the Analytical Sciences, Vol. 2, Society for Analytical Chemistry, London, 1972.
13 R. N. Heistand, Rev. Anal. Chem., 2 (1975) 193.
14 L. S. Bark, J. Therm. Anal., 12 (1977) 266.
15 A. E. Beezer, MTP. Int. Rev. Sci., T. S. West (Ed.), Phys. Chem. Series 1, Butterworth, London, 1973, p. 71.
16 L. S. Bark, Cron. Chim., 41 (1973) 18.
17 J. M. Sturtevant, in C. H. W. Hirs and S. N. Timasheff (Eds.), Methods of Enzymology, Vol. 26, Academic Press, New York, 1972, p. 227.
18 A. E. Beezer and H. J. V. Tyrrell, Sci. Tools, 19 (1972) 13.
19 H. D. Brown, Biochemical Microcalorimetry, Academic Press, New York, 1969.
20 A. P. Fletcher, Am. Lab., 5 (1973) 42.
21 A. E. Beezer, Thermochim. Acta, 7 (1973) 241.
22 A. C. Censullo, J. A. Lynch, D. A. Waugh and J. Jordan, in R. S. Porter and J. F. Johnson (Eds.), Analytical Calorimetry, Vol. 3, Plenum Press, New York, 1974, p. 271.
23 I. Wadso, in R. Pain and B. Smith (Eds.), New Techniques in Biophysics and Cell Biology, Vol. 2, Wiley, New York, 1974, p. 85.
24 C. Spink and I. Wadso, in D. Glick (Ed.), Methods of Biochemical Analysis, Vol. 23, Wiley-Interscience, New York, 1975, p. 1.
25 R. N. Goldberg, E. J. Prosen and B. R. Staples, Anal. Biochem., 64 (1975) 68.
26 R. N. Goldberg and G. T. Armstrong, Med. Instrum., 8 (1974) 30.
27 S. N. Pennington, Enzyme Technol. Dig., 3 (1974) 105.
28 L. D. Bowers, Biochemical and Clinical Applications of Thermoanalytical Chemistry, Diss. Abs., Int. B., 36 (1976) 6110.
29 P. W. Carr, W. D. Bostick, L. M. Canning, Jr. and R. H. Callicott, Am. Lab., 8 (1976) 45.
30 K. Levin, in H. C. Curtis and M. Roth (Eds.), Clinical Biochemistry, Principles and Methods, Walter de Gruyter, Berlin, 1974.
31 K. Levin, Clin. Chem. (NY), 23 (1977) 929.
32 N. N. Rehak and D. S. Young, Clin. Chem. (NY), 24 (1978) 1414.
33 B. Tan, Ph.D. Dissertation, University of Otago, N.Z., 1979.
34 L. D. Bowers and P. W. Carr, Thermochim. Acta, 10 (1974) 129.
35 L. D. Bowers and P. W. Carr, Thermochim. Acta, 11 (1975) 225.
36 E. B. Smith, C. S. Barnes and P. W. Carr, Anal. Chem., 44 (1972) 1663.
37 H. A. Skinner, in H. D. Brown (Ed.), Biochemical Microcalorimetry, Academic Press, New York, 1969, p. 1.
38 J. M. Sturtevant, in A. Weissberger (Ed.), Techniques of Organic Chemistry, 3rd edn., Part I, Wiley, New York, 1959.
39 P. W. Carr, Thermochim. Acta, 3 (1972) 427.
40 D. J. Eatough, J. Therm. Anal., 14 (1978) 45.
41 L. D. Hansen, T. E. Jensen, S. Mayne, D. J. Eatough, R. M. Izatt and J. J. Christensen, J. Chem. Thermodynam., 7 (1975) 919.

42 J. J. Christensen, R. M. Izatt and L. D. Hansen, Rev. Sci. Instrum., 36 (1965) 779.
43 J. J. Christensen, J. W. Gardener, D. J. Eatough, R. M. Izatt, P. J. Watts and R. M. Hart, Rev. Sci. Instrum., 44 (1973) 481.
44 L. D. Hansen, R. M. Izatt, D. J. Eatough, T. E. Jensen and J. J. Christensen, Anal. Calorim., R. S. Porter and J. F. Johnson (Eds.), Vol. 3, Plenum Press, New York, 1974, p. 7.
45 N. V. Beaudette and N. Langerman, Anal. Biochem., 90 (1978) 693.
46 R. Weber, G. Blanc, G. Peuschel and F. Hagedorn, Anal. Chim. Acta, 86 (1976) 79.
47 R. Weber, Adv. Autom. Anal., 7th Technicon Int. Congr., 2 (1977) 357.
48 F. Hagedorn, G. Peuschel and R. Weber, Analyst (London), 100 (1975) 810.
49 J. Brandstetr, J. Therm. Anal., 14 (1978) 157.
50 F. Hagedorn and G. Peuschel, Z. Anal. Chem., 227 (1975) 177.
51 J. Rusz-Szorad and A. Halasz, Hung. Sci. Instrum., 32 (1975) 25.
52 J. A. Lynch and J. Jordan, Pittsburgh Conference on Analytical Chemistry and Applied Spectroscopy, Paper No. 54, Cleveland, OH, March, 1974.
53 N. D. Jespersen and J. Jordan, Anal. Lett., 3 (1970) 323.
54 P. W. Carr, E. B. Smith, S. R. Betso and R. H. Callicott, Anal. Calorim., R. S. Porter and J. F. Johnson (Eds.), Vol. 3, Plenum Press, New York, 1974, p. 457.
55 E. B. Smith, Ph.D. Dissertation, Univ. of Georgia, 1972, Diss. Abstr., Int. B., 33 (1973) 4165.
56 E. B. Smith and P. W. Carr, Anal. Chem., 45 (1973) 1688.
57 K. M. Kate, L. Vitello, G. C. Kresheck and G. Vanderkooi, Biopolymers, 18 (1979) 1889.
58 S. J. Rehfeld, D. J. Eatough and L. D. Hansen, Biochem. Biophys. Res. Commun., 66 (1975) 2.
59 D. J. Eatough, T. E. Jensen, H. F. Loken, S. J. Rehfeld and L. D. Hansen, Thermochim. Acta, 25 (1978) 289.
60 J. Jordan and T. G. Alleman, Anal. Chem., 29 (1957) 9.
61 R. H. Callicott and P. W. Carr, Clin. Chem., 22 (1976) 1084.
62 D. H. Waugh, Ph.D. Dissertation, Pennsylvania State Univ. (1978), Diss. Abs., Int. B., 39 (1979) 4854.
63 W. D. Bostick and P. W. Carr, Clin. Chem., 20 (1974) 1435.
64 W. D. Bostick and P. W. Carr, Anal. Chem., 46 (1974) 1095.
65 A. Cornish-Bowden, Principles of Enzyme Kinetics, Butterworth, London, 1976.
66 P. Monk and I. Wadso, Acta Chem. Scand., 23 (1969) 29.
67 C. D. McGlothlin and J. Jordan, Anal. Chem., 47 (1975) 1481.
68 J. K. Grime, B. Tan and J. Jordan, Anal. Chim. Acta, 109 (1979) 393.
69 J. K. Grime, K. R. Lockhart and B. Tan, Anal. Chim. Acta, 91 (1977) 243.
70 H. K. O'Farrell, S. K. Chattopadhyay and H. D. Brown, Clin. Chem., 23 (1977) 1853.
71 S. N. Pennington, H. D. Brown, A. B. Patel and S. K. Chattopadhyay, Anal. Lett., 2 (1969) 247.
72 B. Chance, in D. Glick (Ed.), Methods of Biochemical Analysis, 23 (1976) 1.
73 J. K. Grime and K. R. Lockhart, Anal. Chim. Acta, 106 (1979) 251.
74 N. N. Rehak and D. S. Young, Clin. Chem., 22 (1976) 1177.
75 A. Anders, H. Schaefer, B. Schaarschmidt and I. Lamprecht, Arch. Dermatol. Res., 265 (1973) 173.
76 R. B. Kemp, Proc. 1st. Eur. Biophys. Cong., 4 (1971) 381.
77 D. M. Yourtee, H. D. Brown, S. K. Chattopadhyay, D. Phillips and W. J. Evans, Anal. Lett., 8 (1975) 41.
78 D. L. Phillips and D. M. Yourtee, Anal. Lett., 9 (1976) 235.
79 J. Konickova and I. Wadso, Protides Biol. Fluids, Proc. Colloq., 20 (1973) 535.
80 J. K. Grime and E. D. Sexton, Anal. Chim. Acta, in press.
81 N. N. Rehak and D. S. Young, Clin. Chem., 23 (1977) 1153.
82 C. D. McGlothlin and J. Jordan, Anal. Chem., 47 (1975) 786.

83 R. N. Goldberg, E. J. Prosen, B. R. Staples, R. N. Boyd, G. T. Armstrong, R. L. Berger and D. S. Young, Anal. Biochem., 64 (1975) 68.
84 R. N. Goldberg, Clin. Chem., 22 (1976) 1685.
85 C. D. McGlothlin and J. Jordan, Clin. Chem., 21 (1975) 741.
86 J. K. Grime and B. Tan, Anal. Chim. Acta, 107 (1979) 319.
87 N. N. Rehak, G. Janes and D. S. Young, Clin. Chem., 23 (1977) 195.
88 J. K. Grime and K. R. Lockhart, Anal. Chim. Acta, 108 (1979) 363.
89 W. N. Aldridge, Biochem. J., 46 (1950) 451.
90 R. D. O'Brien, Toxic Phosphorus Esters, Academic Press, New York, 1960, p. 76.
91 J. Konickova and I. Wadso, Acta Chem. Scand., 25 (1971) 2360.
92 A. E. Beezer and C. D. Stubbs, Talanta, 20 (1973) 27.
93 J. N. Baldridge and N. D. Jespersen, Anal. Lett., 8 (1975) 683.
94 J. N. Baldridge, Ph.D. Dissertation, University of Texas at Austin, 1977, Diss. Abs. Int. B., 38 (1978) 3158.
95 G. G. Guilbault, Enzymatic Methods of Analysis, Pergamon, Oxford, 1970.
96 K-B. Augustinsson, Acta Physiol. Scand., 15 (1948) Suppl. 52.
97 J. K. Grime and B. Tan, Anal. Chim. Acta, 106 (1979) 39.
98 H. Lineweaver and D. Burk, J. Am. Chem. Soc., 56 (1934) 658.
99 G. S. Eadie, J. Biol. Chem., 146 (1942) 85.
100 B. H. J. Hofstee, J. Biol. Chem., 199 (1952) 357.
101 G. N. Wilkinson, Biochem. J., 80 (1961) 324.
102 J. E. Dowd and D. S. Riggs, J. Biol. Chem., 240 (1965) 863.
103 N. D. Jespersen and K. Barclay, Anal. Lett., 8 (1975) 33.
104 A. E. Beezer, T. I. Steenson and H. J. V. Tyrrell, Protides Biol. Fluids, Proc. Colloq., 20 (1973) 563.
105 A. E. Beezer, T. I. Steenson and H. J. V. Tyrrell, Talanta, 21 (1974) 467.
106 M. Tribout, S. Paredes and J. Leonis, Biochem. J., 153 (1976) 89.
107 R. S. Schifreen, D. A. Hanna, L. D. Bowers and P. W. Carr, Anal. Chem., 49 (1977) 1929.
108 K. Mosbach and B. Danielsson, Biochim. Biophys. Acta, 364 (1974) 140.
109 K. Mosbach, B. Danielsson and B. Mattiasson, Biochem. Soc. Trans., 7 (1979) 11.
110 B. Danielsson and K. Mosbach, in K. Mosbach (Ed.), Methods in Enzymology, Vol. 44, Academic Press, New York, 1976, p. 667.
111 K. Mosbach, B. Danielsson, A. Borgerud and M. Scott, Biochim. Biophys. Acta, 403 (1975) 256.
112 B. Mattiasson, B. Danielsson and K. Mosbach, Anal. Lett., 9 (1976) 867.
113 N. N. Rehak, J. Everse, N. O. Kaplan and R. L. Berger, Anal. Biochem., 70 (1976) 381.
114 L. D. Bowers and P. W. Carr, Clin. Chem., 22 (1976) 1427.
115 L. D. Bowers, L. M. Canning, Jr., C. N. Sayers and P. W. Carr, Clin. Chem., 22 (1976) 1314.
116 L. M. Canning, Jr. and P. W. Carr, Anal. Lett., 8 (1975) 359.
117 W. Marconi, F. Bartoli, F. Morisi and F. Pittalis, Int. J. Artif. Organs, 2 (1979) 159.
118 B. Danielsson, K. Gadd, B. Mattiasson and K. Mosbach, Anal. Lett., 9 (1976) 987.
119 H. L. Schmidt, G. Krisam and G. Grenner, Biochim. Biophys. Acta, 429 (1976) 283.
120 B. Mattiasson, K. Mosbach and A. Svensen, Biotechnol. Bioeng., 14 (1977) 1643.
121 B. Danielsson, K. Gadd, B. Mattiasson and K. Mosbach, Clin. Chim. Acta, 81 (1977) 163.
122 B. Mattiasson, B. Danielsson and K. Mosbach, in L. B. Wingard and E. K. Pye (Eds.), Enzyme Engineering, Vol. 3, Plenum Press, New York, 1978, p. 453.
123 B. Mattiasson, B. Danielsson, C. Hermansson and K. Mosbach, FEBS Lett., 85 (1978) 203.
124 B. Mattiasson, B. Danielsson and K. Mosbach, Anal. Lett., 9 (1976) 217.
125 B. Danielsson and K. Mosbach, FEBS Lett., 101 (1979) 47.
126 L. J. Forrester, D. M. Yourtee and H. D. Brown, Anal. Lett., 7 (1974) 599.

127 C. L. Cooney, J. C. Weaver, S. R. Tannenbaum, D. V. Faller, A. Shields and M. Jahnke, in E. K. Pye and L. B. Wingard (Eds.), Enzyme Engineering, Vol. 2, Plenum Press, New York, 1974, p. 411.
128 J. C. Weaver, C. L. Cooney, S. P. Fulton, P. Schuler and S. R. Tannenbaum, Biochim. Biophys. Acta, 452 (1976) 285.
129 J. C. Weaver, C. L. Cooney, S. R. Tannenbaum and S. P. Fulton, T. M. H. Chang (Ed.), in Biomedical Applications of Immobilized Enzymes and Proteins, Vol. 2, Plenum Press, New York, 1977.
130 S. Rich, R. M. Ianniello and N. D. Jespersen, Anal Chem., 51 (1979) 204.
131 C. Tran-Minh and D. Vallin, Anal. Chem., 50 (1978) 1874.
132 N. D. Jespersen, Ph.D. Dissertation, Pennsylvania State University, 1971, Diss. Abs., Int. B., 33 (1972) 59.
133 B. Mattiasson, C. Borrebaeck, B. Sanfridson and K. Mosbach, Biochim. Biophys. Acta, 483 (1977) 221.
134 C. Borrebaeck, J. Borjeson and B. Mattiasson, Clin. Chim. Acta, 86 (1978) 267.
135 B. Mattiasson, FEBS Lett., 77 (1977) 107.

Analytica Chimica Acta, 118 (1980) 227—231

THE FORMATION OF AMINES IN THE ANALYTICAL PYROLYSIS OF NITRO AND AZO COMPOUNDS

M. F. KUTTER, P. P. SCHMID and W. SIMON*

Department of Organic Chemistry, Swiss Federal Institute of Technology, Universitätstrasse 16, CH-8092 Zürich (Switzerland)

(Received 19th March 1980)

SUMMARY

The analytical pyrolysis of aromatic nitro and azo compounds on metal supports yields the corresponding amines, which are the major volatile products. This reduction is mainly due to effects of the support. The origin of the hydrogen under high vacuum conditions is established. It is shown that the sample preparation can be of great importance.

Reaction paths in the analytical pyrolysis of compounds of low volatility under high vacuum conditions have rarely been studied in detail [1, 2]. Our experience in pyrolysis/gas chromatography as well as pyrolysis/mass spectrometry indicates that the pyrolysis of a compound depends to a surprising degree on apparently minor details of the sample preparation. An example is the pyrolysis/mass spectrometry of aromatic nitro and azo compounds. Under certain conditions the corresponding amines are observed as the main products. With regard to the origin of the hydrogen in the vacuum of the mass spectrometer, the following possibilities may be considered: (1) inter- and/or intra-molecular exchange among sample molecules; (2) solvent residues or other contaminations on the sample support; (3) substances adsorbed on the ion source area (e.g. water); (4) absorbed hydrogen of the sample support.

In Curie-point pyrolysis the ferromagnetic sample supports are often inductively heated and annealed in a hydrogen atmosphere for cleaning purposes [3]. Although the cleaning of metal surfaces through the reduction of organic material is very efficient [4, 5], the simultaneous absorption of atomic hydrogen is well documented [6]. Of the different cleaning methods tested, reductive cleaning has indeed been highly recommended for analytical pyrolysis [5] in view of the good reproducibility achieved in the distribution of the thermal fragments observed. In this paper, the origin of hydrogen in the formation of amines when nitro or azo compounds are pyrolysed on metal supports is discussed.

EXPERIMENTAL

Instrumentation

Curie-point pyrolysis mass spectrometry. A Varian MAT 112 mass spectrometer (double focusing, reversed Nier-Johnson geometry) equipped with an Incos data system 2400 and a pyrolysis unit was used as described earlier [7]. The operating conditions were: ionisation energy, 21 eV (nominal); ion source temperature, 230°C; direct inlet probe heating rate, 5°C s^{-1} up to 360°C; high frequency, 610 kHz, 1.5 kW.

Sample supports. Ferromagnetic tubes (35/29 steel, 16 mm long, 1.6 mm o.d., 1.4 mm i.d., supplied by La Nationale S.A., CH-1211 Genève, Switzerland) were heated inductively in a stream of hydrogen or deuterium (8 ml min^{-1}, deuterium produced by electrolysis of D_2O). The hydrogen content of the iron tubes was determined by hot extraction in a high vacuum at 600°C [8]. Platinum tubes (10 mm long, 1.4 mm o.d., thickness 0.04 mm) were also tested.

Sample preparation

An aliquot (1 or 2 μl) of a solution containing 0.1% (w/v) of the sample dissolved in methanol-d_0, methanol-d_4 or in carbon disulphide was spread over the inner surface of the ferromagnetic tube and the solvent evaporated.

The substances used were nitrobenzene-d_5 (99.5% D, Stohler, CH-3044 Innerberg), nitrobenzene-d_0, *o*-nitrobiphenyl and *p*-nitrocinnamic acid (purum, Fluka AG, CH-9470 Buchs) and 1-phenylazonaphthalene. Three other azo compounds, taken from a collection of dyes (Department of Chemical Engineering, Swiss Federal Institute of Technology) were also examined: 1-phenyl-naphth-2-ol-6,8-disulphonic acid (compound I), 1-(*p*-methoxyphenyl)-naphth-2-ol-6,8-disulphonic acid (compound II), and 1-(*p*-chlorophenyl)-naphth-2-ol-6,8-disulphonic acid (compound III).

RESULTS

The pyrolysis of aromatic nitro and azo compounds on ferromagnetic supports yields the corresponding amines in pyrolysis/gas chromatography (with hydrogen or helium as carrier gas) as well as in pyrolysis/mass spectrometry. The formation of these amines is observed in the pyrolysis of nitro compounds such as *o*- and *p*-nitrocinnamic acid, *o*-nitrocinnamic aldehyde, *o*-nitrobiphenyl, α-nitrostyrene, and 2,4-dinitrostilbene. The molecular ions of the amines are dominant in all pyrolysis mass spectra of nitro as well as of azo compounds. An example is given in Fig. 1. Results of the pyrolysis of several compounds on metal tubes pretreated in deuterium are presented in Table 1. Mean intensities of 4—6 measurements are given, from which the corresponding intensities obtained in the pyrolysis on hydrogen-treated supports have been subtracted. The degree of deuteration is compared to the complete exchange of both hydrogen atoms of the amine. The variability

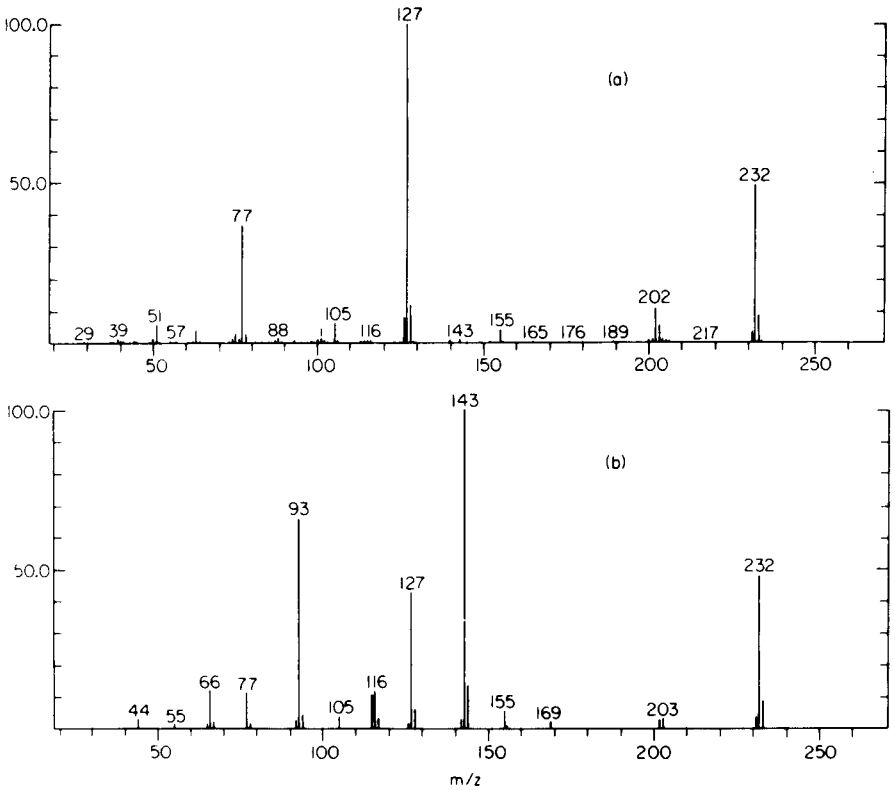

Fig. 1. Mass spectra of 1-phenylazonaphthalene. (a) E.i. mass spectrum of the sample introduced with the direct probe; (b) pyrolysis mass spectrum of the sample on hydrogen-treated iron tube.

of the deuteration, as calculated by error-propagation procedures, is 20% RSD. The hydrogen content of iron tubes pretreated in a stream of hydrogen has been determined with the results presented in Table 2. To study the influence of the solvent on the pyrolysis products, fragmentations were carried out on 1-phenylazonaphthalene in the presence of hydrogen-containing as well as hydrogen-free solvents (see Table 3). As indicated in Table 4 intermolecular exchange of hydrogen is significant.

DISCUSSION

The pyrolysis of aromatic nitro and azo compounds leads to the corresponding amines. The results in hand clearly show that this effect is due to several contributions. An important one is the hydrogen retained during the pretreatment of the metal sample supports with hydrogen (see Table 1). Even if the pyrolysis is carried out in platinum tubes not exposed to a hydrogen atmosphere, amines are among the main products. As shown in

TABLE 1

Formation of amines with sample tubes pretreated with deuterium

Sample	Product	Degree of deuteration of $-NH_2$ to $-ND_2$ (%)	Sample support	Solvent
Nitrobenzene	Aniline	9.4	Fe	CS_2
o-Nitrobiphenyl	*o*-Phenylaniline	10.3	Fe	CS_2
p-Nitrocinnamic acid	*p*-Aminocinnamic acid	12.8	Fe	CH_3OH
Compound I	Aniline	8.6	Fe	CH_3OH
Compound II	*p*-Methoxyaniline	8.6	Fe	CH_3OH
Compound III	*p*-Chloroaniline	3.2	Fe	CH_3OH
1-Phenylazo-naphthalene	1-Naphthylamine	10.6	Fe	CH_3OH
Compound III	*p*-Methoxyaniline	2.9	Pt[a]	CH_3OH
Nitrobenzene-d_5	Aniline-d_5	14.2	Pt[a]	CH_3OH

[a]Deuterium-treated platinum tubes were inserted into deuterium-free iron tubes and heated inductively.

TABLE 2

Hydrogen content of iron tubes annealed in a stream of hydrogen

Treatment after annealing	Hydrogen content	
	(ppm)	(nmol)
No further treatment	0.06 ± 0.02	3.1
1 μl CS_2 applied and evaporated	0.08 ± 0.02	4.1
1 μl CH_3OH applied and evaporated	0.10 ± 0.02	5.2

TABLE 3

Pyrolysis of 1-phenylazonaphthalene on hydrogen- and deuterium-treated iron tubes with different solvents

Solvent	Pretreatment of iron tube	Degree of deuteration of $-NH_2$ to $-ND_2$ (%)
Methanol-d_0	Hydrogen	Reference
Methanol-d_4	Hydrogen	3.5
Methanol-d_0	Deuterium	10.6 (see Table 1)
Carbon disulphide	Deuterium	14.4

Table 2 the amount of hydrogen present in the sample support can be considerable in terms of the sample size. In the case of the pyrolysis of 1 μg (8.13 nmol) of nitrobenzene, 3.1 nmol of hydrogen (see Table 2) is sufficient to transform up to 20% of the sample to the amine. It is rather surprising that the introduction of nitrobenzene, *p*-nitrocinnamic acid and 1-phenylazonaphthalene into the ion source of the mass spectrometer by means of a

TABLE 4

Pyrolysis of nitrobenzene-d_0 and nitrobenzene-d_5 with carbon disulphide as solvent

Sample (on deuterium-pretreated iron tube)	Reference (on hydrogen-pretreated iron tube)	Degree of deuteration of $-NH_2$ to $-ND_2$ (%)
Nitrobenzene-d_0	Nitrobenzene-d_0	9.4 (see Table 1)
Nitrobenzene-d_5	Nitrobenzene-d_5	17.0[a]

[a] Assuming full deuteration of the phenyl moiety.

direct inlet probe and using the same sample supports (ferromagnetic and platinum tubes) does not lead to a significant formation of amines. Apparently the heating rate of 5°C s^{-1} in the direct inlet probe, as compared to the rate of about 3000°C s^{-1} in the Curie-point pyrolysis, leads predominantly to evaporation of the intact sample (see Fig. 1).

The hydrogen contribution from solvent residues is small but nevertheless significant; it is demonstrated in Table 3. Methanol-d_4 causes a deuteration amounting to 3.5%. On deuterium-treated sample supports this contribution by solvent residues is about the same. The degree of deuteration is 3.8% smaller when methanol-d_0 is used instead of the hydrogen-free solvent carbon disulphide, because of competition by hydrogen stemming from solvent molecules. It is therefore very probable that water adsorbed in the ion-source area also participates in such exchange reactions.

The importance of intermolecular exchange of hydrogen and deuterium is shown in Table 4. The difference in the deuteration of aniline-d_0 and aniline-d_5 is due to intermolecular exchange of hydrogen and deuterium.

REFERENCE

1 M. A. Posthumus, N.M.M. Nibbering and A. J. H. Boerboom, Org. Mass Spectrom., 11 (1976) 907.
2 M. A. Posthumus and N. M. M. Nibbering, Org. Mass Spectrom., 12 (1977) 334.
3 J. P. Schmid, P. P. Schmid and W. Simon, Chromatographia, 9 (1976) 597.
4 E. L. Richter and W. A. Schmidt, Surf. Sci., 15 (1969) 498.
5 W. Windig, P. G. Kistemaker, J. Haverkamp and H. L. C. Meuzelaar, J. Anal. Appl. Pyrol., 1 (1979) 39.
6 K. Hauffe and S. R. Morrison, Adsorption, Walter de Gruyter, New York, 1974, p. 63.
7 P. P. Schmid and W. Simon, Anal. Chim. Acta, 89 (1977) 1.
8 H. K. Feichtinger, J. -M. Locarnini and B. Marincek, Mater. Tech., 6 (1978) 67.

Analytica Chimica Acta, 118 (1980) 233—241

DETECTION OF METAL IONS WITHOUT INTERFERENCE FROM DISSOLVED OXYGEN BY REVERSE PULSE AMPEROMETRY IN FLOW-INJECTION SYSTEMS AND LIQUID CHROMATOGRAPHY

PAUL MAITOZA and DENNIS C. JOHNSON*

Department of Chemistry, Iowa State University, Ames, Iowa 50011 (U.S.A.)

(Received 17th March 1980)

SUMMARY

Reverse pulse amperometry (r.p.a.) is used to monitor fluid streams for the presence of electroactive metal ions using a mercury electrode without the requirement of deaeration. The technique is based on the application of an unsymmetrical square wave with a large negative initial potential for deposition of the metal ion followed by a positive potential pulse for anodic stripping of the metal. The analytical signal is measured during the stripping process at a potential where dissolved oxygen is not reduced. R.p.a. is applied at a polarographic detector in flow-injection systems and ion-exchange chromatography for detection of several ions of transition and heavy metals in aqueous solutions.

The use of normal pulse and differential pulse methods for the amperometric monitoring of fluid streams for electroactive analytes has been studied by various workers [1—3]. Kissinger [4] has outlined several approaches based on pulsed-potential waveforms in a review of electrochemical detectors in liquid chromatography. Advantages of the pulsed mode of detection can include the maintenance of electrode activity, a decreased dependence of the detector response on the flow rate of the fluid stream, and increased analytical sensitivity. Rapid-scan square-wave polarography at a dropping mercury electrode (DME) has also been used in conjunction with liquid chromatography to obtain voltammetric characterization for each chromatographic peak [5]. All these polarographic techniques, however, suffer from the requirement of removal of dissolved oxygen from the sample and the fluid stream prior to application for cathodic reactions. Dissolved oxygen is electroactive at a mercury electrode for $E \leqslant 0$ V vs. SCE and a significant effort is required to maintain the dissolved oxygen in the fluid stream at an undetectable level. Dissolved oxygen can be removed with reducing agents such as ascorbic acid [6] and sodium sulfite [7]; with nitrogen-activated glass nebulizers [8]; or, most commonly, by purging with pure nitrogen or helium gas. All these approaches have major disadvantages for electroanalysis in fluid streams: the reducing agents have limited useful pH ranges; the nebulizers introduce significant dead-volume and are, therefore, incompatible with requirements for high resolution in high-performance

liquid chromatography; and the purging of all solutions is inconvenient, time-consuming, expensive in the case of helium, and virtually useless if the flow analyzer is constructed from teflon tubing which is readily permeated by oxygen. The later problem, in particular, led us to consider reverse pulse amperometry (r.p.a.).

The voltammetric basis for r.p.a. is easily understood after a brief comparison of the waveforms for normal pulse polarography (n.p.p.) and reverse pulse polarography (r.p.p.) as applied for cathodic reactions. The potential—time waveforms for n.p.p. and r.p.p. are shown in Fig. 1 by curves A and B, respectively. In n.p.p., the initial potential, E_i, has a value positive of $E_{1/2}$ for the cathodic wave; and the applied potential is "scanned" by way of regular increases in the amplitude, ΔE, of negative potential pulses of short duration, t_p, which are added to E_i at regular time intervals, T. For application of n.p.p. at a dropping mercury electrode, the lifetime of each mercury drop is terminated at the conclusion of the period T. In r.p.p., E_i is chosen at a value negative of $E_{1/2}$ in the potential region where the cathodic reaction is controlled by mass transport; and the potential is "scanned" by way of increasingly positive pulses. In both techniques, the faradaic current is measured at the end of each pulse when the charging current resulting from ΔE has decayed to an insignificant value.

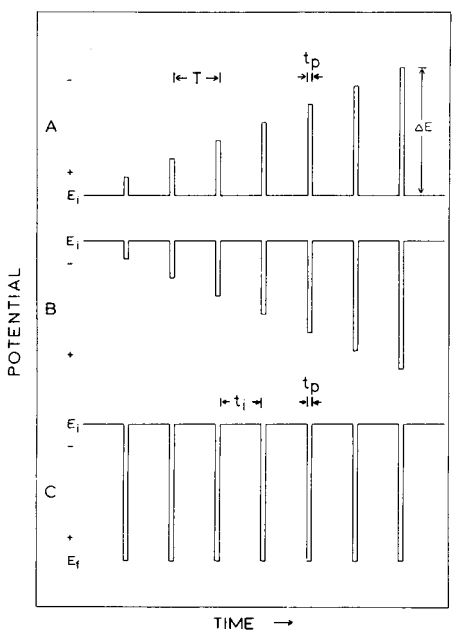

Fig. 1. Potential—time waveforms. E_i = Initial potential, E_f = final potential, ΔE = pulse height, T = pulse period, t_p = pulse width, t_i = time at initial potential. Curves: (A) normal pulse polarography; (B) reverse pulse polarography; (C) reverse pulse amperometry.

The potential—time waveform for r.p.a. is illustrated in Fig. 1 by curve C. The initial potential is chosen at a value for the mass transport-limited reduction of the analyte and a large, constant value of ΔE is applied so the final potential, $E_f = E_i + \Delta E$, is at a value for the oxidation of the product of the initial reaction at E_i. In the case of many metal ions, a metal amalgam is formed at E_i, as illustrated by $M^{n+} + ne^- \rightleftharpoons M(Hg)$, which is entirely analogous to the process of accumulation in voltammetric stripping methods. Anodic stripping of the metal commences with application of the potential pulse to E_f and the faradaic current for the oxidation is measured at the conclusion of the pulse, t_p. As described here for a dropping mercury electrode, the process of deposition and stripping occurs once for each drop. With proper selection of E_f, there is no faradaic contribution to the analytical signal from the reduction of dissolved oxygen.

R.p.p. and r.p.a. are not restricted to cathodic reactions which produce metal amalgams. Any product of a reaction at E_i which is soluble in the solvent phase and remains in the diffusion layer at the electrode surface can also, in principle, be detected following application of ΔE to a value of E_f suitable for the reverse of the initial reaction. As described here, r.p.p. corresponds to the technique of pulse polarography with scan reversal suggested by Oldham and Parry [9] for characterizing the reversibility of electrode reactions. Recently, Osteryoung and Kirowa-Eisner [10] demonstrated the applicability of r.p.p. for the determination of organic compounds known to have irreversible reductions but where the product of the cathodic reaction is reversibly oxidized. The possibility is also suggested that r.p.p. might permit detection of compounds for which the primary reaction occurs only for potentials where decomposition of the solvent occurs.

EXPERIMENTAL

Instrumentation

Polarograms were obtained with a static mercury drop electrode (Model 303, EG and G Princeton Applied Research, Princeton, New Jersey). Amperometric detection for the flow-injection systems and ion-exchange chromatography was by a polarographic detector (Model 310, EG and G Princeton Applied Research) with a static dropping mercury electrode (SDME) or a hanging mercury drop electrode (HMDE). The "small" size of the mercury drop (ca. 0.010 cm^2) was selected for all work. The glass capillary was cleaned and siliconized as described later.

Potential control and current measurement were made with a polarographic analyzer (Model 174A, EG and G Princeton Applied Research). The instrument was operated in the PULSE mode. The potential limits for r.p.a. were set by selecting the appropriate negative value of E_i; the value of ΔE was scanned in a positive direction to give the desired value of E_f, and the scan function was then set to HOLD. All values of electrode potential were measured versus the Ag/AgCl electrode with a solution saturated in AgCl and

KCl as the filling solution. The counter electrode was a platinum wire. Polarograms were recorded on an X—Y recorder (Model 7035, Hewlett-Packard Co., Pasadena, California). Detection peaks for all procedures were recorded on a stripchart recorder (Model SR-204, Heath-Schlumberger Instruments, Benton Harbor, Michigan).

All tubing, tube-end fittings and valves used in the ion-exchange chromatograph were Cheminert (Laboratory Data Control, Riviera Beach, Florida). Tubing (0.787-mm i.d.) was teflon, tube-end fittings were polypropylene and valves were Kel-F. The sample loop of the sample injection valve had a capacity of 0.206 ml. Flow of the fluid stream was provided by a Gilson HP Minipuls-2 peristaltic pump (Gilson Medical Electronics, Inc., Middletown, Wisconsin). The pulse dampener was an inverted T-tube containing a bubble of air (ca. 0.5 ml) in series with an adjustable needle valve, for generating back-pressure, constructed from Kel-F in the workshop. The ion-exchange column (4-mm i.d. × 100 mm) was packed with a low-capacity, sulfonated, cation-exchange resin (45—53 μm; Dionex Corp., Sunnyvale, California). This column was virtually equivalent to the Dionex No. 030233 Cation-Separator Column. The flow-injection analyzer was the same system as used for chromatography with the ion-exchange column removed.

Chemicals

All chemicals were analytical-reagent grade (Mallinckrodt Chemical Works, St. Louis, Missouri) except where noted. Mercury was triply distilled. Water was demineralized after a single distillation. The glass capillary of the polarographic detector was siliconized with a 5% solution of dichlorodimethylsilane (99% purity; Aldrich Chemical Co.) prepared in carbon tetrachloride (Certified ACS; Fisher Scientific Co.).

Siliconization procedure [11]. The glass capillary was cleaned by aspiration of 3 M nitric acid for 5 min, followed by aspiration with water for 10 min. The capillary was briefly aspirated in air, placed in an oven at 70°C for 1 h, and allowed to cool in a desiccator. The tip of the capillary was submerged into a freshly prepared solution of 5% dichlorodimethylsilane for 5 min; this caused the siliconizing solution to be drawn about halfway up the bore of the tube by capillary action. Finally, the capillary was aspirated in air for 10 min and was then ready for use. When not in use, the tip of the capillary was submerged in water without detachment from the detector.

RESULTS AND DISCUSSION

Discrimination against dissolved oxygen

The major advantage of r.p.a. over amperometric detection at constant potential for detection of metal ions is the ability to discriminate against direct faradaic interference by dissolved oxygen. This is illustrated by Fig. 2 which contains polarograms obtained by n.p.p. and r.p.p. for lead(II) in the presence and absence of dissolved oxygen. Only the cathodic wave for electro-

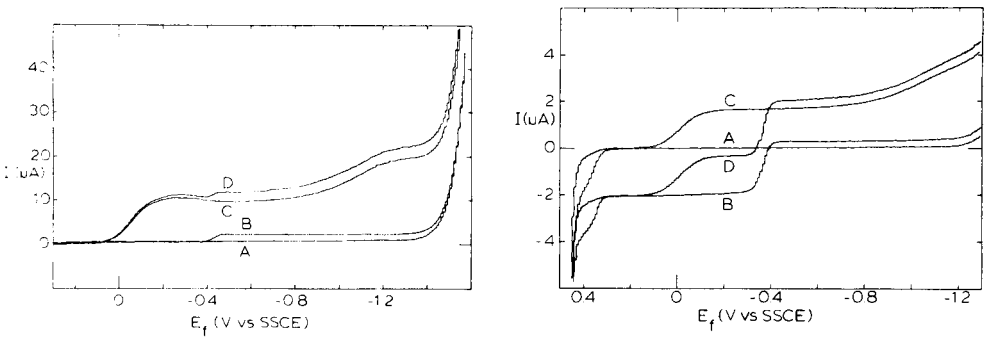

Fig. 2. (a) Normal pulse polarograms (E_i = +0.30 V, T = 2 s, ϕ = 5 mV s^{-1}), and (b) reverse pulse polarograms (E_i = −1.30 V, T = 2 s, ϕ = 5 mV s^{-1}). Medium, 0.01 M H_2SO_4 + 0.05 M Na_2SO_4. Curves: (A) oxygen-free residual curve; (B) oxygen-free + 10^{-4} M Pb(II); (C) air-saturated; (D) air-saturated + 10^{-4} M Pb(II).

deposition of lead(II) as the lead amalgam is observed by n.p.p., and accurate measurement of the limiting faradaic current for low levels of lead(II) can be accurately made only after removal of dissolved oxygen. R.p.p. yields waves for both the cathodic deposition and anodic dissolution of the lead. Oxygen again interferes with measurement of the cathodic wave for lead(II), but the limiting current for the anodic wave can be measured without a background current from reaction of oxygen in the potential region +0.1 V to +0.3 V vs. Ag/AgCl. Based on the information in Fig. 2(b), appropriate conditions for detection of lead(II) by r.p.a. would be E_i = −0.5 to −1.3 V and E_f = +0.2 V. Increasing the negative value of E_i increases the number of electroactive species which can be detected simultaneously with lead(II) by r.p.a. The anodic wave at +0.4 V results from chloride which is present in the cell of the detector by leakage of the filling solution from the reference electrode.

Peaks are shown in Fig. 3 for detection of zinc(II) by flow-injection analysis without benefit of deaeration to illustrate further the advantages of r.p.a. for eliminating interference by dissolved oxygen. Curve A is for determination of 6.5 ppm Zn(II) by n.p.a.; the sample and blank solutions contained the same concentration of supporting electrolyte as the carrier stream. Application of a large constant offset potential in the polarographic analyzer was necessary to bring the signal on scale for n.p.a. and the high uncertainty in the background current is attributed to fluctuation in the concentration of oxygen. The detection limit for n.p.a. (signal/noise =2) is estimated to be approximately 1 ppm Zn(II). The detection peak of 0.65 ppm zinc(II) by r.p.a. is shown by curve B (Fig. 3). Background noise is much lower for r.p.a. than n.p.a. and the detection limit is estimated to be a factor of 100× smaller.

Neither dissolved oxygen nor hydrogen peroxide, which is produced by reduction of oxygen at $-1.0 < E_i < 0.0$ V vs. Ag/AgCl, are anodically detected at $0.1 < E_f < 0.3$ V. However, chemical interference by these compounds

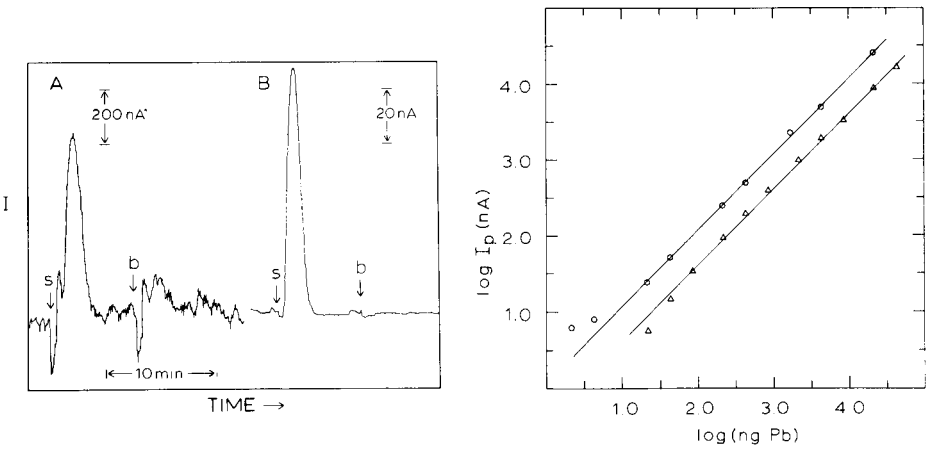

Fig. 3. Comparison of response for n.p.a. and r.p.a. Conditions: no column in analyzer; T = 2 s, RC filter = 0.3 s, V_f = 1.0 ml min^{-1}, V_s = 0.206 ml; 0.01 M H_2SO_4 + 0.05 M Na_2SO_4; (s) sample injection; (b) blank injection. Curves: (A) n.p.a. (E_i = +0.20 V, E_f = −1.20 V, 6.5 ppm Zn(II)); (B) r.p.a. (E_i = −1.20 V, E_f = +0.20 V, 0.65 ppm Zn(II)).

Fig. 4. Calibration curves for the determination of lead(II) by r.p.a. at the HDME (○) and SDME (△). Conditions: E_i = −1.20 V, E_f = +0.20 V, T = 2 s, V_f = 1.0 ml min^{-1}, V_s = 0.206 ml; 0.3 M tartaric acid + 0.02 M NaCl, pH 3.30. The lines shown have a slope of unity.

would occur in the detection of metal ions by r.p.a. if oxygen or hydrogen peroxide present at the electrode surface could chemically strip the deposited metal for $E = E_f$:

$$2M(Hg) + nO_2 + 2nH^+ \rightarrow 2M^{n+} + nH_2O_2$$

$$2M(Hg) + nH_2O_2 + 2nH^+ \rightarrow 2M^{n+} + 2nH_2O$$

Chemical interference by oxygen is not likely to be significant because the surface concentration of oxygen is zero during t_i for $E_i < 0.0$ V vs. Ag/AgCl; and the anodic signal is measured for a very short value of t_p, e.g. ca. 50 ms for the PAR 174A. Chemical interference by hydrogen peroxide is of concern only for $-1.0 < E_i < 0.0$ V where peroxide is the product of the reduction of oxygen. The absence of a chemical interference by oxygen in the detection of lead(II) can be observed in Fig. 2(b) by comparison of curves B and D at +0.2 V. The conclusion for lead(II) cannot be taken as applicable for all metals to be detected by r.p.a. and these possible interferences are under study at the present time.

Determination of lead(II) in the flow-injection system

Twenty successive injections of 640 ng Pb(II) were made during a period of 35 min. The average value of the peak heights was 270 nA with a relative standard deviation of 2.6%. The major source of uncertainty in the peak height resulted from variation in the area of the mercury drop in the polarographic detector. The siliconization of the capillary was repeated whenever

the drop-to-drop fluctuations of the faradaic signal exceeded approximately 5%. It was noted that, for siliconized capillaries, the application of a large negative value of E_i, e.g., < -1.3 V vs. Ag/AgCl, caused flow of solution into the bore of the capillary tube with the result that the mercury column broke within the tube. This phenomenon was also noted to be dependent on the identity of the supporting electrolyte.

Detection peaks of r.p.a. at the HMDE had a similar peak height but showed somewhat greater tailing than for the SDME. The tailing results from the fact that not all the deposited metal is stripped from the electrode during the application of E_f for the time t_p. Hence, several pulse cycles are required to eliminate the deposited metal totally from the electrode after the concentration of the metal ion in the stream has decreased to zero. Calibration curves based on peak height are shown in Fig. 4 for lead(II) in the approximate range 10 ng—40 μg for the 0.206-ml injection, which corresponds approximately to 0.2 μM—1 mM. The estimated detection limit is 13 ng (0.06 ppm) for the SDME and 2 ng (0.01 ppm) for the HMDE. Straight lines with a slope of unity have been superimposed on the data for comparison. Deviation from the expected slope is appreciable for the SDME at low concentrations of lead(II). The cause of the curvature is not known at the present time. It should be noted, however, that the case of mass transport to spherical electrodes in a stream has not been solved mathematically and the expectation of a linear correspondence between peak current and concentration is actually based on general experience in electroanalytical methods.

Selectivity of r.p.a.

A current—potential curve obtained by r.p.p. is shown in Fig. 5 for a mixture of Zn(II), Pb(II) and Cu(II). The solution was deaerated with nitrogen to simplify the interpretation of the polarogram. The value of E_i was -1.3 V and for $E_f = -1.3$ V, i.e., $\Delta E = 0$, the net current is cathodic resulting from simultaneous electrodeposition of the three metals. Three anodic waves are observed at -1.0 V, -0.4 V, and $+0.05$ V corresponding to Zn(II), Pb(II) and Cu(II), respectively. To assist in the interpretation of the polarogram, consider the reactions for $E_f = -0.2$ V. The net signal is the algebraic sum of the anodic currents for dissolution of Zn(Hg) and Pb(Hg), and the cathodic current for deposition of copper(II). For $E_f = +0.2$ V, the signal is the result of anodic dissolution of the three metals. When attempts are made to increase the selectivity of r.p.a. by judicious choice of parameters for the pulse waveform, there is little flexibility available in the choice of E_f if interference from dissolved oxygen is to be avoided. As illustrated by Fig. 5, E_i can be chosen so that the anodic current at $E_f = +0.2$ V results only from detection of copper(II). However, it is not possible under these circumstances to detect zinc(II) exclusive of Cu(II) and Pb(II) for $E_f = +0.2$ V. The use of $E_i = -1.3$ V and $E_f = -0.8$ V for detection of zinc(II) would be hampered by the large uncertainty in the background signal for oxygen.

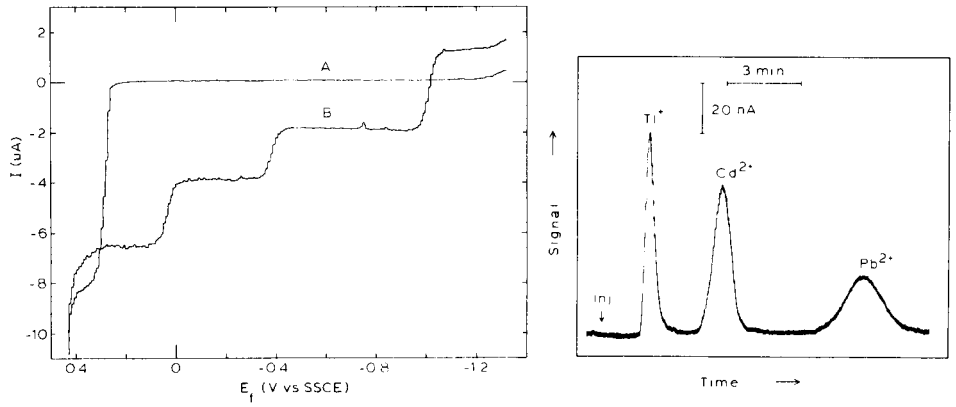

Fig. 5. Reverse pulse polarograms for a solution of Cu(II), Pb(II) and Zn(II). Conditions: $E_i = -1.30$ V, $T = 2$ s, $\phi = 5$ mV s^{-1}; 0.01 M H_2SO_4 + 0.05 M Na_2SO_4. Curves: (A) oxygen-free; (B) oxygen-free + 10^{-4} M in each metal.

Fig. 6. Chromatographic separation of Tl(I), Cd(II) and Pb(II) with detection by r.p.a. Conditions: $E_i = -1.20$ V, $E_f = +0.20$ V, $T = 2$ s, $V_f = 1.0$ ml min^{-1}; 0.01 M H_2SO_4 + 0.05 M Na_2SO_4 as eluent and electrolyte. Column: low-capacity, sulfonated, cation-exchange resin (45—53 μm), 4 mm-i.d. × 100 mm. Sample: 0.206 ml, 1.0×10^{-5} M in each metal.

Application of r.p.a. for analysis of complex mixtures is best made in conjunction with ion-exchange chromatography. The ionic eluents used in this technique fulfil the requirement of high conductivity for electroanalysis and the column effluent need not be mixed with a separate solution of supporting electrolyte prior to passing through the detector. A chromatogram is shown in Fig. 6 for separation of Tl(I), Cd(II) and Pb(II) in the cation-exchange column with detection by r.p.a. at the SDME. The base-line separation was acheived within 15 min for the isocratic elution with 0.01 M H_2SO_4 containing 0.05 M Na_2SO_4. The remaining parameters relevant to the separation are given in the legend to Fig. 6. No attempt was made to regulate the level of oxygen in the sample or eluent.

Conclusions

Reverse pulse amperometry at a polarographic detector appears to offer much promise for detection of metal ions in flow-injection systems and ion-exchange chromatography without interference from dissolved oxygen. Interference is expected from the presence of any species which is directly electroactive at E_f; or which produces an anodic wave at E_f by forming a slightly dissociated compound with Hg(I,II), e.g., halides, CN^-, S^{2-}, EDTA, etc. This information must be considered when selecting the carrier solution for flow-injection systems and the eluent for ion-exchange chromatography. Work is in progress to characterize r.p.a. further for detection in fluid streams as to dependence on flow rate and timing parameters.

Financial support from Dionex Corporation, Sunnyvale, California, is gratefully acknowledged.

REFERENCES

1 D. G. Swartzfager, Anal. Chem., 48 (1976) 2189.
2 A. MacDonald and P. D. Duke, J. Chromatogr., 83 (1973) 331.
3 K. Stulik and V. Hora, J. Electroanal. Chem., 70 (1976) 253.
4 P. T. Kissinger, Anal. Chem., 49 (1977) 447A.
5 J. Wang, E. Ouziel, Ch. Yarnitsky and M. Ariel, Anal. Chim. Acta, 102 (1978) 99.
6 T. M. Florence and Y. J. Farrar, J. Electroanal. Chem., 41 (1973) 127.
7 S. Kikuchi, K. Honda and S. Kim, Bull. Chem. Soc. Jpn., 27 (1954) 65.
8 C. Yarnitsky and E. Ouziel, Anal. Chem., 48 (1976) 2024.
9 K. B. Oldham and E. P. Parry, Anal. Chem., 42 (1970) 229.
10 J. Osteryoung and E. Kirowa-Eisner, Anal. Chem., 52 (1980) 62.
11 R. W. Andrews, University of Alabama, Birmingham, private communication, August 1979.

Analytica Chimica Acta, 118 (1980) 243—256

A DIRECT DIFFERENTIAL PULSE ANODIC STRIPPING VOLTAMMETRIC METHOD FOR THE DETERMINATION OF THALLIUM IN NATURAL WATERS

J. E. BONELLI*, H. E. TAYLOR and R. K. SKOGERBOE**

U.S. Geological Survey, Mail Stop 407, Denver Federal Center, Denver, CO 80225 (U.S.A.)

(Received 11th February 1980)

SUMMARY

A dual direct method for the ultratrace determination of thallium in natural waters by differential pulse anodic stripping voltammetry (d.p.a.s.v.) is presented. D.p.a.s.v. at the hanging mercury drop electrode and at the mercury film electrode is used in the concentration ranges 0.5—100 $\mu g\ Tl\ l^{-1}$, and 0.01—10 $\mu g\ Tl\ l^{-1}$, respectively. Quantification is aided by the technique of standard additions. The response of the method is optimized for typical natural surface water matrices. An intercomparison of thalium determinations performed by the two anodic stripping methods and electrothermal-atomization atomic absorption spectrometry on normal and thallium-spiked surface water samples demonstrates equivalent accuracy within the range where atomic absorption is applicable. The method appears free from serious interferences.

The lack of a direct, convenient and rapid analytical method for thallium with adequate sensitivity for water resource monitoring has limited extensive determination of naturally occurring concentration levels of thallium in surface waters. Because of the recent inclusion of thallium on the U.S. Environmental Protection Agency's list of priority pollutants [1] and steadily increasing emissions of this element to the environment, particularly from fossil fuel combustion [2], the authors sought to develop an analytical method for thallium that met the above criteria.

Existing analytical techniques applicable to thallium determinations in waters include neutron activation [3, 4], spark-source mass spectrometry [5, 6], electrothermal-atomization atomic absorption spectrometry [7—9], optical emission spectroscopy [6, 10], spectrophotometry [11], and anodic stripping voltammetry [12—16]. Anodic stripping voltammetry is a natural choice as a technique for determination of thallium in natural waters; thallium is reduced reversibly on mercury in most supporting electrolytes and concentrated amalgams may be obtained [17]. The inherent sensitivity of the technique is realized with the use of the differential pulse stripping mode [18] and the rotating mercury film electrode (m.f.e.) [19]. In a similar application, anodic stripping voltammetry has been widely used for determinations

**Department of Chemistry, Colorado State University, Fort Collins, CO 80523, U.S.A.

of thallium in urine and blood serum [20—22 and references therein].

With the exception of anodic stripping voltammetry, each of the techniques mentioned above exhibits one or more undesirable features, such as (a) requirements for laborious preconcentration steps, (b) matrix separations to eliminate interferences, and (c) access to expensive and sophisticated analytical facilities. Of the available anodic stripping voltammetric methods for thallium in waters, one involves preconcentration of thallium on a chelating resin [12], another involves preconcentration of thallium by coprecipitation [13], followed by d.p.a.s.v. at the hanging mercury drop electrode (h.m.d.e.), or direct current (d.c.) anodic stripping voltammetry at the mercury-graphite electrode, respectively. The first method requires a 3-day preconcentration procedure and a 4-l sample volume to obtain a limit of detection of 0.6 ng Tl l^{-1}. The second method is more rapid (3 h), requires a 100-ml sample, and obtains a determination limit of 10 ng Tl l^{-1}. The method reported here requires no preconcentration, or at most one hour, a sample volume of 25 ml and obtains a detection limit of 10 ng Tl l^{-1}. This limit may be extended by appropriate alteration of experimental parameters, or by use of preconcentration steps.

EXPERIMENTAL

Instrumentation

D.p.s.a.v. determinations were carried out with an EG&G Princeton Applied Research Corp. (PAR) Model 174A Polarographic Analyzer and Model 315 Electroanalysis Controller. The voltammetric cell was a borosilicate glass polarographic cell (PAR K60) with a molded plastic cell top (PAR K66). Current/potential curves were recorded on a Houston Instruments Model 2000 X-Y recorder. Optimized instrumental operating parameters are summarized in Table 1.

Electrodes

The working electrodes used were the PAR 9323 h.m.d.e. (Metrohm E-410) and a Tokai EB-6 (type GCA) 6-mm glassy carbon rod encapsulated in epoxy resin. A Pine Instruments electrode rotator Model #PIR was employed with the glassy carbon substrate on which the thin mercury film was electrodeposited. The reference electrode was Ag/AgCl (sat. KCl) isolated from the sample solution by a porous Vycor silica bridge, to which all potentials were referred. The auxiliary electrode was a 20-gauge platinum wire.

Reagents

All chemicals used were reagent-grade or better. Water was obtained from a commercial water purification system and used without further purification; local tapwater was analyzed and found to contain no detectable thallium. Only ultrapure nitric acid was used for reagent preparation; reagent grade nitric acid (as a 20% water solution) was used for cleaning glassware.

TABLE 1

Summary of optimized operating parameters

Parameter	Optimum setting or condition	Parameter	Optimum setting or condition
Instrumental		*Chemical*	
Mode	Differential pulse	Supporting electrolyte/ buffer (pH 4.5—4.6)	0.06 M $HC_2H_3O_2$
Conditioning potential	0.0V (h.m.d.e.); —0.1V (m.f.e.)		0.05 M $KC_2H_3O_2$
Deposition potential	—0.8V		0.001 M EDTA
Potential scan rate, ν	5 mV s^{-1}	m.f.e. plating solution	0.06 M $HC_2H_3O_2$
Pulse frequency	2 Hz		0.05 M $KC_2H_3O_2$
Pulse modulation amplitude	50 mV		0.0008 M Hg^{2+}
Final potential	0.0V (h.m.d.e.); —0.1V (m.f.e.)		

The supporting electrolyte/buffer (1.53 M acetic acid, 1.42 M potassium acetate) solution was prepared by reacting 17.3 g of anhydrous potassium carbonate with 35.4 g (33.8 ml) of glacial acetic acid adding water very slowly. When the reaction was complete, sufficient water was added to bring the total volume up to 200 ml.

The EDTA stock solution was prepared by dissolving 4.16 g of tetrasodium-EDTA in enough water to yield 100 ml of solution. A mercury stock solution (used for preparation of the m.f.e.) was made by dissolving 0.201 g of mercury in 1.0 ml of nitric acid and diluting with water to 100 ml.

The thallium stock standard solution (1000 mg l^{-1}) was prepared by dissolving 130.3 mg of oven-dried (110°C) thallium(I) nitrate in 10.0 ml of nitric acid and adding sufficient water to yield 100 ml of solution. Working thallium standard solutions were prepared fresh daily from this stock standard solution by appropriate serial dilutions in 0.02 M nitric acid.

Cylinder nitrogen used for purging solutions was passed through a vanadium-(II) chloride solution to remove traces of oxygen, as described by Meites [23].

Procedures

All glassware was soaked in 20% (1 + 4) nitric acid for at least one hour prior to use. It is recommended that water samples be collected and preserved with nitric acid in accordance with accepted procedures [24].

Electrode preparation. The m.f.e. is prepared on the exposed 6-mm end of the glassy carbon rod encapsulated in a cylindrical sheath of chemically resistant epoxy resin. The electrode surface is faced off flat on a lathe, and then wet-ground by hand on a glass plate with a succession of abrasives starting with 400-, followed by 600-grit silicon carbide and finally γ-alumina, to produce a mirror-like finish. The electrode is then mounted in the rotator and immersed in a plating solution made from 22.0 ml of water, 1.0 ml of supporting electrolyte/buffer, and 2.0 ml of the mercury stock solution. After purging the solution with nitrogen for 5 min with electrode rotation at 3600 revolutions per min (rpm), a d.c. potential of —0.25 V is applied for

5 more minutes, with nitrogen bubbling as the only means of stirring. Subsequently, the electrode is rotated at 3600 rpm for 10 min at −0.25 V [19].

During a typical film-plating operation, about 0.2 coulomb of charge will be passed; assuming 100% current efficiency and homogeneous coverage, the resulting mercury film will be about 500 nm thick, well within the thin-film range [19, 25]. Electrodes prepared in this way have been successfully used for one complete day's work. Since the analytical performance of the m.f.e. degrades with time, it is recommended that a new m.f.e. be prepared daily.

Analysis of waters. The following procedure is suitable for the analysis of waters with concentrations of 0.5 to 100 μg Tl l^{-1} with the h.m.d.e. To a 25.0 ml sample in a polarographic cell, add 1.0 ml acetate supporting electrolyte/buffer, 0.25 ml EDTA solution and a small magnetic stirring bar. Purge the solution with prepurified nitrogen gas for 5 min. Extrude a fresh mercury drop from the electrode — a 3-division (0.02 cm^2) drop has been found satisfactory. Condition the electrode for 1.5 min with stirring at −0.1 V, deposit 60 s with stirring at −0.8 V and equilibrate 15 s at −0.8 V without stirring. Initiate the stripping scan with instrument parameters shown in Table 1 and record the current/potential curve. A well-formed peak at about −0.42 V corresponds to thallium oxidation, the height of which is proportional to thallium concentration. An appropriate small-volume spike of the working thallium standard solution is added, and the above procedure repeated. Three additions are required to provide a linear standard additions plot from which the original thallium concentration can be calculated directly [26, 27]. Higher precision can be obtained by using the same electrode drop for a succession of four scans on each sample. However, caution must be exercised when surface-active organic materials or large amounts of copper are present; in these cases it may be prudent to use a fresh electrode drop for each scan.

Analysis of waters with concentrations of 0.01—10 μg Tl l^{-1} is carried out at the m.f.e. exactly as in the preceding paragraph with the exceptions that (a) no magnetic stirring bar is used; electrode rotation at 3600 rpm is used to effect solution stirring; (b) the electrode is conditioned and the stripping scan is terminated at −0.1 V; (c) the deposit time is 600 s; and (d) the thallium oxidation peak appears at about −0.56 V.

The choice of a 25-ml sample is merely for convenience. There is no reason that significantly smaller sample volumes cannot be used, provided that the usual limitations on a.s.v. are not exceeded (for a detailed discussion, see [17, 28]).

RESULTS AND DISCUSSION

Response optimization

To provide for the widest possible concentration working range, the method was optimized for thallium determinations in natural water matrices. Previous reports, though few in number, have clearly indicated that concen-

trations of thallium in natural waters do not exceed 50 ng Tl l^{-1} [12, 13]. Our intent was to obtain the greatest sensitivity of determination, consistent with sound analytical practice and reasonable expenditure of time and effort, per sample analysis. It is anticipated that most, if not all, unpolluted water samples will have thallium concentrations that fall within the working range of the m.f.e. (0.01—10 μg Tl l^{-1}). Response optimization experimentation was, therefore, concentrated on the m.f.e. portion of the method.

The response optimization experiments can be broadly divided into two categories, instrumental parameters and chemical parameters.

Instrumental parameters. The differential pulse stripping mode was employed because of its inherent sensitivity and operational simplicity with modern instrumentation [18, 19, 29].

Of the parameters affecting the total quantity of thallium preconcentrated into the m.f.e. during the deposition step (which is proportional to the stripping peak current), the instrumental parameters of deposition time, electrode rotation rate, and deposition potential are the most important. Figure 1 (a—c) shows dependences of the observed stripping peak current on each of these parameters. As expected [19], the stripping peak current is roughly proportional to deposition time and the square root of the electrode rotation rate, and roughly independent of deposition potential in the range investigated. In agreement with Neeb [30], the stripping peak current was found to fall off rapidly at deposition potentials more negative than −1.1 V.

The instrumental parameters of pulse rate, pulse amplitude, and potential scan rate are to a degree interactive and affect the stripping step, and, consequently, the observed stripping peak current. Figure 1 (d—f) show these dependences and their respective selected optimum values. Instrumental parameters were chosen for optimum response in all but two cases, deposition time and electrode rotation rate. This was to retain a reasonable time commitment per determination and to prevent the possibility of solution cavitation in some samples during the deposition step [19]. If a lower detection limit is desired, deposition time and/or electrode rotation rate may be increased within reasonable limits.

Chemical parameters. Various chemical parameters, such as supporting electrolyte concentration, solution pH and ligand concentration, markedly affect deposition and stripping processes. These chemical parameters were response-optimized within limitations imposed by the expected variability of the natural water matrices. Figure 2 shows dependences of the observed stripping peak current on the supporting electrolyte and EDTA concentrations. In both cases, the apparent maximum response was not chosen. The optimum supporting electrolyte/buffer concentration was chosen on the basis of maximizing analytical response, while providing adequate buffer capacity to deal with acidified samples (for preservation), and widely variant sample alkalinity, along with sufficient ionic strength to overwhelm the possible effects of large amounts of dissolved solids. Sufficient supporting

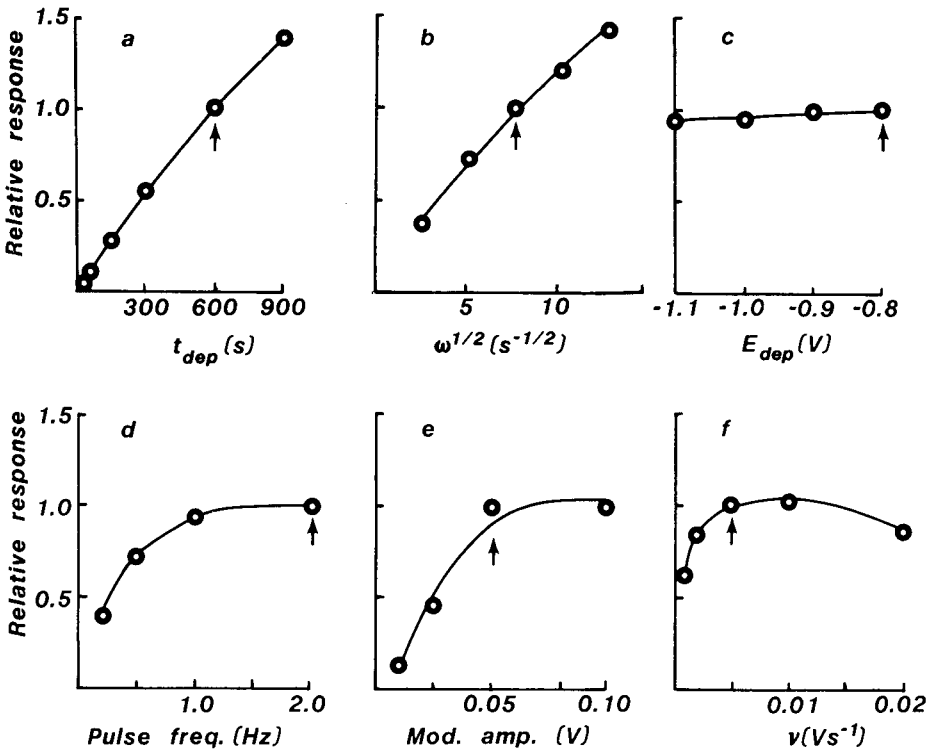

Fig. 1. Response optimization of instrumental parameters. (a) Deposition time; (b) electrode rotation rate; (c) deposition potential; (d) pulse frequency; (e) pulse modulation amplitude; (f) potential scan rate. Synthetic water samples containing approximately 2 μg Tl l^{-1} were analyzed at the rotating m.f.e. Non-varied instrumental parameters were held constant at the values shown in Table 1. Arrows show chosen optimum parameters.

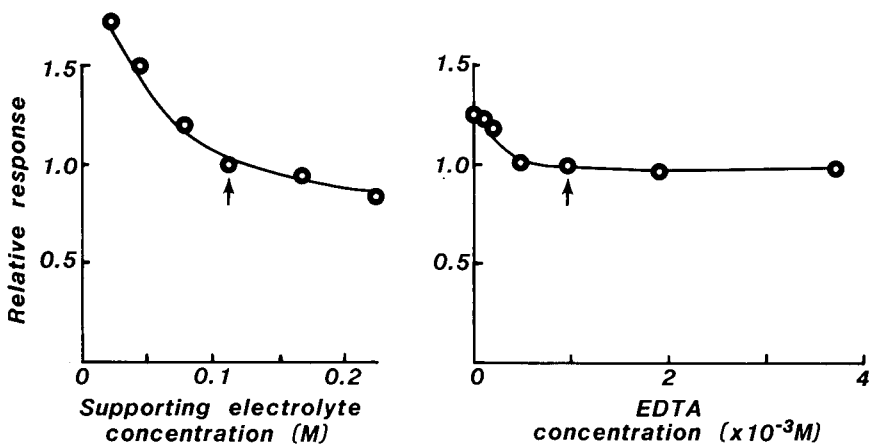

Fig. 2. Response optimization of chemical parameters. (a) Supporting electrolyte/buffer concentration (acetate buffer); (b) EDTA concentration. Synthetic water samples containing approximately 2 μg Tl l^{-1} were analyzed at the rotating m.f.e. Instrumental parameters are shown in Table 1. Arrows show chosen optimum parameters.

electrolyte concentration is also necessary to avoid the effects of large uncompensated solution resistance on the measurement [31]. Optimum EDTA concentration was chosen to provide an adequate margin of safety from interference by cadmium, lead, and copper.

The effect of mercury film thickness may also be loosely regarded as a chemical parameter. Although it has been shown theoretically [25] and verified experimentally [19] that the stripping peak current is not, within limits, a function of mercury film thickness, Batley and Florence [29] have claimed superior analytical performance for mercury film electrodes formed in situ (i.e., simultaneous film and analyte deposition). We have chosen in this application a m.f.e. thin enough to adhere to thin-film behavior, but thick (voluminous) enough to minimize the effects of co-deposited metals (especially copper), which may saturate or otherwise alter the electrode. Stulikova [32] suggested that more homogeneous electrode coverage with mercury is obtained at applied film plating potentials less than −0.8 V. We have found no performance advantage in doing so.

Analytical ranges

The working ranges, sensitivities, and detection limits of the two d.p.a.s.v. methods described here and similar data for a representative electrothermal-atomization atomic absorption spectrometric method [33], are seen in Table 2. Definitions for sensitivity and detection limit found in Skogerboe [34] were used for these calculations. Because these method parameters are to a small degree dependent on the matrix, values are reported for one of the natural water matrices discussed in the accuracy and precision section. The working range is given here as that concentration space bounded by the detection limit and the upper limit tested for which a suitably linear working curve may be obtained. This upper limit includes provision for the standard additions quantification technique; e.g. the m.f.e. method gives suitably linear working curves up to 40 μg Tl l^{-1}. A sample d.p.a.s.v. voltammogram for a standard additions determination of thallium in a natural water sample is seen in Fig. 3. Note that the operative detection limitation of the method is the applied potential dependence of the background which precludes the use of higher amplifier gains. Consequently, appropriate instrumental modi-

TABLE 2

Sensitivity and detection limits in natural water matrix number 31

Method	Working range ($\mu g\ l^{-1}$)	Sensitivity γ ($l\ \mu g^{-1}$)	Detection limit ($\mu g\ l^{-1}$)[a]
E.t.a.a.a.	1.0—10	2.9	1.0
D.p.a.s.v./h.m.d.e.	0.5—100	5.2	0.6
D.p.a.s.v./m.f.e.	0.01—10	138	0.01

[a] $\alpha = 0.05$, $\nu = 2$.

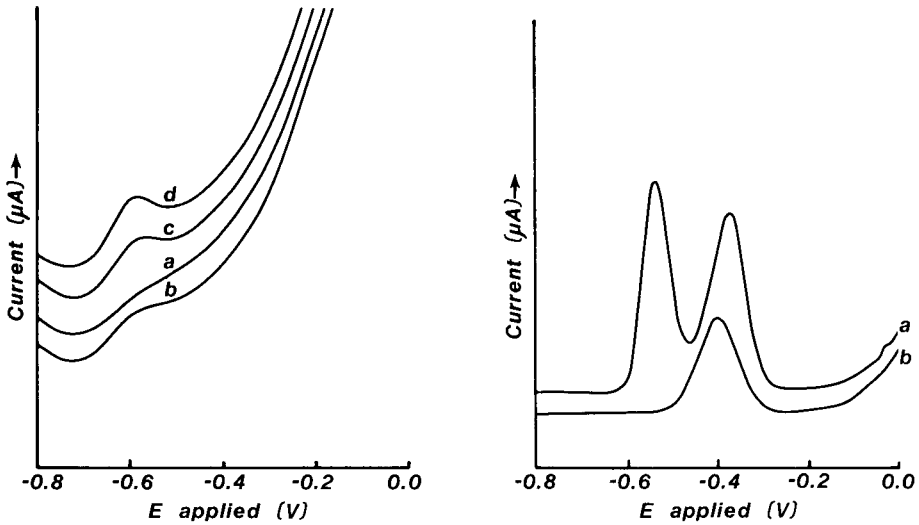

Fig. 3. Standard additions determination of thallium at the m.f.e. (a) Natural water sample containing approximately 0.02 μg Tl l^{-1}; (b) water + 0.049 μg Tl l^{-1}; (c) water + 0.098 μg Tl l^{-1}; (d) water + 0.147 μg Tl l^{-1}. Analytical conditions are specified in the procedure section.

Fig. 4. D.p.a.s.v. of Cd, Pb, and Tl at the h.m.d.e. (a) Without added EDTA; (b) with added EDTA. All 3 constituents present at approximately 5 μg l^{-1}. Analytical conditions are specified in the procedure section.

fications or use of other instrumentation could potentially decrease the detection limit of the method.

Interferences

Because of similarity of oxidation potentials of the Cd(Hg) and Pb(Hg) amalgams to the Tl(Hg) amalgam [17], cadmium and lead were expected to be major interferents. EDTA has been used to mask cadmium and lead in polarographic determinations of thallium [23, 35], and its use has been documented for a.s.v. thallium determinations as well [12]. Although thallium is sufficiently resolved from cadmium and lead at the m.f.e. to permit quantification in acetate medium at comparable concentrations [36], it is necessary to add EDTA in this circumstance because cadmium and lead are invariably present at much higher concentrations than thallium in natural waters. In addition, thallium is less well resolved from cadmium and lead at the h.m.d.e. (see Fig. 4). Within the working ranges specified in the previous section, cadmium and lead were found not to interfere up to 100 μg l^{-1}, provided that the pH of the analysis solution is not below 3.5 (which could be due, for example, to excessive acidification of samples for trace metal preservation prior to analysis), and that the total hardness (calcium plus magnesium) does not exceed 500 mg l^{-1}. Both of these circumstances lead to incomplete masking of the cadmium and lead by the added EDTA, because of competitive reactions with H_3O^+ and Ca^{2+} and Mg^{2+}.

Although EDTA complexes of cadmium and lead are reduced at applied potentials more negative than the thallium deposition potential (−0.8 V), the copper—EDTA complex is reduced (albeit slowly) at −0.8 V. The ill-formed and unreproducible copper stripping peak in this medium occurs at about −0.2 V. The presence of co-reduced copper in the electrode amalgam does not interfere in the thallium determination, provided that the solubility of copper in mercury is not exceeded [37]. This is only likely in the case of the m.f.e., since the electrode volume is significantly smaller than an h.m.d.e.

Several experiments were performed with synthetic and natural water samples to determine the effects of co-deposited copper with thallium at the m.f.e. In general, it was found that while up to 5 mg Cu l^{-1} could apparently be tolerated when 1 μg Tl l^{-1} was determined, visible alteration of the m.f.e. could be seen at copper concentrations between 0.5 and 1.0 mg l^{-1}. The m.f.e. was transformed from a normal dull grey appearance to a highly reflective metallic appearance under these circumstances. This was found to be due to saturation of the mercury film with copper, resulting in a change in the surface tension of the amalgam. Since the effective surface area and composition of the electrode are important analytical parameters, it is suggested that thallium determinations in the presence of more than 0.5 mg Cu l^{-1} are suspect. It was verified that successful thallium determinations at the m.f.e. may be carried out with no interference from copper, if the copper concentration is less than 0.5 mg l^{-1}. This copper interference is not a significant limitation, since copper concentrations in natural waters rarely exceed 0.2 mg l^{-1} [38].

Peak current suppression interferences are likely in solutions that contain large amounts of organic material, soaps, detergents, surfactants, or other surface-active materials. It was shown that wet-ashing the sample just to dryness (not baking) in the presence of nitric acid effectively eliminates this interference and gives 100% recovery of a thallium spike in an unpreserved atmospheric precipitation sample, in which algal growth was evident, at the 50 ng Tl l^{-1} level. It is unfortunately not possible to make a general statement concerning the vulnerability of this method to interference by surface-active constituents. Such effects are invariably compound-specific and matrix-dependent.

A positive interference has very occasionally been observed that was attributed to a strongly potential-dependent simultaneous electrode reaction, in which both the reactant and product remained in solution. This type of interference may be effectively dealt with by algebraic subtraction of zero deposition time-peak currents from those observed under normal operating conditions [39]. Two previously reported interfering elements of this latter type [39, 40], iron and manganese, were found not to interfere with thallium determinations up to 0.5 and 5.0 mg l^{-1}, respectively. No evidence of intermetallic compound formation between thallium and other metals in the electrode amalgam has been observed.

The proposed d.p.a.s.v. method appears free from serious interference from

other unknown sources likely to be found in natural water samples. This is demonstrated by spike recovery data obtained in natural water matrices of documented chemical composition. Two of the U.S. Geological Survey Standard Reference Water Sample (SRWS) matrices (see below) were selected and spiked with 2.00 μg Tl l^{-1}. Both SRWS 56 and 59 originally contained no detectable thallium. SRWS 56 is unique in the current library of samples because of its large quantity of dissolved solids (1200 mg l^{-1}), while SRWS 59 is fairly typical of the remainder of the SRWS series prepared for trace elemental determination. Determination of thallium in spiked SRWS 56 and 59 by d.p.a.s.v. at the m.f.e. resulted in 101 ± 8 and 93 ± 7% recoveries, respectively. Of the known potential interferents, SRWS 56 has been found to contain 9.9 μg Cd l^{-1}, 19.6 μg Pb l^{-1}, and 196 μg Cu l^{-1}; and SRWS 59 has been found to contain 4.4 μg Cd l^{-1}, 16.8 μg Pb l^{-1}, and 239 μg Cu l^{-1}.

Accuracy and precision

An intercomparison of thallium determinations on normal and thallium spiked surface water samples by d.p.a.s.v. and electrothermal-atomization atomic absorption spectrometry (e.t.a.a.a.) was used to evaluate the relative accuracy of this proposed analytical method. A total of fifteen samples was used in the intercomparison, of two general types: six of the samples were from the U.S. Geological Survey's Standard Reference Water Sample (SRWS) program, and nine others were selected from the large number of surface water samples submitted to the U.S. Geological Survey's National Water Quality Laboratory (Denver) for analysis.

The SRWS program [41] prepares and distributes four natural water samples per year to about eighty academic, State and Federal water analysis laboratories for chemical determinations as part of a comprehensive quality control program. Two of the most recent samples (SRWS Nos. 65 and 67) contained thallium, and several of the cooperating laboratories performed thallium determinations on both SRWS 65 and 67 by e.t.a.a.a.

These two SRWS, in addition to three selected natural water samples (by

TABLE 3

Results of methods intercomparison on SRWS. All table entries are in units of μg Tl l^{-1} at the 95% confidence level; see text for additional details

Matrix	Approximate spike addition	E.t.a.a.a. (This laboratory)	D.p.a.s.v./ h.m.d.e.	D.p.a.s.v./ m.f.e.	Most probable concentration
SRWS 65	0	4.4 ± 0.6	4.5 ± 1.2	4.3 ± 0.8	4.3 ± 1.2[a]
SRWS 65	5	9.6 ± 1.0	9.5 ± 0.7	9.6 ± 0.1	—
SRWS 67	0	5.6 ± 0.4	6.3 ± 1.0	5.6 ± 0.5	5.8 ± 1.7[b]
SRWS 67	5	8.7 ± 1.2	10.3 ± 1.8	9.5 ± 1.0	—

[a]Three laboratories. [b]Four laboratories.

TABLE 4

Results of methods intercomparison on selected natural water samples. All table entries are in units of μg Tl l^{-1} at the 95% confidence level; see text for additional details.

Natural water matrix	Approximate spike addition	E.t.a.a.a.	D.p.a.s.v./ h.m.d.e.	D.p.a.s.v./ m.f.e.
29	0	<1	—	<0.01
29	1	<1	1.0 ± 0.5	1.0 ± 0.1
29	10	10.0 ± 0.6	10.0 ± 1.7	9.3 ± 0.9
31	0	<1	—	0.045 ± 0.015
31	1	<1	0.7 ± 0.7	1.0 ± 0.4
31	5	7.0 ± 0.4	4.5 ± 1.4	5.0 ± 1.5
70	0	<1	—	<0.01
70	5	3.3 ± 0.8	4.6 ± 0.5	4.8 ± 0.3
70	10	7.9 ± 1.0	8.5 ± 2.2	9.4 ± 1.2
99	0	<1	—	<0.01
99	5	4.6 ± 0.4	4.8 ± 0.2	4.2 ± 0.5

virtue of their relatively high concentrations of cadmium and lead) were prepared for analysis by e.t.a.a.a. and the two d.p.a.s.v. methods in this laboratory by spiking each of them (if necessary) with thallium at three approximate concentration levels. A direct comparison of analytical results obtained by the three methods is shown in Tables 3 and 4. Each entry in these tables is the result of a single determination; the reported uncertainties are due to different sources of error.

Table 3 gives the results of the methods intercomparison on the SRWS. The uncertainties shown in the three methods columns reflect the error in the concentration estimates associated with the linear correlation of the standard addition concentration with the analytical technique response [42] at the 95% confidence level. The uncertainties shown in the last (most probable concentration) column are one standard deviation of the mean of thallium determinations by several laboratories, reported as one value per laboratory to the nearest μg Tl l^{-1}. SRWS 65 has been found to contain, in addition to thallium: 11.8 μg Cd l^{-1}, 38.4 μg Pb l^{-1}, and 27.0 μg Cu l^{-1}. Figure 5 shows an example of a standard additions determination of thallium in SRWS 67 at the m.f.e. by d.p.a.s.v.

Table 4 shows the results of methods intercomparison on the selected natural water samples. Reported uncertainties reflect the error in the concentration estimates associated with the linear correlation of the analytical technique response with the standard addition concentration. Sample matrix 29 was found to contain, in addition to thallium: 8 μg Cd l^{-1}, 67 μg Pb l^{-1}, and 2 μg Cu l^{-1}; sample matrix 31: 6 μg Cd l^{-1}, 20 μg Pb l^{-1}, and 4 μg Cu l^{-1}; sample matrix 70: 10 μg Cd l^{-1}, 140 μg Pb l^{-1}, and 4 μg Cu l^{-1}. Sample matrix 99 was laboratory-deionized water; sample matrix 29 was taken from the South Platte River near Roscoe, NE, U.S.A.; sample matrix 31 was taken from the Republican River near Orleans, NE, U.S.A.; and sample matrix 70 was taken from the Big Blue River near Seward, AK, U.S.A.

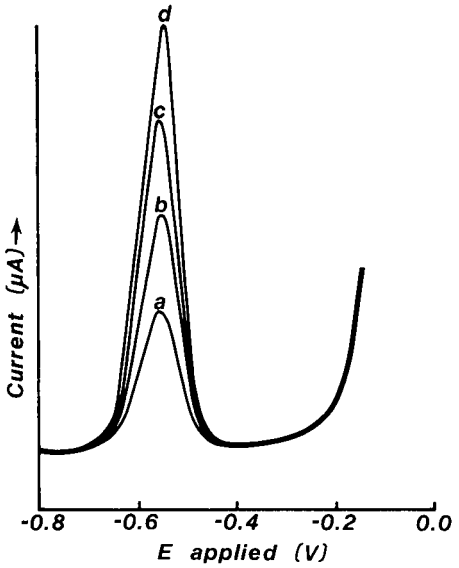

Fig. 5. Standard additions determination of thallium at the m.f.e. (a) SRWS 67; (b) SRWS 67 + 3.8 μg Tl l^{-1}; (c) SRWS 67 + 7.6 μg Tl l^{-1}; (d) SRWS 67 + 11.4 μg Tl l^{-1}. Conditions are specified in the procedure section.

Data in Table 3 give the best estimate of accuracy of the d.p.a.s.v. methods compared to independent thallium determinations by several laboratories using e.t.a.a.a. Within the specified error of the most probable concentrations, the results obtained in our laboratory with the two d.p.a.s.v. methods and an e.t.a.a.a. method are indistinguishable from the most probable concentrations (also obtained by e.t.a.a.a.). Thus, no bias is evident for thallium determinations in this concentration range by the three methods, and the relative accuracy of both d.p.a.s.v. methods is seen to be at least equivalent to e.t.a.a.a.

The most meaningful estimate of attainable precision of the d.p.a.s.v. methods is illustrated by replicate thallium determinations on a representative sample over a long time period. The most recently issued Standard Reference Water Sample containing thallium, SRWS 69, was chosen to demonstrate the replicate precision of the method. Ten thallium determinations in SRWS 69 were carried out over a period of two months on random days, using the m.f.e. method here described. The mean concentration of thallium in SRWS 69 was found to be 0.59 ± 0.04 μg l^{-1} (±7% relative standard deviation), which illustrates that excellent precision may be obtained even at thallium concentration levels accessible only to the d.p.a.s.v. technique. The cooperating laboratory data for thallium in SRWS 69 were not used in the accuracy assessment above, because only one other laboratory provided thallium determinations.

Techniques of quantification

Three techniques of quantification available for d.p.a.s.v. determinations are standard curve, standard additions, and internal standard. Each of these techniques has been discussed widely [28, 36]. The standard curve technique is the least time-consuming, however, at present its use in this application would be impractical. The efficiency of the deposition and stripping steps are dependent on cell geometry, electrode placement, solution viscosity, temperature, ionic strength and several other factors. It is not possible at present, to reproduce the experimental conditions well enough to obtain suitable accuracy of determination between standards and samples. Furthermore, analytical characteristics of the m.f.e. change slowly with time, which would make frequent restandardization necessary.

The internal standard approach offers a tempting alternative to standard additions, because of its ease and rapidity [36]. This approach, however, relies on the assumption of similar chemical behavior of both analyte and internal standard element. Thallium is probably present in both the +1 and +3 oxidation states in natural waters [12], and is relatively unaffected by the EDTA ligand. It is unlikely that a similar internal standard element, determinable by d.p.a.s.v. under these conditions, could be found.

The present investigations showed that the standard additions technique gives satisfactory analytical results for thallium determinations in a wide variety of natural water matrices, and is the technique of choice for best accuracy and precision of determination.

Applications

The d.p.a.s.v. method described here is being used for routine thallium determinations in natural water samples submitted to the U.S. Geological Survey Central Laboratory (Denver). This method has also been used to investigate the occurrence of thallium in several samples of atmospheric deposition waters (wet and dry precipitation) collected by the U.S. Geological Survey's precipitation monitoring network. The results of this investigation will appear elsewhere [43].

This work was presented in part at the 30th Pittsburgh Conference on Analytical Chemistry and Applied Spectroscopy, Cleveland, Ohio, U.S.A., in March 1979. The assistance of Mr. Gary Perryman on the e.t.a.a.a. thallium determinations is gratefully acknowledged.

REFERENCES

1 L. H. Keith and W. A. Telliard, Environ. Sci. Technol., 13 (1979) 416.
2 I. C. Smith and B. L. Carson, Trace Metals in the Environment, Vol. 1 Thallium, Ann Arbor Science, Ann Arbor, 1977, p. 36.
3 A. D. Matthews and J. P. Riley, Anal. Chim. Acta, 48 (1969) 25.
4 D. F. C. Morris and R. A. Killick, Talanta, 4 (1960) 51.
5 R. L. Brown, M. L. Jacobs and H. E. Taylor, Am. Lab., 4 (November 1972) 29.
6 R. L. Davison, D. F. S. Natusch, J. R. Wallace and C. A. Evans, Jr., Environ. Sci. Technol., 8 (1974) 1107.

7 G. P. Sighinolfi, At. Absorpt. Newsl., 12 (1973) 136.
8 A. S. Curry, J. F. Read and A. R. Knott, Analyst, 94 (1969) 744.
9 C. R. Parker, Water Analysis by Atomic Absorption Spectroscopy, Varian Techtron, London, 1972, p. 20, 22.
10 D. M. Shaw, Geochim. Cosmochim. Acta, 2 (1952) 118.
11 E. L. Kothny, Analyst, 94 (1969) 198.
12 G. E. Batley and T. M. Florence, J. Electroanal. Chem., 61 (1975) 205.
13 L. V. Shevchenko, V. P. Portretnyi and V. T. Chuiko, J. Anal. Chem. USSR, 32 (1977) 1448.
14 R. Neeb, Fresenius Z. Anal. Chem., 190 (1962) 98.
15 J. Dieker and W. E. Van der Linden, Fresenius Z. Anal. Chem., 274 (1975) 97.
16 V. Zitko, W. V. Carson and W. G. Carson, Bull. Environ. Contam. Toxicol., 13 (1975) 23.
17 F. Vydra, K. Stulik and E. Julakova, Electrochemical Stripping Analysis, Ellis Horwood, Chichester and Halsted Press, J. Wiley, New York, 1976, p. 203.
18 J. B. Flato, Anal. Chem., 44 (1972) 75A.
19 T. R. Copeland, J. H. Christie, R. A. Osteryoung and R. K. Skogerboe, Anal. Chem., 45 (1973) 2171.
20 U. Eisner and M. J. Ariel, J. Electroanal. Chem., 11 (1966) 26.
21 D. I. Levit, Anal. Chem., 45 (1973) 1291.
22 J. P. Franke, P. M. J. Coenegracht and R. A. de Zeeuw, Arch. Toxicol., 34 (1975) 137.
23 L. Meites, Polarographic Techniques, J. Wiley, New York, 1965, p. 89.
24 E. Brown, M. W. Skougstad and M. J. Fishman, Techniques of Water Resources Investigations of the U.S. Geological Survey, Methods for Collection and Analysis of Water Samples for Dissolved Minerals and Gases, Book 5, U.S. Government Printing Office, Washington, DC, 1970, Chapter A1.
25 R. A. Osteryoung and J. H. Christie, Anal. Chem., 46 (1974) 351.
26 J. P. Franke, R. A. de Zeeuw and R. Hakkert, Anal. Chem., 50 (1978) 1374.
27 K. L. Ratzlaff, Anal. Chem., 51 (1979) 232.
28 E. Barendrecht, in A. J. Bard (Ed.), Electroanalytical Chemistry, Vol. 2, M. Dekker, New York, 1967, p. 53.
29 G. E. Batley and T. M. Florence, J. Electroanal. Chem., 55 (1974) 23.
30 R. Neeb, Fresenius Z. Anal. Chem., 171 (1959) 321.
31 T. R. Copeland, J. H. Christie, R. K. Skogerboe and R. A. Osteryoung, Anal. Chem., 45 (1973) 995.
32 M. Stulikova, J. Electroanal. Chem., 48 (1973) 33.
33 Analytical Methods for Atomic Absorption Spectrophotometry Using the HGA Graphite Furnace, Perkin-Elmer, Norwalk, Connecticut, 1977.
34 R. K. Skogerboe, in J. A. Dean and T. C. Rains (Eds.), Flame Emission and Atomic Absorption Spectrometry, Vol. 1, M. Dekker, New York, 1969, Chapter 13.
35 E. Temmerman and F. Verbeek, J. Electroanal. Chem., 19 (1968) 423.
36 T. R. Copeland, R. A. Osteryoung and R. K. Skogerboe, Anal. Chem., 46 (1974) 2093.
37 T. R. Copeland and R. K. Skogerboe, Anal. Chem., 46 (1974) 1257A.
38 J. D. Hem, Study and Interpretation of the Chemical Characteristics of Natural Water, 2nd edn., Geological Survey Water-Supply Paper 1473, U.S. Government Printing Office, Washington, DC, 1970, p. 202.
39 J. E. Bonelli, R. K. Skogerboe and H. E. Taylor, Anal. Chim. Acta, 101 (1978) 437.
40 M. Ariel, U. Eisner and S. Gottesfeld, J. Electroanal. Chem., 7 (1964) 307.
41 M. W. Skougstad and M. J. Fishman, in Proceeding of the AWWA Water Quality Technology Conference, American Water Works Association, Denver, 1975, p. XIX—1.
42 B. Ostle, Statistics in Research, The Iowa State University Press, Ames, 1963, p. 170.
43 J. E. Bonelli, L. J. Schroder, R. K. Skogerboe and H. E. Taylor, Atmos. Environ., in press.

Analytica Chimica Acta, 118 (1980) 257—269

A STUDY OF THE ELECTROCHEMICAL CHARACTERISTICS OF SOME THIOLS BY DIFFERENTIAL PULSE POLAROGRAPHY AND OTHER ELECTROCHEMICAL TECHNIQUES

RONALD L. BIRKE* and MARIA MAZORRA

City University of New York, Department of Chemistry, The City College, New York, New York 10031 (U.S.A.)

(Received 26th December 1979)

SUMMARY

A study of some low-molecular-weight odorous thiols at mercury electrodes has been made by differential pulse polarography (d.p.p.), d.c. polarography, linear-sweep voltammetry, and coulometric measurement on linear-sweep reduction. Linear current versus concentration plots are found for individual thiols, in aqueous 0.2 M sodium hydroxide by using d.p.p. at thiol concentrations from ca. 2×10^{-7} M to 10^{-4} M. A linear trend between peak potential and molecular weight was found for homologous series, but the method cannot be used for qualitative identification because of peak shifts in multicomponent mixtures. The electrode reactions show quasireversible behavior. At concentrations of thiol greater than 10^{-4} M, the single peak splits into two peaks and film formation occurs. Charge density versus concentration plots indicate that the quantity of adsorbed material is several monolayers.

The electrochemical behavior of sulfhydryl compounds has been investigated in great detail by the classical d.c. polarographic method [1, 2] since these compounds are of interest in a wide range of biological, pharmaceutical, and industrial chemical areas. More recently pulse polarography has been applied to sulfhydryl compounds which are biologically important [3—5] and to several odorous low-molecular-weight sulfhydryl compounds [6] which are of interest in the petrochemical industry. Differential pulse polarography (d.p.p.) with a cathodic pulse was found by the latter two studies [5, 6] to be sensitive and reproducible at concentrations below which a monolayer of mercury thiolate forms on the dropping mercury electrode (DME). The electrochemical mechanism giving rise to the d.p.p. wave was proposed, independently [5, 6], to be the reduction of a mercury thiolate compound originally produced by an anodic process before the cathode pulse is applied. This mechanism assumes that the reduction process is at least quasireversible. The reversibility of the cathodic pulse wave for thiols is further investigated in this paper.

Peter and Rosset [6] studied several low-molecular-weight thiols in a nonaqueous medium of methanol—benzene (3 : 1) with an acetic acid—acetate buffer where the thiols are in their molecular form. In the present

work, the electroanalytical behavior of similar compounds in aqueous basic media where the thiols are in the thiolate (RS^-) form has been investigated. With this medium one does not have to protect against loss of thiol by volatilization and all the thiols employed were found to dissolve at the low concentrations used except for 1-dodecanethiol which had the largest molecular weight (202). Several differences in electrochemical behavior were noted between the aqueous and nonaqueous media and these will be discussed later.

In addition to d.p.p., d.c. polarographic and cyclic voltammetric studies were made at mercury electrodes in order to investigate the electrode process. The latter investigation included experiments dealing with the measurement of charge passed on reducing mercury thiolate films.

EXPERIMENTAL

Chemicals

The thiols used were 1-butanethiol (Pfaltz and Bauer), benzyl mercaptan (Evans Chemetics), 1-decanethiol and β-phenylethyl mercaptan (K and K Laboratories), thiolphenol (Hilton-Davis Chemical Co. Div.), 1-nonanethiol (Columbia Organic Chemical Co.), furfuryl mercaptan (Felton Chemical Co.) and 1-hexanethiol and 2-mercaptoethanol (Eastman Chemical Co.). These compounds were used without further purification, by mixing microquantities directly into nitrogen-deaerated supporting electrolytes. The supporting electrolytes were 0.2 M NaOH, 0.1 M Na_2CO_3, and 0.2 M Na_2HPO_4 of pH 12.9, pH 11.3 and pH 9.0, respectively.

Some comparison experiments were performed with L(+)-cysteine (Fisher Scientific Co. reagent grade). Stock solutions (0.01 M) were prepared fresh daily by dissolving the weighed reagent in a nitrogen-deaerated buffer solution. The buffer was 0.2 M in both Na_2HPO_4 and KH_2PO_4 leading to a pH of 6.80.

The mercury used for the hanging mercury drop electrode and the dropping mercury electrode was Fisher Scientific Co. Instrumental Grade.

Instrumentation

The polarographic measurements were made using the previously described procedures, equipment, and electrochemical cell [5]. Cyclic voltammetry was done with a PAR model 175 Universal Programmer, a PAR model 173 potentiostat and an MFE 815 plotamatic x—y recorder. Coulometric measurements were made with a PAR model 179 digital coulometer attachment to the 173 potentiostat. A Metrohm microburette E410 hanging mercury drop electrode was used in the cyclic voltammetric and coulometric experiments and a fixed number of turns was employed each time which gave a measured area of 0.0269 cm^2. In all runs a fresh hanging drop was allowed to preequilibrate at a fixed potential in deaerated solution. The scan rate was fixed at 50 mV s^{-1}; the scan was started going in a positive potential direction and

reversed after passing completely through the oxidation peaks. Both the current and integrated reduction current (charge) were recorded on the return sweep. All potentials quoted are with reference to the saturated calomel electrode.

The d.p. polarographic pulse duration and sampling time were the same as previously given [5]. The drop time τ was always 1 s and the scan rate 4 mV s^{-1}. The mass flow rate was 1.86 mg s^{-1} giving an area of 0.00129 cm^2. The mercury column height was 84 cm.

RESULTS AND DISCUSSION

Differential pulse polarographic characteristics

Differential pulse polarograms of 1-butanethiol, 1-hexanethiol, 1-nonanethiol, 1-decanethiol, benzyl mercaptan, β-phenylethyl mercaptan, thiophenol, furfuryl mercaptan, and 2-mercaptoethanol were run in 0.2 M sodium hydroxide. The polarograms were run with both an anodic pulse and a cathodic pulse, and for each polarity scanning in either potential direction reproduced the same waveform. A typical d.p. polarogram of 1-butanethiol is shown in Fig. 1 for a cathodic and an anodic pulse both scanned from a positive to negative potential. In all cases the cathodic pulse gave narrower waves with larger peak magnitudes than the anodic pulse as previously observed with other thiols under different conditions [5, 6]. The anodic wave in this example had a peak half-width of ca. 85 mV while the cathodic peak half-width was 58 mV. The sizeable narrowing of the peak half-width in the cathodic case is caused by the nature of the electrode process which indicates that reduction of an adsorbed compound is taking place. Calibration plots of peak current versus concentration were made for 2-mercaptoethanol, 1-butanethiol, benzyl mercaptan, β-phenylethyl mercaptan, 1-nonanethiol, and 1-decanethiol. These plots were constructed for both a cathodic and an anodic pulse waveform and were found to be linear, in the concentration range ca. 2×10^{-7} M to ca. 1×10^{-4} M. For concentrations below 2×10^{-7} M plots are curved concave upward as they approach the zero-current intercept. Similar behavior was also noted in nonaqueous media [6]. At concentrations above ca. 10^{-4} M the single wave splits into two waves with a new wave coming at more positive potentials in all cases (Fig. 2). Similar behavior for the cathodic waves of cysteine and glutathione has been reported [5]. As seen in Fig. 2 for the benzyl mercaptan both the cathodic and anodic waves show the splitting phenomenon. The new wave at more positive potential is attributed to the formation of an additional layer on top of a monolayer of mercury thiolate. It can also be seen from these curves that the magnitude of the more negative anodic wave (B) is larger now than the more negative cathodic wave (A) which might be expected in the presence of film formation. On the other hand, calibration plots from cathodic waves showed less scatter. The new wave which forms at a more positive potential in Fig. 2 continues to increase as the concentration of thiol is increased while the wave

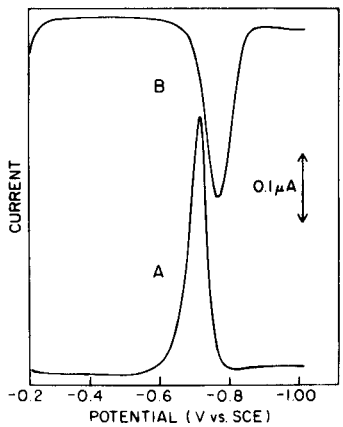

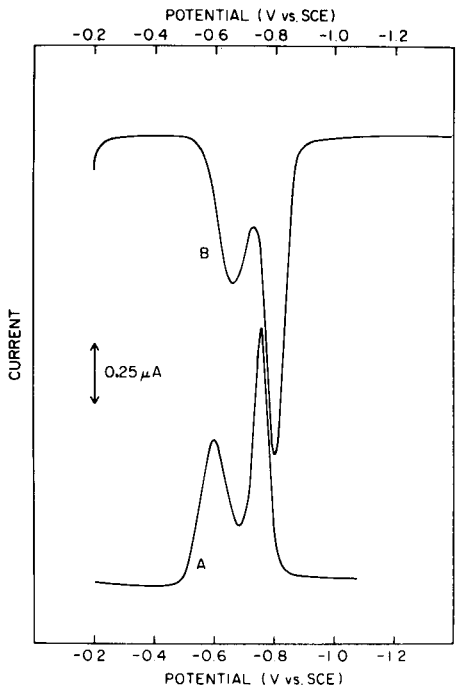

Fig. 1. D.p.p. current—potential curves for 5.58×10^{-5} M 1-butanethiol in 0.2 M NaOH (pH 12.9). Polarographic conditions are ΔE 50 mV; τ 1.00 s; scan rate 4.00 mV s^{-1}. (A) Cathodic pulse; (B) anodic pulse.

Fig. 2. D.p.p. current—potential curves for 2.90×10^{-4} M benzyl mercaptan in 0.2 M NaOH (pH 12.9). Polarographic conditions as in Fig. 1. (A) Cathodic pulse; (B) anodic pulse.

at the original potential tends to level off. This behavior is exhibited in Fig. 3 which shows the current versus concentration curves for the two potentials. At the higher concentrations there is a great deal of scatter as shown in the dotted curve in Fig. 3 and it does not appear that quantitative determination can be accomplished in this part of the current versus concentration plot. The leveling off with increase in concentration of the peak height measured at a more negative potential is indicative of an adsorption process. Addition of the nonionic surfactant Triton X-100 (1 ml of 0.005% to 50 ml of electrolyte solution) did not cause a shift in peak potentials nor did it change the thiol concentrations at which the splitting phenomenon was observed to begin.

The value of the peak potentials for the cathodic and anodic pulse should follow the equation $E_p = E_{1/2} - (\Delta E/2)$ for a reversible electrode process [7, 8] where ΔE is taken with sign. For a reversible process one would expect to calculate the same $E_{1/2}$ for all pulse magnitudes and for different polarities.

Table 1 gives values of $E_{1/2}$ calculated for several pulse magnitudes for a cathodic and an anodic pulse. The values of $E_{1/2}$ calculated for 1-butanethiol are quite similar except for ΔE = 100 mV. Benzyl mercaptan shows more

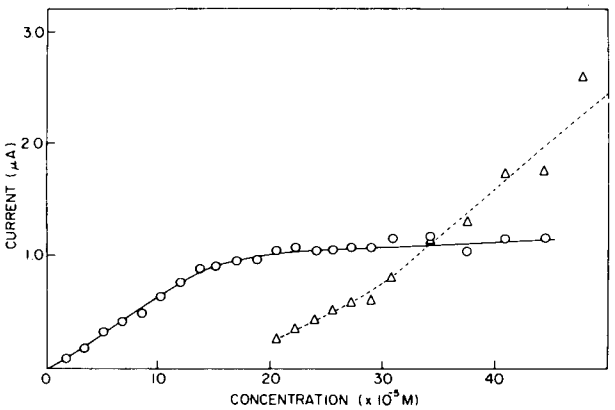

Fig. 3. D.p.p. current as a function of concentrations for benzyl mercaptan. Polarographic conditions as in Fig. 1. (○) $E_p = -0.75$; (△) $E_p = -0.60$ V.

variation between cathodic and anodic pulse especially for the higher pulse magnitudes. The fact that the anodic current is not equal to the cathodic current for both species indicates some degree of irreversibility or that the processes are different.

The value of $E_p^c - E_p^a$ should equal ΔE for a reversible process. Recent unpublished theoretical work in this laboratory shows that $E_p^c - E_p^a$ decreases from ΔE for a quasireversible process but then increases to the pulse magnitude ΔE as the electron transfer becomes completely irreversible for soluble species. The main process which controls the position of the d.p.p. peak is an oxidation to produce a soluble species (see below) and thus these results may be pertinent. The values of $E_p^c - E_p^a$ in Table 1 for 1-butanethiol and benzyl mercaptan are very close to the pulse magnitude. In Table 2 the values of $E_p^c - E_p^a$ for a homologous series of alkanethiols are shown for a fixed ΔE of −50 mV. Since $E_p^c - E_p^a$ is 25 mV, 27 mV and 20 mV for 1-hexane-

TABLE 1

Peak potential data as a function of pulse height

ΔE (mV)	E_p^c (V)	$E_{1/2}^{calc}$ (V)	E_p^a (V)	$E_{1/2}^{calc}$ (V)	$E_p^c - E_p^a$ (mV)
1-Butanethiol (7×10^{-5} M)					
100	−0.670	−0.720	−0.785	−0.735	115
50	−0.715	−0.740	−0.765	−0.740	50
20	−0.735	−0.745	−0.755	−0.745	20
10	−0.740	−0.745	−0.750	−0.745	10
Benzyl mercaptan (5×10^{-5} M)					
100	−0.695	−0.745	−0.830	−0.780	135
50	−0.740	−0.765	−0.795	−0.775	55
20	−0.760	−0.770	−0.780	−0.770	20
10	−0.765	−0.770	−0.775	−0.770	10

TABLE 2

Peak potentials for a series of alkanethiols[a]

Compound	E_p^c (V)	E_p^a (V)	$E_p^c - E_p^a$ (mV)	$W_{1/2}^c$ (mV)
1-Butanethiol	−0.715	−0.765	50	56
1-Hexanethiol	−0.785	−0.810	25	56
1-Nonanethiol	−0.876	−0.903	27	71
1-Decanethiol	−0.907	−0.927	20	76

[a] $\Delta E = -50$ mV.

thiol, 1-nonanethiol, and 1-decanethiol, respectively, these electrode processes are probably quasireversible. The fact that $E_p^c - E_p^a = \Delta E$ for 1-butanethiol and benzyl mercaptan indicates that electron transfer for these systems is closer to reversible than for the other thiols. These data must be reconciled with the fact that the cathodic and anodic currents are not equal. If the cathodic process involves the reduction of a film of mercury thiolate and the anodic process involves diffusion of thiol, then one might expect differences in peak-current heights.

Another parameter which can be used to ascertain irreversibility is the width of the peak at half peak height, $W_{1/2}$. Table 2 shows that $W_{1/2}^c$ grows larger for the higher-molecular-weight compounds, indicating increased irreversibility as the molecular weight is increased. Since $W_{1/2}^a$ is about 85 mV for the anodic peak of 1-butanethiol, this value again indicates a more nearly reversible system since the theoretical value is 98.2 mV for a 1-e transfer with a 50-mV pulse magnitude. Polarographic studies discussed below indeed indicate that a 1-e transfer producing a soluble species occurs for the anodic reaction.

An interesting empirical correlation between peak potential and molecular weight of two homologous series was found (Table 3). The alkanethiols show a nearly linear shift in cathodic peak potential with molecular weight. In addition, the homologous series of phenyl-substituted thiols (thiol phenol, benzyl mercaptan, and β-phenylethyl mercaptan) also shows a linear shift of E_p^c with molecular weight. The two thiols tested, 2-mercaptoethanol and furfuryl mercaptan, which are not members of either series, do not lie on the straight lines. These straight-line plots may represent linear free-energy correlations. Indeed, the shift of E_p^c to more negative potentials for the series of phenyl-substituted thiols is in the direction of less electron-withdrawing power of the phenyl ring yielding a more nucleophilic thiolate, RS^-. The more nucleophilic thiolate would tend to form more stable complexes with mercury(I) formed by oxidation of the mercury electrode. This correlation is consistent with the electrode mechanism discussed below.

The fact that E_p^c shifts with different thiols in aqueous solution is in direct contrast to the behavior of similar thiols in a methanol—benzene solvent for which very small shifts were obtained, and it was concluded that d.p.p. was

TABLE 3

Peak potential for a cathodic pulse for various thiols as a function of molecular weight[a]

Compound	M.w. (g mol^{-1})	E_p^c (V)	Compound	M.w. (g mol^{-1})	E_p^c (V)
2-Mercaptoethanol	78	−0.58	Thiophenol	110	−0.66
1-Butanethiol	90	−0.70	Furfuryl mercaptan	114	−0.65
1-Hexanethiol	118	−0.78	Benzyl mercaptan	124	−0.72
1-Nonanethiol	160	−0.87	β-Phenylethyl mercaptan	138	−0.78
1-Decanethiol	174	−0.90			

[a] $\Delta E = -50$ mV.

not useful for qualitative analysis [6]. However, it does not appear that qualitative analysis is possible in the present case since polarograms of multicomponent mixtures of the thiols in aqueous solution showed effects of one thiol on the others yielding shifts of E_p^c for a given thiol. Similar results were obtained for $E_{1/2}$ values with mixtures of thiols when integral pulse polarography with anodic pulses was used.

The effect of pH on the d.p. polarographic characteristics of the thiols was investigated with three thiols: 1-butanethiol, benzyl mercaptan, and 1-decanethiol individually in 0.2 M NaOH (pH 12.9), 0.1 M Na_2CO_3 (pH 11.3) and 0.2 M Na_2HPO_4 (pH 9.00). For the benzyl mercaptan system the most linear behavior for peak current versus concentration plots was found for the 0.2 M NaOH electrolyte (Fig. 4, A). In this system a large decrease in sensitivity (slope) is seen with the pH 9.0 electrolyte although there is little difference in sensitivity between the sodium carbonate and sodium hydroxide media. With 1-butanethiol (Fig. 4, B) there is a large decay in sensitivity as the pH decreases.

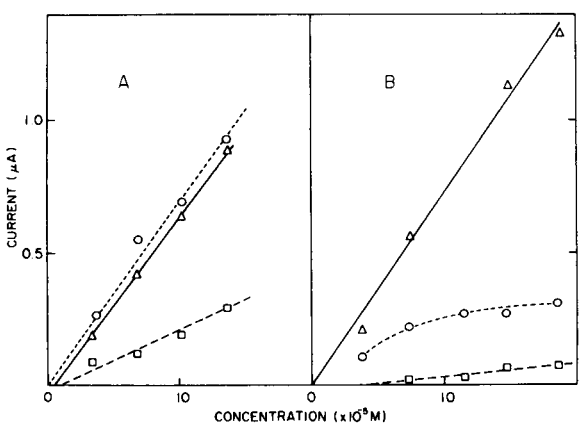

Fig. 4. D.p.p. current vs. concentration for (A) benzyl mercaptan and (B) 1-butanethiol as a function of pH. (△) 0.2 M NaOH (pH 12.9); (○) 0.1 M Na_2CO_3 (pH 11.3); (□) 0.2 M Na_2HPO_4 (pH 9.0).

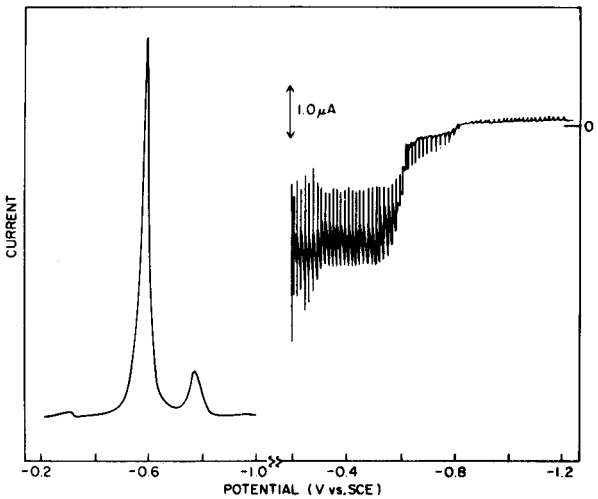

Fig. 5. D.p.p. current—potential curve and d.c. polarogram of 7.17×10^{-4} M benzyl mercaptan in 0.2 M NaOH. D.p.p. conditions as in Fig. 1. The d.c. polarographic scan rate was 4 mV s^{-1} with a free-falling DME.

Values of peak potential were found to shift very slightly negative with an increase in pH. However, this shift was not measured over a large enough pH range to determine the pK_a value of the sulfhydryl group since the range investigated was from 9.0 to 12.9. The small value of $\Delta E_p/\Delta pH$ (ca. -0.01) indicates that for the thiols studied the predominant species in solution is the thiolate anion.

D.c. polarography

For concentrations below 2×10^{-4} M in thiol, plots of E_{DME} vs. log $[(i_d - i)/i]$ were made for anodic currents at a number of different concentrations. Table 4 shows these data; it is seen that the slopes and $E_{1/2}$ values are independent of concentration within experimental error. The value of the slope in the case of benzyl mercaptan corresponds to Nernstian behavior for a 1-e transfer. This indicates that for benzyl mercaptan and perhaps 1-decanethiol the anodic electron-transfer process at pH 12.9 is $RS^- + Hg = HgSR + e^-$, where both RS^- and HgSR are soluble since if an insoluble complex were

TABLE 4

Slope of E_{DME} vs. log $[(i_d - i)/i]$ as a function of concentration

Benzyl mercaptan			1-Decanethiol		
Conc. (M)	Slope	$E_{1/2}$ (V)	Conc. (M)	Slope	$E_{1/2}$ (V)
3.40×10^{-5}	0.053	−0.721	1.93×10^{-5}	0.044	−0.886
6.83×10^{-5}	0.060	−0.725	3.86×10^{-5}	0.043	−0.894
1.37×10^{-4}	0.057	−0.726	7.73×10^{-5}	0.040	−0.890
1.71×10^{-4}	0.060	−0.725	1.55×10^{-4}	0.043	−0.894

formed the halfwave potential would vary as a function of concentration. Such a variation of E_p^c with concentration was found in a nonaqueous medium [6]. Mercury(I) thiolates are known to be insoluble in aqueous solution and to disproportionate [6], thus the charge-transfer reaction is probably followed by a disproportionation reaction $2HgSR = Hg + Hg(SR)_2$ (s), leading to an overall electrode process of $2RS^- + Hg = Hg(SR)_2$ (s) + $2e^-$. This set of reactions has been suggested in other polarographic studies of thiols [1, 9]. The actual mercury(I) species may be the condensed ion Hg_2^{2+} and not Hg^+ for which there is little evidence in solution.

The shape of the d.c. polarograms for benzyl mercaptan, 1-butanethiol, and 1-decanethiol shows a prewave and a main wave which is typical of the d.c. polarographic behavior of thiols [1]. The prewave has the characteristics of an adsorption prewave and above a certain concentration reaches a constant height while the total current of the main wave at more positive potentials continues to increase in a linear manner with concentration. The same type of phenomenon was also seen for d.p.p. in Fig. 3. For benzyl mercaptan, the $E_{1/2}$ value of the prewave is roughly −0.77 V and that of the second wave or main wave is −0.58 V. This main wave first appears clearly at a thiol concentration of 7.1×10^{-4} M. Figure 5 shows the d.p. and d.c. polarograms for benzyl mercaptan at a concentration of 7.1×10^{-4} M. It is seen that the

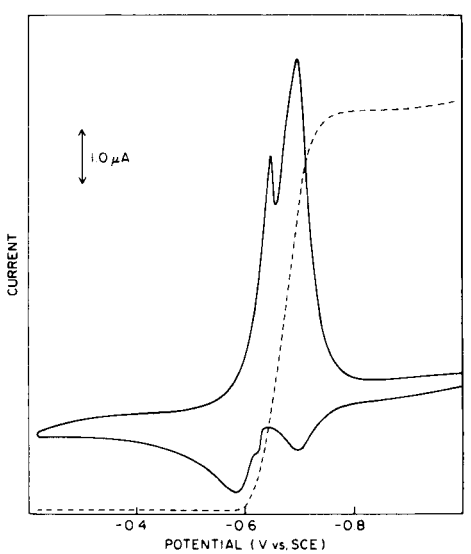

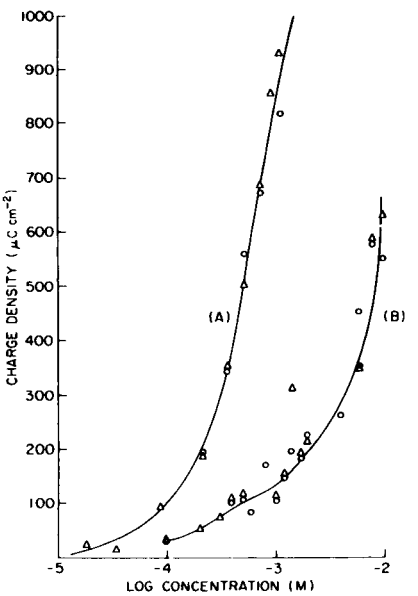

Fig. 6. (—) Linear-sweep current—potential curve for 2.56×10^{-4} M benzyl mercaptan in 0.2 M NaOH. (- - -) Charge—potential curve for the return sweep in the negative potential direction. Sweep rate, 50 mV s^{-1}.

Fig. 7. Charge density vs. log concentration for (A) benzyl mercaptan and (B) cysteine. (○) and (△) indicate runs made on different days.

current in the −0.7 V region is clearly inverted and of a capacitive nature. This type of current is indicative of a film which completely blocks the faradaic process. Since the data in Table 4 indicate that the product of the electrode reaction is soluble in solution, the blocking film can only be attributed to the formation of a surface layer of $Hg(SR)_2$ by a fast follow-up chemical reaction.

In the d.p. and d.c. polarograms of the 7.1×10^{-4} M solution of benzyl mercaptan in Fig. 5, three waves are discernible corresponding to the polarographic prewave, main wave and a third small wave which has a maximum at −0.28 V in the d.c. polarogram. The occurrence of a third wave at still more positive potentials possibly indicates that the electrode may be covered with still a third type of mercury(II) thiolate deposit. Canterford and Buchanan [10] found three d.c. waves in the polarogram of sulfide ion at 7×10^{-4} M and four d.c. waves above 1.1×10^{-3} M. They explain these waves by the deposition on the mercury surface of three successive layers of HgS which inhibit dissolution of the mercury as HgS_2^{2-}. In a previous publication [5], the two peaks found in the d.p. polarogram of cysteine at concentrations above 4×10^{-4} were ascribed to monolayer and multilayer formation. The use of the term multilayer was only meant to indicate that a film of thickness greater than a monolayer is formed, the exact nature of this layer being unknown. Similar phenomena are certainly taking place with the thiols investigated in the present study.

Integrated reduction current for cyclic voltammetry

In order to investigate film formation further, the integrated reduction current (charge) following scan reversal was studied in a cyclic voltammetry experiment. The cyclic voltammograms were run by pre-equilibrating a fresh mercury drop in a stirred solution at a potential around −1.0 V and then scanning in a quiet solution in the positive potential direction to around −0.2 V where the scan was reversed. Both the current versus potential curve and the charge versus potential curve were recorded. Similar experiments have been performed by Stankovich and Bard [11] for the cysteine system, and it was found that pre-equilibration time did not affect the results. In the work reported here, these voltammetric and coulometric curves were investigated for benzyl mercaptan and 1-butanethiol at pH 12.9 and for cysteine at pH 6.8. Figure 6 shows typical curves for benzyl mercaptan at 2.56×10^{-4} M. The anodic voltammetric waves with peaks at ca. −0.70 V and −0.58 V have a diffusion-controlled character and correspond to the $E_{1/2}$ values found for the d.c. polarographic oxidation waves. The reduction waves formed on scan reversal decay sharply, which indicates that surface layers are being reduced. Very similar behavior has been observed for cysteine where cathodic current spikes were attributed to the formation of a tight or complete monolayer [11]. In these linear sweep experiments [11] the anodic peak current versus concentration curve was found to level off at concentrations where the compact film forms, which is identical to the behavior reported in Fig. 3 for the d.p.p. method.

Charge density versus concentrations plots for benzyl mercaptan and cysteine are given in Fig. 7. The Q vs. concentration curve for benzyl mercaptan (Fig. 7A) was found to be more reproducible than the plot for cysteine (Fig. 7B), as can be seen from the experimental points taken for two sets of identical but independent experiments run at different times. In agreement with the proposal that the product of the electrode process $Hg(SR)_2$ is the blocking species, it is seen in Fig. 7(A) that there is little adsorbed material in the 10^{-5}–10^{-4} M region but that beyond 10^{-4} M the charge grows rapidly as the concentration of the thiol is increased. Similar behavior was found for 1-butanethiol except that the plot appeared to be rounding off in the 10^{-3}–10^{-2} M range. For cysteine (Fig. 7B) it appears that there is a plateau around 100 μC cm^{-2} but that the charge begins to grow rapidly above a concentration of 10^{-3} M. Stankovich and Bard [11] found that the charge density versus concentration plot for cysteine (pH 7.4) reached a maximum around 80 μC cm^{-2}. In their plot, the concentration does not exceed 10^{-3} M and there is a great deal of scatter in the data. We have gone beyond 10^{-3} M in [RSH] and found that for cysteine, benzyl mercaptan, and 1-butanethiol the charge density grows rapidly above 2×10^{-4} M and exhibits values of several hundreds μC cm^{-2}. The shape of the cathodic current—potential curve in the linear sweep experiment is very sharp and symmetrical or has a spike on top of a symmetrical peak at these large concentrations. This behavior indicates qualitatively that most of the reduction is for an adsorbed film even though there may be a small amount of reduction of diffusing $Hg(SR)_2$.

Assuming a very large maximum coverage of around 10^{-9} mol cm^{-2} corresponding to an area of 16 Å^2 per molecule or a monolayer coverage of 200 μC cm^{-2}, the charge density at high concentration still indicates several monolayers or a multilayer of film formation. The cathodic current spikes (Fig. 6) are typical and have been attributed to interactions between the R-part of adsorbed species causing a tight packing [11]. The nature of this tight packing or compact layer is not clear. Stankovich and Bard suggested that for cysteine the tight packing may involve a hydrogen bond between the $-NH_2$ group on one molecule and the $-COOH$ group of an adjacent molecule. We have seen the same type of spike (Fig. 6) in the cathodic branch of the cyclic voltammogram of benzyl mercaptan where such hydrogen bonding is not possible, suggesting that there may be another mechanism.

The behavior found in the Q vs. concentration plots, which show a semi-plateau region followed by a rapidly increasing adsorption, is typical of multilayer adsorption from solution [12]. In the present case, this phenomenon may correspond to the formation of a two-dimensional monolayer followed by physical adsorption of $Hg(SR)_2$ in a three-dimensional film. An alternative possibility is successive monolayers of varying structure stacked one upon the other with the nature of the first layer being quite different from succeeding layers. It is also possible that the large charge densities found at the larger concentrations are the result of the reduction of nonadhering $Hg(SR)_2$; however, the nature of the d.p. polarograms and of the cathodic c.v. curves

is consistent with reduction of adsorbed species. In the analogous case of oxidation of 1 M sodium sulfide in alkaline solution at a mercury electrode two successive monolayers of HgS have been found [13]. The charge density of the first layer was 179 ± 16 μC cm^{-2} while that of the second layer was 228 ± 23 μC cm^{-2} indicating different structures for the two layers. In the d.p. polarogram of benzyl mercaptan (Fig. 5), the third peak at −0.3 V is not seen until concentrations around 7×10^{-4} M which corresponds to an integrated reduction current in the cyclic voltammetric experiment of ca. 700 μC cm^{-2}. This peak does not indicate that a second monolayer has been formed since the charge density where the third peak appears is certainly equivalent to many monolayers. The peak, therefore, must indicate further changes in the film structure as the concentration reaches 7×10^{-4} M.

CONCLUSION

The d.p. polarographic method with a negative polarity pulse for low-molecular-weight thiols can be used from around 10^{-7} M to 10^{-4} M in an aqueous basic medium. The cathodic electrode process is a quasireversible reduction of either a HgSR or $Hg(SR)_2$ adsorbed layer which becomes more irreversible as the alkane chain-length increases. The anodic process is different from the cathodic one and involves the formation of a soluble mercury(I) thiolate which may be in equilibrium with the insoluble compound. The HgSR can disproportionate yielding mercury and adsorbed $Hg(SR)_2$. The linear shift of cathodic peak potential for a homologous series of thiols is most likely related to an increase in irreversibility caused by increased electron density at the sulfhydryl group.

The film formation that occurs on oxidation of RSH for concentrations greater than 10^{-4} M at a mercury electrode becomes passivating after a monolayer of $Hg(SR)_2$ has been formed. If the electrode potential is made more positive, it is possible for mercury to get through the film to form additional $Hg(SR)_2$ which forms additional layers of solid on the electrode. The detailed structure of the film is not known but it is thought to be a two-dimensional monolayer at the mercury surface followed by a three-dimensional multilayer of $Hg(SR)_2$ which contacts the aqueous solution. This monolayer multilayer structure is preferred to that of a compact or tight monolayer which cannot explain the very large charge-density values found when the film is reduced.

Acknowledgement is made to The City University of New York for a Faculty Research Award Grant RF-11426 made under the Professional Staff Congress—Board of Higher Education Grants Program to R.L.B.

REFERENCES

1 M. Brezina and P. Zuman, Polarography in Medicine, Biochemistry and Pharmacy, Interscience, New York, 1958, p. 470.

2 J. Heyrovsky and J. Kuta, Principles of Polarography, Academic Press, New York, 1966.
3 C. A. Mairesse-Ducarmois, G. J. Patriarche and J. L. Vanderbalck, Anal. Chim. Acta, 71 (1974) 165.
4 C. A. Mairesse-Ducarmois, G. J. Patriarche and J. L. Vanderbalck, Anal. Chim. Acta, 76 (1975) 299.
5 M. Youssefi and R. L. Birke, Anal. Chem., 49 (1977) 1380.
6 F. Peter and R. Rosset, Anal. Chim. Acta, 79 (1975) 47.
7 R. L. Birke, Anal. Chem., 50 (1978) 1489.
8 J. W. Dillard, J. J. O'Dea and R. A. Osteryoung, Anal. Chem., 51 (1979) 115.
9 R. S. Sexena and G. L. Khandelwohl, J. Indian Chem. Soc., 53 (1976) 564.
10 D. R. Canterford and A. S. Buchanan, J. Electroanal. Chem., 45 (1973) 193.
11 M. T. Stankovich and A. J. Bard, J. Electroanal. Chem., 75 (1977) 487.
12 A. W. Adamson, Physical Chemistry of Surfaces, Interscience, New York, 1967, p. 407.
13 R. D. Armstrong, D. F. Porter and H. R. Thirsk, J. Phys. Chem., 72 (1968) 2300.

Analytica Chimica Acta, 118 (1980) 271—276

CATHODIC STRIPPING DETERMINATION OF IRON AT A PLATINUM ELECTRODE MODIFIED BY ADSORPTION OF ADENOSINE-5′-MONOPHOSPHATE

JAMES A. COX* and MARCIN MAJDA

Department of Chemistry and Biochemistry, Southern Illinois University at Carbondale, Carbondale, IL 62901 (U.S.A.)

(Received 15th February 1980)

SUMMARY

Irreversible adsorption of adenosine-5′-monophosphate onto platinum yields an electrode surface which is readily plated by formation of a non-labile complex with iron(III) present initially in solution or formed by oxidation of iron(II). A negative potential scan subsequent to a 60-s deposition step produces a cathodic stripping peak, the height of which is proportional to the sum of the Fe(III) and Fe(II) concentrations in solution. Oxalate can be used to mask the response to Fe(III). The method is shown to be applicable to determinations of Fe(III) and Fe(II) in the concentration range 10^{-8}—10^{-6} mol l^{-1}.

The optimum electrode for stripping analysis is one which permits the test species to be deposited as a thin film. The resulting stripping peaks are narrower and higher than those from deposits of a metal into a hanging mercury drop or a mercury pool electrode and, therefore, result in greater sensitivity and resolution. Unfortunately, simple solid electrodes often fail as indicators for stripping methods, particularly for the analysis of mixtures. Problems include the effect of structure of the electrode surface and of the deposit on the stripping behavior, the effect of area on the sensitivity, and interference by surface oxides [1]. The use of mercury film electrodes can alleviate these problems but in turn introduces possible interference arising from intermetallic compound formation and related phenomena as well as errors from film thickness variation.

A recent paper [2] described the modification of a platinum electrode by irreversible adsorption of a monolayer of adenosine-5′-monophosphate and the behavior of the iron(III)/iron(II) couple at that electrode. Because previously reported stripping methods for iron(III) and iron(II) [3—9] are not completely satisfactory, this electrode was evaluated for determinations of these species by cathodic stripping voltammetry. In this work, iron(III) initially in solution and that obtained by oxidation of iron(II) is collected at the modified electrode through formation of a relatively nonlabile complex of iron(III) with the immobilized adenosine-5′-monophosphate. Subsequent reduction to the iron(II) complex gives the stripping peak. The lability of the reduction product prevents any memory effect.

EXPERIMENTAL

The experiments were performed with a Princeton Applied Research Model 170 Electrochemistry System. All potentials were recorded and reported vs. a saturated calomel reference electrode.

Iron stock solutions were prepared from ACS Reagent Grade $Fe(NH_4)_2(SO_4)_2 \cdot 6H_2O$ and $Fe(NH_4)(SO_4)_2 \cdot 12\ H_2O$. Monochloroacetic acid was recrystallized from water and distilled; the 81—82°C fraction was collected.

Adenosine-5'-monophosphate (AMP) was obtained from Sigma Chemical Company. The 99% assay sodium salt was stored at −18°C except for 30 min prior to weighing. The solutions were freshly prepared for each use.

The modified electrode substrates were platinum wires (1 mm diameter, 5 mm long) heat-sealed into soft glass tubing. Based upon previous reports [10, 11], the platinum was cleaned in chromic acid for 15 min, rinsed, and transferred to deaerated 0.5 M perchloric acid. The pretreatment was completed by applying 50—100 20-s potential step cycles between −0.3 V and 1.3 V and 20—50 potential scan cycles at 50 mV s^{-1} between −0.26 V and 1.05 V; the scan was stopped at 0.1 V. The platinum was rinsed and transferred to a deaerated 2×10^{-3} M AMP solution which was buffered at pH 3.5 with 0.1 M chloroacetate. The potential was cycled between −0.05 V and 0.40 V for 5 min at 200 mV s^{-1} to complete the modification. The electrode was stored in distilled water until needed. Storages of at least 2 weeks can be used. The characteristics of the Pt—AMP electrode have been reported elsewhere [2].

Results and discussion

The experiments were generally performed in pH 3.5 chloroacetate buffer [2]. Cyclic voltammetric experiments at 200 mV s^{-1} are characterized by anodic and cathodic peaks at a coincidental potential of 0.08 V. The same results are obtained with either iron(II) or iron(III) as the solution component. The peak currents are proportional to scan rate. These data are consistent with the electrode process involving the oxidation and reduction of surface-bound electroactive species, Fe(II)—AMP and Fe(III)—AMP [2]. At potentials positive of 0.4 V the oxidation of iron(II) in solution is observed.

Also noteworthy is that the Fe(III)—AMP complex is non-labile whereas Fe(II)—AMP is labile [2]. Therefore, if the Pt—AMP electrode is held negative of 0.1 V, iron is essentially removed from the electrode surface for situations in which the iron(II) concentration in the solution is below ca. 10^{-5} M so that Fe(II)—AMP approaches complete dissociation. This permits design of the cathodic stripping voltammetric experiment in a manner which is free of electrode history effects.

The experiment begins with the Pt—AMP electrode held at −0.05 V in a stirred, deaerated sample which is buffered at pH 3.5. Stepping the potential to 0.4 V initiates the pre-electrolysis. After a prescribed time the stirring is

stopped; following a 10-s rest, the electrode is scanned from 0.4 to —0.05 V at 200 mV s^{-1}. As shown in Fig. 1, the Fe(III)—AMP which is accumulated by the pre-electrolysis is reduced at 0.08 V. The peak height and area are both proportional to the iron concentration in the sample; for convenience only the former is reported.

Because of the limited number of phosphate sites available at the Pt-AMP electrode, the pre-electrolysis times used are much shorter than those in stripping experiments with electrodes such as the hanging mercury drop. Nevertheless the sensitivity and linear working range are sufficient to permit routine determinations at trace levels. With a 60-s pre-electrolysis, the linear range is 10^{-8}—10^{-6} M iron(II). Eight-point working curves over that range have the following linear least-squares characteristics: slope, 1.42 μA μM^{-1}; intercept, 0.04 μA; correlation coefficient, 0.9996; relative standard deviation of the slope, 1.7%.

When iron(III) is the sample component, the experiment is performed in an identical manner. When the potential is stepped to 0.4 V, accumulation is accomplished by an ion-exchange or direct-complexation reaction. Not surprisingly, the sensitivity is about the same as when iron(II) is the sample component. Eight-point working curves over the range 10^{-6}—10^{-8} M iron(III) have the following characteristics: slope, 1.39 μA μM^{-1}; intercept, 0.04 μA; correlation coefficient, 0.9993; slope standard deviation, 2.5%. Thus, the method directly responds to the total Fe(II) and Fe(III).

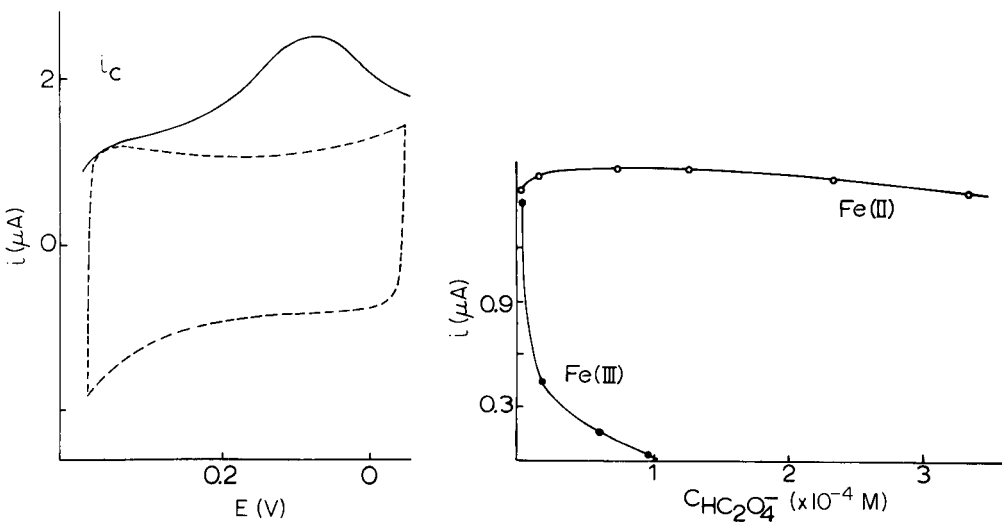

Fig. 1. Cathodic stripping voltammetry of iron at the Pt—AMP electrode. 9.4 x 10^{-7} M iron (II) in 0.03 M chloroacetate at pH 3.5; 60-s pre-electrolysis at 0.4 V; scan rate, 200 mV s^{-1}. Broken line is a cyclic voltammogram in the same solution.

Fig. 2. Evaluation of oxalate as a masking agent for iron(III). Cathodic stripping experiment as in Fig. 1. Iron(III) and iron(II) concentrations were 1 x 10^{-6} M.

Increasing the pre-electrolysis time to 120 s diminishes the linear range to 2×10^{-9}—1×10^{-7} M but increases the overall sensitivity. For iron(III) standards the working curve characteristics in this concentration range are: slope, 2.88 μA μM^{-1}; intercept, 0.05 μA; correlation coefficient, 0.9995; standard deviation, 2.6%.

When the variation of the characteristics of the Pt—AMP electrode and of the electrochemical experiment are considered together, the relative standard deviation of the peak current is about 4%. For example, when the cathodic stripping experiment was performed with a different Pt—AMP electrode for each of a series of 1.00×10^{-6} M iron(II) solutions, the peak currents which were obtained were 1.46, 1.53, 1.49, 1.37, and 1.50 μA. These results were obtained with a 60-s pre-electrolysis.

The irreversibility of the AMP adsorption at platinum and the stability of the Pt—AMP electrode were tested by performing multiple determinations of iron(II) at the 10^{-6} M level over a period of a few days with the same electrode. A 1.1×10^{-6} M iron(II) solution which was buffered at pH 3.6 was used throughout the experiment. The Pt—AMP electrode was stored in deaerated buffer between trials. Under these conditions, 16 experiments were performed in 49 h (7 times in the first 12 h) with variable intervals between trials. Each of the 16 experiments was repeated 3—5 times to obtain a representative current. The average of the 16 peak current values which were so obtained was 1.51 μA, and the relative standard deviation was 3.6%. The data attest to the stability of Pt—AMP.

In order to achieve such results, certain precautions must be taken. Desorption of AMP will occur if the electrode is polarized outside of the range 0.6 to −0.1 V in pH 3.5 solution. Further, forcing a current of above 0.3 mA cm^{-2} even within this potential range will alter the electrode behavior.

The sensitivity is a function of pH, so the samples must be buffered in order to obtain reproducible results. With a 5×10^{-5} M iron(II) sample, a series of experiments which were performed with a 1-min pre-electrolysis at pH values of 1.5, 2.0, 2.5, 3.0, 3.2, 3.4, and 3.5 yielded peak currents of 1.93, 2.52, 4.24, 5.53, 6.21, 6.49, and 6.60 μA. The use of pH 3.5 afforded the greatest sensitivity in this range as well as the least error caused by slight variations of acidity. At lower pH values the proton will compete for the phosphate complexing site; above pH 3.8 the deposition of iron(III) onto the Pt—AMP surface as a hydrated oxide can occur and introduce error.

As the cathodic stripping experiment responds directly to the total iron(II) and iron(III), determinations of each of these species in a mixture must employ masking. Oxalate was found to be useful for masking the iron(III). The effect of oxalate concentration on the stripping peak currents for iron(II) and iron(III) is summarized in Fig. 2. Oxalate in a 100-fold excess completely suppresses the Fe(III) peak but does not decrease that of Fe(II). In fact, as is seen in Fig. 2, the iron(II) peak is actually increased by about 6%. A blackened cell was used to minimize the known photochemically-induced reduction of iron(III) by oxalate [12].

The determination of iron(II) in the presence of large excesses of iron(III) cannot be performed by this approach. When the molar ratio of oxalate to iron(II) exceeds 300, the stripping peak is shifted into the potential range of discharge of the supporting electrolyte. Thus, only 3-fold excesses of iron(III) can be masked.

The success of the masking experiment indicates that the reported method would be subject to interference by complexing agents for iron(III) and iron(II). As noted in the pH study, hydroxide can also interfere.

Metals which can interact with AMP and thus block the phosphate sites were also considered as possible interferences. Based upon formation constants of the metal—AMP complexes [13], the interference of calcium, copper and cobalt ions was evaluated; the log K_1 values are 1.4, 2.6, and 3.2, respectively. The decrease of i_{pc} obtained after 60-s electrolysis in a 1×10^{-6} M iron(II) solution at pH 3.5 was measured as a function of the interfering metal concentration. Up to a 1000-fold molar excess of cobalt(II) did not alter the peak current. A 200-fold excess of calcium(II) caused an 8% current decrease. A 10-fold excess of copper(II) decreased the cathodic peak by 25%.

As the formation constant of the copper(II) complex is the only one which approaches that for iron(III) complexes with adenosine phosphates [13, 14], the interference by copper(II) is expected. Other metals should only slightly affect the stripping behavior.

In conclusion, the present study describes a rather simple means for the determination of trace levels of iron(II) and iron(III). Perhaps more important is the demonstration of the use of a modified electrode for an indicator in stripping analysis. The low, reproducible background current which is characteristic of an electrode coated with an organic film permits in turn the reliable measurement of sub-microampere faradaic currents. Hence, short pre-electrolysis times can be used with stripping methods.

This work was presented in part at the 178th National American Chemical Society Meeting, Washington, D.C., 1979. Partial support for M.M. was provided by the U.S. State Department through the Eastern European Universities Exchange Program grant to SIU-C. The work was partially supported by the National Science Foundation grant CHE 7908660.

REFERENCES

1 F. Vydra, K. Stulik and E. Julakova, Electrochemical Stripping Analysis, Halsted Press, New York, 1976, Ch. 1.
2 J. A. Cox and M. Majda, Anal. Chem., 52 (1980) 861.
3 W. Kemula and Z. Galus, Bull. Acad. Polon. Sci. Ser. Sci. Chim., 7 (1959) 729.
4 W. Haerdi, J. Buffle and D. Monnier, J. Electroanal. Chem., 23 (1969) 81.
5 J. Buffle, W. Haerdi and D. Monnier, J. Electroanal. Chem., 23 (1969) 89.
6 J. Buffle, D. Monnier and W. Haerdi, Chimia, 21 (1967) 578.
7 C. Olson and R. N. Adams, Anal. Chim. Acta, 29 (1963) 358.
8 Kh. Z. Brainina and E. Roizenblat, Zh. Anal. Khim., 18 (1963) 1392.
9 C. C. Young and H. A. Laitinen, Anal. Chem., 44 (1972) 457.
10 R. F. Lane and A. T. Hubbard, J. Phys. Chem., 77 (1973) 1401.

11 H. Angerstein-Kozlowska, B. E. Conway and W. B. A. Sharp, J. Electroanal. Chem., 43 (1973) 9.
12 C. P. Keszthelyi, N. E. Takvoryan and A. J. Bard, Anal. Chem., 47 (1975) 249.
13 R. S. J. Phillips, Chem. Rev., 66 (1966) 501.
14 C. R. Gaucher and J. F. Taylor, J. Biol. Chem., 239 (1964) 2251.

Analytica Chimica Acta, 118 (1980) 277—283

AN IMPROVED HYDROGENATION—MICROCOULOMETRIC METHOD FOR THE DETERMINATION OF NITROGEN IN ORGANIC MATERIALS INCLUDING COAL AND HEAVY RESIDUAL OILS

P. J. ZEEN and M. C. VAN GRONDELLE*

Koninklijke/Shell-Laboratorium, (Shell Research B.V.) Amsterdam (The Netherlands)

(Received 19th October 1979)

SUMMARY

The reliability of the Dohrman hydrogenation—microcoulometric system for the determination of nitrogen in organic products has been improved by replacing the troublesome platinum-black indicator electrode by a glass electrode. This involves a simple modification of the microcoulometer. The applicability of the method has been extended to cover coal and asphaltenes by using a basic flux. These samples previously gave low results.

The hydrogenation—microcoulometric method for the determination of nitrogen in organic materials by the Dohrman system has been reported in detail [1—3]. The sample is vaporized in a stream of hydrogen and hydrogenated over a hot nickel catalyst, chemically bound nitrogen being converted to ammonia. The gas stream is passed through lithium hydroxide to remove acidic gases and then to a titration cell where the ammonia is automatically titrated with electrolytically generated hydrogen ions. The end-point is indicated potentiometrically by a platinized-platinum pH electrode. The method is rapid and sensitive and performs well with a wide variety of organic products.

In this laboratory, the method was used initially for the analysis of relatively low-boiling organic products such as distillates but gradually the field of application was extended to include high-boiling products and chemicals such as epoxy resins. Later, the analysis of coal samples became of interest, but such samples gave rise to several problems. First, the platinum-black sensor was rapidly poisoned by traces of organic products resulting from incomplete hydrogenation of the sample; this occurs when high-boiling samples are analysed, or when the nickel catalyst is poisoned by sulfur compounds. Secondly, coals and other samples which leave a carbonaceous residue in the sample boat on hydrogenation, give low results because the chars retain some nitrogen [4, 5] even at 1000°C.

In this paper, it is shown that the nitrogen trapped in carbonaceous residues can be released, and a titration system is described which is not affected by incompletely hydrogenated species.

EXPERIMENTAL

Apparatus

A diagram of the apparatus is shown in Fig. 1.

Hydrogenation system. The hydrogenation system is shown in Fig. 2. It consists of a quartz tube (16-mm internal diameter) packed with a 10-cm bed of granular nickel catalyst (Dohrman Instruments) which is maintained at 850°C by means of a tube furnace; the inlet section is held at 950°C by a supplementary heating coil. Hydrogen is passed through the tube at a rate of 400 ml min^{-1}, 50 ml min^{-1} of which is humidified to prevent coking [6,7] of the catalyst. The humidifier is simply a wash bottle filled with water. The outlet section of the hydrogenation tube is maintained at 300°C and contains a small quartz scrubber tube filled with granular lithium hydroxide to remove any acidic gases formed during hydrogenation.

Titration system. The titration cell used is similar to that described by Martin [7], but the platinum-black sensor electrode is replaced by a glass pH electrode. Glass electrodes are unaffected by the presence of incompletely hydrogenated products. Other pH electrodes such as the antimony and carbon electrodes are unsuitable because of their slow response. The high electrical impedance of the glass electrode, however, was not compatible with the type

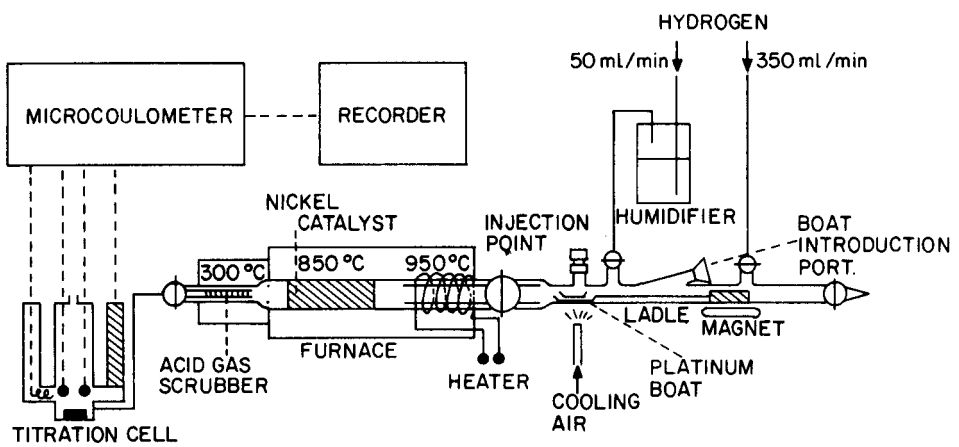

Fig. 1. Diagram of apparatus.

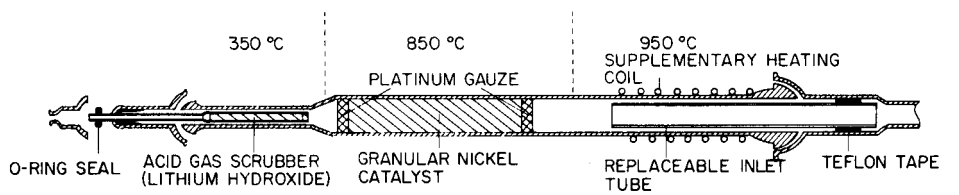

Fig. 2. Hydrogenation system.

of Dohrman microcoulometer used here, and so a Dohrman model C250 microcoulometer was modified (by Techmation) for use with glass electrodes. This was achieved by placing a suitable operational amplifier between the glass electrode and the sensor input of the coulometer. A diagram of the modification is shown in Fig. 3. The modified coulometer could still be used with normal low-impedance titration cells.

The cell electrolyte used is a 1% solution of potassium sulfate [8]. The bias potential corresponding to a suitable pH (6.0—7.0) can be determined by filling the cell with a buffer solution and adjusting the bias potential until a null balance is obtained. With the electrodes tested, this bias potential was negative and the polarity of the bias battery had to be changed. This can be done by using the switching circuit (Fig. 3) incorporated into the modified version of the microcoulometer.

Release of nitrogen from coal and heavy residual products

A method for the determination of nitrogen in residual products including asphaltenes, with a nickel boat and nickel powder has been described by Drushel [5]. However, this method cannot be used for the analysis of coal samples. With such samples, a basic flux was found satisfactory; this not only releases the nitrogen but retains, to a large extent, elements such as sulfur and chlorine which may deactivate the catalyst. This technique was described by Ter Meulen [4], who used barium carbonate with a steam/hydrogen gas flow. The flux melts the residue and ensures that carbon is converted to volatile products, thus releasing any nitrogen that may be trapped in the residue. Barium carbonate did not give satisfactory results in the present work, as broad tailing titration peaks and low recoveries were obtained. Several basic metal oxides and hydroxides were then tested as the flux for the analysis of a coal sample with a known nitrogen content. Table 1 shows that only BaO, $Na(OH)_2$ and LiOH gave good results; NaOH and KOH were not tested as these are known to attack quartz severely at high temperatures. Pure lithium hydroxide was finally selected because it gave the lowest blank value and, unlike barium oxide or hydroxide, did not tend to fuse the sample boat to the quartz tube.

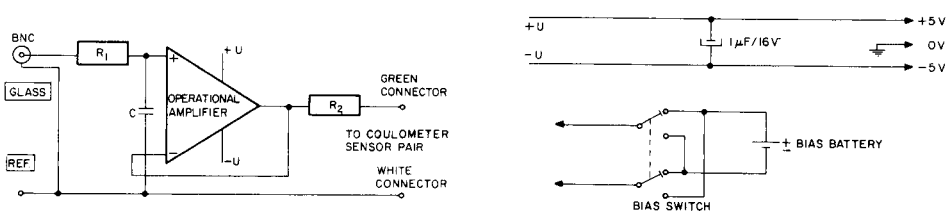

Fig. 3. High-impedance input adaptor and bias switching circuit.

TABLE 1

Coulometric analysis of a coal sample with various fluxes (nitrogen content, 1.05% by Kjeldahl method)

Flux	Peak shape	%N
Without flux	Broad tailing	0.80
LiOH	Sharp with little tailing	1.06
$Ba(OH)_2$	Sharp with little tailing	1.04
BaO	Sharp with little tailing	1.05
$BaCO_3$	Broad with tailing	1.04
$Ca(OH)_2$, CaO, $Mg(OH)_2$, MgO, $MgCO_3$	Broad with prolonged tailing	Not measurable

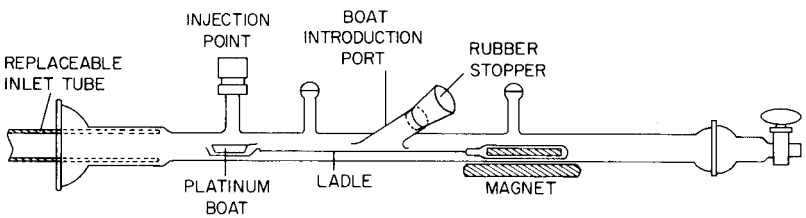

Fig. 4. Sample introduction system. The ball joints for the gas inlets are S 13/6.

Sample introduction system

The sample introduction system is shown in Fig. 4. Solid samples are weighed into a boat (covered with flux, if necessary) and placed on the ladle via the boat introduction port. Care must be taken to avoid introduction of atmospheric nitrogen into the system when the stopper is replaced. Liquid samples can be injected directly into the boat via the injection facility. The boat can then be moved into the hot inlet section by means of a magnet. The replaceable inlet tube makes it possible to prevent lithium hydroxide from coming in contact with the hydrogenation tube, which would shorten its service life.

Sample preparation and procedure

Heterogeneous solid samples such as coal should be ground to a particle size of less than 88 μm. If the whole sample passes a 88-μm sieve after grinding, microanalyses can be carried out with a precision as good as that obtained when the standard macro methods for coal are used.

The apparatus is first checked by using a standard sample of quinoline in kerosine, which is injected directly into the sample boat via the injection point (Fig. 4). The boat is then moved into the hot inlet of the hydrogenation tube with a magnet. The nitrogen content of the standard is calculated from the titration peak obtained; when necessary, the coulometer gain and/or bias are/is adjusted to give sharp titration peaks.

Solid samples can be dissolved in a suitable nitrogen-free solvent and

injected, or directly weighed, into the sample boat. The boat is placed on the ladle for introduction (Fig. 4). Coals and other samples which tend to leave a carbonaceous residue on hydrogenation are covered with lithium hydroxide (ca. 10 mg). Blank runs are done in all cases.

RESULTS AND DISCUSSION

Hydrogenation to ammonia

For the complete hydrogenation of most organic materials on granular nickel, a temperature of at least 800°C is necessary [7]. In the present system, amounts up to 3 mg of most samples were completely hydrogenated at this temperature. With larger samples, the gas effluent had a typical aromatic smell resulting from incompletely hydrogenated material and visible deposits were sometimes present in the outlet tube.

With a new catalyst, recoveries were low even though the sample was completely hydrogenated. The recovery also depended on the total amount of nitrogen present in the sample. This effect is related to decomposition of the ammonia formed, because at 850°C the equilibrium of the reaction, $2\ NH_3 \rightleftharpoons N_2 + 3H_2$, lies to the right. It can be seen from Fig. 5 that even at very low nitrogen concentrations a recovery of no more than about 20% can be expected at 850°C if equilibrium is established. However, with an old catalyst and a low nitrogen concentration, the rate of the decomposition reaction is usually very slow and during the short residence time of the ammonia in the hydrogenation tube (<30 s) hardly any dissociation takes place (see Fig. 6). With a new active catalyst, however, the rate of dissociation can be high enough to cause a significant loss of ammonia, particularly with

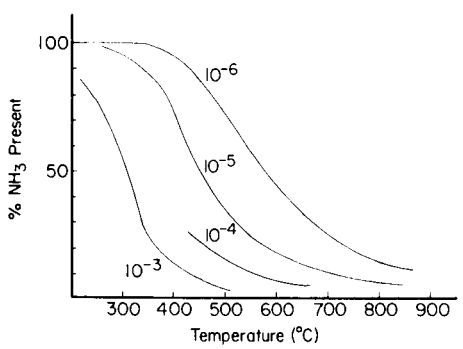

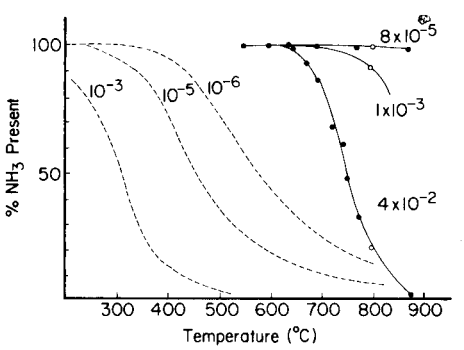

Fig. 5. Equilibrium ($2\ NH_3 \rightleftarrows N_2 + 3H_2$) calculated as a function of temperature and nitrogen concentration for a total pressure of 1 bar; % NH_3 is calculated from (NH_3-N/total N) × 100. The numbers on the curves indicate the nitrogen concentration in g l^{-1}.

Fig. 6. Effect of temperature and nitrogen concentration on the recovery of ammonia with an "old" tube. The numbers on the curves indicate the nitrogen concentration in g l^{-1}. (- - -) Calculated equilibrium concentration; (——) measured in outlet gas, for injections of ammonia.

high nitrogen intakes in the sample, because the reaction rate increases with increasing ammonia concentration. Accordingly, new and overactive catalysts have to be "conditioned" for optimum performance. A lasting deactivation of the catalyst was achieved by partially coating it with carbon and stable sulfides through repeated injections of a high-sulfur crude oil, e.g. by injecting ten 3-μl portions over a period of 1 h. After this treatment, samples containing up to 1 μg of nitrogen could be injected before significant dissociation of the ammonia occurred, and recoveries between 95 and 100% were obtained.

Effect of sulfur on catalytic activity

Samples containing up to a few percent of sulfur interfere with the determination because sulfur temporarily deactivates the catalyst by formation of nickel sulfide, and this leads to low recoveries. The catalytic hydrogenation activity is usually completely restored within 20 min because nickel sulfide decomposes slowly. The introduction of smaller amounts of sulfur, e.g. 25 μg, will also deactivate the catalyst to some extent; and although 100% of the nitrogen may be recovered, traces of incompletely hydrogenated sample may pass into the system.

Performance of the glass electrode

Traces of incompletely hydrogenated materials which enter the cell when the catalyst is not in optimum condition seriously affect the platinum-black electrode. The glass electrode, however, remains unaffected; even when the cell is visibly contaminated with organic material, the titration proceeds normally and the cell stability is not influenced.

The titration cell was used with several electrodes with impedances between 8 and 100 MΩ and diameters between 6 and 16 mm. Most electrodes performed well: a complete set-up, with cell and glass microelectrode (Type 76 R 221 NS from Electrofact, Radiumweg 20, Amersfoort, The Netherlands), is available (Techmation N.V., Schipol-Oost, The Netherlands). A good combined electrode (Type S700C, Intek Ltd., 88 Brewery Road, London, H 79 NS) is also satisfactory. The stability of these electrodes is good enough to allow detection of down to 0.5 mg of nitrogen. Although the titration speed was not as fast as with the hydrogen electrode, the titration was usually complete within 1 min. The titration proceeded more quickly when 1% K_2SO_4 served as the electrolyte instead of a sodium sulfate solution.

The function of lithium hydroxide

Various coal samples and some heavy residue materials, which in the absence of a flux, give low results, were analysed with lithium hydroxide as the flux. The results compared well with those obtained by the standard Kjeldahl method but tended to be a little higher. This tendency was also recorded by Ter Meulen [4]. The results are given in Table 2. The lithium hydroxide probably acts by forming carbon monoxide and lithium carbide from the carbonaceous residue: $2LiOH + 3C \rightarrow CO + Li_2C_2 + H_2O$.

TABLE 2

Comparison of results obtained by the microcoulometric—flux method and the Kjeldahl method

Sample	Kjeldahl (%N)	Microcoulometer (%N) With flux	Without flux	Sample	Kjeldahl (%N)	Microcoulometer (%N) With flux	Without flux
Coal A	1.72	1.78	1.20	Heavy crude oil A	0.57	0.59	0.52
Coal B	1.69	1.75	—	Heavy crude oil B	0.59	0.58	0.55
Coal C	1.58	1.64	—	Vacuum dist. residue A	0.44	0.45	0.40
Coal D	0.36	0.34	—	Vacuum dist. residue B	0.82	0.83	0.50
Coal E	0.41	0.43	—	Vacuum dist. residue C	0.35	0.40	0.35
Coal F	1.05	1.06	0.80	Asphaltenes from a			
Coal G	1.70	1.69	1.04	long residue	0.66	0.70	0.46

The carbide then reacts further with water to give acetylene and lithium hydroxide again: $Li_2C_2 + 2H_2O \rightarrow 2LiOH + C_2H_2$. In this way the carbonaceous residue is completely converted to gaseous products and occluded nitrogen is released.

The present system has been in full use now for about two years and has proved to be almost trouble-free.

We thank Techmation, the Dohrman agents in The Netherlands, for assistance with the modified electronic circuitry.

REFERENCES

1 J. A. McNulty, New Instrumental Methods of Analysis: Microcoulometric Titrating System, American Gas Association, Chemical and Engineering Session, Baltimore, MD, May 23, 1966.
2 D. R. Rhodes, J. R. Hopkins and J. C. Guffy, Anal. Chem., 43 (1971) 556.
3 L. A. Fabbro, L. A. Filachek, R. L. Iannacone, R. T. Moore, R. J. Joyce, Y. Takahashi and M. E. Riddle, Anal. Chem., 43 (1971) 1671.
4 M. H. Ter Meulen, Bull. Soc. Chim. Belg., 49 (1940) 103.
5 H. V. Drushel, Am. Chem. Soc., Div. Petr. Chem., Repr. 21, (1) (1976) 146.
6 I. J. Oita, Anal. Chem., 40 (1968) 1753.
7 R. L. Martin, Anal. Chem., 38 (1966) 1209.
8 R. Belcher (Ed.), Instrumental Organic Elemental Analysis, Academic Press, London, 1977.

Analytica Chimica Acta, 118 (1980) 285–292

EXTRACTION BASED ON THE FLOW-INJECTION PRINCIPLE
Part 5. Assessment with a Membrane Phase Separator for Different Organic Solvents

LAGE NORD

Department of Analytical Chemistry, Royal Institute of Technology, S-100 44 Stockholm (Sweden)

BO KARLBERG

Bifok AB, Box 5024, S-194 05 Upplands-Väsby (Sweden)

(Received 10th March 1980)

SUMMARY

Several membrane phase separators have been designed and tested for use in a flow-injection extraction manifold. The membrane is sandwiched between two pieces of perspex with grooves facing the membrane. A PTFE membrane with polyethylene backing proved to be most suitable. With this type of phase separator the total dispersion in the extraction system is less than that obtained with the conventional T-piece separator. Alcohols, alkanes, chlorinated hydrocarbons and aromatic solvents pumped at a flow rate of 0.5–1.0 ml min^{-1} can be segmented with aqueous phase and later separated from it with a recovery of up to 95%. The organic phase passing through the detector flow cell is not contaminated by the aqueous phase to any measurable extent.

In previous parts of this series [1–4] extraction systems based on the flow-injection principle have been described. The phase separator comprised a T-piece glass fitting into which a teflon fibre string was inserted at one of the bends [1]. The segmented stream, with alternating water and chloroform segments, from the teflon extraction coil was led into the T-piece, the inlet of which was positioned horizontally. The chloroform segments were joined at the contact with the fibre string and by differential pumping part of this joined stream was taken out through the downwardly positioned outlet. The remaining fraction of the chloroform was forced out, together with the aqueous phase, upwards through the opposite outlet. Further improvements in extraction by f.i.a. required a redesign of various parts of the system, especially the phase separator, which should ideally function for solvents of both greater and smaller density than water.

Several phase separators have been constructed for use in continuous flow systems; a review has been given by Furman in his monograph [5]. It is apparent that there are three main groups of phase separators. First, the chamber separator takes advantage of the density difference only, and the collected phase is removed either at the top or at the bottom. Secondly, there is the two-material separator, which utilizes the difference in properties

of two different materials and their respective affinity to the two phases; the working principle for this separator is to rejoin the segments and then to direct the joined stream. It is obvious that the difference in densities of the two solvents can also guide the design in this case. Thirdly, there is the membrane separator, which consists of a lipophilic membrane that expels the aqueous phase but lets through the organic phase. This type of phase separator seems to have the most universal application since it is possible to combine the properties of the two previous types.

Some of these have been used in flow-injection systems for solvent extraction. Bergamin et al. [6] determined molybdenum by the thiocyanate method after extraction with isoamyl alcohol. The phase separator was of the chamber type and made of perspex. Kawase et al. [7] used two phase separators in series in order to achieve separation in an extraction system involving water, methanol, and chloroform. The first separator was a T-piece separator of the conventional type [1] while the second was a membrane separator provided with a stirring device. Anionic surfactants were determined as an ion-pair with methylene blue. Klinghoffer et al. [8] investigated the extraction of lead solutions by dithizone in carbon tetrachloride at different pH values, using a T-piece separator. Cockshott et al. [9] have described the construction of a two-material separator. In contrast, Kina et al. [10] have measured the fluorescence of an extracted species without any phase separation at all.

The requirements of a phase separator in an f.i.a. system are not only that a complete separation should be obtained for several types of organic solvents but also that the dispersion of the injected and extracted sample should be kept as small as possible. For this reason the volume of the phase separator must be small. Further, the materials used for construction must be inert to attack by solvents. These requirements present problems of design and construction, and there is considerable scope for further experimentation. The aim of this study was to investigate the performance of the most sophisticated type of phase separator, namely the membrane separator, in an f.i.a. system.

EXPERIMENTAL

Apparatus

The equipment comprised the following items: two eight-channel peristaltic pumps (FIA 08, Bifok AB, Sweden); a chromatographic injector (Rheodyne, Berkeley, U.S.A.) with a volume of approximately 50 μl; a conventional segmentor [1] with two adjustable teflon tubes, and an extraction coil of teflon; a phase separator of new design as described in detail below; and a spectrophotometer (LC-55, Perkin-Elmer) with an 8-μl flow cell. Pump tubes were standard tygon for aqueous solutions; Solvaflex for alcoholic solvents, isooctane, and cyclohexane; and Acidflex for chloroform and toluene. All other connection tubes were of teflon.

Reagents

All chemicals and solvents were of analytical grade except for 1-octanol, ethyleneglycol and bromocresol green which were of purum quality. The organic solvents were shaken with aqueous phase to establish solubility equilibria between the two phases.

Test procedure

Figure 1 shows a typical manifold used to study the performance of different phase separators and to study the influence of various flow rates. Dispersion, or rather peak-shape, studies were carried out with 1-pentanol or chloroform as the organic phase. The test solution was injected via the chromatographic valve. With 1-pentanol as the organic phase, the aqueous test solution was 1.7×10^{-4} M bromocresol green, which was extracted in its acid form. With chloroform as the organic phase, the aqueous test solution was 3.6×10^{-5} M caffeine. After phase separation, the absorbance of the organic phase was measured at 435 nm or 275 nm, respectively. In some experiments, the flow of organic phase through the flow cell, z, was controlled separately with the aid of a second pump.

Durability studies of different membranes involved pumping aqueous and organic phases, without any sample injections being made. Instead, the stability of the baseline was taken as an indication of possible contamination of the flow cell by water as a result of insufficient separation. Such contamination manifested itself as a step-wise, significant change of the baseline.

Description of the phase separator

Figure 2 illustrates the working principle of the phase separator. The membrane is sandwiched between two pieces of perspex, each of which has a groove facing the membrane. The inlet and outlet bores were 0.8 mm i.d. In some studies teflon pieces were used instead of perspex. Groove dimensions are listed in Table 1. All phase separators of the membrane type were manufactured by Bifok AB (Upplands-Väsby, Sweden) for the purpose of this study. The separator was positioned as shown in Fig. 2 when the organic solvent in question was lighter than water and was inverted when solvents heavier than water were used.

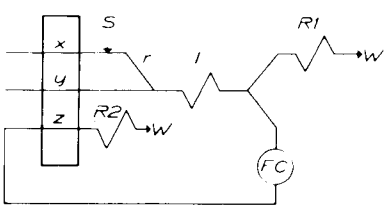

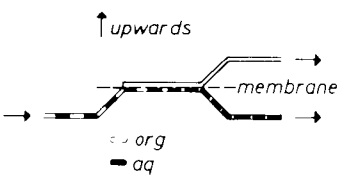

Fig. 1. Manifold used in the study of phase separators. Flows: x is the aqueous phase, y the organic phase and z the organic phase through the flow cell. $R1$ and $R2$ are restrictors, l is the extraction coil and r the reaction coil. S is the injection port and W is waste.

Fig. 2. Working principle of the membrane phase separator.

TABLE 1

Groove dimensions of phase separators used

No.	Length (mm)	Width (mm)	Depth (mm)	Material
1	35	2.0	0.3	perspex
2	35	0.5	1.2	perspex
3	70	1.2	0.5	perspex
4	20	1.2	0.5	perspex
5	35	1.2	0.5	teflon

RESULTS AND DISCUSSION

Durability of different membranes

The selection of a suitable membrane for flow systems is complicated by the number of parameters that can be varied (e.g., flow rate, type of organic phase, and separator design), and an unacceptable number of experiments would be required for a systematic evaluation. Consequently, some simple tests were devised to evaluate several membranes roughly. The results are given in Table 2. If the membrane still functioned after a minimum of 2 h, the test was interrupted.

Membranes with backing were more durable than membranes without. Though apparently very durable in this test, the cellulose acetate membranes deteriorated in, for instance, chloroform. Compared with teflon membranes, cellulose acetate membranes are much less hydrophobic and they also absorb water when they are dry (i.e., when they have not been pre-soaked by organic phase). For these reasons, the PTFE membranes with polyethylene backing were preferred for further investigations.

Groove dimensions of the phase separator

A fundamental criterion of the groove design was established at an early stage of this work: the volume of the groove should be at least 4—5 times larger than the volume of an individual segment of aqueous phase. The reason for this is that the groove must not, at any time whatsoever, be exclusively filled by the aqueous phase; if this happens, water will be sucked through and the membrane will be destroyed. A typical segment volume in extraction based on the flow-injection principle is about 3 μl. The minimum volume of a separator should thus exceed 15 μl. This of course refers to the groove that holds the segmented stream and not to the groove for the recipient stream.

As can be seen in Table 1, the cross-sectional area of the different grooves was kept constant. Separators 1 and 2 have equal lengths but different areas of the membrane available for solvent penetration. This means that the flux of solvent per membrane area unit differs significantly and that a membrane in separator 1 is subjected to less mechanical stress than a membrane in separator 2. When pentanol was used as the organic phase and the flow rates

TABLE 2

Tenacity and durability of different membranes
[Organic phase, 1-pentanol; phase separator, no. 1; restrictors R1 = 6 m (0.5 mm i.d.) and R2 = 0; extraction coil, 0.4 m (0.5 mm i.d.)]

Membrane type	Pore size (μm)	Durable for more than 2 h Test No.				Flow rates (ml min^{-1})		
		1	2	3	4	x	y	z
1. PTFE with polyethylene backing[a]	1.0	Yes	Yes	Yes	—	0.9—1.0	1.1—1.2	0.8—0.9
2. PTFE with polyethylene backing[a]	0.5	1.6[b]	Yes	Yes	Yes	0.9—1.0	1.1—1.2	0.8—0.9
3. Cellulose acetate	1.0	Yes	Yes	—	—	0.9—1.0	1.1—1.2	0.8—0.9
4. Cellulose acetate and nitrate	0.8	0.3[b]	0.5[b]	—	—	0.9—1.0	1.1—1.2	0.8—0.9
5. Cellulose acetate and nitrate	5.0	0[b]	—	—	—	0.9	1.0	0.6
6. PTFE tape	—	0[b]	—	—	—	0.8	1.0	0.7
7. PTFE without polyethylene backing	5.0	0[b]	—	—	—	0.4	0.4	0.3

[a]Obtained from millipore.
[b]Total lifetime of the membrane (h).

(ml min^{-1}), specified in Fig. 1, were x = 0.9—1.0, y = 1.0—1.1 and z = 1.0, the membranes in separator 1 remained useful for more than 2 h whilst in separator 2 they broke after about 10 min.

A similar comparison between separators 3 and 4 gave results that were in favour of the longer grooves, i.e. separator 3. In all, the conclusion of the experiments was that a large membrane area, achieved either by making the grooves shallower and wider, or by making the separator longer, or both, is to be recommended. The volume of the separator cannot, however, be increased indefinitely since the dispersion will increase correspondingly. Thus, separators 2 and 4 were rejected at this stage.

Different organic solvents tested

Many organic solvents are useful in batch extraction procedures, but in continuous flow systems involving a peristaltic pump, the number of organic solvents is limited because of chemical deterioration of the pump tubes. Unfortunately, the displacement bottle technique [5] is inconvenient to apply in this case, because a defined fraction of the organic phase has to be sucked off at a constant rate. In Table 3 are listed some phase systems for which separation with a PTFE membrane (no. 1, Table 1) is possible. The test time for each extraction system was at least 2 h. Two independent tests were performed in each case; no contamination of the flow cell by the polar phase was found.

TABLE 3

Some phase systems in which phase separation is possible with membrane no. 1.

Non-polar phase	Polar phase	Flow rates (ml min^{-1})			Phase separa no.
		x	*y*	*z*	
n-Butanol	0.015 M HNO_3 (aq.)	0.7	0.6—0.7	0.6—0.7	1
n-Pentanol	0.015 M HNO_3 (aq.)	0.9—1.0	1.0—1.1	1.0	1
n-Octanol	0.015 M HNO_3 (aq.)	1.0	1.0—1.1	0.7—0.8	1
iso-Octane	Water	0.9—1.1	1.1	1.0	1
Chloroform	Methanol + water (1 + 1)	0.9	1.1	0.7	5
Toluene	Water	0.9	1.0—1.1	0.8	5
Cyclohexane + n-Pentanol (8 + 2)	Water	1.1	1.1	0.9—1.0	1
Cyclohexane	Ethylene glycol	0.9	1.0	0.8	1

Segmentation failed for n-butanol when higher flow rates than those listed in Table 3 were used, and segmentation was difficult to control for the chloroform—methanol—water system. However, regular segments were easily obtained for the other phase systems.

Influence of the phase separator on the peak shape

Each part of the system — from the injection site up to the flow cell — contributes to the total dispersion. In this context, the concept of dispersion covers all processes which cause changes in the concentration profile of the sample plug in the system. By definition, the total dispersion consists of a combination of dispersion processes, each of which is associated with a certain part in the system, i.e. the dispersion is multiplicative [11]. This assumes that the dispersion processes occur independently in each part. The phase separator unit is a physically defined part of the system and it would be of interest to know its absolute contribution to the total dispersion, but this is difficult to determine. If, however, one phase separator is replaced with another one, the change of the total dispersion is easily determined. For analytical purposes, it is sufficient to know this change regardless of whether it arises strictly within the separator unit or not.

Any comparison of two phase separators should include the variation of the fraction of the organic phase sucked through the membrane in order to distinguish possible differences. The result of a comparison between the T-piece and one of the membrane type separators is shown in Fig. 3. The comparison was done with chloroform as the organic phase because the T-piece separator was designed for this organic solvent. In Fig. 3 peak heights and peak widths (at 5% peak height) are plotted against the percentage of the organic phase passing through the flow cell. The original T-piece separator [1] is slightly inferior to the membrane phase separator (no. 5, Table 1) with respect to these two characteristics of dispersion. However, the difference is more pronounced at higher fraction values. It was experimentally verified

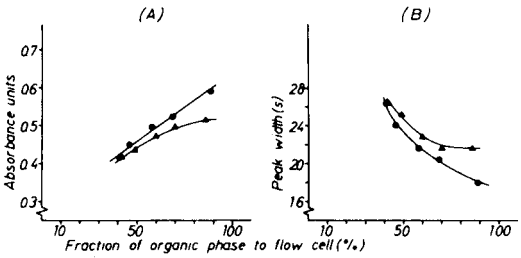

Fig. 3. Comparison of phase separators. (•) Membrane type; (▲) T-piece type. Peak heights (A) and peak widths (B) are plotted vs. fraction of organic phase to flow cell. The peak widths (in s) were measured at 5% of the peak-height value. x = 0.82—0.84 ml min^{-1}, y = 1.05—1.09 ml min^{-1}, r = 0.4 m (0.5 mm), l = 2 m (0.8 mm), $R1$, $R2$ = 3 m (0.5 mm).

that the stream-splitting achieved with a teflon T-piece in a simple single-phase system gave rise to a curve similar to that obtained for the T-piece separator in the two-phase system. As expected, a plot of peak areas vs. fraction of organic phase (instead of peak heights and widths as shown in Fig. 3) gave two coinciding straight lines intersecting the origin. Peak area in this connection means the product of absorbance and volume.

With the other phase separators, a straight line was obtained when the peak height was plotted against the fraction of the pentanol phase sucked through the membrane. For phase separator 1, the slope was 0.17 A.U. and the intercept 0.14 A.U. for y = 0.85 and x = 0.97 ml min^{-1}. Phase separators 2 and 4 were not, for the reasons mentioned above, included in this extended study. With phase separator 1, the peaks were about 10% higher throughout than the peaks obtained with separator 3. This result is easily explained by the larger volume of the latter separator.

So far only phase separators have been considered in which the directions of both the recipient and the segmented streams are the same. In a series of experiments with pentanol as the organic phase, the direction of the recipient stream was reversed. No significant decrease of the dispersion was observed. The durability of the membranes was not investigated for the reversed direction of the recipient stream.

Conclusions

Controlled dispersion is one of the cornerstones in flow injection analysis. With regard to dispersion in an extraction flow injection system, the phase separation step can contribute to the total dispersion to a large extent. This work shows that there are at least two means to decrease this contribution: first, by an appropriate design of the phase separator, and secondly, by increasing the separated fraction of the organic phase. The membrane phase separator causes a lower dispersion than the T-piece separator especially at high fraction values. It is important to realize that a significant decrease in dispersion really occurs when the separated fraction is increased; typically this decrease is about 30% when the fraction value changes from 0.4 to 0.9.

The membrane separator described here should be useful in practical f.i.a. applications for the additional reasons that the PTFE membrane is very durable, and that several phase separations can be performed for which the T-piece separator fails.

This work was supported by the Swedish National Board for Technical Development. The authors are indebted to Prof. D. Betteridge and Prof. F. Ingman for valuable comments on the manuscript.

REFERENCES

1 B. Karlberg and S. Thelander, Anal. Chim. Acta, 98 (1978) 1.
2 B. Karlberg, P. A. Johansson and S. Thelander, Anal. Chim. Acta, 104 (1979) 21.
3 B. Karlberg and S. Thelander, Anal. Chim. Acta, 114 (1980) 129.
4 P. A. Johansson, B. Karlberg and S. Thelander, Anal. Chim. Acta, 114 (1980) 215.
5 W. B. Furman, Continuous Flow Analysis, Theory and Practice, M. Dekker, New York, 1976, pp. 52 and 141.
6 H. Bergamin F°, I. X. Medeiros, B. F. Reis and E. A. G. Zagatto, Anal. Chim. Acta, 101 (1978) 9.
7 I. Kawase, A. Nakae and M. Yamanaka, Anal. Chem., 51 (1979) 1640.
8 O. Klinghoffer, J. Růžička and E. H. Hansen, Talanta, 27 (1980) 169.
9 I. D. Cockshott, R. Payne and P. B. Copsey, Research disclosure nr 18721, November 1979.
10 K. Kina, K. Shiraishi and N. Ishibashi, Talanta, 25 (1978) 295.
11 J. Růžička and E. H. Hansen, Anal. Chim. Acta, 99 (1978) 37.

Analytica Chimica Acta, 118 (1980) 293—299

AN ACCURATE MODEL FOR SAMPLE DROPLET ACCELERATION IN AN AIR—ACETYLENE FLAME

RICHARD E. RUSSO and GARY M. HIEFTJE*

Department of Chemistry, Indiana University, Bloomington, IN 47405 (U.S.A.)

(Received 13th March 1980)

SUMMARY

The experimentally observed velocity of an aerosol droplet in an air—acetylene flame is compared to the velocity calculated through a new mathematical model. The experimental droplet velocity is measured by means of stroboscopic photography of a stream of individual droplets sent into a flame at a known frequency and traveling very reproducible trajectories. Because the temporal spacing between these droplets is known, a measure of the instantaneous droplet location enables their velocity to be calculated. The droplet acceleration model was modified by incorporating into it a radially changing flame rise velocity, which was assumed constant in earlier treatments. Excellent agreement is found between calculated and measured droplet acceleration in the flame.

An aerosol droplet of sample solution, directed into an analytical flame or plasma, will rapidly accelerate toward the moving gas velocity. The rate and degree of approach of the droplet to the flame gas velocity is important both fundamentally and practically in analytical spectrometry. For example, the differential velocity between the droplet and the flame (or resulting particle and the flame) governs whether or not convective mass transport is significant in desolvation and vaporization. Also, droplet acceleration affects the eventual distribution of analyte atoms throughout the flame, which in turn influences analytical sensitivity, precision, and linearity of the working curve.

In particular, the horizontal acceleration of droplets as they enter a flame has been shown to be responsible for some of the lateral spread of atom populations [1]. More importantly, the vertical acceleration of aerosol droplets determines the distribution of analyte atoms above the burner, and therefore contributes to the optimal viewing height in the flame. It is also this vertical acceleration which determines the amount of time before a droplet (or particle) reaches the flame gas velocity, at which time convective mass transport becomes negligible in its influence on the atomization processes.

A mathematical expression has been formulated to model the vertical acceleration of aerosol droplets in a flame or plasma [2]. However, the time-dependent droplet velocity calculated through this expression does not

accurately predict the velocity actually observed. The apparent oversight in this previous work [2, 3] is that flame rise velocity was assumed to be constant across the burner. Unfortunately, this assumption leads to greater theoretical than observed droplet acceleration; in the experimental test of the model, droplets were injected into the flame in a direction perpendicular to its flowing axis, so that they experienced a radially changing flame velocity. Moreover, in the present study it was found that the measured droplet velocity in the flame is affected significantly by the droplet introduction rate. At droplet introduction rates greater than 2 kHz, the droplets bunch together, forming a quasi-continuous stream of solution. The flame then must accelerate the entire stream instead of individual entities, thereby leading to different behavior than expected for acceleration of single droplets. In the present paper, the agreement between theoretical and experimental results is improved by incorporating a measured, radially changing flame rise velocity into the acceleration expression, and by controlling carefully the droplet introduction rate. Significantly, theoretical results are shown to compare quite favorably with the measured droplet velocity over the entire droplet lifetime in the flame.

THEORY

The droplet acceleration expression is derived from Newton's Second Law, $a = F/m$, where a is the acceleration of the droplets, m is their mass, and F is the algebraic sum of forces acting on the droplets in the flame. There are two such forces: the viscous drag of the rising flame gases which serves to accelerate the droplets, and gravitational attraction, which tends to retard them. For a laminar flame and spherical droplets, viscous drag can be expressed by Stoke's Law as: $3\pi\eta d(V - V_d)$, where η is the average viscosity of the flame gases, d is the diameter of the droplets, and V and V_d are the velocities of the flame and droplet, respectively. Gravitational attraction is mg, where g is the gravitational constant.

Unfortunately, droplet diameter and mass are not constant in the flame because of ongoing desolvation. Therefore, time-dependent relations for droplet mass and diameter must be incorporated into the foregoing treatment. The time dependence of droplet size during desolvation has been determined [4] to be, $d^2 = d_0^2 - kt$, where d is the droplet diameter at time t after its entry into the flame, d_0 is the initial droplet diameter, and k is the desolvation rate constant. Upon substitution of the two time-dependent forces into Newton's Second Law, the droplet acceleration expression becomes

$$a = [18\eta(V - V_d)]/[\rho(d_0^2 - kt)] - g \tag{1}$$

where ρ is the density of the aerosol droplet.

In an earlier treatment [2], this expression was integrated to calculate the droplet velocity in the flame. However, direct integration is valid only

if one assumes the flame velocity to be constant over the entire lifetime of the droplet. We have found that this assumption is not valid, especially when a droplet generator [4] is used to inject the aerosol droplets into the flame. In this situation, used to test the proposed model, droplets are introduced into the flame in a direction perpendicular to the flame flow and therefore experience a parabolic flame rise velocity gradient as they penetrate the flame. Consequently, to obtain agreement between the proposed model and results obtained using the droplet generator, one should determine experimentally the flame velocity profile, relate this profile to the time-dependent horizontal droplet position, and then integrate the acceleration expression. Unfortunately, such a procedure leads to a fourth-order dependence of acceleration on flame rise velocity, making integration difficult and laborious. Instead, a numerical approach was chosen in the present study. In this approach, the acceleration expression is directly evaluated at very small time intervals by using an experimentally mapped flame rise velocity.

EXPERIMENTAL

In the measurement of droplet velocities, a droplet generator is used to inject uniform-sized aerosol droplets into the flame with reproducible, isochronal spacing [4, 5]. Because of this reproducibility, a single high-intensity flash photograph reveals the trajectory and spatial relationship of droplets in the flame, from which their instantaneous and spatially dependent velocities can be deduced. Figure 1 of an earlier paper [4] shows such a single-flash photograph, with a droplet introduction rate of 1000 droplets per second.

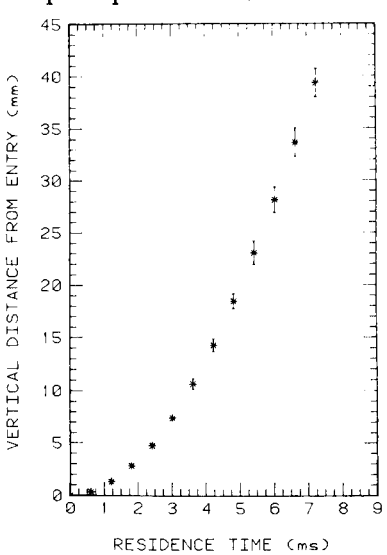

Fig. 1. Droplet trajectory in the flame. Initial droplet diameter, 68 μm. Introduction rate, 1.6 kHz. Error bars indicate ± 95% confidence limits.

In the present study, droplets were introduced into the flame in a slightly downward direction in order to establish a zero-vertical-velocity droplet location. Experimentally, vertical droplet positions were obtained by direct measurements above this reference droplet. Of course, small variations in individual droplet positions exist because of air currents around the apparatus. Therefore, droplet positions from several photographs were averaged to obtain an experimental curve of droplet position against droplet residence time in the flame (Fig. 1). Each droplet position in Fig. 1 represents the average of five different photographs in which all droplet generator and flame conditions were the same. Error bars in Fig. 1 represent 95% confidence limits, indicating that a standard deviation of less than 6% exists on the distance traveled by the droplets. If necessary, the magnitude of this error could be decreased by averaging additional photographs or by shielding the experimental apparatus from ambient air currents.

The time-dependent horizontal position of the droplets in the flame was also measured from the single-flash photographs. Coupled with knowledge of the rise velocity of the flame as a function of position across the burner (horizontal flame rise-velocity profile), this measurement enables one to calculate the flame velocity that each droplet experiences as it traverses the flame. The method of obtaining flame rise-velocity profiles is described elsewhere [6]. The rise-velocity profile for the air-acetylene flame used in this study is shown in Fig. 2. Asterisks in Fig. 2 represent the flame rise velocity values measured at a particular burner location; again, error bars show the 95% confidence limits. Not surprisingly, the relationship between rise velocity and position across the flame was found to fit a second-order

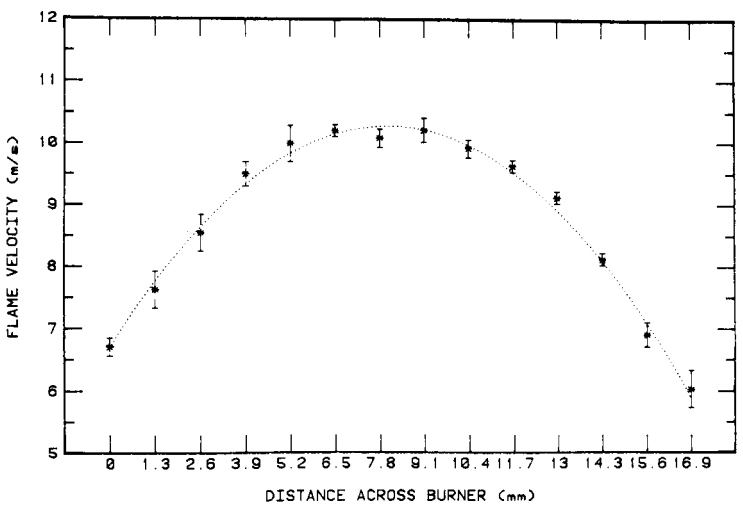

Fig. 2. Spatial velocity profile in stoichiometric (fuel/oxidant = 0.13) air—acetylene flame. Asterisks represent measured velocities; dotted line is the curve obtained from second-order fit (correlation coefficient = 0.99).

polynomial expression with a correlation coefficient of 0.99. The smooth parabolic curve (dotted), obtained from this polynomial expression, is what one would expect from Poiseuille's equation for a laminar flow system. The velocity of the flame that each droplet experiences with respect to spatial position can be easily found from this polynomial (or from Fig. 2), and direct evaluation of the acceleration expression at short time intervals then becomes possible.

A barium chloride solution (100 mg Ba l^{-1}; density, 1.0 g ml^{-1}) was used in the droplet generator reservoir. The initial droplet diameter was measured to be 68 ± 2 μm, by the MgO technique [7]. Droplet introduction rates were kept below 2 kHz in order to minimize the slip-stream effect [8]. Flame gas viscosity was calculated, by statistical mechanics, to be 660 micropoise for a flame temperature of 2450 K [9]. This average flame temperature was measured over the flame region of study using the sodium line-reversal technique [10].

RESULTS AND DISCUSSION

The random spatial distribution of droplets produced by a conventional nebulizer makes it unlikely that one droplet will strongly affect the acceleration or velocity of another. However, with the droplet generator used in the present study, droplets follow identical trajectories through the flame and can affect each other by developing a slip-stream [8]. Understandably, this slip-stream effect is most marked when droplets are closely spaced; visual changes in droplet velocity (spacing) are evident at droplet introduction frequencies greater than 2 kHz. Because this slip-stream effect, if pronounced, tends to shield each droplet somewhat from the viscous forces of the flowing flame gases, upward droplet acceleration is somewhat lowered at high droplet introduction rates.

This reduction in acceleration is evident by examination of Fig. 3, in which all experimental conditions were the same except for the droplet introduction rate. At an introduction rate of 2.8 kHz, droplets approach the flame velocity more slowly than at 1.6 kHz. To obtain a measure of droplet velocity consistent with the developed theoretical model, a low droplet introduction rate (1.6 kHz) was employed in the present study. At this rate, the slip-stream effect should be negligible [8].

Figure 4 compares droplet velocity curves calculated through the acceleration expression with the curve obtained experimentally at a droplet introduction rate of 1.6 kHz. The upper theoretical curve represents the droplet velocity calculated by assuming a constant flame rise velocity of 10.0 m s^{-1}. The lower curve was calculated by incorporating the spatially changing flame rise velocity (cf. Fig. 2) into the acceleration expression and evaluating it at small, discrete time intervals. As expected, the predicted acceleration is too great when a constant average flame rise velocity is assumed. In contrast, the curve incorporating a spatially changing flame rise velocity

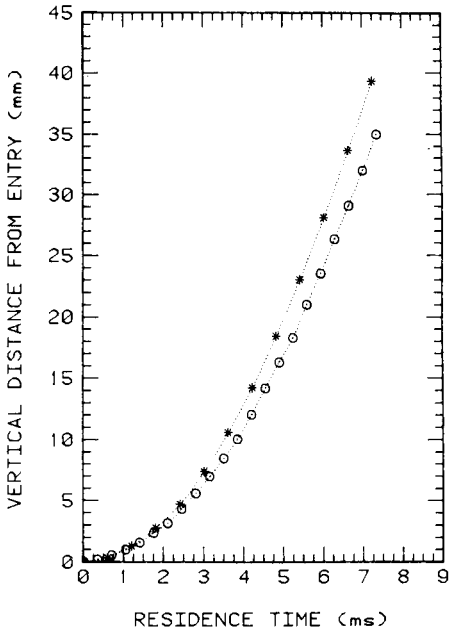

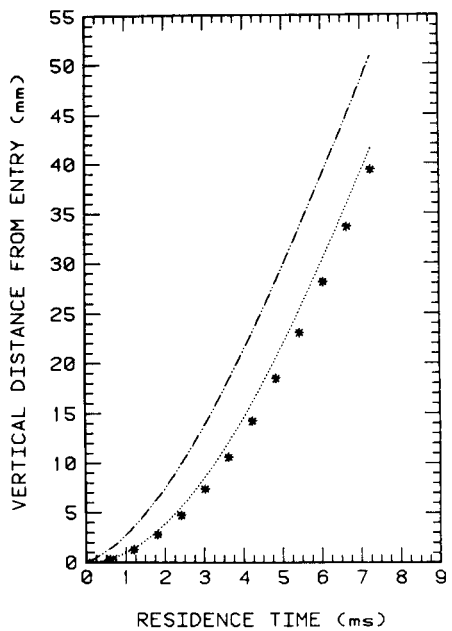

Fig. 3. Measured droplet velocity in the air—acetylene flame. All droplet generator and flame conditions are the same, except for the droplet introduction rate: (○) 2.8 kHz; (*) 1.6 kHz.

Fig. 4. Comparison of measured droplet velocity with that calculated through the acceleration expression (eqn. 1). (*) Measured; (—··—) calculated assuming rise velocity is constant across flame; (· · · ·) calculated using horizontally changing flame rise velocity.

(lower curve) agrees within experimental error with observed velocities over the entire lifetime of a desolvating droplet. Clearly, a spatially changing flame rise velocity must be considered in order to model droplet acceleration accurately when a droplet generator is used for nebulization. In conventional nebulizer systems, however, droplets usually enter the flame vertically and a constant flame rise velocity in the acceleration expression should provide close agreement with observed behavior.

Additional but small improvement in the droplet acceleration model is possible. For example, the existing expression does not take into account the change in density which occurs as droplets desolvate and become more concentrated. Also, a changing flame viscosity could be incorporated into the model. Such a change probably occurs as a result of changing flame temperature and water vapor concentration in the vicinity of the droplets. Inspection of the acceleration expression reveals that both of these modifications would improve agreement with experiment. Finally, it is not yet certain that the effect of one droplet on another is completely removed at the droplet introduction rate employed in this work. In order to measure the true droplet trajectory (velocity) in the flame, it would be necessary to inject a single droplet and monitor its path with a high-speed motion camera.

In our view, the improved agreement between experiment and theory which the above three modifications would yield does not justify the substantial complications which they would introduce into both the existing model and its verification. In most cases, the agreement obtained in this study would be sufficient to predict both the spatial distribution of atoms in an analytical flame and the amount of time required for introduced droplets (or particles) to reach the flame rise velocity.

This paper was presented in part at the annual meeting of the Federation of Analytical Chemistry and Spectroscopy Societies, Philadelphia, PA, Sept., 1979. The work was supported in part by the National Science Foundation through grant CHE 77-22152 and in part by the Office of Naval Research.

REFERENCES

1 B. V. L'Vov, L. P. Kruglikova, L. K. Polzik and D. A. Katskov, J. Anal. Chem. USSR, 30 (1975) 545.
2 C. B. Boss and G. M. Hieftje, Anal. Chem., 49 (1977) 2112.
3 C. B. Boss, Ph.D. Thesis, Indiana University, 1977.
4 G. M. Hieftje and H. V. Malmstadt, Anal. Chem., 40 (1968) 1860.
5 G. M. Hieftje and H. V. Malmstadt, Anal. Chem., 41 (1969) 1735.
6 C. B. Boss and G. M. Hieftje, Appl. Spectrosc., 32 (1978) 377.
7 K. R. May, J. Sci. Instrum., 27 (1950) 128.
8 G. J. Bastiaans and G. M. Hieftje, Anal. Chem., 45 (1973) 1994.
9 D. A. McQuarrie, Statistical Mechanics, Harper and Row, New York, 1976, Ch. 16.
10 W. Snelleman, in Flame Emission and Atomic Absorption Spectroscopy, J. A. Dean and T. C. Rains (Eds.), M. Dekker, New York, 1969, Vol. 1, Ch. 7.

Analytica Chimica Acta, 118 (1980) 301—306

THE DETERMINATION OF MANGANESE BY ELECTROTHERMAL ATOMIC ABSORPTION SPECTROMETRY WITH A GRAPHITE FURNACE AT CONSTANT TEMPERATURE

D. C. MANNING and WALTER SLAVIN*

The Perkin-Elmer Corporation, Main Avenue, Norwalk, CT 06856 (U.S.A.)

(Received 14th February 1980)

SUMMARY

Many of the interferences reported earlier for the determination of manganese in a graphite furnace were not found when a modern graphite furnace was used. At high levels of chloride matrix, an interference which was observed in the modern furnace was reduced when manganese was determined under constant temperature conditions. In this work, the sample was introduced on a tungsten wire after the graphite furnace had reached a constant, preset temperature. Drying and ashing were accomplished outside the atomization furnace, reducing contamination from matrix materials.

Experiments to reduce interferences in the graphite furnace [1—4] have been continued with a study of manganese. In this work, the experimental conditions used were similar to those recently described [3], the sample being introduced into the graphite furnace at constant temperature. This method involves depositing and drying the sample on a tungsten wire, and then inserting the wire and sample residue into the furnace which has been heated to the desired equilibrium temperature. The earlier experiments [3] showed that interferences in the determination of lead and thallium were reduced by this sampling method.

This paper describes the effects of matrix interferences in the determination of manganese when this wire sampling technique was used. In this work, the system was changed from that described earlier [3]. The standard graphite sample tube was replaced by a modified tube having an extension tube of smaller diameter at right angles (Fig. 1). The extension provided a region for the sample to be ashed or charred in a way that reduced the probability that the volatilized product would condense on the graphite furnace walls. This is in contrast to the usual procedure of ashing within the furnace tube. If a relatively high flow of purge gas is maintained into the furnace ends and out of the extension during ashing, relatively little of the volatilized matrix products diffuses into the furnace.

Several workers have studied interferences when determining manganese in the graphite furnace. These workers [5—10] have used various furnace systems, with different operating characteristics. Some authors imply that

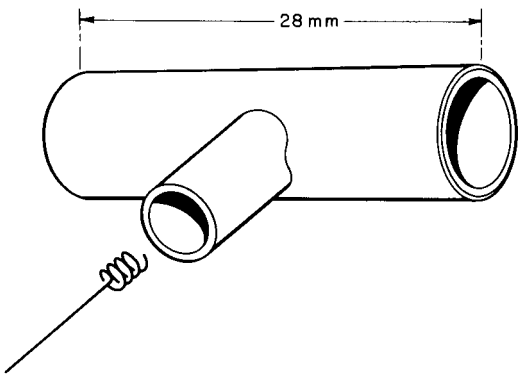

Fig. 1. Graphite tube modified for the tungsten wire sampling system.

their results pertain to graphite furnaces generally. Our experience indicates that there is considerable performance variation among furnaces of different design, and even within a single design if the experimental conditions are not the same.

Barnard and Fishman [5] reported no manganese interference from 1% NaCl or KCl solutions. They found significant (about 80%) suppression of manganese absorbance from 0.5% $MgCl_2$; the interferences were erratic. Bonilla [6] reported no or negligible interference on 0.5 ng of manganese from 250 ng of Zn, Cu, Mg, Na, and K, all added as the chloride. However, in his work, large amounts of nitric acid were present, which probably facilitated removal of the chloride in the charring step (800°C for 70 s).

McArthur [7] observed that manganese could be determined in saline water (up to 3.5% NaCl) provided that about 9% (w/v) ammonium nitrate was added to samples and standards, and that the samples were charred at a slow heating rate. Belling and Jones [8] found serious interference from Na, K, Ca, and Mg chlorides and resorted to extraction of the manganese prior to its determination.

Smeyers-Verbeke et al. [9] investigated the interference of several chemical compounds on manganese at a number of concentrations, and found $CaCl_2$, $LaCl_3$, and $MgCl_2$ to provide the most severe interference, in that order. Hageman et al. [10] also investigated interferences on manganese by 15 chemical compounds, and found $CaCl_2$, $MgCl_2$ and $ZnCl_2$ to be most severe, in that order.

L'vov [11] has shown that the interference resulting from an excess of chlorides in the sample on the absorption of the analyte comes about by the formation of a relatively volatile chloride of the analyte whose dissociation is incomplete in the gas phase. He showed quantitatively that the chloride compounds in the sample resulted in a vapor phase equilibrium between the free analyte and the chloride of the analyte, which depended on the quantity of chloride present, the temperature and the dissociation energy of the metal chloride species, among other factors.

The interferences of $CaCl_2$ and $MgCl_2$ on manganese were investigated here by using the Perkin-Elmer Model HGA-500 graphite furnace. The objective was to compare this furnace system with systems reported in the literature with respect to interferences, and also to establish the expected reduction of interference when the wire sampling method was used.

EXPERIMENTAL

The Perkin-Elmer Model 5000 atomic absorption spectrophotometer and the Model HGA-500 graphite furnace were used in this work. Because of the modified tube design, the temperature display on the Model 500 control unit did not indicate the correct temperature in the tube. True graphite tube temperatures were established by calibrating the indicated controller reading with an automatic recording pyrometer viewing the graphite tube interior. The Ircon Modline Series 2000 recording pyrometer was used for the temperature range from 850 to 3000°C. Absorbance was recorded on a Model 056 strip-chart recorder, and also on a Model PRS-10 printer-sequencer. Integrated absorbance readings were used in all cases. The furnace conditions for sampling from the wall were those recommended by the manufacturer. Conditions for wire sampling are listed in Table 1.

The heating sequence used with the wire was similar to that described previously [3] except for the addition of a charring step at 1000°C (step 2). The sample droplet was dispensed onto the wire coil which was then moved forward to about 1 mm in front of the extension tube. Sufficient power was applied to the furnace to bring the extension tube to about 500°C. Radiation from the extension tube together with the heated argon flowing out of the tube removed the solvent and left the dry residue on the tungsten wire. When the drop had dried, the wire was moved into the extension tube where the residue was charred at 1000°C. After the sample was charred, the furnace was cooled, the wire was withdrawn from the extension tube, and sufficient power was applied to bring the furnace to 2200°C. The recorder was turned on after 7 s of the 4th program step had elapsed. This was sufficient time for the tube to reach its equilibrium temperature. The spectrometer was instructed to begin reading the absorbance signal after 8 s of the 4th program step had

TABLE 1

Furnace program for wire sampling[a]

Step	1 (dry)	2 (char)	3 (cool)	4 (atomize)	5 (reference)
Temp. (°C)	500*	1000	50	2200	2200
Hold (s)	25	20	10	12	4

[a]In all cases the ramp setting was 1.

elapsed. The wire was plunged into the tube at the same time as the reading began. The absorption peak was integrated during the following 3.6 s. A second absorption signal, the blank, was recorded immediately after, with the wire in the optical beam and the furnace at the same temperature, step 5. The sample absorption signal was the difference between the two values.

For wire sampling, the solution used (5 μl) contained 0.04 μg Mn ml^{-1} (0.2 ng Mn) and varying amounts of matrix materials. For wall sampling, 20-μl aliquots (0.8 ng Mn) of the same solutions were applied.

RESULTS

The results obtained, together with literature reports, for $MgCl_2$ are summarized in Fig. 2A. The ratio of the weight of $MgCl_2$ to that of manganese is plotted on a log scale against percent recovery of manganese. The recovery is defined as the ratio of the integrated absorbance of the solution containing manganese and the matrix compound, divided by the integrated absorbance of the solution containing manganese alone. In order to compare the results from this work directly with those of some of the previous workers, several sets of data are included in Fig. 2A. Smeyers-Verbeke et al. [9], using the Model HGA-72, reported an enhancement at low concentrations of $MgCl_2$, turning to a suppression at higher concentrations. In data not plotted on Fig. 2A, Hageman et al. [10], using the CRA-63, found only 24% recovery at a weight ratio of 10^4. When these workers used the Woodriff constant-temperature furnace, they found that the interference was less than 10% at the same ratio (shown as limits in Fig. 2).

Results for $CaCl_2$ are summarized in Fig. 2B. Again data from Smeyers-Verbeke et al. [9] and a set of limits from the Woodriff furnace study reported by Hageman et al. [10] are included. Using the CRA-63, Hageman et al.

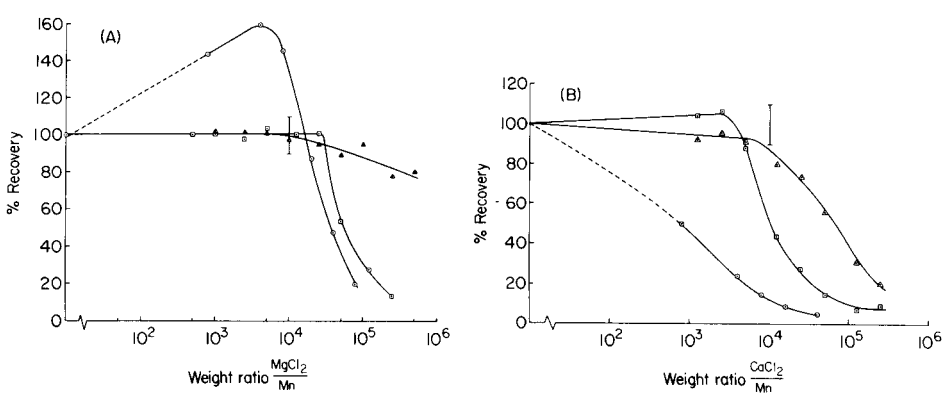

Fig. 2. Percent recovery of manganese observed in the presence of varying concentrations of (A) $MgCl_2$ and (B) $CaCl_2$. (⊙) Smeyers-Verbeke et al. [9] using the HGA-72; (⊡) this work, sampling from the wall; (△) this work, sampling from the wire. The bars show the limits given by Hageman et al. [10] for their constant-temperature furnace.

found less than 10% recovery at a weight ratio of 10^3 and essentially total loss of signal at a weight ratio of 10^4. These points are not plotted in Fig. 2B.

DISCUSSION

Several points can be made from these data. First, let us compare the several systems that report wall sampling. When the Perkin-Elmer Model HGA-500 system is used with sampling on the wall as recommended by the manufacturer, the enhancement reported by Smeyers-Verbeke et al. [9] at lower $MgCl_2$ concentrations is not seen. The recovery of manganese reported by Hageman et al. [10] with the Woodriff furnace is not different from that found with the conventional HGA-500 furnace and sampling from the wall. The severe suppression found by these workers with the CRA-63 was not observed under the present experimental conditions.

The $CaCl_2$ results (Fig. 2B) produce a similar pattern. The suppression of manganese absorbance is greater than found in the $MgCl_2$ matrix. Hageman et al. [10] using the Woodriff constant-temperature furnace, found less than 10% interference at a ratio of 10^4. However, using the CRA-63, they reported complete suppression of the manganese signal at a ratio of 10^4 with $CaCl_2$, and a 90% suppression at a ratio of 10^3. The results reported by Smeyers-Verbeke et al. [9], reproduced in Fig. 2B, show a more severe suppression of manganese absorbance than was found with wall sampling on the HGA-500.

As was stated earlier, integrated absorbance was used in this work. Although it is usually not stated, prior workers have probably used peak absorbance. It is possible that part of the decrease in the matrix effects observed here compared with literature reports is due to integration of the signal. However, only a small part of the improved performance of wall sampling from the HGA-500 can be attributed to the handling of the data.

While the interference effects of both $MgCl_2$ and $CaCl_2$ were not very severe when manganese was determined on the wall of the HGA-500, the effects were even smaller when sampling from the wire in the constant-temperature furnace.

There is good agreement between the present results for determining manganese on the wire in a constant-temperature furnace and those published by Hageman et al. [10] for the Woodriff constant-temperature furnace. The present measurements were carried to higher ratios of the interfering compounds than the earlier measurements.

The theory of L'vov [11] suggests that the degree of interference for different chlorides should be related to the dissociation energy, D_0, of the MCl. The large difference in D_0 between calcium and magnesium chlorides, 94 and 75 kcal mol^{-1}, respectively, should make $MgCl_2$ a significantly greater problem than $CaCl_2$. Even correction of the results in Fig. 2 to a mole basis leaves $CaCl_2$ the greater problem as an interference. This is probably because more $MgCl_2$ than $CaCl_2$ is removed during the char step, because of the greater volatility of the former.

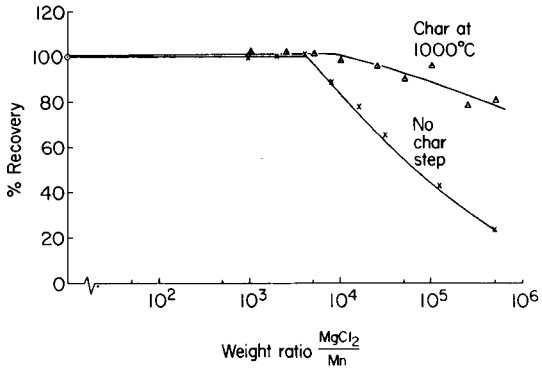

Fig. 3. Percentage recovery of manganese observed in the presence of varying concentrations of $MgCl_2$. (△) Charring at 1000°C; (x) no charring.

The charring step is important in reducing the chloride interference. Figure 3 shows the $MgCl_2$ interference on manganese. The data were taken by wire sampling, with and without charring at 1000°C. The marked difference in results is presumably due to the loss of chlorides in the charring step because of the destruction of magnesium chloride. Manganese can be charred at 1000°C, which is a high enough temperature to remove much of the $MgCl_2$ matrix. In the determination of lead [2] it is not possible to char at greater than 600°C without risking loss of lead. It is unlikely that very much chloride is removed at 600°C.

In the present experiments, no large difference in interference effects was seen between the L'vov Platform sampling system [2] and the wire sampling system. This is understandable, since the objective of both techniques is to introduce the sample into an environment that has reached thermal equilibrium. However, the wire technique should be applicable to high-temperature elements.

It is emphasized that the wire sampling technique is being used to study analytical performance. In its present form, it is not sufficiently convenient to be recommended for routine use.

We thank our colleagues, including Sabina Slavin and Frank J. Fernandez, for helpful discussions and for suggestions concerning the manuscript.

REFERENCES

1 D. C. Manning and W. Slavin, Anal. Chem., 50 (1978) 1234.
2 W. Slavin and D. C. Manning, Anal. Chem., 51 (1979) 261.
3 D. C. Manning, W. Slavin and S. Myers, Anal. Chem., 51 (1979) 2375.
4 W. Slavin, S. Myers and D. C. Manning, Anal. Chim. Acta, 117 (1980) 267.
5 W. M. Barnard and M. J. Fishman, At. Absorpt. Newsl., 12 (1973) 118.
6 E. Bonilla, Clin. Chem., 24 (1978) 471.
7 J. M. McArthur, Anal. Chim. Acta, 93 (1977) 77.
8 G. B. Belling and G. B. Jones, Anal. Chim. Acta, 80 (1975) 279.
9 J. Smeyers-Verbeke, Y. Michotte, P. Van Den Winkel and D. L. Massart, Anal. Chem., 48 (1976) 125.
10 L. Hageman, A. Mubarak and R. Woodriff, Appl. Spectrosc., 33 (1979) 226.
11 B. V. L'vov, Spectrochim. Acta, Part B, 33 (1978) 153.

Analytica Chimica Acta, 118 (1980) 307—311

DIRECT ATOMIC ABSORPTION SPECTROMETRIC DETERMINATION OF CHROMIUM, COBALT AND NICKEL IN FISH PROTEIN CONCENTRATE AND DRIED FISH SOLUBLES

F. J. LANGMYHR* and S. ORRE

Department of Chemistry, University of Oslo, Oslo 3 (Norway)

(Received 12th February 1980)

SUMMARY

Solid-sampling atomic absorption spectrometry was used for the determination of chromium, cobalt and nickel in four types of fish protein concentrate and a sample of dried fish solubles. The samples (0.3—10 mg) were introduced through the injection port of the graphite furnace by means of a special injector. The metals in the fish protein concentrate were determined from peak height measurements, by comparison with the International Atomic Energy Agency reference standard Dried Fish Solubles as the solid standard. The contents (in ppm) of chromium, cobalt and nickel were found to lie in the ranges 0.2—1.8, 0.07—0.3, and 0.7—2.8, respectively; the relative standard deviations were 5—16%.

Fish protein concentrate (f.p.c.) constitutes an important protein and trace element source which has not been fully utilized in human nutrition. The extended use of this important nutrient makes it highly desirable to know the content not only of the main constituents but also of the trace metals.

The conventional atomic absorption spectrometric (a.a.s.) methods for trace analysis of f.p.c. are plagued by lengthy and tedious procedures for dry or wet ashing, separation and concentration. The advent of the direct sampling technique has facilitated the analysis of these materials, and the technique has been applied successfully to the determination of mercury [1], cobalt, manganese and zinc [2], and cadmium, copper, manganese and lead [3] in samples of fish and f.p.c.

In this paper, methods are presented for direct a.a.s. determination of chromium, cobalt and nickel in four samples of f.p.c. and a sample of dried fish solubles.

EXPERIMENTAL

Apparatus

The measurements were made with a Perkin-Elmer (PE) 400S instrument equipped with two lamps for background correction and with a Pye-Unicam SP9-01 atomizer and graphite tubes of the standard type. The instrumental

TABLE 1

Instrumental parameters

	Chromium	Cobalt	Nickel
Lamp current (mA)	12	30	30
Wavelength (nm)	357.9	240.7	232.0
Spectral bandwidth (nm)	0.7	0.2	0.2
Heating program			
Drying	40 s, 100°C	40 s, 100°C[a]	40 s, 100°C
Ashing	40 s, 800°C	50 s, 500°C[b]	50 s, 500°C
		50 s, 1000°C	50 s, 1000°C
Atomization	8 s, 2700°C	8 s, 2700°C	8 s, 2700°C
Tube cleaning	8 s, 2800°C	8 s, 2800°C	8 s, 2800°C
Tube blank	8 s, 2700°C	8 s, 2700°C	8 s, 2700°C

[a]The drying time in the determination of cobalt in the decomposed IAEA sample was 100 s.

[b]For sample (d) the ashing program was: 30 s, 200°C; 30 s, 300°C; 100 s, 400°C; 50 s, 500°C; 50 s, 600°C; 60 s, 1000°C.

parameters are listed in Table 1. Single-component hollow-cathode lamps were used. The argon flow rate was 3.0 l min^{-1}.

The problems originating from the evaporation of large amounts of salts during the atomization step were solved by equipping the atomizer with silica windows and inlets at both ends for the purging gas (argon). With this arrangement, the absorbing species were rapidly removed through the injection port. Although this modification reduced the sensitivity of the measurements by about 25%, it was compensated for by enabling greater amounts (up to 10 mg) to be analyzed.

The solid samples were placed in the middle of the graphite tube by means of a specially-made stainless steel injector which could be introduced through the injection port.

Weighings were made with a microbalance. The acids were of Suprapur quality (Merck).

Samples and sample preparation

The samples analyzed in the present study were: (a) a solid reference sample of dried fish solubles (code no. A-6/1975) issued by the International Atomic Energy Agency (IAEA, Vienna, Austria); this sample was also applied as the solid standard; (b) a sample of functional f.p.c. (product no. 305) of blue whiting prepared from fish without head and entrails; (c) a sample of functional f.p.c. prepared from fillet of blue whiting; (d) a sample of functional f.p.c. prepared from fillet of pollack; and (e) a sample of conventional f.p.c. Type B-Norse Fish Powder. Sample (e) is produced commercially, whereas the other samples were products from pilot plants.

With the exception of sample (e), the materials were received as finely ground powders; sample (e) was pulverized in an agate mortar and pestle.

Preliminary work

Portions of the samples were dried at 110 ±5°C. The losses of mass (in percent) were: sample (a) 6.6; (b) 5.4; (c) 5.9; (d) 5.4; and (e) 6.5.

The volatilization of the three metals from aqueous standard solutions without and with an added excess of sodium chloride, and from all the solid samples, was studied by pyrolyzing suitable portions at temperatures ranging from 300°C to 1700°C, and then atomizing the analytes at 2700°C. From aqueous solutions without and with added sodium chloride (the amount added corresponding to four times the concentration present in f.p.c.), chromium was not detected until the temperature reached 1400°C. When the solid standard and the samples were heated, the first chromium signals were observed at about 1300°C. The presence or formation of volatile chromium compounds had to be taken into account; for this reason an ashing temperature of 800°C was chosen. According to Jones et al. [4], chromium is not lost by pyrolyzing brewer's yeast at 800°C, this sample contains relatively large concentrations of organic chromium compounds.

Similar experiments with cobalt and nickel standard solutions without and with sodium chloride demonstrated that no losses of the analytes occurred below 1100°C. Because of the low content of cobalt in the samples, it was difficult to establish the appearance temperature for this element; for nickel, however, the first signals appeared at about 1300°C.

Decomposition and analysis of the solid standard

A 4-g portion of the IAEA sample was dry-ashed at 700°C in a platinum dish, 5 ml of concentrated nitric acid was added, and the residue was dissolved by heating. The solution was diluted to 50 ml.

The contents of the three metals in the solid and in the decomposed sample were determined by the method of standard additions. The heating programs given in Table 1 were used. The three analytes were first determined by adding metal standard solutions to portions of the solid sample; procedural details are given in Table 2. The same standard additions method was then used to establish the content of the metals in the decomposed sample; details pertaining to these measurements are again given in Table 2. Regression analysis was used to calculate the analytical data.

TABLE 2

Procedural data for the analysis of the solid and dissolved IAEA sample

Element	Solid sample		Dissolved sample	
	Mass range taken (mg)	Solutions added (ppm)[a]	Volume taken (μl)	Solutions added (ppm)[a]
Cr	0.27—0.38	0, 0.04, 0.08, 0.16,	10	0, 0.04, 0.08, 0.16,
Co	1.93—2.87	0, 0.192, 0.384, 0.576, 0.768	50	0, 0.48, 0.72, 0.96, 1.44
Ni	0.55—0.85	0, 0.32, 0.64, 0.96, 1.28	10	0, 0.32, 0.64, 0.96, 1.28

[a]In all cases, four standard addition curves were plotted; 5-μl volumes of the solutions were added.

The averages ($\bar{x}$) from the 8 standard addition curves and the corresponding relative standard deviations (s_r) were as follows (the values in parentheses are the accepted laboratory averages from IAEA): chromium, $\bar{x}$ = 0.74 ppm, $\bar{s}_r$ = 15% (0.785 ppm), cobalt, $\bar{x}$ = 0.27 ppm, $\bar{s}_r$ = 13% (0.242 ppm); and nickel, $\bar{x}$ = 2.8 ppm, s_r = 16% (not reported). All data refer to samples dried at 110°C.

On the assumption that the IAEA data represent the true values, the differences between these data and those of the proposed method were compared by *t*-tests. The differences for chromium and cobalt were found to be insignificant.

General procedure for analysis of solid samples

With the IAEA sample as the solid standard, the contents of the three metals were determined in the four f.p.c. samples. The analyses were made by alternate atomization of suitable amounts (see Table 3) of samples and standards, and the results were calculated by relating the peak height of sample 1 with that of standard 1, etc. Instrumental parameters are given in Table 1.

TABLE 3

Analytical data for chromium, cobalt and nickel in f.p.c.

Sample[a]	Mass range taken (mg)		$\bar{x}$[b]	s_r	N
	Sample	Standard			
Chromium					
b	0.63—1.15	0.70—1.15	0.33	8	9
c	0.28—0.51	0.35—0.87	1.8	5	12
d	0.68—1.00	0.64—1.05	0.30	10	12
e	0.78—1.23	0.60—1.27	0.18	5	16
Cobalt					
b	3.00—3.64	3.41—4.37	0.33	11	12
c	4.02—4.98	4.09—4.80	0.17	16	12
d	7.57—10.60	2.89—3.40	0.068	7	12
e	3.62—4.14	3.27—4.00	0.27	10	12
Nickel					
b	1.54—2.50	1.64—2.40	0.97	16	13
c	1.43—2.61	1.69—2.48	2.5	5	13
d	3.00—3.45	1.63—2.90	0.68	10	10
e	1.24—2.43	1.06—2.21	2.3	6	14

[a](b)—(e) refer to type of sample (see Experimental).

[b]The average result (in ppm) with relative standard deviation (s_r, %) and number (N) of samples and standards atomized.

RESULTS

The results obtained by the use of the proposed method are listed in Table 3. In view of the small sample amounts and the low concentrations of the analytes, the precision of the proposed methods is acceptable, and does not indicate any inhomogeneous distribution.

The present results for chromium are lower than most of the earlier data [5—9]; there are reasons to believe that some of the previous values are too high. The present results for cobalt agree well with previous data from a.a.s. and neutron activation analysis [2, 10—12]. No data were found in the literature for the content of nickel in f.p.c. produced from the raw materials involved here. However, in South African f.p.c. [13], nickel was present in the range 0.7—4.8 ppm; the results obtained by the proposed method lie in a similar range.

As is apparent from Table 3, the contents of chromium and nickel are higher in sample (c) than in the other samples of functional f.p.c. (samples b and d). This sample (c) had been in longer and closer contact with processing equipment made of stainless steel, and this could be a factor contributing to the higher levels of chromium and nickel.

The authors thank the Research Institute of the Norwegian Herring Oil and Meal Industry, 5064 Straumsgrend, for providing the samples of fish meal, and Dr. J. Opstvedt for commenting on the manuscript.

REFERENCES

1 T. Hadeishi, Appl. Phys. Lett., 21 (1972) 438.
2 G. Lundgren and G. Johansson, Talanta, 21 (1974) 257.
3 F. J. Langmyhr and J. Aamodt, Anal. Chim. Acta, 87 (1976) 483.
4 G. B. Jones, R. A. Buckley and C. S. Chandler, Anal. Chim. Acta, 80 (1975) 389.
5 R. R. Kifer, W. L. Payne, D. Miller and M. E. Ambrose, Feedstuffs, 40 (1968) 36.
6 R. R. Kifer, W. L. Payne and M. E. Ambrose, Feedstuffs, 41 (1969) 18.
7 J. H. Soares, Jr., D. Miller and M. E. Ambrose, Feedstuffs, 42 (1970) 65.
8 E. W. Toepfer, W. Mertz, E. E. Roginski and M. M. Polansky, J. Agric. Food Chem., 21 (1973) 69.
9 E. G. Zook, J. J. Powell, B. M. Hackley, J. A. Emerson, J. R. Brooker and G. M. Knobl, Jr., J. Agric. Food Chem., 24 (1976) 47.
10 G. Lunde, J. Sci. Food Agric., 19 (1968) 432.
11 G. Lunde, J. Sci. Food Agric., 24 (1973) 416.
12 K. Julshamn and O. R. Braekkan, At. Absorpt. Newsl., 12 (1973) 139.
13 Annual Report of the Fisheries Industry Research Institute, South Africa, Cape Town, 1974, p. 42.

Analytica Chimica Acta, 118 (1980) 313—323

IDENTIFICATION AND QUANTIFICATION OF POLYNUCLEAR AROMATIC COMPOUNDS IN SYNTHOIL BY ROOM-TEMPERATURE PHOSPHORIMETRY

T. VO-DINH*, R. B. GAMMAGE and P. R. MARTINEZ

Health and Safety Research Division, Oak Ridge National Laboratory, Oak Ridge, Tennessee 37830 (U.S.A.)

(Received 20th December 1979)

SUMMARY

Room-temperature phosphorimetry (r.t.p.) is used to identify and quantify polynuclear aromatic compounds in a synthetic fuel (Synthoil). Several trace and major components, benzo[a]pyrene, chrysene, fluorenes, fluoranthene, phenanthrene, and pyrene, have been identified and determined at concentrations ranging from tens to thousands of parts-per-million. The selectivity of the r.t.p. analysis is greatly improved by using selective heavy-atom perturbation and synchronous excitation scanning.

With the goal of producing viable and environmentally acceptable fossil energy sources, much effort has recently been devoted to developing analytical methods that are sensitive and simple enough to be employed on a routine basis. The polynuclear aromatic compounds (PNA) originating from coal conversion processes have received particular attention because some of them are carcinogenic [1]. Because of the extreme complexity of these fossil-fuel-derived samples, the identification of the organic components usually requires a series of sophisticated, time-consuming and relatively expensive separation and spectrochemical measurements.

Although it is often necessary to characterize as many compounds as possible in a sample, there is an equal need for simple, rapid, and reliable methods that can give, within a reasonably short time (within a few hours or one day), a qualitative or semi-quantitative indication of the major components in a complex environmental sample. Such a method would be most suitable as a pre-screening tool for processing large numbers of environmental samples.

This paper reports on the relatively rapid and simple method based on room-temperature phosphorimetry (r.t.p.) for identification and quantification of PNA compounds in a Synthoil sample (a coal liquid from a hydrodesulfurization process). Room-temperature phosphorimetry is a relatively new method for organic trace determinations that has recently generated considerable interest among analytical spectroscopists [2—21]. First reported by Roth [17] and later by Schulman and Walling [18], the phosphorescence

at room temperature of organic compounds adsorbed on solid surfaces was first put to analytical use by Winefordner and co-workers [2–7]. One important feature of the r.t.p. technique is the possibility of using external heavy-atom perturbers in order to enhance the phosphorescence emission of individual compounds [4–6, 11, 15]. The technique of selective heavy-atom perturbation (SEHAP) was recently used to characterize targeted components only in synthetic mixtures [11]. In the present work, SEHAP is used for identification and determination of PNAs in Synthoil. Several trace and major components, including benzo[a]pyrene, chrysene, fluoranthene, fluorene, phenanthrene and pyrene, are determined at concentrations from tens to thousands ppm. The selectivity of the technique was improved by using synchronous scanning [10, 22].

EXPERIMENTAL

Apparatus

All r.t.p. measurements were conducted with a Perkin-Elmer spectrofluorimeter (Model 43A, Perkin-Elmer, Norwalk, Conn.) with a phosphoroscope attachment. The instrumental details were given previously [10, 11]. For synchronous rather than fixed excitation phosphorescence measurements, the excitation and emission monochromators are locked together at a fixed wavelength difference of $\Delta\lambda$. The excitation light source was a 150-W xenon arc lamp. The detector was a R777 photomultiplier (Hamamatsu Company) that has a useful photocathode spectral response from 185 nm to 700 nm. All the measurements were conducted with a 5-nm spectral bandwidth.

Reagents

The PNA compounds (technical grade) were commercially available. Schleicher and Schuell paper filters (Type 2040A) were used as substrate for the measurements. The Synthoil sample (0.15 g) was provided by the Analytical Chemistry Division of the Oak Ridge National Laboratory (ORNL). The chromatographic column was packed with magnesium silicate (Florisil, 100/200 mesh; Floridin Co., Berkeley Springs, W. Va.). All compounds were dissolved in ethanol and all heavy-atom salts in ethanol—water mixtures (volume ratio, 1:1).

Procedures

The procedures used to prepare the samples for r.t.p. measurements were similar to those reported in previous papers [4, 10]. In general, 3 μl of sample solution was spotted on a 0.6-cm diameter filter paper circle mounted on finger-type sample holders. The paper was pretreated with heavy atoms by spotting 3 μl of 0.5 M heavy-atom solution (lead acetate, sodium iodide, cesium iodide, or sodium bromide). After a drying period of about 3 min under an infrared heating lamp, the samples were transferred to the sample

compartment for spectroscopic measurements. Since 20 sample holders (6 cm long) were constructed, 20 different samples could be processed simultaneously. One advantage of the r.t.p. method is the small amount of sample required for each measurement. Only 0.15 g of Synthoil was used for the entire assay.

Two types of sample subjected to r.t.p. analysis were an unfractionated sample that had been diluted in methylene chloride (sample 1), and a sample that had undergone coarse extraction (sample 2). Several solvent extraction methods could be used for coal-derived products. A liquid—liquid extraction procedure using dimethyl sulfoxide has been recently developed for isolating polycyclic organic matter from complex mixtures of organic compounds [23]. A separation technique using solvents of increasing polarity is also available [24]. The extraction procedures used for this work are standard and already described previously [25, 26]. These procedures were the same as those used to fractionate synthetic crude oils from coal for biological testing.

The coarse extraction [25, 26] provides acidic, basic and neutral fractions. The organic solvent was methylene chloride. After sodium hydroxide and hydrochloric acid extractions, both phases were filtered to remove insoluble matter. The acidic and basic portions were stored for later studies. The neutral portion that contains the polyaromatic hydrocarbons was examined by r.t.p. For the quantification of benzo[a]pyrene, this neutral portion was also passed through a Florisil column to remove the polar components. These extraction procedures took about two hours.

RESULTS AND DISCUSSIONS

Rapid screening of the unfractionated Synthoil

Measurements were first conducted with the unfractionated Synthoil sample to explore the analytical usefulness of r.t.p. for rapid prescreening. It is noteworthy that the Synthoil sample was almost black. Diluted in methylene chloride (5 mg ml^{-1}), the sample still remained brownish because of insoluble particulates. Figure 1 serves to illustrate the usefulness of r.t.p. even with a raw Synthoil sample that had not been subjected to any fractionation procedure. It shows the r.t.p. spectrum of 15 μg of an unfractionated Synthoil sample using the excitation wavelength at 343 nm (optimal absorption wavelength for pyrene). The r.t.p. spectrum unambiguously reveals the presence of pyrene. For comparison, the r.t.p. spectrum of pure pyrene is also shown in Fig. 1 (dashed curve). Note that the broad bands at about 540 nm are due to the phosphorescence background of the paper whereas the narrower bands at 595 nm and 650 nm are characteristic of pyrene [21]. These data demonstrate that r.t.p. allows identification, within a few minutes, of a major component in an unfractionated real-life sample, thus permitting the rapid and simple detection of indicator PNA compounds.

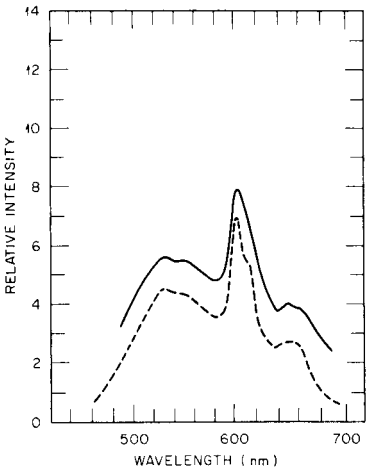

Fig. 1. Rapid r.t.p. screening of an unfractionated Synthoil sample. (—) Unfractionated Synthoil sample; (- - -) pure pyrene. λ_{ex} 343 nm.

Analysis of the fractionated sample

Figure 2 shows the r.t.p. spectra from Synthoil that had been subjected to coarse fractionation (sample 2). The sample was spotted onto filter paper that had been pretreated with either cesium iodide, lead acetate, or sodium iodide. In previous work [11], it was demonstrated that each heavy atom is able to induce the phosphorescence of a specific compound in a very selective manner. In this study the effect was used to improve the overall analysis of Synthoil. Combined with the selectivity offered by the selection of the excitation, this SEHAP technique is a valuable tool in the identification of several major and trace PNA compounds in Synthoil.

Considering the complexity of the sample, the r.t.p. spectra of Synthoil in Fig. 2 exhibit reasonably well-resolved structure. The spectral details are drastically altered by varying the excitation wavelength and the heavy atom. For example, with λ_{ex} = 343 nm and lead acetate providing the heavy atom, the r.t.p. spectrum is practically devoid of phenanthrene (Phe) or fluorene (Flu), and chrysene (Chy) but is rich in pyrene (Pyr) and fluoranthene (Fluo). With λ_{ex} = 304 nm and cesium iodide, phenanthrene and fluorenes (fluorene and methyl fluorenes) can be easily observed. On the other hand, chrysene is best identified with λ_{ex} = 330 nm and sodium iodide as the heavy-atom salt. The combination of excitation wavelengths and heavy atoms in Fig. 2 was chosen to illustrate the dependence of the r.t.p. spectra of Synthoil on these experimental factors. The three excitation wavelengths are, however, not optimal (except for pyrene and chrysene) for each individual compound. The actual determination of the individual compounds uses other excitation wavelengths which fall into the strongest absorption bands for each of them.

The criteria for selection of the appropriate heavy-atom perturber can

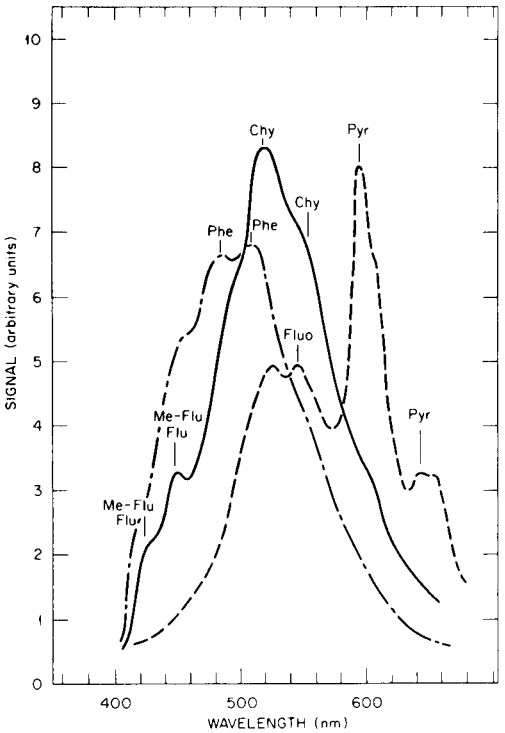

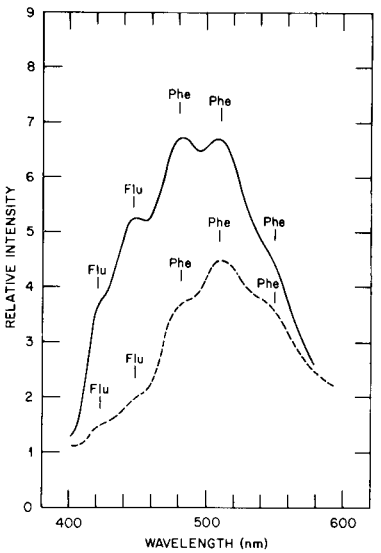

Fig. 2. Effect of various heavy atoms and excitation wavelengths on the r.t.p. spectra of Synthoil. (—) NaI, λ_{ex} 330 nm; (- . -) CsI, λ_{ex} 304 nm; (- - -) $Pb(OAc)_2$, λ_{ex} 343 nm.

Fig. 3. Effect of cesium iodide and lead acetate on the r.t.p. spectra of Synthoil. (—) CsI; (- - -) $Pb(OAc)_2$; λ_{ex} 295 nm.

sometimes be different for a pure compound and for the same compound in a mixture. For a pure compound, the choice of the most effective heavy atom is solely determined by the phosphorescence enhancement factor, f^{HA}, induced by the perturber (f^{HA} being defined as the ratio of the phosphorescence signal with heavy atom to that without heavy atom [11]). In a complex mixture, spectral interferences from neighboring emissions are also of major importance. If the individual compounds are considered, lead acetate is the best heavy-atom salt because it induces the strongest enhancement in the phosphorescence intensity of each compound in Synthoil. It is, however, not the best choice for several components because its effect is less selective than other heavy atoms. In some cases, the heavy-atom perturber that induces a weaker enhancement in the phosphorescence of a given compound of interest can be preferable if it provides little or no enhancement of the emission from other components.

Consider the identification of 1-methylfluorene and phenanthrene. Lead acetate induces the strongest phosphorescence enhancement for these two

components. The phosphorescence of 1-methylfluorene is strongly overlapped by the neighboring emission of phenanthrene (at 474 nm) if lead acetate is used. The use of cesium iodide decreases the interference from phenanthrene but the overlap between the two emissions is still significant (Fig. 2). As shown, sodium iodide is the best choice to observe 1-methylfluorene in Synthoil because it induces much less enhancement in phosphorescence from the interfering phenanthrene than does lead acetate or cesium iodide.

Figure 3 illustrates the selectivity of the heavy-atom effect. The two r.t.p. spectra of Synthoil, measured under identical experimental conditions (λ_{ex} = 295 nm), show the variation of the spectral structure with the heavy atom.

Another example is the choice of cesium iodide to identify phenanthrene in Synthoil. Although sodium iodide would also be a good perturber for pure phenanthrene, the cesium salt is a more suitable choice with Synthoil because it induces less interference from chrysene. The quenching properties of the perturber can also be important to render the determination more accurate. For example, silver nitrate appears to reduce the phosphorescence of fluorene, thus allowing an easier observation of fluoranthene and chrysene. It induces a general increase in the phosphorescence intensity of Synthoil but also causes a significant blurring of the spectral structure, thus making the analysis less effective [21].

Improved selectivity by synchronous excitation

The use of various excitation wavelengths and different heavy atoms is sufficient in most cases to identify the major PNAs present in Synthoil. A possibility exists for further improving the selectivity of the analysis. The methodology based on synchronous excitation [19] has been recently applied to r.t.p. [9, 10]. To obtain a synchronous spectrum, both excitation and emission wavelengths are simultaneously scanned while the wavelength interval between them ($\Delta\lambda$) is kept constant. This technique can significantly enhance the selectivity of phosphorescence determinations in complex mixtures. Noteworthy is the possibility of exploiting the singlet—triplet energy splitting as an additional factor of selectivity. The use of a $\Delta\lambda$ value that is optimized to the singlet—triplet properties of a given compound usually renders its detection more effective than with conventional fixed excitation. The use of the synchronous excitation method for rapidly identifying pyrene was discussed previously [10]. In the present work, the synchronous technique was useful in providing more accurate identification and quantification of several other PNAs in Synthoil.

A practical example of the benefits of synchronous versus conventional fixed excitation is given in Fig. 4. With CsI as the heavy-atom perturber and λ_{ex} = 270 nm, the r.t.p. spectrum of Synthoil exhibits a shoulder at ca. 430 nm. Because of its diffuse appearance, this band has limited analytical usefulness. In contrast, the synchronous r.t.p. spectrum, with $\Delta\lambda$ = 125 nm, exhibits at

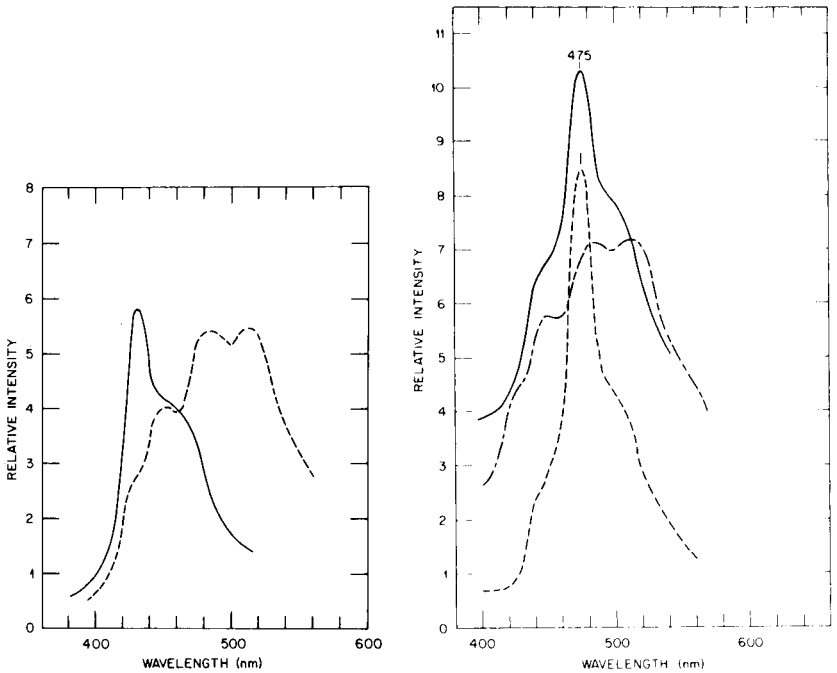

Fig. 4. Improved selectivity with the synchronous scanning technique. (- -) fixed λ_{ex} 270 nm; (—) synchronous with $\Delta\lambda$ = 125 nm. CsI.

Fig. 5. Identification of phenanthrene in Synthoil by synchronous r.t.p. (—) Synthoil, $\Delta\lambda$ = 180 nm; (- - -) phenanthrene, $\Delta\lambda$ = 180 nm; (— - —) Synthoil, λ_{ex} 295 nm. CsI.

433 nm a sharp band that can be assigned to fluorenes (fluorene and its methyl derivatives).

Another example underscores the improvement in selectivity achieved by the synchronous technique. Figure 5 shows the r.t.p. spectrum of Synthoil with λ_{ex} = 295 nm and CsI as the heavy-atom salt. Spectral overlap from fluorenes and chrysene is a major source of interference in r.t.p. analysis of Synthoil. The synchronous excitation method with a $\Delta\lambda$ value optimized to phenanthrene however, can reduce this interference. Illustrated in Fig. 5 are the synchronous r.t.p. spectra of Synthoil and of the pure phenanthrene compound. Both values $\Delta\lambda$ = 180 nm and λ_{ex} = 295 nm are optimized to phenanthrene. Whereas the fixed-excitation spectrum exhibits a broad band (at 475 nm) with a significant interference from the neighboring emission of fluorenes, the synchronous spectrum shows a sharper peak characteristic of phenanthrene with less spectral overlap from fluorenes. Overall, the decrease of the interference emissions and the band-width narrowing process combine to enhance the selectivity of the r.t.p. analysis of Synthoil.

Quantification

Great care must be taken in conducting quantitative r.t.p. work. Since r.t.p. is a surface-measurement technique, the linear ranges of the analytical curves are usually more limited ($\approx 10^3$) than those encountered in luminescence of solutions ($\approx 10^5$). Saturation effects occur at high concentrations [7]. In addition, interferences from the other components (inner-filter effect) and matrix effects from the substrate and heavy atoms can cause distortion of the spectral bands and saturation effects. It is worth mentioning that theoretical expressions for surface-intensity measurements predict the linearity of analytical curves over only a limited concentration range [7].

Test measurements were first conducted to ensure that the sample was sufficiently diluted (Fig. 6). Phosphorescence intensities were measured with samples of decreasing concentration to find the linear range of the calibration curves. The starting sample (referred as sample with dilution factor = 1) was 150 mg/100 ml of Synthoil in methylene chloride. This sample was successively diluted and the r.t.p. signals of chrysene, fluorene, and phenan-

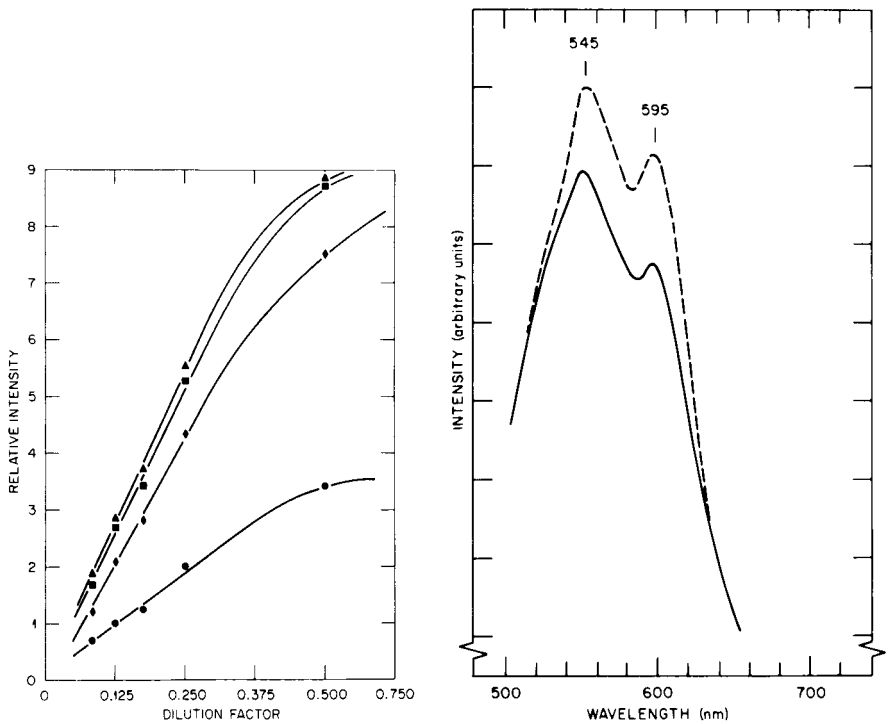

Fig. 6. Determination of the linear range of working curves: (▲) for chrysene at 518 nm; (■) for phenanthrene at 475 nm; (♦) and (●) for 1-methyl-fluorene at 428 nm and 450 nm, respectively.

Fig. 7. R.t.p. spectrum of Synthoil spiked with phenanthrene. (—) Synthoil; (- - -) Synthoil spiked with phenanthrene. λ_{ex} 295 nm.

threne were measured at each stage. Note that dilution does not eliminate background interferences but provides a simple and rapid means of determining the concentration ranges where quantification is feasible. The results in Fig. 6 indicate that the original sample was too concentrated for quantitative work and had to be diluted by at least a factor equal or higher than 4 (i.e., dilution factor $f \leqslant 0.25$). Most determinations, therefore, were performed with at least 10-fold dilutions. Detection limits for pure PNA compounds such as benzo[a]pyrene (BaP), chrysene, fluoranthene, fluorene, phenanthrene, and pyrene are 0.5 ng, 0.30 ng, 0.50 ng, 0.2 ng, 0.07 ng, and 0.1 ng, respectively.

These determinations of PNAs were first performed by comparing the signal intensities to those in the calibration curves of the pure compounds. The second method consisted in spiking the sample with known amounts of the component of interest. This latter method also provides a confirmation of the spectral assignments of the phosphorescence bands of Synthoil. Figure 7 gives one example of the spiking method, showing a portion of the r.t.p. spectrum of Synthoil before and after being enriched with phenanthrene.

The present r.t.p. methods can identify five compounds in Synthoil (BaP, chrysene, fluoranthene, phenanthrene, and pyrene) and quantify four of these. Data for chrysene were not meaningful because of the strong interference from phenanthrene and fluoranthene. Fluorenes can only be identified as a group. The results of r.t.p. determinations of the PNAs are given in Table 1. Although the relative standard deviation in the measurements of pure compounds is 7%, the precision of the analysis of the Synthoil sample is conservatively estimated to be 30% because of the mutual interferences among various components, and the strong background of Synthoil.

Because of the strong background, the detection of BaP in Synthoil is less accurate than for pure BaP. This interference is due to the 100-fold

TABLE 1

R.t.p. determination of PNA compounds in Synthoil

Compound	λ_{ex} ($\Delta\lambda$)[a] (nm)	Heavy atom	Concentration (ppm)[b]
Benzo[a]pyrene	395	$Pb(OAc)_2$	50 ± 18
Chrysene	330	$Pb(OAc)_2$	NQ[c]
Fluoranthene	365	$Pb(OAc)_2$	460 ± 160
Fluorenes	270 (125)	NaI	NQ[c]
Phenanthrene	295 (180)	CsI	2100 ± 700
Pyrene	343	$Pb(OAc)_2$	5500 ± 1600

[a]The value of $\Delta\lambda$ is given when the synchronous excitation technique is more selective than the conventional fixed-excitation method.
[b]Values given with the estimated absolute errors (30% inaccuracy).
[c]NQ = Not quantified because of spectral interference.

greater abundance of pyrene: the emission of the strongly phosphorescent pyrene produces a tail that is responsible for a strong background at the BaP emission wavelength. The measured concentration of BaP in Synthoil was found to be 50 ± 18 ppm [25]. Other laboratories have determined BaP in this same Synthoil in a round-robin involving fractionation and chromatographic techniques and the results obtained varied between 29 ppm and 96 ppm. R.t.p. can offer a simple method for monitoring BaP even when it is present only as a trace component.

Synthoil has also been previously analyzed in this laboratory by gas chromatography (g.c.) [26]. Within the experimental 30% accuracy, the r.t.p. data agree with the g.c. results. Anthracene phosphoresces at a wavelength longer than 700 nm, a region in which the photomultiplier tube currently being used is too insensitive. Addition of a photomultiplier tube responsive to longer wavelengths should permit easy discrimination as well as determinations of anthracene.

The data in Table 1 confirm that pyrene is the most abundant high-boiling PNA compound in Synthoil, a result that is in keeping with the data obtained by rapid r.t.p. screening of the unfractionated sample.

Conclusion

The applicability of the r.t.p. method in the analysis of a real-life coal liquid sample has been demonstrated. Although r.t.p. is not a technique intended to provide a complete analysis of complex samples such as coal liquids that might contain 100—200 components, it can find useful applications in the analysis of coal-derived products at various levels. R.t.p. is suitable for routine screening of large numbers of samples because it is simple and inexpensive. It also requires no cryogenic equipment and uses only inexpensive filter papers for sample substrates. Unfractionated samples can be directly monitored in order to profile one or two major components within a few minutes. Parent PNA profiling is useful for characterizing different types of fugitive emissions [27].

The r.t.p. technique also finds application if a more detailed analysis is required. A longer time (2—4 h) is required since the sample has to be coarsely fractionated and calibration curves for various compounds have to be measured beforehand. This type of analysis can provide qualitative as well as quantitative characterization of five major PNA components in such a complex sample as Synthoil. In practical analyses of environmental systems, a 30% inaccuracy is sometimes adequate for preliminary characterization.

This research was sponsored by the Office of Health and Environmental Research, U.S. Department of Energy under contract W-7405-eng-26 with the Union Carbide Corporation.

REFERENCES

1 C. E. Searle (Ed.), Chemical Carcinogens, ACS Monograph 173, Library of Congress, Washington D.C., 1976, p. 253.
2 S. L. Wellon, R. A. Paynter and J. D. Winefordner, Spectrochim. Acta, Part A, 30 (1974) 2133.
3 R. A. Paynter, S. L. Wellon and J. D. Winefordner, Anal. Chem., 46 (1974) 736.
4 T. Vo-Dinh, E. L. Lueyen and J. D. Winefordner, Anal. Chem., 48 (1976) 1186.
5 T. Vo-Dinh, E. L. Lueyen and J. D. Winefordner, Talanta, 24 (1977) 146.
6 T. Vo-Dinh, G. L. Walden and J. D. Winefordner, Anal. Chem., 49 (1977) 1126.
7 T. Vo-Dinh and J. D. Winefordner, Appl. Spectrosc. Rev., 13 (1977) 261.
8 P. G. Seybold and W. White, Anal. Chem., 47 (1975) 1199.
9 T. Vo-Dinh, R. B. Gammage, A. R. Hawthorne and J. H. Thorngate, Environ. Sci. Technol., 12 (1978) 1297.
10 T. Vo-Dinh and R. B. Gammage, Anal. Chem., 50 (1978) 2054.
11 T. Vo-Dinh and J. H. Hooyman, Anal. Chem., 51 (1979) 1915.
12 C. D. Ford and R. J. Hurtubise, Anal. Chem., 51 (1979) 659.
13 R. M. A. Von Wandruszka and R. J. Hurtubise, Anal. Chem., 48 (1976) 1784.
14 E. L. Bower and J. D. Winefordner, Anal. Chim. Acta, 101 (1978) 319; 102 (1978) 1.
15 I. M. Jakovljevic, Anal. Chem., 49 (1977) 2048.
16 C. G. de Lima and E. M. de M. Nicola, Anal. Chem., 50 (1978) 1658.
17 M. J. Roth, Chromatographia, 30 (1967) 270.
18 E. M. Schulman and C. Walling, Science, 178 (1972) 53.
19 G. J. Niday and P. G. Seybold, Anal. Chem., 50 (1978) 1577.
20 R. M. A. Von Wandruszka and R. J. Hurtubise, Anal. Chem., 48 (1976) 1784.
21 T. Vo-Dinh and R. B. Gammage, Anal. Chim. Acta, 107 (1979) 261.
22 T. Vo-Dinh, Anal. Chem., 50 (1978) 396.
23 D. F. S. Natusch and B. A. Tomkins, Anal. Chem., 50 (1978) 1492.
24 F. K. Schweighard and B. M. Thames, Anal. Chem., 50 (1978) 1382.
25 ORNL-Annual Progress Report, Oak Ridge National Laboratory — Period Ending November 20, ORNL-5360 (1977), p. 56.
26 C. H. Ho and B. R. Clark, Coal Technology Program Annual Interim Report for Fiscal Year Ending June 20, ORNL-5208 (1976), p. 96.
27 A. Bjorseth, in P. W. Jones and P. Leber (Eds.), Polynuclear Aromatic Hydrocarbons, Ann Arbor Science, Ann Arbor MI, p. 371.

Analytica Chimica Acta, 118 (1980) 325—331

FLUORESCENCE LIFETIMES AS A DISTINGUISHING PROPERTY OF MEMBERS OF DRUG SERIES

L. J. CLINE LOVE* and LINDA M. UPTON

Department of Chemistry, Seton Hall University, South Orange, N.J. 07079 (U.S.A.)

(Received 13th December 1979)

SUMMARY

The fluorescence lifetimes of antidepressant drugs, benzimidazoles, barbiturates and antimalarial drugs are reported for several different chemical environments. The quantum yields and natural fluorescence lifetimes are also reported for the latter two drug families. Structurally similar members of each drug group were qualitatively distinguished through temporal resolution, and the sensitivity of fluorescence enhanced by proper choice of chromophore environment.

Difficulties often arise in the determination of drugs because of the low therapeutic dose concentrations and the spectral similarities between the drugs and their metabolites. Although the sensitivity of fluorescence techniques has long been a recognized advantage for quantitative work at low concentrations, spectral selectivity has not always been achievable, especially for initial qualitative identification of structurally similar species. Often metabolites or drug series differ only in an attached functional group, thereby retaining the same fluorophore center which gives rise to the same spectrum for both it and its drug parent or homologue.

Many drugs fluoresce and have a characteristic fluorescence lifetime in the 1—200 ns range, which is easily measurable by the time-correlated single photon technique. Examples follow which show that in some cases, fluorescence lifetimes, τ_F and τ_0, are useful in the identification of compounds. In addition, for some drugs, the measured fluorescence lifetime may be the only selective fluorescence property.

In order to utilize fluorescence lifetimes effectively in the determination of members of drug series, the chemical environment must be a known or controlled quantity. Examples are given to show the possible effect of chromophore environment on τ_F and τ_0. A discussion of the possible application of fluorescence lifetimes to the identification of drug series based on these findings will be presented.

FUNDAMENTAL PRINCIPLES

The fluorescence lifetime of a compound is a measure of the time a molecule exists in an excited state before it loses the excess energy by emission of a photon. This deactivation back to the ground state can proceed by numerous mechanisms [1]. Radiative deactivation by fluorescence is characterized by the decay constant, k_F. Radiationless transitions depopulate the first excited singlet state by internal conversion, k_{ic}, intersystem crossing, k_{ix}, or by various quenching processes, $k_q(Q)$, where (Q) is the concentration of quencher.

The particular modes of deactivation can affect the value of the experimentally determined excited-state lifetime of the chemical species [2]. The experimental fluorescence lifetime, τ_F, is given by the reciprocal of the sum of all the decay constants operative in the system, for example:

$$\tau_F = 1/[k_F + k_{ic} + k_{ix} + k_q(Q)]$$

It is apparent that in the absence of all decay processes competing with k_F, the fluorescence lifetime is a maximum value, called the natural lifetime, τ_0. As more mechanisms are made available for non-fluorescent deactivation of the molecule, the measured fluorescence lifetime becomes shorter. Some environmental factors affecting τ_F include solvent polarity, pH, hydrogen bonding, temperature, viscosity, ionic strength and quenching. If the chemical environment of the fluorophore, i.e. both the solvent and the substituents attached to the chromophore, is carefully controlled, the experimental excited-state lifetimes are potentially useful for qualitative work. This is possible only if conditions are rigidly maintained so as to render all of the modes of deactivation constant. Many similar compounds with virtually identical absorption and fluorescence spectra do exhibit measurably different singlet state lifetimes [3, 4]. The use of fluorescence lifetimes, then, holds promise for the qualitative determination of compounds which are difficult to determine spectrally.

Measurement of both the experimental fluorescence lifetime and the fluorescence quantum yield, Φ, enables the calculation of the natural lifetime, τ_0, of the excited state [5]. This unique, intrinsic property of a molecule is calculated from the relationship $\tau_0 = \tau_F/\Phi = 1/k_f$, where Φ is the ratio of the number of emitted photons to the number of absorbed photons. If no competing processes to the fluorescence decay path are present, the quantum yield would equal unity and the experimental lifetime would correspond to the natural lifetime.

Use of both the experimental fluorescence lifetime and the calculated natural lifetime allows separation of the effects arising from the molecular excited-state intrinsic radiative deactivation rate from the effects caused by other physical processes and chemical effects [6]. These lifetimes are related as shown by the equation

$$(1/\tau_F) - (1/\tau_0) = k_{ic} + k_{ix}$$

for the case where internal conversion and intersystem crossing are the most important decay paths. In the determination of these excited-state lifetimes, the effects of the environment of the chromophore on several of its photochemical and photophysical properties may be observed by use of this relationship [7].

EXPERIMENTAL

Fluorescence lifetimes reported here were measured by the time-correlated single photon method, which is relatively fast and reliable [2, 3]. Quantum yields are measured by the same instrumentation [8] and τ_0 can be calculated. The detailed procedures and instrumentation have been described elsewhere [2, 3, 8, 9] and need not be repeated. Generally, the data presented here were collected using the basic ORTEC electronic systems, including the ORTEC Model 9352 nanosecond flashlamp, Model 457 time-to-amplitude converter, and Model 463 constant fraction discriminator. The single photons were detected using an RCA 8850 photomultiplier equipped with a rhodamine B quantum counter to eliminate the differential wavelength response. The data were analyzed by both a reiterative convolution program [9] and a plot program on an Interdate 7/16 mini-computer. All of the lifetimes reported were from experimental data with good fit to single exponential decays.

RESULTS AND DISCUSSION

A common compound used as a standard in fluorescence measurements is acridine [10]. It is a prime example of the profound effect a solvent can have on the fluorescence lifetimes, τ_F and τ_0. The data are presented in Table 1. The fluorescence lifetime increases by a factor of 60 in going from an ethanolic to a sulfuric acid solvent system. Since longer-lived species are more easily and precisely determined with greater accuracy, the choice of solvent in this case can greatly improve the reliability of the results.

Antidepressants

Table 2 presents the effect of solvents on the fluorescence lifetimes of the antidepressant drugs, amitriptyline (I) and protriptyline (II). In the solvents from 0.1 M acid to chloroform, the lifetimes of the two compounds are effectively the same within one to three standard deviations. However, in the sodium hydroxide solvent, the lifetimes are sufficiently different for reliable resolution. Environment can indeed be manipulated in this case to optimize the selectivity of the determination. The observed lifetimes for both compounds decrease as the solvent polarity decreases, with the exception of protriptyline in sodium hydroxide. This latter observation may be due to some quenching process allowed in base, such as intramolecular exciplex formation between the amine group and the ring system following neutralization of the hydrochloride from the amino group at the end of the exocyclic

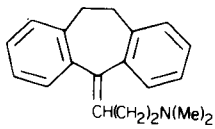

(I)

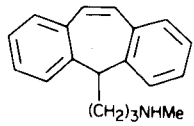

(II)

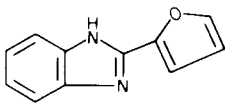

(III)

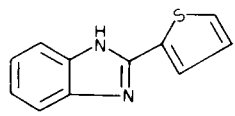

(IV)

TABLE 1

Fluorescence lifetimes of acridine

Solvent	τ_F[a](ns)	Φ[b]	τ_0 (ns)
Ethanol	0.6	0.020	30
0.05 M Sulfuric acid	37.5	0.500	75
0.1 M Hydrochloric acid	6.1	—	—

[a] ±0.3ns (1σ). [b] ±0.001 (1σ).

carbon chain. This may not be allowed in amitriptyline because of steric or charge effects. The quantum yield of amitriptyline is much lower than protriptyline in all solvents, probably because its relatively longer natural lifetime allows more time for the processes that compete with fluorescence to take place.

Benzimidazoles

Table 3 shows the fluorescence lifetimes for the benzimidazole compounds III and IV. When the oxygen heteroatom is replaced by the slightly less electronegative sulfur heteroatom, lifetime differences are seen. In all the solvents used, except strong acids, the compounds could probably be distinguished through their lifetimes. Acidic solvents cause the common chromophore to predominate over the substituent effect on the deactivation of the excited state. In these solvents the furyl and thienyl rings are protonated and the proposed charge-transfer transition cannot take place. The transition energies become very similar to acidified benzimidazole, and the transition occurring may be the usual benzimidazole transition. Again a particular environment may be chosen to provide selectivity.

Barbiturates

Table 4 presents some fluorescence data for oxy- and thiobarbiturates (formula V where R_1 and R_2 are hydrocarbon groups). Little trend is seen

TABLE 2

Fluorescence lifetimes [τ_F in ns ±0.3 ns (1σ)] of some antidepressants

Solvent	Amitriptyline	Protriptyline	Solvent	Amitriptyline	Protriptyline
0.1 M HCl	3.4	3.0	Ethyl acetate	2.4	2.9
Water	3.8	4.1	Chloroform	1.6	2.1
Acetonitrile	3.2	3.8	1% NaOH/methanol	3.3	1.8
Methanol	2.5	3.4			

TABLE 3

Fluorescence lifetimes [τ_F in ns ± 0.3 ns (1σ)] of benzimidazoles

Solvent	2-(2-Furyl)[a]	2-(2-Thienyl)[b]	Solvent	2-(2-Furyl)[a]	2-(2-Thienyl)[b]
Water	1.9	0.8	Sodium hydroxide	1.3	0.3
Ethanol	1.2	0.6	Hydrochloric acid	0.5	0.5
Ether	1.3	0.9	Sulfuric acid	1.4	1.4

[a]Compound III. [b]Compound IV.

TABLE 4

Lifetimes and quantum yields of some barbiturates

Compound	τ_f (ns)[a]	Φ_f	τ_0 (μs)[b]
Barbital	40	0.0028	14
Butethal	33	0.0029	11
Butalbital	21	0.0009	23
Phenobarbital	19	0.0006	32

[a]±1 ns (1σ). [b]Error is as much as 30%.

with substituent changes. The determination of barbiturates by their fluorescence properties is very limited because of their very weak fluorescence. The fluorescence lifetimes are unusually long and the natural lifetimes are in the microsecond range. Those with unsaturated groups in the 5-position (butalbital and phenobarbital) have much lower quantum yields than those with no unsaturation in that position (barbital and butethal). They also have longer natural lifetimes. Thus, the saturated and unsaturated barbiturates may be distinguished through natural lifetime or relative quantum yield. These data indicate that excited-state natural lifetimes are potentially useful for identifying specific molecular structural features among compound groups.

Atabrines

The experimental and calculated fluorescence lifetimes for a homologous series related to atabrine (formula VI) have been presented [3]. The observed

lifetimes, τ_F, in an acidic hydrogen bonding solvent (aqueous 0.1 M HCl) varied with the number, n of -CH_2-groups on the exocyclic nitrogen from τ_F = 12.7 ns for n = 1 to τ_F = 1.3 ns for n = 7. Thus, the primary difference among the molecules of the series, carbon chain length, can be made to affect an excited-state property, τ_F, in this type of solvent [3, 11]. The absorption and fluorescence spectra of all the series members in all solvents tried were superimposable. In all non-acidic solvents the lifetimes are identical among the series. Therefore, fluorescence lifetimes in acidic solvents provide the only identification of these molecules, through time resolution. Through this investigation a sensitive and selective approach to a qualitative identification has been optimized.

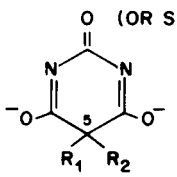

(V)

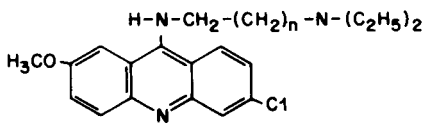

(VI)

Compounds for which fluorescence lifetimes may be particularly useful then, are those which have identical chromophores linked to different substituents, such as structures (V) and (VI). In these cases, the spectral properties of the series of compounds may be too similar for sufficient spectral resolution. The substituents, however, may cause different modes of deactivation from the excited singlet state to predominate and thus affect τ_F and/or τ_0 [7], to produce useful temporal resolution.

Solvents may, in the same manner as substituents, affect the fluorescence lifetimes. They can cause lifetimes and lifetime differences to increase, concomitantly increasing sensitivity, and they can promote excited states with significantly different lifetimes by actually changing the type of electronic transition occurring in one type of solvent versus another [3]. Through investigation of solvent properties such as dielectric constant, pH, polarity, hydrogen bonding ability, etc., the best matrix for optimal analysis may be chosen, or the effect of a biological matrix may be estimated and controlled. When there are small lifetime differences between compounds, a simple change in solvent polarity can increase the lifetime differences simply by lengthening lifetimes.

In conclusion, fluorescence lifetimes, both measured and natural, hold promise for sensitive and selective determination of difficult drugs and metabolites through nanosecond time resolution. Knowledge of environmental effects is necessary to bring control and optimization to the analysis and enhance the selectivity.

The financial assistance of the Analytical Division of the American Chemical Society through an award of a full year fellowship to L. M. U. is

gratefully acknowledged. Research support provided by the State of New Jersey Independent Colleges and Universities Utilization Act is also gratefully acknowledged.

REFERENCES

1 C. Parker, Photoluminescence of Solutions, Elsevier, Amsterdam, 1968.
2 L. J. Cline Love and L. A. Shaver, Anal. Chem., 48 (1976) 264A.
3 L. J. Cline Love, L. M. Upton and A. W. Ritter, Anal. Chem., 50 (1978) 2059.
4 L. M. Upton, Ph.D. Thesis, Seton Hall University, NJ, 1978.
5 S. J. Strickler and R. A. Berg, J. Chem. Phys., 37 (1962) 814.
6 J. B. Birks (Ed.), Organic Molecular Photophysics, J. Wiley, New York, Vol. 1, 1973, Vol. 2, 1975.
7 E. L. Wehry (Ed.), Modern Fluorescence Spectroscopy, Plenum Press, New York, Vol. 1, 1976.
8 L. J. Cline Love and L. M. Upton, Anal. Chem., 51 (1979) 1941.
9 L. J. Cline Love and L. A. Shaver, Anal. Chem., 52 (1980) 154.
10 S. Udenfriend, Fluorescence Assay in Biology and Medicine, Academic Press, New York, 1969.
11 L. J. Cline Love, P. C. Tway and L. M. Upton, Anal. Chem., 52 (1980) 311.

Analytica Chimica Acta, 118 (1980) 333—340

APPLICATION OF THE ELECTROCHEMILUMINESCENCE OF LUMINOL TO THE DETERMINATION OF COPPER

KEIJO E. HAAPAKKA and JOUKO J. KANKARE*

Department of Chemistry, University of Turku, SF-20500 Turku 50 (Finland)

(Received 2nd April, 1980)

SUMMARY

The electrochemiluminescence of aqueous alkaline luminol solutions has been studied by using rapid alternate positive and negative electrical pulses. Traces of copper are shown to change the proportion of the light emitted during the positive and negative pulses, measurement of which gives a linear log—log calibration plot for 1×10^{-7} to 6×10^{-6} M copper in glycine buffer at pH 10.15. Out of ten common cations tested only Hg(II), Pb(II) and Mn(II) interfered.

Analytical determinations based on chemiluminescent reactions are among the most sensitive. The sensitivity of the other luminescence methods, fluorescence and phosphorescence, is also high, but they have the problem of stray light from the excitation source. Background radiation presents little problem in the methods where one of the primary reagents participating in the chemiluminescent reaction is to be determined. For instance, hydrogen peroxide may be determined with high sensitivity by using its chemiluminescent reactions with luminol [1] or esters of oxalic acid [2]. A number of methods, however, use the catalytic influence of a third component on the chemiluminescence; for example, a number of metal ions may be determined by their catalytic influence on the luminol—hydrogen peroxide reaction [1].

Chemiluminescence is a dynamic process, which means that the reagents should be pumped or injected into the reaction zone where the resulting light is measured. Some of the inconvenience of handling flowing liquids can be circumvented by using electrolytic generation of at least one of the reagents. In addition, a new element of selectivity is obtained by varying the excitation voltage. This process is called electrogenerated chemiluminescence or electrochemiluminescence.

Luminol (3-aminophthalhydrazide) was one of the earliest known synthetic compounds exhibiting chemiluminescence. Its electrochemiluminescence was also the earliest known phenomenon of its kind. The mechanism of the latter has been extensively studied by Kuwana and co-workers [3—5], but no report on its analytical exploitation has been published. The aim of this paper is to show that trace metal analysis is feasible using the catalyzed electrochemiluminescence of luminol.

EXPERIMENTAL

Apparatus

The cell used for generating electrochemiluminescence is shown in Fig. 1. The working electrode (B) was a platinum coil wound on a glass tube and supported in both ends by PTFE collars. The supporting glass tube (D) also served as an oxygen inlet. The reference electrode was a saturated calomel electrode (A) and the auxiliary electrode (C) a short platinum wire. The emission was measured from the side by a RCA 1P28 photomultiplier tube.

A block diagram of the apparatus is shown in Fig. 2. Most of the electronic circuitry was constructed using a modular system (McKee-Pedersen Instruments, Danville, Calif.). The square-wave generator consisted of conventional circuitry with a couple of integrated circuits. The amplitude of the square-wave could be accurately controlled. The gated integrator (lock-in amplifier) was as described previously [6]. The average anode current of the photomultiplier was maintained constant by a feedback loop consisting of operational amplifiers OA1 and OA2 and a programmable high-voltage supply (MP-1030A). Output from OA1 was demodulated by the lock-in amplifier and recorded on a strip-chart recorder.

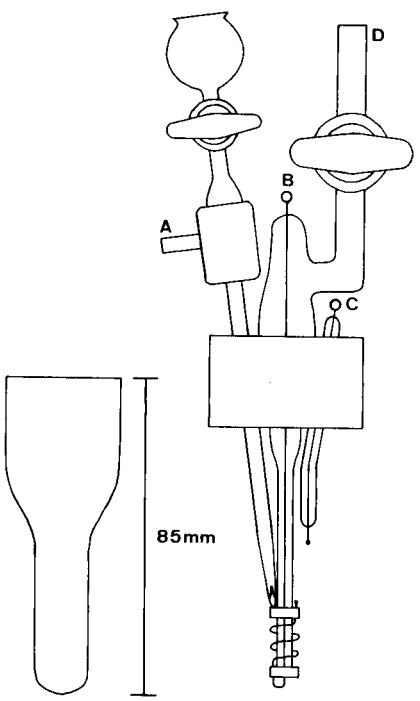

Fig. 1. Cell for generating electrochemiluminescence.

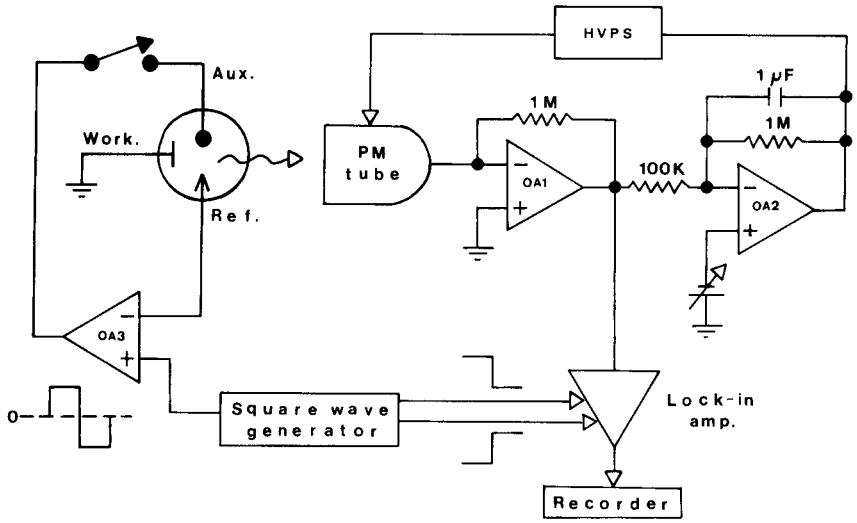

Fig. 2. Circuitry for pulsed electrochemiluminescence apparatus.

Reagents

The water used was distilled once from a conventional large-scale stainless steel unit and then from a quartz double distillation unit. Luminol (Fluka AG, pract.) was crystallized from hot (80°C) 1 M sodium hydroxide solution. The crystals of the sodium salt of luminol were filtered off, redissolved in water, and precipitated by neutralizing with 0.5 M hydrochloric acid. The precipitate was filtered off and washed with water. The purity of luminol could not be assessed from its melting point because of decomposition. Molar absorptivity was chosen as the criterion of purity because previous information about its value was available. The value of the molar absorptivity at 347.5 nm in 0.1 M sodium hydroxide solution was 7480 l mol^{-1} cm^{-1} for the purified luminol, compared to 6980 l mol^{-1} cm^{-1} for the unpurified compound. The molar absorptivities reported previously are 7440 l mol^{-1} cm^{-1} [5] and 7470 l mol^{-1} cm^{-1} [7].

Stock solutions of luminol were prepared by dissolving purified luminol in 0.02 M sodium hydroxide solution to give a 0.01 M luminol solution. Solutions of luminol prepared by dilution of the stock solution were stored in a polypropene bottle under nitrogen.

All the other reagents were of analytical grade; their solutions were also stored in polypropene bottles.

Procedure

The sample solution (10 ml) with appropriate amounts of sodium chloride, glycine buffer and luminol, was pipetted into the cell, and oxygen was bubbled through the solution for 5 min. The cell was immediately transferred into the measuring chamber and the cell voltage set to the required value. The output from the lock-in amplifier was followed by a recorder and the maximum emission intensity measured.

RESULTS AND DISCUSSION

Both the chemiluminescent and electrochemiluminescent reactions of luminol take place only in alkaline solutions. Heavy metal ions present may be precipitated or adsorbed as hydroxides on the walls, under the alkaline conditions, unless a complexing agent is added. However, the metal complexes formed should not be too stable or vacant coordination sites should be available, to preserve the catalytic efficiency of the metal ions. For instance, EDTA forms very stable complexes, and inhibits completely the catalytic influence of metal ions on the luminol—hydrogen peroxide reaction [8].

Copper(II) has a profound influence on the intensity of chemiluminescence of the reaction between luminol and hydrogen peroxide. On the other hand, copper(II) and glycine do not form higher than 1:2 complexes to any significant extent, so that two coordination sites are left available for the potential catalytic effect. Hence copper(II) in a glycine buffer was chosen to test the feasibility of electrochemiluminescence of luminol for trace metal analysis.

During the preliminary experiments, it was soon found that the addition of copper(II) had no dramatic effect on the total intensity of the electrochemiluminescence of luminol. However, when a pulse excitation was used with alternate positive and negative pulses applied to the working electrode and the shape of the light pulses was observed, it was found that copper(II) had a considerable effect, even in trace quantities, on the rise and fall times of the light pulses (Fig. 3). The effect on the rise and the fall times is somewhat different and consequently increased copper(II) concentration causes increased asymmetry in the shape of the light pulse. Gated integration proved to be an excellent method for measuring this asymmetry. The halves of the light pulses corresponding to the positive and negative excitation pulses were integrated and subtracted from each other. The average output of the photomultiplier was kept constant by a feedback system so that the only contribution to the signal was the relative inequality of the pulse halves.

The emission—time response obtained in this way had a sharp initial peak and subsequent slowly varying amplitude as shown in Fig. 4. A minimum was

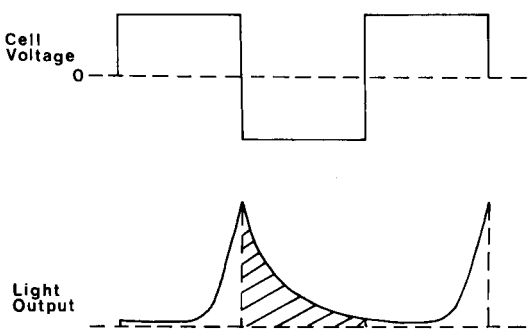

Fig. 3. Cell voltage pulses and corresponding light pulses.

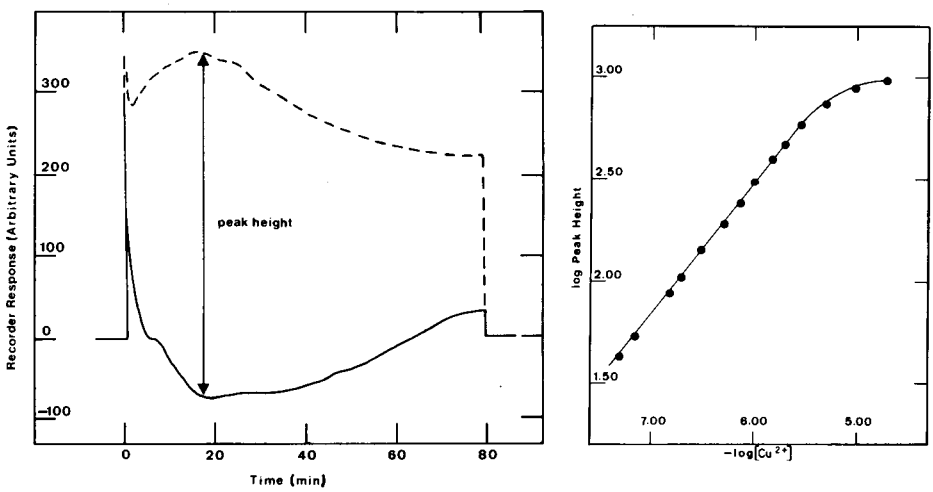

Fig. 4. Electrochemiluminescence signals for solutions of luminol with (— — —) and without (——) added copper(II).

Fig. 5. Log—log calibration curve for copper(II). Conditions: pulse amplitude 1160 mV, pulse width 44.0 ms, pH 10.15, luminol concentration 1.00×10^{-4} M, glycine concentration 5.00×10^{-2} M, sodium chloride added to give an ionic strength of 0.11.

obtained with a solution without added copper and a maximum obtained after 20 min with copper-containing solutions. The signal was reproducible, and could be used to measure copper, as can be seen in the calibration graph (Fig. 5).

Attempts were made to maximise the response for copper(II) and minimize the blank emission by varying the pulse amplitude (Fig. 6), pulse duration (Fig. 7), pH (Fig. 8) and luminol concentration (Fig. 9). The conditions for minimal blank value and greatest response to copper were those given in the caption to Fig. 5. This log—log plot is linear from 6×10^{-6} M down to at least 1×10^{-7} M copper. The slope is 0.64, showing that the response function is highly non-linear.

The method of measurement (light-pulse asymmetry) does not allow any conclusions easily to be drawn on the possible mechanism of the electrochemiluminescence of luminol. If the plausible proposition of Kuwana et al. [3—5] is adopted, i.e., that the primary intermediate in the electrochemiluminescence is the one-electron oxidation product of the luminol anion, the catalytic effect of copper(II) on the shape of the light pulses can be predicted. During the positive pulse this oxidation product is formed and simultaneously its chemiluminescent reaction with oxygen and/or hydrogen peroxide catalyzed by copper(II) begins. This reaction continues during the negative pulse when more hydrogen peroxide is formed, but the intensity is greater during the positive pulse.

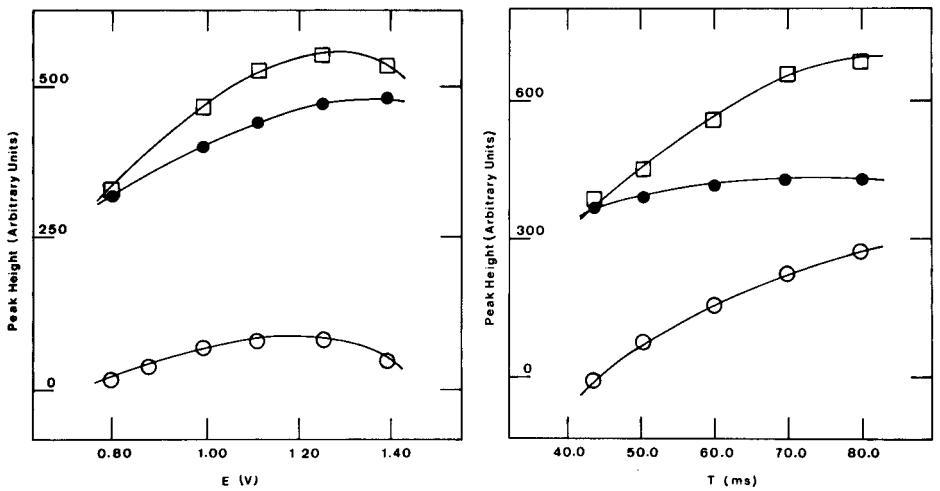

Fig. 6. Effect of pulse amplitude on the response signal. Conditions as Fig. 5, except for pulse width 50.0 ms. [Cu^{2+}]: (□) 5 × 10^{-5} M, (○) 0, (•) difference signal.

Fig. 7. Effect of pulse width on the response signal. Conditions as Fig. 5, except for pulse amplitude 1000 mV. [Cu^{2+}]: (□) 5.0 × 10^{-5} M, (○) 0, (•) difference signal.

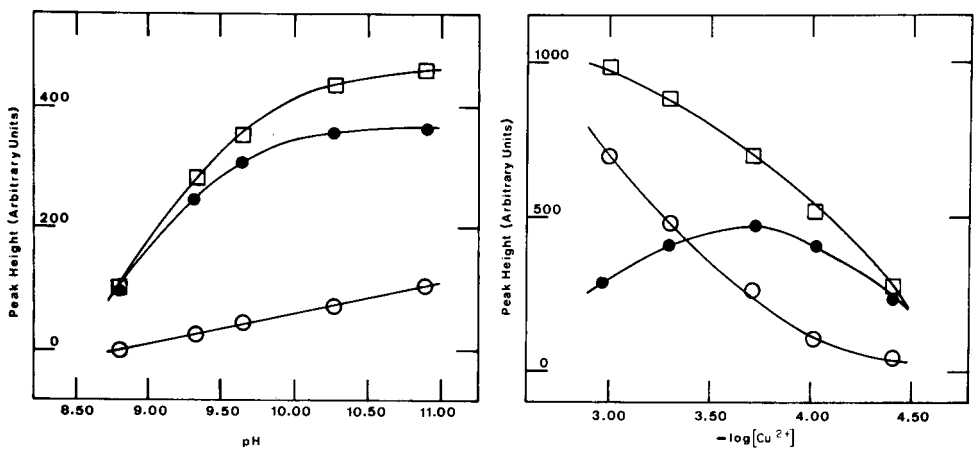

Fig. 8. Effect of pH on the response signal. Conditions: pulse amplitude 1000 mV, pulse width 50.0 ms, luminol concentration 1.00 × 10^{-4} M, glycine concentration 5.00 × 10^{-2} M, sodium chloride added to give an ionic strength of 0.11. [Cu^{2+}]: (□) 5 × 10^{-5} M, (○) 0, (•) difference signal.

Fig. 9. Effect of luminol concentration on the response signal. Conditions as Fig. 8, except for, pulse width 55.0 ms and pH 10.15 [Cu^{2+}]: (□) 5 × 10^{-5} M, (○) 0, (•) difference signal.

Interference by other metal ions

Table 1 shows the influence of ten metal ions on the electrochemiluminescence of luminol catalyzed by copper(II). It is seen that Cd(II), Co(II), Ni(II), Zn(II), Al(III), Cr(III) and Fe(III) do not produce appreciable interference even at ca. 7-fold molar concentration. This is interesting, especially for Co(II) and Cr(III) which do have a considerable influence on the normal chemiluminescent reactions of luminol. Hg(II) and Mn(II) increase the response and Pb(II) has an inhibitory influence. A partial explanation for the different behavior of metal ions is provided by the complexation with the buffer medium. Cadmium(II), Co(II), Ni(II), Cr(III) and Zn(II) are known to form 1:3 complexes with glycine and thus all the coordination sites of the metal ion are blocked for catalytic action. The 1:3 complexes of Cu(II), Hg(II), Mn(II) and Pb(II) do not have significant stabilities and vacant coordination sites for complexation with luminol and/or electrogenerated hydrogen peroxide are available. Some corroboration is given by the studies of Kovats [9] according to which the square-planar complexes of transition metals catalyze the decomposition of hydrogen peroxide, whereas the corresponding octahedral complexes are ineffective.

The inhibitory effect of lead(II) may be due to the anodic formation of lead dioxide, which is one of the most potent catalysts for the decomposition of hydrogen peroxide [10].

CONCLUSION

There are numerous methods capable of determining copper(II) at the same or even lower concentration levels than the method presented in this paper. The main purpose of this paper, however, is to point out the potenti-

TABLE 1

Effect of ten common cations on the determination of copper(II) (Conditions as in Fig. 5.)

Cation[a]	Cation conc. (M)	Peak height (arbitrary units)	Cation[a]	Cation conc. (M)	Peak height (arbitrary units)
—	—	100	Hg(II)	5.0×10^{-6}	158
Cd(II)	1.0×10^{-5}	99		1.0×10^{-6}	122
Co(II)	1.0×10^{-5}	101		5.0×10^{-7}	100
Ni(II)	1.0×10^{-5}	100	Mn(II)	5.0×10^{-6}	163
Zn(II)	1.0×10^{-5}	101		1.0×10^{-6}	130
Al(III)	1.0×10^{-5}	100		5.0×10^{-7}	119
Cr(III)	1.0×10^{-5}	102		2.0×10^{-7}	111
Fe(III)	1.0×10^{-5}	98	Pb(II)	5.0×10^{-6}	44
				1.0×10^{-6}	86
				5.0×10^{-7}	98

[a] All solutions are 1.5×10^{-6} M in copper(II).

alities of trace analytical methods based on electrochemiluminescence. It is quite possible that further optimization may extend the present method to lower concentrations, and the use of other sequestering agents and electrochemiluminescent systems may allow the determination of other elements. A more exact geometry of the working electrode may allow easier interpretation of the results and give a clue to the mechanism of the processes. Work along these lines is in progress.

Financial support for this work from the Emil Aaltonen Foundation and the National Council for Sciences, Finland, is gratefully acknowledged.

REFERENCES

1 W. R. Seitz and M. P. Neary, Anal. Chem., 46 (1974) 188A, and references cited therein.
2 D. C. Williams III, G. F. Huff and W. R. Seitz, Anal. Chem., 48 (1976) 1003.
3 T. Kuwana, B. Epstein and E. Seo, J. Phys. Chem., 67 (1963) 2243.
4 T. Kuwana, J. Electroanal. Chem., 6 (1963) 164.
5 B. Epstein and T. Kuwana, Photochem. Photobiol., 4 (1965) 1157; 6 (1967) 605; J. Electroanal. Chem., 15 (1967) 389.
6 J. J. Kankare and K. E. Haapakka, Anal. Chim. Acta, 111 (1979) 79.
7 E. K. Hodgson and I. Fridovich, Photochem. Photobiol., 18 (1973) 451.
8 W. R. Seitz, W. W. Suydam and D. M. Hercules, Anal. Chem., 44 (1972) 957.
9 Z. Kovats, Magy. Kem. Folyoirat, 69 (1963) 98; Chem. Abstr., 59 (1963) 2368f.
10 W. C. Schumb, C. N. Satterfield and R. L. Wentworth, Hydrogen Peroxide, Reinhold, New York, 1955, p. 479.

Analytica Chimica Acta, 118 (1980) 341—358

A CRITICAL EVALUATION OF SHORT-LIVED AND LONG-LIVED NEUTRON ACTIVATION PRODUCTS FOR TRACE ELEMENT DETERMINATIONS

R. E. TOUT and A. CHATT*

Trace Analysis Research Centre, Department of Chemistry, Dalhousie University, Halifax, Nova Scotia, B3H 4J1 (Canada)

(Received 19th December 1979)

SUMMARY

The application of short-lived nuclides in routine instrumental neutron activation analysis can reduce total experimental time per sample. The experimental sensitivities of short- and long-lived thermal neutron activation products of 32 elements are compared. The advantages of using short-lived nuclides are evaluated by comparing the precision, accuracy, and detection limits, using both short- and long-lived nuclides, for elemental determinations in biological, environmental and geological standard reference materials.

Instrumental neutron activation analysis (i.n.a.a.) is a well-established analytical technique for multielement determinations in a variety of complex sample matrices. The half-lives of the neutron activation products generally used in i.n.a.a. measurements span many orders of magnitude of time; e.g., lead concentrations have been determined [1] by using the ^{207m}Pb nuclide ($t_{1/2}$ = 0.8 s) while cobalt is routinely determined through ^{60}Co ($t_{1/2}$ = 5.24 years). In order to approach the maximum sensitivity obtainable by i.n.a.a. for each of several elements in a given sample, it is usually necessary to perform a series of experiments with different irradiation, decay and counting periods, optimized for the detection of nuclides with a specific range of half-lives. Thus the attractiveness of i.n.a.a. as a simultaneous multi-element technique is often partly negated by it also being a multi-experiment technique.

Some elements, under thermal neutron bombardment, produce only one nuclide which can conveniently be utilized for i.n.a.a., e.g. ^{207m}Pb ($t_{1/2}$ = 0.8 s), ^{20}F (11 s), ^{27}Mg (9.5 min), ^{51}Cr (27.8 d), ^{160}Tb (72.1 d); in such cases, the half-life of the nuclide under investigation dictates the length of sample irradiation, decay, and counting periods, and thus the total experiment time per determination. There are, however, several elements which produce more than one γ-ray emitting nuclide by thermal neutron capture; this is because either they possess more than one stable isotope in the natural state or they form a radioactive metastable state in addition to the expected (n, γ) product. Both types of activation products are illustrated by the nuclides of selenium, which are listed in Table 1. It is feasible to use any of these nuclides

TABLE 1

Comparison of total experimental time for determining Sc and Se by i.n.a.a.

Element	Activation reaction	Cross-section (barns)	Nuclide half-life	Irradiation time (t_i)	Decay time (t_d)	Counting time (t_c)	Total experiment time ($t_i + t_d + t_c$)
Sc	$^{45}Sc(n, \gamma)^{46}Sc$	13	84 d	16 h	~7 d	1 h	~8 d
	$^{45}Sc(n, \gamma)^{46m}Sc$	10	20 s	90 s	15 s	90 s	195 s
Se	$^{74}Se(n, \gamma)^{75}Se$	30	120 d	16 h	~7 d	1 h	~8 d
	$^{76}Se(n, \gamma)^{77m}Se$	22	17.5 s	90 s	15 s	90 s	195 s
	$^{78}Se(n, \gamma)^{79m}Se$	0.36	3.9 min				
	$^{80}Se(n, \gamma)^{81}Se$	0.5	18 min				
	$^{80}Se(n, \gamma)^{81m}Se$	0.1	57 min				
	$^{82}Se(n, \gamma)^{83}Se$	0.004	25 min				
	$^{82}Se(n, \gamma)^{83m}Se$	0.05	70 s				

for elemental determinations; the maximum sensitivity obtainable for each nuclide depends on its nuclear data and the proximity of experimental conditions to the optimum timing parameters. The use of the short-lived nuclides of elements for routine i.n.a.a., in preference to their longer-lived activation products, can significantly reduce the total experimental time, which in turn can lead to more efficient use of reactor and counting facilities, and thus make this analytical technique more cost-effective. However, the effect on important analytical parameters such as precision, accuracy, and sensitivity of measurements by the use of short-lived nuclides will have to be evaluated prior to their exclusive application in routine determinations. The objective of the present study is critically to evaluate and compare the usefulness of short- and long-lived reactor-flux thermal-neutron activation products for trace multielement determinations in biological, environmental and geological standard reference materials (SRM).

For the purpose of the work reported here, the short-lived nuclides are arbitrarily defined as having half-lives less than 1 h and the long-lived nuclides as having half-lives longer than 12 h. At least 38 elements (listed in Table 3) are known to be capable of producing both short- and long-lived nuclides by thermal neutron capture. Using a standard set of 'short' and 'long' irradiation, decay and counting conditions, the sensitivities for the best short- and long-lived nuclides of 32 of these elements have been determined. Eleven SRM of various types have been analysed by applying the standard experimental conditions. The precision and accuracy of measurements using short- and long-lived nuclides have been compared. The elemental detection limits of the 32 short- and long-lived pairs of nuclides have also been calculated for the SRM analyzed. From these results it can be evaluated whether or not short-lived nuclides (with their time-saving advantage) can be applied exclusively, by using one set of experimental conditions, for the analysis of a variety of matrix types.

EXPERIMENTAL

The sensitivities of short- and long-lived nuclides were determined by irradiating monoelement comparator standards. These were prepared by depositing between 1 and 5,000 μl of '1,000 ppm atomic absorption standard solutions (Alfa-Ventron Corporation)' on Nuclepore polycarbonate membranes. The spotted membranes were evaporated to dryness at low heat under an infrared lamp and then sealed in polyethylene sample capsules. These monoelement comparator standards were also used for determining elemental content of the SRM.

The biological, environmental, and geological SRM analysed were provided by a number of agencies. The U.S. National Bureau of Standards (NBS) supplied the Spinach (NBS SRM-1570), Orchard Leaves (NBS SRM-1571), Bovine Liver (NBS SRM-1577), Bituminous Coal (NBS SRM-1632a) and Sub-bituminous Coal (NBS SRM-1635). The U.S. Geological Survey (USGS) provided the Granite (USGS G-2), Peridotite (USGS PCC-1) and Marine Mud (USGS MAG-1). The soil (IAEA S-5) was obtained from the International Atomic Energy Agency (IAEA), the Fish Flour (ICES Intercalibration in 1975) from the International Council for the Exploration of the Sea (ICES), and the Pepperbush (NIES No. 1) from the Japanese National Institute for Environmental Studies (NIES). The SRM were freeze-dried according to the methods prescribed by the respective agencies, and weighed into 1.5-ml polyethylene vials which were then heat-sealed.

All samples and standards were irradiated in the Dalhousie University SLOWPOKE-2 Reactor (DUSR) at a flux of either 1×10^{11} or 5×10^{11} n cm^{-2} s^{-1}. The details of operating range, composition, homogeneity, and reproducibility of the DUSR neutron flux have been reported [2]. Samples, standards, and Cu and Fe flux monitors were irradiated for 90 s and 16 h for the study of short- and long-lived nuclides, respectively.

Gamma-ray spectra of all irradiated materials were acccumulated using a spectrometry system consisting of a 60-cm^3 Canberra Ge(Li) detector (full width at half-maximum of 1.9 keV at the 1332.4-keV γ-ray of ^{60}Co, peak-to-Compton ratio of 35:1, and an efficiency of 9.5%) linked to a Tracor Northern 50MHzADC and a TN-11 model 4096-channel pulse-height analyser.

RESULTS AND DISCUSSION

The use of short-lived neutron activation products in preference to longer-lived nuclides can lead to a significant reduction of total experimental time. A comparison of two possible sets of i.n.a.a. timing parameters than can be used for determining scandium and selenium through their most sensitive short- and long-lived nuclides is shown in Table 1. Scandium is present in the natural state only as ^{45}Sc which produces ^{46}Sc ($t_{1/2}$ = 84 d) and ^{46m}Sc ($t_{1/2}$ = 20 s) on irradiation with thermal neutrons, whereas selenium has

six naturally occurring isotopes which give rise to seven nuclides with half-lives ranging from as short as 17.5 s to as long as 120 d (Table 1). The advantage in time-saving brought about by the use of the short-lived nuclides of these two elements is obvious as the total experimental time can be reduced from more than a week to 3.25 min. The selection of the experimental conditions used for determining these and other nuclides are discussed below.

Table 2 shows the two standard sets of irradiation, decay and counting times used in this work for determination by short- and long-lived nuclides. Like all sets of timing parameters used in multi-element i.n.a.a. studies, these values are a compromise and are obviously better suited to some of the nuclides (listed in Table 3) than others. The short irradiation time (t_i = 90 s), decay time (t_d = 15 s), and counting time (t_c = 90 s) are optimum for nuclides with half-lives ranging between 10 s and about 3 min. For example, for ^{46m}Sc and ^{77m}Se the t_i is approximately equal to 5 × $t_{1/2}$ (Table 1) so that the activities of the nuclides are close to their saturation levels. In studies involving short-lived nuclides, the t_d should be as short as possible. Although 10 s is the shortest feasible manual transfer time at the DUSR facility [3], a t_d of 15 s was selected to ensure easily achieved reproducibility of nuclides with half-lives as short as 6.5 s. A t_c of 90 s (approximately 5 × $t_{1/2}$ of ^{46m}Sc and ^{77m}Se) covers the period over which most of the induced activity of the short-lived nuclide is measured. A large sample-to-detector distance (ca. 45 mm) was needed to study the short-lived nuclides in the highly active SRM samples, when irradiated and counted as described above, in order to maintain the dead time at a reasonable level.

In studies involving long-lived nuclides, the t_i and t_c should be as long as possible to obtain minimum detection limits. However, the realistic values of t_i and t_c (Tables 1 and 2) were those imposed by the availability of irradiation and counting times. The value assigned to t_d is the principal component of the experiment time when analysis is performed using long-lived nuclides. For optimum detection limits, t_d should be sufficiently long so that the contribution from any undesired short-lived nuclide to the background activity of the sample is minimal. Although the selected t_d of approximately

TABLE 2

Standard experimental conditions for determining short- and long-lived nuclides

	t_i	t_d	t_c	Sample-detector distance (mm)	Flux (n cm^{-2} s^{-1})	Sample size (mg)
'Short' half-life conditions	90 s	15 s	90 s	~45	1 × 10^{11} 5 × 10^{11}	25—250
'Long' half-life conditions	16 h	~7 d	1 h	~5	5 × 10^{11}	50—250

TABLE 3

Nuclear data and sensitivity ratios of short- and long-lived nuclides

Element	Short-lived nuclide used	Half-life	Energy of most intense γ-ray (keV)	Long-lived nuclide used	Half-life	Energy of most intense γ-ray (keV)	Sensitivity ratio of long- to short-lived nuclides
Antimony	^{122m}Sb	4.2 min	61	^{122}Sb	2.8 d	564	4.1×10^{3}
Barium	^{139}Ba	84 min	166	^{131}Ba	12 d	124	4.5×10^{1}
Bromine	^{80}Br	18 min	617	^{82}Br	36 h	554	1.5×10^{2}
Cadmium	^{111m}Cd	49 min	245	^{115}Cd (^{115m}In)	54 h (4.5 h)	335[a]	8.9×10^{2}
Calcium	^{49}Ca	8.9 min	3083	^{47}Ca (^{47}Sc)	4.7 d (3.43 d)	160[a]	1.2×10^{1}
Cerium	^{139m}Ce	55 s	746	^{141}Ce	33 d	145	>1
Cobalt	^{60m}Co	10.5 min	59	^{60}Co	5.3 y	1173	1.5×10^{1}
Copper	^{66}Cu	5.2 min	1039	^{64}Cu	12.8 h	1346	1.3×10^{-2}
Dysprosium	^{165m1}Dy	1.3 min	108	^{159}Dy	140 d	58	<1
Gadolinium	^{161}Gd	3.6 min	361	^{153}Gd	240 d	99	9.8×10^{0}
Gallium[b]	^{72}Ga	14 h	835	^{72}Ga	14 h	835	1.9×10^{1}
Germanium	^{75m}Ge	49 s	139	^{77}Ge	12 h	263	1.3×10^{-3}
Hafnium	^{179m}Hf	19 s	214	^{181}Hf	45 d	133	1.5×10^{0}
Indium	^{116m1}In	54 min	417	^{114m}In	50 d	192	1.2×10^{0}
Iridium	^{192m1}Ir	1.4 min	58	^{192}Ir	74 d	317	2.2×10^{4}
Mercury	^{199m}Hg	43 min	158	^{203}Hg	47 d	279	3.6×10^{3}
Molybdenum	^{101}Mo	15 min	590	^{99}Mo	67 h	140	6.8×10^{3}
Neodymium	^{151}Nd	12 min	116	^{147}Nd	11 d	91	1.2×10^{2}
Niobium	^{94m}Nb	63 min	871	^{94}Nb	2×10^{4} y	702	<1
Osmium	^{190m}Os	9.9 min	187	^{193}Os	31 h	139	not detd.
Palladium	^{109m}Pd	4.7 min	188	^{109}Pd	13.5 h	88	4.4×10^{-1}
Platinum	^{199}Pt	30 min	540	^{195m}Pt	4.1 d	99	1.6×10^{2}
Rhenium	^{188m}Re	18.7 min	106	^{186}Re	3.8 d	137	5.6×10^{3}
Rubidium	^{86m}Rb	1 min	556	^{86}Rb	18.7 d	1078	4.2×10^{0}
Samarium	^{155}Sm	23 min	104	^{153}Sm	47 h	103	1.7×10^{3}
Scandium	^{46m}Sc	20 s	142	^{46}Sc	84 d	889	4.8×10^{0}
Selenium	^{77m}Se	17.5 s	161	^{75}Se	120 d	136	2.6×10^{0}
Silver	^{110}Ag	24 s	658	^{110m}Ag	250 d	658	1.8×10^{0}
Strontium	^{87m}Sr	2.8 h	388	^{85}Sr	64 d	514	1.9×10^{1}
Tantalum	^{182m}Ta	16 min	172	^{182}Ta	115 d	1121	2.2×10^{3}
Tellurium	^{131}Te	25 min	150	^{123m}Te	120 d	159	9.7×10^{0}
Thorium	^{233}Th	22 min	87	^{233}Th (^{233}Pa)	22 min (27 d)	312[a]	8.0×10^{2}

TABLE 3 (continued)

Element	Short-lived nuclide used	Half-life	Energy of most intense γ-ray (keV)	Long-lived nuclide used	Half-life	Energy of most intense γ-ray (keV)	Sensitivity ratio of long- to short-lived nuclides
Tin	^{125m}Sn	9.7 min	332	^{113}Sn	120 d	255	<1
Tungsten[c]	^{187}W	24 h	479	^{187}W	24 h	479	8.0×10^2
Uranium	^{239}U	24 min	75	^{239}U (^{239}Np)	24 min (2.4 d)	106[a]	5.8×10^1
Xenon	^{137}Xe	3.9 min	662	^{133m}Xe	2.3 d	233	not detd.
Ytterbium	^{177m}Yb	6.5 s	104	^{175}Yb	100 h	396	1.6×10^3
Zinc	^{69m}Zn	13.8 h	439	^{65}Zn	240 d	1115	1.4×10^3

[a]The γ-ray peak measured at this energy is due to daughter radiations resulting from the β^- decay of the isotope of interest. (Parentheses indicate the daughter nuclide and associated half-life.) [b] ^{70}Ga with 21.0-min half-life was not studied here. [c]Short-lived tungsten nuclides were not studied here.

7 d was designed to encompass nuclide half-lives of between 12 h and 2×10^{-4} years, it favours the relatively 'shorter-lived' of the long-lived nuclides. After 7-d decay, the activity of the SRM samples was such that a minimal sample-detector distance of ca. 5 mm could be used.

Table 3 lists 38 elements which are known to produce more than one thermal neutron activation product, with half-lives ranging from less than 1 h to more than 12 h. The sensitivity (counts per μg of the element) of each of the short- and long-lived nuclides was calculated from the most intense photopeak of the most active product under the experimental conditions given in Table 2. Among all the short-lived activation products of an element detected using the short experimental conditions, the most sensitive nuclide was not always the one with a 'short' half-life as defined for this study, e.g. ^{139}Ba ($t_{1/2}$ = 1.4 h) was found to have a greater sensitivity than ^{137m}Ba ($t_{1/2}$ = 2.6 min). Similarly, ^{87m}Sr ($t_{1/2}$ = 2.8 h) and ^{69m}Zn ($t_{1/2}$ = 13.9 h) were found to be the most sensitive nuclides for determining these two elements using the short experimental conditions (Table 2).

Although the most intense photopeak of the most active nuclide of each element was used in calculating the sensitivity, it was not always possible to use the same peak for determining the elemental content of the SRM, because of interfering reactions or overlapping γ-ray peaks in the accumulated spectrum. An example of an interfering reaction encountered in this work was ^{47}Ti (n, p)^{47}Sc which gave rise to errors in calcium determinations in geological materials containing significant amounts of titanium. The interference of γ-rays of similar energy was observed in the determination of hafnium, where its most sensitive γ-ray peak at 133.1 keV (from ^{181}Hf) was found to be interfering with the 133.7-keV γ-ray peak of ^{131}Ba in several samples; therefore, the alternative 482.2-keV photopeak of ^{181}Hf was used.

The sensitivity ratio of long- to short-lived nuclide for an element (Table 3) gives an indication of how useful a particular short-lived nuclide might be in determining that element. A ratio of one shows that the sensitivities of the short- and long-lived nuclides are about the same, values less than one indicate that the use of the short-lived nuclide should be more favourable than the long-lived, and the opposite is true for ratios greater than one. Although it is evident from Table 3 that the number of values greater than one far exceeds those less than one (by 30 to 6), the relative usefulness of the short- and long-lived nuclides will also depend on the actual concentration of the particular element in a given sample as well as on the contribution of the other elements comprising the sample matrix. If the concentration of the element of interest in a matrix is above the detection limit obtained using short experimental conditions, the concentration of that element can be determined through the short-lived nuclide even though the sensitivity ratio of the long- to short-lived nuclides is greater than unity. The effect of background activity in a γ-ray spectrum on the relative applicability of short- and long-lived nuclides can be demonstrated by the determination of calcium. The ratio of sensitivities for calcium (Table 3) shows the long-lived nuclide to be more sensitive than the short-lived one. However, the background activity in the region of the 3083-keV photopeak of ^{49}Ca ($t_{1/2}$ = 8.9 min) is almost certain to be very much lower than around the 160-keV photopeak of ^{47}Sc ($t_{1/2}$ = 3.43 d). Consequently, the magnitude of the two detection limits for calcium will probably be much closer in actual sample matrices than the ratio of sensitivities would at first suggest (Table 3).

In order to evaluate the matrix effect fully for a range of sample types used in i.n.a.a., various biological, environmental and geological SRM (Table 4) were analyzed. The total activity of the irradiated samples was invariably found to be greater for the short experimental condition than the long, which was generally due to the presence of ^{28}Al ($t_{1/2}$ = 2.3 min). The ^{28}Al nuclide can be produced by three reactions with neutrons of the range of energies present in the DUSR: $^{27}Al(n,\gamma)^{28}Al$, $^{28}Si(n,p)^{28}Al$, and $^{31}P(n,\alpha)^{28}Al$. The last two reactions are important in analyses of materials with high silicon content (such as geological samples) and high phosphorus levels (such as some biological samples). Known concentrations of aluminium, phosphorus and silicon of the eleven SRM analyzed in this work are shown in Table 4. The aluminium concentrations of the ICES Fish Flour and the IAEA Soil are given as only approximate values and are not corrected for contributions from phosphorus and silicon owing to the lack of appropriate data.

Sample masses of approximately 250 mg of each of the SRM were irradiated, as recommended by some of the suppliers, to eliminate errors arising from inhomogeneity. If such a sample mass produced a dead time of greater than 10% (measured by the ADC), the normal operating flux of 5×10^{11} n cm^{-2} s^{-1} was reduced by a factor of five. In the event that the resulting dead time was still too high, then the sample mass was reduced. From Table 4 it can be seen that both flux and sample mass had to be reduced only for the

TABLE 4

The Al, P and Si content and experimental parameters of materials analyzed

Sample material	Al($\mu g\ g^{-1}$)	Si(%)	P(%)	Short-lived nuclides			Long-lived nuclide	
				Avg. mass of sample (mg)	Flux ($\times 10^{11}$ n $cm^{-2}s^{-1}$)	ADC dead time (%)	Avg. mass of sample (mg)	Flux ($\times 10^{11}$ n $cm^{-2}s^{-1}$)
Fish Flour (ICES)	~60[a]	—	—	252.9	5	8	252.9	5
Bovine Liver (NBS SRM-1577)	35.5[b]	0.00167[b]	1.36[b]	255.1	5	3	255.1	5
Spinach (NBS SRM-1570)	870 ± 50[c]	—	0.55 ± 0.02[c]	258.2	1	5	258.2	5
Orchard Leaves (NBS SRM-1571)	410[b]	0.048[b]	0.21 ± 0.01[d]	253.2	5	7	253.2	5
Pepperbush (NIES No. 1)	567 ± 30[a]	—	—	250.2	1	6	250.2	5
Soil (IAEA S-5)	~8%[a]	—	—	25.6	1	20	252.7	5
Bituminous Coal (NBS SRM-1632a)	3.07%[e]	—	—	52.0	1	14	254.2	5
Subbituminous Coal (NBS SRM-1635)	0.32%[f]	—	—	51.5	1	2	219.2	5
Granite (USGS G-2)	8.15%[g]	32.3[g]	0.061[g]	26.1	1	19	51.7	5
Peridotite (USGS PCC-1)	0.39%[g]	19.6[g]	0.0009[g]	50.4	1	3	55.9	5
Marine Mud (USGS MAG-1)	8.7%[h]	23.2[h]	0.14[h]	28.9	1	18	49.4	5

[a]This work. [b]Ref. 5. [c]Ref. 17. [d]Ref. 18. [e]Ref. 24. [f]Ref. 26. [g]Ref. 9. [h]Ref. 29.

analyses of geological materials because of their high aluminium and silicon levels. In a number of cases, the dead time obtained was still significantly higher than desirable even when sample mass was reduced to as little as 25 mg (Table 4). The low levels of aluminium in the biological SRM did not necessitate any reduction in either sample size or flux, except for the NBS Spinach where the flux had to be reduced. The quantities of phosphorus present in the biological SRM were insufficient to influence the ^{28}Al response greatly; it was determined that, under the short experimental conditions used here, approximately 440 times as much phosphorus was needed to produce the same ^{28}Al signal as that due to the aluminium alone.

Thus the analysis of the geological SRM using the short experimental conditions is already at a disadvantage, compared to the analysis based on the long experimental conditions, because of the lower flux and sample masses, as well as the greater sample to detector distance (Tables 4 and 2). Sample masses smaller than the standard 250 mg were also used for the long irradiations of the USGS Standard Rocks because of their high sodium contents.

Elemental content (average of three determinations) of the eleven SRM analyzed by short and long experimental conditions are shown in Table 5. It can be seen that only in the biological SRM with a low aluminium content were a significant number of elements determined when the short irradiation

conditions were used. For example, in the ICES Fish Flour more elements could be determined in a total experiment time of 3.25 min than by using the long irradiation conditions described in Table 2. However, in most of the SRM analyzed, especially those with high aluminium content (and hence a small sample mass was irradiated at a low flux using short experimental conditions), more of the elements listed in Table 3 were determined by using long-lived nuclides rather than short-lived ones.

Five elements, namely Br, Ca, Hf, Rb and Sc, were determined using both sets of experimental conditions in one or more of the SRM analyzed. A comparison of the results obtained for these elements (Table 5) will show the usefulness of their short-lived nuclides in routine elemental analyses. Bromine was determined by both sets of experimental conditions only in the ICES Fish Flour; the agreement between the two values was good, and both values (within the limit of quoted errors) coincided with the literature value [4]. Although bromine could not be determined by its short-lived nuclide in the NBS Bovine Liver and Spinach, its detection limits were near the concentrations reported in the literature [5—7].

Calcium was determined in four biological SRM using the long experimental conditions but could only be determined in two of these SRM by using short timing parameters although the detection limits of calcium through its short-lived nuclide (Table 5) were lower than the actual calcium concentrations in the other two biological SRM (Spinach and Pepperbush). This observation indicates that if the background counts under a photopeak tend to zero (e.g. the 3083-keV peak of ^{49}Ca), Currie's L_D value [8] is insufficient to describe the detection limit.

Hafnium concentrations were determined in four of the geological and environmental SRM analyzed. It was possible to determine the hafnium content of USGS G-2 by both short- and long-lived nuclides, and the agreement between the two values is good although both are slightly higher than those reported in the literature [9, 10]; this difference may be due to the small sample size used in this study (Table 4). The amounts of hafnium in the other three geological and environmental SRM were only measured using the long-lived nuclide but in each case the amount was not greatly in excess of the detection limit for the short-lived hafnium nuclide, indicating that optimized short experimental conditions are probably viable for hafnium determinations in a number of geological samples.

Although rubidium concentrations were determined in five of the SRM, the short experimental conditions were successfully applied to only one, namely the NBS Bovine Liver. It can be seen from Table 5 that the short-lived rubidium nuclide not only produced a result closer to the certified value than the long-lived nuclide, but also gave a lower detection limit. However, a two-week decay of the long-lived nuclide produced a greatly improved detection limit of 3 $\mu g\ g^{-1}$ for rubidium. The rubidium concentrations of the Orchard Leaves and Pepperbush SRM are not greatly exceeded by their respective detection limits; however, the elevated detection limits for the

TABLE 5

Elemental content of materials analyzed using short- and long-lived nuclides

Sample material	Elements	Content (in $\mu g\ g^{-1}$ unless otherwise stated)		
		Short-lived nuclide (detection limit)	Long-lived nuclide (detection limit)	Literature value
Fish Flour (ICES)	Br	50.4 ± 7.3 (17)	50.0 ± 3.8 (0.9)	43.6 ± 4.0[a]
	Ca,%	1.25 ± 0.12 (0.1)	1.57 ± 0.16 (0.3)	1.67 ± 0.104[a]
	Se	1.37 ± 0.37 (1.3)	<2.1	1.35 ± 0.11[a]
	Others[b]	Al, Cl, I, Mn, Na	As, Fe, K, Na	
Bovine Liver (NBS SRM-1577)	Br	<9.9	11 ± 1 (0.6)	9.37[d], 11.34[e], 11.1[f]
	Cu	177 ± 19 (37)	<6500	193 ± 10[c], 190[g], 170 ± 8[g], 177[h]
	Mo	<510	3.4 ± 0.7 (0.8)	(3.4)[c], 3.0[d], 3.4 ± 0.2[g], 3.71[h]
	Rb	18.7 ± 0.9 (9.7)	16.5 ± 1.2 (10.5)	18.3 ± 1.0[c], 18.7[e], 18.7 ± 1.5[a]
	Se	1.1 ± 0.4 (0.74)	<1.55	1.1 ± 0.1[c], 1.51[e], 1.01 ± 0.4[i]
	Zn	<1.2%	137 ± 9 (25)	130 ± 13[c], 128 ± 12[a], 134[h], 137[j]
	Others[b]	Al, Cl, Mn, Na	Fe, K, Na	
Spinach (NBS SRM-1570)	Br	<65	55.3 ± 3.8 (1.2)	(54)[k], 45.0 ± 3.3[g], 47.2 ± 0.5[l]
	Ca,%	<0.86	1.37 ± 0.07 (0.34)	1.35 ± 0.03[k], 1.49 ± 0.1[l]
	Co	<26	1.6 ± 0.1 (0.34)	(1.5)[k], 1.49 ± 0.05[g], 1.76 ± 0.01[l]
	Sc	<0.34	0.15 ± 0.03 (0.06)	(0.16)[k], 0.17 ± 0.02[g], 0.17 ± 0.004[l]
	Sm	<12	0.033 ± 0.004 (0.012)	0.08 ± 0.02[g]
	Others[b]	Al, Cl, Mg, Mn, Na	Fe, K, Na	
Orchard Leaves (NBS SRM-1571)	Ba	<230	37 ± 11 (28)	(44)[m]
	Br	<19	11.0 ± 0.7 (0.4)	(10)[m], 8.2 ± 0.6[g]
	Ca,%	1.81 ± 0.24 (0.11)	2.46 ± 0.09 (0.22)	2.09 ± 0.03[m], 2.00 ± 0.08[g]
	Co	<1.3	0.26 ± 0.12 (0.33)	(0.2)[m], 0.16 ± 0.02[g]
	Rb	<15.5	11.3 ± 2.9[p] (4.7)	12 ± 1[m]
	Sb	<99	3.3 ± 0.2 (0.03)	2.9 ± 0.3[m], 2.85 ± 0.06[g]
	Sc	<0.097	0.075 ± 0.005 (0.015)	0.052 ± 0.003[i]
	Sm	<3.1	0.088 ± 0.008 (0.006)	0.105 ± 0.004[g]

Pepperbush (NIES No. 1)	Ba	<1200	143 ± 19 (21)	
	Br	<120	1.9 ± 0.3 (0.4)	
	Ca,%	<0.83	1.6 ± 0.2 (0.2)	1.45[q]
	Cd	<2400	6.4 ± 0.6 (1.0)	(8)[q]
	Co	<37	21.7 ± 1.5 (0.35)	(21)[q]
	Rb	<88	84 ± 9 (5.3)	
	Sb	<510	0.20 ± 0.03 (0.03)	
	Sc	<0.44	0.052 ± 0.010 (0.020)	
	Sm	<15	0.033 ± 0.006 (0.006)	
	Zn	<6.3%	350 ± 30 (12)	328[q]
	Others[b]	Al, Mn	As, Cs, Fe, K, La, Na	
Soil (IAEA S-5)	Ba	<1.9%	503 ± 70[p] (96)	561 ± 53[s], 422[t]
	Br	<1300	8.4 ± 0.8 (1.8)	5.4 ± 1.0[s]
	Co	<630	16.3 ± 1.0 (1.9)	14.8 ± 0.76[s]
	Hf	<9.4	7.7 ± 1.2[p] (0.8)	6.30 ± 0.30[s]
	Rb	<1070	158 ± 14 (26.9)	138 ± 7.4[s], 126[t]
	Sb	<8900	19 ± 5 (0.14)	14.3 ± 2.2[s]
	Sc	15.6 ± 0.9 (9.5)	16.7 ± 0.7 (0.10)	14.8 ± 0.66[s]
	Sm	<270	3.9 ± 0.2 (0.02)	5.42 ± 0.39[s]
	Th	<4300	10 ± 0.6 (0.5)	11.3 ± 0.73[s], 11[t]
	U	<160	3.3 ± 0.2 (0.54)	3.04 ± 0.51[b], <6[t]
	W	<1.9%	4.7 ± 1.0 (2.4)	(5.1)[s]
	Yb	<5400	2.2 ± 0.2 (0.26)	2.24 ± 0.20[s]
	Zn	<8.6%	553 ± 36[r] (65)	368 ± 8.2[s], 390[t]
	Others[b]	Al, Mn, V	As, Cr, Cs, Eu, Fe, K, La, Lu, Na, Tb	
Bituminous Coal (NBS SRM-1632a)	Ba	<7500	116 ± 7[p] (58)	110 ± 16[v]
	Br	<550	50 ± 4 (0.83)	45.4 ± 4.7[v]
	Co	<250	6.6 ± 0.5[p] (0.8)	(6.8)[u], 6.6 ± 0.7[v]
	Dy	1.98 ± 0.53 (0.45)	n.d.	1.6 ± 0.2[v]
	Hf	<3.8	1.9 ± 0.3[p] (0.5)	(1.6)[u], 1.6 ± 0.1[v]
	Rb	<410	29 ± 5 (11.5)	(31)[u], 30 ± 5[v]
	Sb	<3500	0.69 ± 0.05 (0.08)	(0.58)[u], 0.63 ± 0.10[v]
	Sc	6.9 ± 0.9 (2.7)	6.3 ± 0.2 (0.04)	(6.3)[u], 6.2 ± 0.7[v]

Table 5—*continued*

Sample material	Elements	Contents (in $\mu g\ g^{-1}$ unless otherwise stated)		
		Short-lived nuclide (detection limit)	Long-lived nuclide (detection limit)	Literature value
Bituminous Coal—*cont'd.*	Sm	<110	1.9 ± 0.1 (0.02)	2.1 ± 0.2[v]
	Th	<1600	4.2 ± 0.2 (0.31)	4.5 ± 0.1[u], 4.5 ± 0.3[v]
	U	<62	1.2 ± 0.1 (0.33)	1.28 ± 0.02[u], 1.4 ± 0.1[v]
	Yb	<2200	1.1 ± 0.1 (0.15)	0.97 ± 0.14[v]
	Others[b]	Al	As, Cr, Cs, Eu, Fe, K, La, Lu, Na	
Subbituminous Coal (NBS SRM-1635)	Ba	<2800	72 ± 17 (29)	72 ± 8[v]
	Br	<170	1.9 ± 0.2 (0.6)	1.0 ± 0.2[v]
	Sb	<1200	0.17 ± 0.4[p] (0.04)	(0.14)[w], 0.14 ± 0.01[v]
	Sc	<1.2	0.70 ± 0.03 (0.02)	(0.63)[w], 0.67 ± 0.07[v]
	Sm	<39	0.27 ± 0.01 (0.007)	0.26 ± 0.03[v]
	Th	<650	0.64 ± 0.05 (0.14)	0.62 ± 0.04[w], 0.62 ± 0.05[v]
	U	<23	0.32 ± 0.04* (0.17)	0.24 ± 0.02[w], 0.23 ± 0.03[v]
	Yb	<780	0.17 ± 0.06 (0.08)	0.17 ± 0.02[v]
	Others[b]	Al	As, Cr, Fe, La, Lu, Na	
Granite (USGS G-2)	Ba	<1.8%	1730 ± 190[p] (320)	1870[x], 1780 ± 90[y]
	Hf	10.2 ± 2.7 (9.2)	10.5 ± 2.3[β] (2.7)	7.35[x], 7.20 ± 0.60[y]
	Sc	<7.3	3.5 ± 0.3 (0.35)	3.7[x], 2.90 ± 0.21[y], 3.5 ± 0.24[z]
	Sm	<260	5.6 ± 0.3 (0.07)	7.3[x], 7.25 ± 0.80[y]
	Th	<4020	24 ± 2 (1.4)	24.2[x], 22.4 ± 0.31[y]
	Yb	<5200	1.6 ± 0.3 (0.8)	0.88[x], 0.75 ± 0.06[y]
	Others[b]	Al	Cr, Cs, Eu, Fe, K, La, Lu, Na	
Peridotite (USGS PCC-1)	Br	<340	3.2 ± 0.8 (2.3)	0.6[x]
	Co	<140	117 ± 6 (1.5)	112[x]
	Sb	<1900	1.6 ± 0.1 (0.16)	1.4[x]
	Sc	8.4 ± 1.2 (1.98)	8.7 ± 0.3 (0.12)	6.9[x]
	Others[b]	Al, Mg, Mn, V	Cr, Fe, Na	

Marine Mud (USGS MAG-1)	Ba	<1.8%	370 ± 50 (260)	311[α]
	Br	<1300	258 ± 18 (5.4)	
	Co	<610	21.3 ± 1.5[p] (5.2)	18.8[α]
	Hf	<9.0	4.4 ± 0.4[p, β] (2.0)	3.15[α]
	Sb	<8750	1.1 ± 0.2 (0.4)	0.83[α]
	Sc	16.8 ± 0.7 (9.2)	17 ± 0.5 (0.24)	16.3[α]
	Sm	<260	5.5 ± 0.5 (0.06)	
	Th	<4200	12.1 ± 0.6[p] (1.1)	13.0[α]
	Yb	<5200	2.4 ± 0.2 (0.7)	
	Others	Al, Mn, V	As, Cr, Cs, Eu, Fe, K, La, Lu, Na	

[a]Ref. 4. [b]Other elements determined in the sample material using short and long experimental conditions. [c]Ref. 12. [d]Ref. 13. [e]Ref. 6. [f]Ref. 7. [g]Ref. 14. [h]Ref. 15. [i]Ref. 3. [j]Ref. 16. [k]Ref. 17. [l]Ref. 18. [m]Ref. 19. [n]Ref. 20. [p]Result computed after a 2-week-decay period for superior counting statistics. [q]Ref. 21. [r]This value is in error due to interference from the intense 1120-keV peak of ^{46}Sc on the 1115-keV peak of ^{65}Zn. [s]Ref. 22. [t]Ref. 23. [u]Ref. 24. [v]Ref. 25. [w]Ref. 26. *Interference from ^{182}Ta peak on ^{239}Np-peak. [x]Ref. 9. [y]Ref. 10. [z]Ref. 27. [α]Ref. 28. [β]See text for details.

geological materials (due to low flux and small sample mass) make the useful application of the short-lived nuclide to routine rubidium determination unlikely. For similar reasons the detection limit of the short-lived scandium nuclide, ^{46m}Sc, is much higher (by a factor of about 100) for the geological SRM than for the biological ones; however, because of relatively high concentrations of scandium in geological SRM, its measurement via ^{46m}Sc could provide a faster alternative for analysis than the longer-lived ^{46}Sc (Table 5). Scandium levels could also be measured in three biological SRM using the long experimental conditions. Agreement between scandium content of geological and environmental SRM determined by both sets of experimental condition is generally good and always within the limits of the measured errors. However, the difference between the detection limits of the long- and short-lived nuclides of scandium was observed to be as high as a factor of 95 in favour of the long-lived nuclide.

Concentrations of copper in the Bovine Liver, dysprosium in the Bituminous Coal, and selenium in the Fish Flour and Bovine Liver were determined using the short-lived nuclides only. Selenium in the last two matrices could also be determined by its long-lived nuclide after a decay of at least two weeks. Eleven elements, Ba, Cd, Co, Mo, Sb, Sm, Th, U, W, Yb and Zn, were only determined in some of the SRM by their long-lived nuclides. In addition to the elemental levels measured by using short-lived nuclides (Table 5), several elements which do not possess an alternative long-lived thermal-neutron activation product (e.g. Al, Cl, I, Mg, Mn and V) were also simultaneously determined in several SRM when analyzed under the short experimental conditions.

Most of the elemental concentrations reported in Table 5, and obtained by using the short and/or long experimental conditions, are generally in good agreement with the literature values although the timing parameters for several of the elements determined were far from optimum. The agreement between our values and the certified values varied between ±5 and 15% for most of the elements studied. Occasionally, the desired degree of accuracy for the elemental levels determined (Table 5) could not be obtained after 1-week decay because of poor counting statistics: barium, cobalt and hafnium in the NBS Bituminous Coal, antimony in the NBS Sub-bituminous Coal, barium in the USGS G-2, and cobalt, hafnium and thorium in the USGS MAG-1. For this reason, where necessary a few elemental concentrations were determined after a 2-week decay period and are appropriately indicated in Table 5. It is obviously possible to achieve a greater accuracy of measurement if the timing parameters are optimized to suit individual nuclides. In most cases, precision of measurement was within ±15%. Both precision and accuracy for measuring short-lived nuclides can be improved by using methods based on pseudo-cyclic and cyclic i.n.a.a. which are presently being developed in this laboratory.

The detection limits of 36 of the elements listed in Table 3 were calculated for four representative SRM, using short- and long-lived nuclides, according

to the method prescribed by Currie for L_D[8]. The number of channels for calculating L_D was taken as equal to the rounded-up integer value of the full width at tenth maximum (f.w.t.m.) resolution of the detector at the γ-ray energy of interest. These channels encompass an area equal to or greater than 96.8% of a Gaussian distribution. The detection limits are presented in Table 6. For the short-lived nuclides, the SRM containing relatively high amounts of aluminium and silicon (e.g. NBS Bituminous Coal and USGS MAG-1) exhibited poor detection limits in comparison to those with low amounts of these two elements (e.g. NBS Bovine Liver and Orchard Leaves). These practical detection limits are different from the approximate detection limits calculated in the absence of background interfering activities [11]. For biological, environmental, and geological samples, the detection limits listed in Table 6 can be utilized to predict if short-lived nuclides can be successfully used for the determination of the elements of interest, in preference to the long-lived alternative nuclides.

CONCLUSIONS

Among the elements which give both short- and long-lived thermal neutron activation products, up to nineteen were detected in the eleven biological, environmental, and geological SRM analyzed by using the standard short and long experimental conditions. The results obtained showed that eleven of the nineteen elements (Ba, Cd, Co, Mo, Sb, Sm, Th, U, W, Yb and Zn) were more readily determined by using the irradiation and counting conditions suited to long-lived nuclides, while the remaining elements (Br, Ca, Cu, Dy, Hf, Rb, Sc and Se) can be successfully determined, in certain types of sample matrices, by means of their short-lived nuclides. Eight additional elements (Al, Cl, I, K, Mg, Mn, Na and V) were also determined by using the short experimental conditions. Where a comparison of the results from the short and long-lived nuclides of the same element was possible the precision and accuracy of both measurements were generally good. The use of these short-lived nuclides in routine measurements, where applicable, can therefore result in not only a significant reduction of total experimental time from more than a week to a few minutes, but can often also produce results equally as accurate as the alternative longer lived nuclides. Thus, in the interest of economy of effort, it is suggested that the sensitivities and detection limits reported in this work be studied with a view to replacing, where possible, multi-experiment approaches involving lengthy decay times with the much shorter ones required for the determination of a number of commonly determined elements by short-lived nuclides. The detection limits of nuclides with half-lives less than 25 s can further be improved by a simple but effective pseudo-cyclic i.n.a.a. method described elsewhere [3]. The sensitivity can also be increased by optimizing timing parameters in an automated cyclic i.n.a.a. method [30, 31]. The use of a low-energy photon detector for improving detection limits is presently being evaluated.

TABLE 6

Comparison of elemental detection limits obtained through short- and long-lived nuclides (in $\mu g\ g^{-1}$)

Element	Bovine Liver (NBS SRM-1577)		Orchard Leaves (NBS SRM-1571)		Bituminous Coal (NBS SRM-1632a)		Marine Mud (USGS MAG-1)	
	Short-lived	Long-lived	Short-lived	Long-lived	Short-lived	Long-lived	Short-lived	Long-lived
Antimony	66	0.042	99	0.03	3,500	0.08	8,700	0.37
Barium	140	35	220	28	7,500	58	18,000	260
Bromine	9.9	0.57	19	0.38	550	0.83	1,300	5.4
Cadmium	270	1.3	460	1.2	3,100	2.4	38,000	11
Calcium	540	2,200	1,100	2,200	18,000	3,200	33,000	14,000
Cerium	—	1.4	—	1.0	—	2.3	—	9.5
Cobalt	4.6	0.77	1.3	0.33	240	0.79	610	5.2
Copper	36	6,500	40	3,500	1,600	9,800	4,000	49,000
Dysprosium	0.036	—	0.03	—	0.45	—	4.8	—
Gadolinium	5.2	6.2	8.8	4.2	300	11	700	42
Gallium	72	18	100	9.7	3,800	30	9,800	150
Germanium	12	37,000	18	30,000	1,700	62,000	6,600	280,000
Hafnium	0.07	0.39	0.11	0.23	3.8	0.48	9.0	2.0
Indium	0.14	1.1	0.24	0.85	8.0	1.8	19	7.8
Iridium	22	0.004	34	0.003	1,200	0.007	3,000	0.03
Mercury	1,100	1.4	1,800	1.1	59,000	2.5	145,000	10
Molybdenum	500	0.79	960	0.55	28,000	1.2	70,000	5.3
Neodymium	140	2.2	230	1.5	8,200	3.1	20,000	13
Niobium	300	—	490	—	19,000	—	46,000	—
Palladium	9.5	200	16	130	520	260	1,300	1,100
Platinum	240	20	410	14	13,000	35	31,000	130
Rhenium	20	0.023	31	0.02	1,100	0.03	2,600	0.13
Rubidium	9.7	11	16	4.7	410	12	1,000	83

Scandium	0.06	0.03	0.097	0.015	2.7	0.04	9.2	0.24
Selenium	0.74	1.6	0.95	1.1	31	2.1	76	8.9
Silver	0.39	1.1	0.77	1.05	22	2.2	56	9.7
Strontium	320	110	510	59	16,000	140	41,000	660
Tantalum	200	0.33	330	0.16	11,000	1.1	26,000	4.0
Tellurium	65	39	100	38	3,300	60	8,400	260
Thorium	34	0.13	50	0.12	1,600	0.31	4,200	1.1
Tin	130	—	200	—	6,500	—	17,000	—
Tungsten	140	0.78	220	0.62	7,400	1.4	18,000	6.6
Uranium	1.2	0.18	1.9	0.15	62	0.33	150	1.4
Ytterbium	41	0.08	63	0.07	2,200	0.15	5,200	0.7
Zinc	12,000	25	10,000	9.6	350,000	28	840,000	170

The authors acknowledge the co-operation of the SLOWPOKE-2 Operations Group, Dalhousie University SLOWPOKE-2 Reactor, for their assistance in irradiations. This research was supported by a research operating grant (A-9977) and a strategic grant (G-0054) from the Natural Sciences and Engineering Research Council of Canada.

REFERENCES

1 A. Egan and N. M. Spyrou, Anal. Chem., 48 (1976) 1959.
2 D. E. Ryan, D. C. Stuart and A. Chattopadhyay, Anal. Chim. Acta, 100 (1978) 87.
3 A. Chattopadhyay and K. N. DeSilva, Trans. Am. Nucl. Soc., 32 (1979) 185.
4 A. Chattopadhyay, K. M. Ellis and K. N. DeSilva, Proc. Int. Symp. on Nuclear Activation Techniques in the Life Sciences 1978, International Atomic Energy Agency, Vienna, 1979, p. 667.
5 R. A. Nadkarni and G. H. Morrison, J. Radioanal. Chem., 43 (1978) 347.
6 G. V. Iyengar, K. Kasperek and L. E. Feinendegen, Phys. Med. Biol., 23 (1978) 66.
7 R. Schelenz and J.-F. Diehl, in P. D. LaFleur (Ed.), Proc. 7th Materials Res. Symp., NBS Spec. Publ. 422, Vol. II, 1976, p. 1173.
8 L. A. Currie, Anal. Chem., 40 (1968) 586.
9 F. J. Flanagan, Geochim. Cosmochim. Acta, 37 (1973) 1189.
10 K. M. Ellis and A. Chattopadhyay, Anal. Chem., 51 (1979) 942.
11 V. P. Guinn and J. Hoste, Int. Symp. Nuclear Activation Techniques in the Life Sciences, International Atomic Energy Agency, Vienna, Paper No. IAEA-SM-227/102, 1978.
12 National Bureau of Standards, Certificate of Analysis, Standard Reference Material 1577, Bovine Liver, Washington, D.C., 1977.
13 R. A. Nadkarni and G. H. Morrison, Anal. Chem., 45 (1973) 1957.
14 H. A. Van der Sloot, G. D. Wals, C. A. Weers and H. A. Das, Netherlands Energy Research Foundation, Petten, Report ECN-79-096, (1979).
15 P. S. Tjioe, J. J. M. deGoeij and J. P. W. Houtman, J. Radioanal. Chem., 37 (1977) 511.
16 G. Guzzi, R. Pietra and E. Sabbioni, EURATOM Report 5282^{e} (1974).
17 National Bureau of Standards, Certificate of Analysis, Standard Reference Material 1570, Spinach, Washington, D.C., 1976.
18 R. A. Nadkarni, Radiochem. Radioanal. Lett., 30 (1977) 329.
19 National Bureau of Standards, Certificate of Analysis, Standard Reference Material 1571, Orchard Leaves, Washington, D.C., 1976.
20 J. C. Laul and R. A. Rancitelli, J. Radioanal. Chem., 38 (1977) 461.
21 K. Okamoto, Y. Yamamoto and K. Fuwa, Anal. Chem., 50 (1978) 1950.
22 R. Dybczyński, A. Tugsavul and O. Suschny, International Atomic Energy Agency, IAEA/RL/46, Vienna, 1978.
23 R. Van Grieken, L. Van't Dack, C. Costa Dantas and H. da Silveira Dantas, Anal. Chim. Acta, 108 (1979) 93.
24 National Bureau of Standards, Certificate of Analysis, Standard Reference Material 1632a, Bituminous Coal, Washington, D.C., 1978.
25 M. R. Sandeman and A. Chatt, to be published.
26 National Bureau of Standards, Certificate of Analysis, Standard Reference Material 1635, Subbituminous Coal, Washington, D.C., 1978.
27 A. Chattopadhyay and S. A. Katz, J. Radioanal. Chem., 46 (1978) 321.
28 A. Katz and L. Grossman, United States Geological Survey, Geological Survey Professional Paper No. 840, 1976, p. 49.
29 F. T. Manheim, J. C. Hathaway, F. J. Flanagan and J. D. Fletcher, United States Geological Survey, Geological Survey Professional Paper No. 840, 1976, 25.
30 R. E. Tout and A. Chatt, Trans. Am. Nucl. Soc., 33 (1979) 233.
31 R. E. Tout and A. Chatt, Anal. Chim. Acta, submitted (1980).

Analytica Chimica Acta, 118 (1980) 359—368

THE MECHANISM OF THE FORMATION AND HYDROLYSIS OF CYCLOHEXANONE OXIME IN AQUEOUS SOLUTIONS

H. EGBERINK* and C. VAN HEERDEN

DSM Corporate Research and Patents Department, Geleen (The Netherlands)

(Received 28th November 1979)

SUMMARY

The rate of formation of cyclohexanone oxime from cyclohexanone and hydroxylamine and the rate of the reverse reaction, the hydrolysis of cyclohexanone oxime, were studied in the pH range 1—7. The relative position and the bell shape of the two experimental reaction-rate curves can be fully explained by supplementing the reaction mechanism proposed by Jencks for the oximation only with the reverse reaction, applying the principle of microscopic reversibility. An essential part of this mechanism is the intermediate formation of a 1:1 adduct of cyclohexanone and hydroxylamine. It is concluded that the concentration of this adduct is negligibly small under all the conditions used here.

Much attention has been given [1—5] to the kinetics of oxime formation from carbonyl compounds on addition of nucleophilic nitrogen compounds, in particular hydroxylamine. The reaction is clearly reversible. For this reason, the measurements reported in the literature have often been made with a large excess of hydroxylamine, so that the reverse reaction does not occur [1—3]. Few data are available on the rate of the reverse reaction, the hydrolysis of oximes [4]. In both the forward and the reverse reactions, the formal reaction-rate constants were found to be strongly pH-dependent.

Jencks [2] has described a generally accepted mechanism for the pH-dependence of the oximation rate. He explains the bell-shaped curve by assuming that in the acidic range, the reaction of the unprotonated hydroxylamine with the carbonyl compound to form a 1:1 adduct is rate-determining, whereas in the basic range the 'acid-catalysed' dehydration of this adduct to oxime is rate-determining:

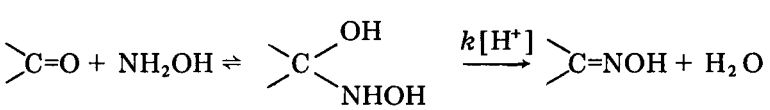

(1)

Recently, Oliveira et al. [1] studied the formation of oxime by differential thermometry. Their measurements led them to propose a completely different mechanism. The momentary generation of heat, detected directly after mixing of the reactants, was assumed to be the result of the adduct formation, with equilibrium being established instantaneously and lying completely towards the adduct formation. In other words, they postulated that the

carbonyl compound, because of the large excess of hydroxylamine, is instantaneously and fully converted to the adduct, which is then transformed to oxime by a slow dehydration reaction. To interpret the pH-dependence of the rate of oxime formation, Oliveira et al. assumed that at low pH values, in addition to the protonated adduct, also an unreactive diprotonated adduct is formed in considerable amounts.

Since the reaction concerned is essentially reversible, it is to be expected that a study of both the oximation reaction and the reverse hydrolysis reaction under comparable conditions would clarify matters considerably. For it must be assumed, from the principle of microscopic reversibility, that the reaction path is identical for both directions. This paper reports the results of such a study, with the reaction conditions often being chosen such that the equilibrium manifested itself in incomplete conversion. This means that the reaction mechanism must not only be capable of describing the initial rate in both directions, but also the rate at which equilibrium is approached under conditions where both reactions proceed simultaneously.

EXPERIMENTAL

Reagents and instrumentation

Hydroxylammonium chloride (chemically pure) was used as received. Cyclohexanone was distilled and stored under nitrogen. Cyclohexanone oxime was crystallized twice from ethanol. The buffer solutions were aqueous phosphate solutions (0.2—1.0 mol l^{-1}) prepared from chemically pure phosphoric acid and disodium hydrogenphosphate. The ionic strength in an aqueous 0.2 mol l^{-1} phosphate buffer was 1.2 mol l^{-1} and was constant during the experiments.

The cyclohexanone and cyclohexanoneoxime concentrations were measured by u.v. absorption spectrophotometry with a Beckman 25 spectrophotometer and quartz cuvettes (path length 10 mm). Additionally, some n.m.r. measurements were carried out with a Varian SC-300 spectrometer. These measurements were done at lower temperatures because of the slow detection. For the pH measurements made before and after the experiments, a combined Schott N61 electrode and a Philips PW 9409 pH meter were used.

Kinetic measurements

The hydroxylammonium chloride and the cyclohexanone were dissolved in the buffer solution at the desired pH. Cyclohexanone oxime was dissolved in distilled water. The temperature was adjusted before each experiment, and kept constant during measurement. For the u.v. measurements on cyclohexanone oxime formation, the hydroxylamine solution was first placed in the sample tube and a concentrated solution of cyclohexanone was quickly added. For the hydrolysis of cyclohexanone oxime, the buffer solution was first introduced and a concentrated cyclohexanone oxime solution was quickly added. The measurements could be started 10—15 s after mixing.

The analytical concentration of cyclohexanone oxime was measured at 222 nm, and that of cyclohexanone at 275 nm. There was no overlap between the peaks. Determination of the molar absorptivities showed that only that of cyclohexanone oxime is very pH-dependent, because cyclohexanone oxime is partially protonated under the measuring conditions used. The hydrolysis reaction was studied initially at a cyclohexanone oxime concentration of 6×10^{-4} mol l^{-1} and the oximation reaction at hydroxylamine concentrations varying from 0.0303 to 0.303 mol l^{-1} with the cyclohexanone concentration always 0.0303 mol l^{-1}. One experiment was done at the very low concentration of 0.0006 mol l^{-1} for both components. In the n.m.r. measurements, the hydroxylammonium chloride was introduced and the cyclohexanone solution was added quickly. The analytical concentrations of hydroxylamine and cyclohexanone were 0.2 mol l^{-1}. The temperature variation covered a range of -11°C to 70°C.

RESULTS

Protonation constants of cyclohexanone oxime and hydroxylamine

Separate u.v. measurements at 222 nm showed that the molar absorptivity of cyclohexanone oxime is highly dependent on the pH of the solution. No such dependence was found for cyclohexanone. It would seem that in the pH range 1—7 not only cyclohexanone oxime but also its protonated form is present. This behaviour must be expected if the molar absorptivity ϵ_{ox} of the free oxime and ϵ_{oxH^+} of the protonated oxime are different. Given the usual assumption that absorption is an additive property, the experimental molar absorptivity ϵ must obey the relation

$$\epsilon = (K_{ox}\epsilon_{ox} + \epsilon_{oxH^+} C_{H^+})/(K_{ox} + C_{H^+}) \qquad (2)$$

where K_{ox} is the protonation constant of the oxime and C_{H^+} is the hydrogen ion concentration (which throughout this paper will be approximated by 10^{-pH}). The solid line in Fig. 1. was calculated with $K_{ox} = 2.3 \times 10^{-2}$ mol l^{-1} from adjusted values of ϵ_{ox} and ϵ_{oxH^+}. The ionic strength was 1.2 mol l^{-1}.

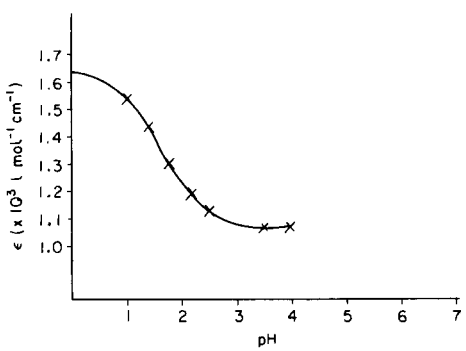

Fig. 1. Molar absorptivity ϵ of cyclohexanone oxime vs. pH. Solid line calculated with $K_{ox} = 2.3 \times 10^{-2}$ mol l^{-1}. (×) Recorded values.

Because of the excellent agreement with the experimental results, this value will subsequently be taken as the protonation constant of cyclohexanone oxime. For cyclohexanone, no such pH-dependence of the molar absorptivity was found from which it was concluded that in the pH range of this study protonation of cyclohexanone can be neglected. The protonation constant of hydroxylamine is known [6] to be 1.04×10^{-6} mol l^{-1}.

Rate constants for the formation and hydrolysis of cyclohexanone oxime

The measurement data for both the formation and the hydrolysis of cyclohexanone oxime (ox) were used to calculate the kinetic constants k_1 and k_2 for the overall equation for the reaction of cyclohexanone (anone) with hydroxylamine:

$$\text{anone} + \text{NH}_2\text{OH} \underset{k_2}{\overset{k_1}{\rightleftharpoons}} \text{ox} + \text{water} \tag{3}$$

and the corresponding formal kinetic equation

$$-\,\mathrm{d}[\text{anone}]_a/\mathrm{d}t = \mathrm{d}[\text{ox}]_a/\mathrm{d}t = k_1[\text{anone}]_a \cdot [\text{NH}_2\text{OH}]_a - k_2[\text{ox}]_a \tag{4}$$

where square brackets indicate the analytical concentration of the component concerned, i.e. the sum of the concentrations of protonated and unprotonated molecules. This kinetic relation, in particular the equality of $-\mathrm{d}[\text{anone}]/\mathrm{d}t$ and $\mathrm{d}[\text{ox}]/\mathrm{d}t$, is based on the assumption that the concentration of any intermediate product, such as the adduct mentioned in the introduction, is negligibly small. Given this assumption the differential equation can be integrated, since the concentrations of components on the right-hand side of the overall reaction equation can only then be expressed directly in terms of conversion of the components on the left-hand side and vice-versa. For the hydrolysis reaction, i.e. with a given initial concentration of cyclohexanone oxime and during the reaction equal increasing concentrations of cyclohexanone and hydroxylamine, the result of integration is

$$k_1 t = \frac{[\text{ox}]_\infty}{([\text{ox}]_0^2 - [\text{ox}]_\infty^2)} \ln \frac{([\text{ox}]_0^2/[\text{ox}]_\infty) - [\text{ox}]}{[\text{ox}] - [\text{ox}]_\infty} \cdot \frac{[\text{ox}]_\infty}{[\text{ox}]_0} \tag{5}$$

$$\text{with } k_1/k_2 = [\text{ox}]_\infty/([\text{ox}]_0 - [\text{ox}]_\infty)^2 \tag{6}$$

Every hydrolysis experiment gives [ox] as a function of time for a given initial concentration $[\text{ox}]_0$. The final concentration $[\text{ox}]_\infty$, after reaction equilibrium has been established, is also determined experimentally. Equation (5) can then be checked with the experimental results by plotting the logarithmic term, which contains experimental quantities only, against time, which should give a straight line. The slope of this line gives k_1, and k_2 can then be calculated by using eqn. (6).

The results of integrating eqn. (4) for the case of cyclohexanone oxime formation, i.e. at a given initial cyclohexanone concentration $[\text{anone}]_0$ and a given initial molar ratio b_0 of hydroxylamine to cyclohexanone, is

$$k_1 t = \frac{[\text{anone}]_0 - [\text{anone}]_\infty}{b[\text{anone}]_0^2 - ([\text{anone}]_0 - [\text{anone}]_\infty)^2} \ln \left[\frac{\{b_0[\text{anone}]_0^2 - ([\text{anone}]_0 - [\text{anone}])([\text{anone}]_0 - [\text{anone}]_\infty)\}([\text{anone}]_0 - [\text{anone}])}{b_0[\text{anone}]_0^2([\text{anone}] - [\text{anone}]_\infty)} \right] \quad (7)$$

with

$$k_1/k_2 = ([\text{anone}]_0 - [\text{anone}]_\infty)/[\text{anone}]_\infty \{(b_0 - 1)[\text{anone}]_0 + [\text{anone}]_\infty\} \quad (8)$$

In this case, too, only experimental quantities are contained in the integrated expression, with the exception of k_1, and the equation can be checked by plotting the logarithmic term as a function of time. This check produced, with great accuracy, a straight line for all oxime formation and hydrolysis experiments. Figure 2 shows representative examples. These results demonstrate than in all experiments the whole course of the reaction satisfies the kinetic relation (4) extremely well right up to equilibrium.

The values for k_1 and k_2 obtained in all these experiments at various pH and temperature values are given in Table 1 for the hydrolysis experiments and in Table 2 for the oximation experiments. In Fig. 3, all results at 28.6°C are plotted against pH. This figure clearly illustrates that consistent values of k_1 and k_2 were obtained, regardless of whether they stemmed from hydrolysis or oximation experiments, regardless of whether the cyclohexanone oxime or the cyclohexanone concentration was measured in these experiments, and regardless of the molar ratio of cyclohexanone to hydroxylamine. The values found for the reaction rate constants k_1 and k_2 correspond well with the results published by Möller and Heckner [3], Vinnik and Zarakhani [4], and Ikonomov [5].

It may be concluded that the progress of reaction (3) to equilibrium is, in the concentration and pH range of this investigation, very well described in both directions by the simple rate equation (4), which is based on the analyti-

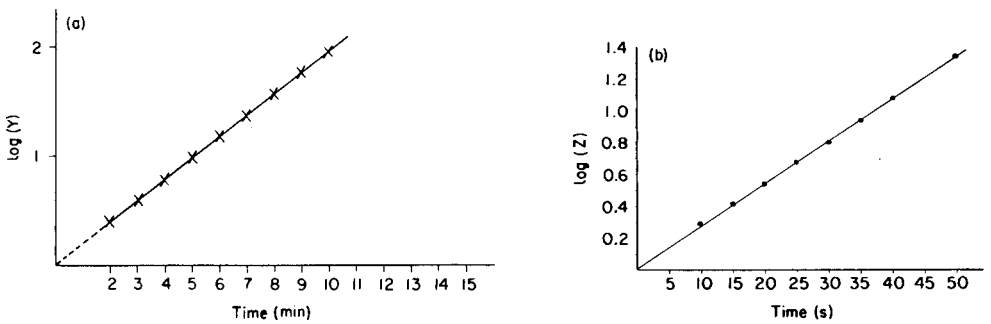

Fig. 2. (a) Hydrolysis of cyclohexanone oxime: log $\{([\text{ox}]_0^2/[\text{ox}]_\infty) - [\text{ox}]\}/\{[\text{ox}] - [\text{ox}]_\infty\}$, represented as log $\{Y\}$, is plotted against time. The slope of the linear section gives the hydrolysis rate constant; T = 28.6°C; pH 1.80. (b) Formation of cyclohexanone oxime: log (Z) vs. time; Z represents the term behind ln in eqn. (7). The slope of the linear section gives the formation rate constant. T = 28.6°C; cyclohexanone = 0.0303 mol l^{-1}; NH_2OH = 0.1516 mol l^{-1}; pH 1.25.

TABLE 1

Hydrolysis of cyclohexanone oxime. Reaction rate constants k_1 and k_2[a] at various pH values and temperatures in a 0.2 mol l^{-1} phosphate buffer (ionic strength 1.2). The decrease in cyclohexanone oxime concentration was followed by u.v. absorption spectrometry at 222 nm. Initial cyclohexanone oxime concentration was 6×10^{-4} mol l^{-1}

pH	$T = 18°C$			$T = 28.6°C$			$T = 50°C$			$T = 70°C$		
	k_2	k_1	$[ox]_\infty$	k_2	k_1	$[ox]_\infty$	k_2	k_1	$[ox]_\infty$	k_2	k_1	$[ox]_\infty$
1.00				0.150	18	3.8×10^{-5}	0.80	60	2.5×10^{-5}	3.0	125	1.4×10^{-5}
1.40	0.129	17.6	4.2×10^{-5}	0.285	44.4	4.8×10^{-5}	1.30	205	4.8×10^{-5}	4.3	271	2.1×10^{-5}
1.80	0.161	24.8	4.6×10^{-5}	0.392	95.0	6.8×10^{-5}	2.0	627	8.4×10^{-5}			
2.18	0.179	53.5	8.1×10^{-5}	0.460	180.5	9.8×10^{-5}						
2.50	0.175	177.6	1.8×10^{-4}	0.435	345.0	1.6×10^{-4}						
2.80	0.167	273.5	2.3×10^{-4}	0.397	369.5	1.7×10^{-4}						
3.29	0.098	484.1	3.4×10^{-4}	0.243	811.1	3.0×10^{-4}						
3.50	0.074	561.3	3.8×10^{-4}	0.178	867.0	3.4×10^{-4}	0.65					
3.92	0.033	893.0	4.7×10^{-4}	0.071	1054	4.3×10^{-4}	0.30	1787	3.5×10^{-4}	0.80	2400	2.9×10^{-4}

[a]The units are min^{-1} for k_2 and 1 mol^{-1} min^{-1} for k_1. The final cyclohexanone oxime concentration, $[ox]_\infty$, is given in mol l^{-1}.

TABLE 2

Cyclohexanone oximation experiments. Reaction rate constants k_1 and k_2 at various pH values and temperatures in a 0.2 mol l^{-1} phosphate buffer (ionic strength 1.2)[a]

pH	Temp. (°C)	$[anone]_0$	$[NH_2OH]_0$	$[ox]_\infty$	Method	Component measured	k_1	k_2
1.00	−11	0.2	0.2	0.17	N.m.r.	[anone], [ox]	0.9	0.005
2.00	−11	0.2	0.2	0.15	N.m.r.	[anone], [ox]	2	0.03
1.00	0	0.2	0.2	0.16	N.m.r.	[anone], [ox]	1.6	0.016
1.50	0	0.2	0.2	0.17	N.m.r.	[anone], [ox]	4.5	0.027
1.00	28.6	0.0303	0.0303	0.017	U.v.	[anone]	20	0.16
1.25	28.6	0.0303	0.0303	0.018	U.v.	[anone]	29	0.24
1.25	28.6	0.0303	0.152	0.029	U.v.	[anone]	33	0.20
1.25	28.6	0.0303	0.303	0.030	U.v.	[anone]	31	0.23
1.50	28.6	0.0303	0.0303	0.019	U.v.	[anone]	50	0.320
2.00	28.6	0.0006	0.0006	0.0001	U.v.	[ox]	160	0.440
4.80	26.8	0.0303	0.0303	0.028	U.v.	[anone]	990	0.011
5.50	28.6	0.0303	0.0303	0.030	U.v.	[ox]	860	<0.001
7.00	28.6	0.0303	0.0303	0.030	U.v.	[anone]	260	<0.001

[a]For units, see footnote to Table 1. All concentrations are given in mol l^{-1}.

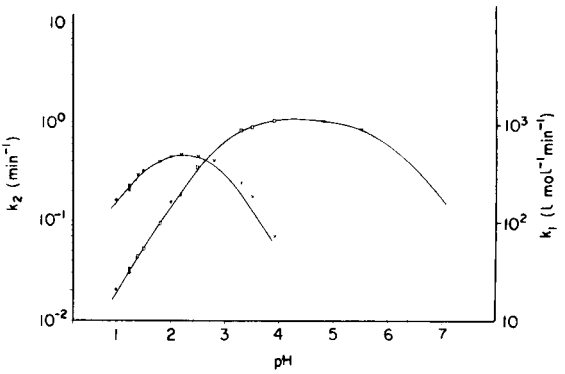

Fig. 3. Formation rate constant k_1 and hydrolysis rate constant k_2 for cyclohexanone oxime vs. pH at 28.6°C. Recorded values: (x) hydrolysis of cyclohexanone oxime and concentration of the oxime followed; (o) formation of cyclohexanone oxime and concentration of cyclohexanone followed. Solid lines are drawn according to formulae (10) and (11).

cal concentrations and characterized by the second-order reaction constant k_1 for the formation of cyclohexanone oxime from cyclohexanone and hydroxylamine and the first-order reaction constant k_2 for the hydrolysis of cyclohexanone oxime. As Fig. 3 shows, both reaction rate constants show a strong dependence on pH, in full agreement with the data found in the literature [3–5].

The reaction mechanism postulated below will have to explain the pH-dependence in both directions simultaneously, i.e. for both k_1 and k_2. Even at this stage, it should be pointed out that the results mentioned above convincingly show that in any mechanism in which an intermediate plays an essential role – and the adduct mentioned in the introduction is generally accepted as an intermediate — the concentration of this compound must always be so small as to be negligible. This conclusion, if correct, rules out the mechanism proposed by Oliveira et al. [1], the essence of which is a direct and complete conversion of cyclohexanone and hydroxylamine to this adduct. These authors based their mechanism on the fast generation of heat detected directly after the reaction components had been mixed. So far, no alternative explanation for this phenomenon offers itself.

The temperature-dependence of cyclohexanone oxime formation and hydrolysis

Plots of ln k_1 and ln k_2 against the reciprocal absolute temperature give, with reasonable accuracy, straight lines (see Fig. 4); the slope of k_2 has the same value at different pH values, but that of k_1 varies considerably with pH. The activation energy thus calculated, independent of pH, is 54.4 kJ mol^{-1} for the rate constant k_2 for oxime hydrolysis and 60.2, 77.8 and 18.4 kJ mol^{-1} at pH values of 1.4, 1.8 and 3.9, respectively, for the rate constant k_1 for oxime formation.

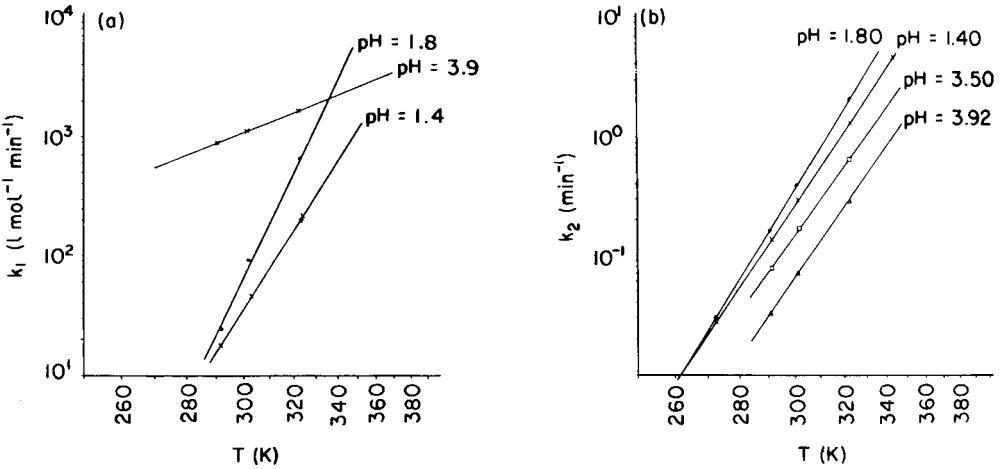

Fig. 4. (a) Oximation rate constant k_1 vs. $1/T$. (b) Hydrolysis rate constant k_2 vs. $1/T$.

Effect of the buffer concentration on the reaction rate constants

Within a limited pH range, it was investigated whether the concentration of the buffer solution influenced the reaction rate constant, ensuring that the buffer capacity was always adequate. In agreement with Jencks' results [2], no appreciable influence was found. The data are shown in Table 3.

DISCUSSION

For a mechanistic interpretation of the experimental results, and in particular of the bell-shaped pH-dependence of the formal reaction constants k_1 and k_2, only those molecular components that can reasonably be expected will be utilized. The mechanism must then consist of a series of reactions of these components with the corresponding reaction rate constant. Besides the adduct mentioned above, in its free and protonated form, it is assumed that free and protonated cyclohexanone oxime, free and protonated hydroxylamine and only free cyclohexanone are present. These protonated molecules will be treated as separate molecules in this reaction mechanism in addition

TABLE 3

Effect of phosphate buffer concentration on reaction-rate constants at 28.6°C.

pH	k_2 (min^{-1})			k_1 (l mol^{-1} min^{-1})		
	Buffer concentration (mol l^{-1})			Buffer concentration (mol l^{-1})		
	0.2	1.0	4.0	0.2	1.0	4.0
1.40	0.28		0.26	44		41
1.80	0.39	0.39		95	97	
2.18	0.46	0.46		180	190	
3.29	0.24	0.26		811	781	

to the unprotonated molecules. Furthermore, it is assumed that the protonation reaction is infinitely fast so that the concentrations of protonated and unprotonated components are at all times determined by the hydrogen ion concentration and the corresponding protonation constant.

The protonation constants of hydroxylamine (1.04×10^{-6} mol l^{-1}) and cyclohexanone oxime (2.3×10^{-2} mol l^{-1}) (see above) can be considered as independently given parameters. The K value of the adduct is an unknown parameter. The mechanism postulated below conforms with the mechanism postulated by Jencks for the oximation reaction. According to Jencks, the decrease in reaction rate with decreasing pH on the left of the maximum in the bell-shaped curve is caused by the decrease in the concentration of free hydroxylamine which only in its unprotonated form can be held responsible for the nucleophilic attack on cyclohexanone to form the adduct. On the right of the maximum, the reaction rate drops with increasing pH, because, according to Jencks, dehydration of the adduct is 'acid-catalysed'; in the present terminology, this is equivalent to saying that the dehydration proceeds only via the protonated adduct. The scheme of Jencks' reaction mechanism is then:

$$\begin{array}{lcccc} \text{anone} + NH_2OH & \underset{k_{-1}^*}{\overset{k_1^*}{\rightleftharpoons}} & \text{adduct} & & \text{oxime} \\ \Big\downarrow\Big\uparrow K_{NH_2OH} & & \Big\downarrow\Big\uparrow K_{\text{adduct}} & & \Big\downarrow\Big\uparrow K_{ox} \\ [NH_3OH]^+ & & \text{adduct } H^+ & \underset{k_{-2}^*}{\overset{k_2^*}{\rightleftharpoons}} & \text{oxime } H^+ + \text{water} \end{array} \qquad (9)$$

Jencks [2] used this scheme only to interpret the rate of the oximation reaction, and moreover for conditions under which the reverse reaction can be neglected (large excess of hydroxylamine). On the principle of microscopic reversibility, this representation was used here to describe the hydrolysis reaction, simply by regarding all reaction steps as reversible. The mechanism is thus characterized by four unknown kinetic constants, viz. the second-order reaction constants k_1^* and the first-order reaction constants k_{-1}^*, k_2^* and k_{-2}^* (pseudo first-order), as well as by the three protonation constants K_{ox}, K_{NH_2OH} and K_{adduct}. All these parameters are considered to be largely independent of pH and concentrations.

To check this reaction mechanism against the experimental data, k_1 and k_2 must be expressed in terms of the above seven parameters. For this purpose, as regards the adduct concentration, the principle of steady-state approximation was used; this is applicable only when the concentration of the intermediate and therefore also its variation per unit time may be neglected in the mass balance. This means that the rate of formation of the adduct can always be equated with its rate of disappearance. A second essential aspect of this derivation is the assumption of instantaneous protonation equilibria. Finally, it should be emphasized that in eqns. (4) defining k_1 and k_2, the analytical concentrations were used, i.e. the sum of the concentrations of protonated and unprotonated components. Derivation is simple in principle but rather long, and is therefore not reproduced here. The results are:

$$k_1 = k_1^* \Big/ \left\{ \left(1 + \frac{k_{-1}^*}{k_2^*} \frac{K_{adduct}}{[H^+]} \right) \left(\frac{[H^+]}{K_{NH_2OH}} + 1 \right) \right\} \quad (10)$$

$$k_2 = k_{-2}^* \Big/ \left\{ \left(1 + \frac{k_2^*}{k_{-1}^*} \frac{[H^+]}{K_{adduct}} \right) \left(\frac{K_{ox}}{[H^+]} + 1 \right) \right\} \quad (11)$$

Because K_{ox} and K_{NH_2OH} are known independently, only the three parameters k_1^*, k_{-2}^* and $k_{-1}^* K_{adduct}/k_2^*$ can be adapted to fit the theoretical relations (10) and (11) with the experimental data for k_1 and k_2. In accordance with the experimental results the formulae (10) and (11) exhibit a maximum at different values of the hydrogen ion concentration; these are given by

$$(H^+)_{max\ k_2} = [K_{ox} \cdot K_{adduct} \cdot k_{-1}^*/k_2]^{1/2} \quad (12)$$

$$(H^+)_{max\ k_1} = [K_{NH_2OH} \cdot K_{adduct} \cdot k_{-1}^*/k_2^*]^{1/2} \quad (13)$$

From this it follows that the distance between the two maxima, expressed in pH units, must be equal to ½ log K_{ox}/K_{NH_2OH} = 2.17 pH units. The very close agreement with the experimental result of 2.1 pH units provides strong support for the correctness of the reaction mechanism proposed, because not a single parameter had to be adapted. The position of the maximum of k_2 at pH 2.2 allows the parameter $(k_{-1}^*/k_2^*).K_{adduct}$ to be calculated as 1.5×10^{-3} mol l^{-1}. After adjusting k_1^* (1.6×10^6 l mol^{-1} min^{-1}) and k_{-2}^* (11 min^{-1}) to the experimental maxima of k_1 and k_2, the whole reaction-rate curve could be calculated. The result is shown by solid lines in Fig. 3. The agreement can be considered as satisfactory, demonstrating the correctness of Jencks' mechanism for both the forward and the reverse reaction. For the hydrolysis reaction, this implies that the adduct, in the pH range 1—7, is formed by hydration of almost only the protonated cyclohexanone oxime, forming the protonated form of the adduct. It is possible, that at pH values above 7 the reaction of unprotonated cyclohexanone oxime to the adduct also plays a role. In this pH range, the concentration of protonated adduct probably becomes very low. Breakdown of the adduct into hydroxylamine and cyclohexanone, finally, occurs only via the free unprotonated adduct.

REFERENCES

1 W. A. de Oliveira, L. Meites and T. Meites, Anal. Chim. Acta, 100 (1978) 245.
2 W. P. Jencks, J. Am. Chem. Soc., 20 (1959) 475.
3 D. Möller and K. H. Heckner, Z. Chem., 6 (1970) 225.
4 M. I. Vinnik and N. G. Zarakhani, Russ. J. Phys. Chem., 34 (1960) 1257.
5 N. N. Ikonomov, Glas. Hem. Drus., Beograd, 32 (1967) 285.
6 P. Lumme, P. Lahermo and J. Tummavuori, Acta Chem. Scand., 19 (1965) 2175.

Analytica Chimica Acta, 118 (1980) 369—372

Short Communication

APPLICATION OF THE CAP-PAIR EFFECT IN REDUCING THE INHIBITION OF ELECTRODE PROCESSES. THE DETERMINATION OF ZINC IN THE PRESENCE OF TWEEN-80

KAZIMIERZ SYKUT*, GRAZYNA DALMATA, BARBARA NOWICKA and JADWIGA SABA

Chemistry Department, The University, Pl. M. Curie-Sklodowskiej3 20031 Lublin (Poland)

(Received 9th January 1980)

Summary. The "cap-pair" effect, which accelerates electrode processes, is shown to be useful in decreasing the effects of inhibitors on reduction processes. The determination of zinc in the presence of Tween-80 is used as an example. In the square-wave polarography of zinc at the 10^{-5} M level, addition of thiourea (10 g l^{-1}) eliminates or greatly reduces the inhibitory action of Tween-80, thus allowing precise determinations.

Many organic substances which are adsorbed at the dropping mercury electrode (DME) inhibit electrode processes; this is reflected in decreasing wave or peak heights in the polarographic curves or even their total repression. The effect is often employed for the determination of surface-active substances, but of course it places severe limits on the direct application of polarographic methods for metals in surface (ground) water, sewage, etc., which are usually polluted with surface-active substances. The employment of polarography in such cases usually requires time-consuming prior removal of surfactants by mineralization. This obstacle may be overcome to some extent by taking advantage of the "cap-pair" effect [1—4], which defines the accelerative influence of organic substances on electrode processes. This effect occurs when: (1) the differential capacity curve of a solution containing the depolarizer and an organic compound at the $E_{1/2}$ value of the depolarizer runs above the differential capacity curve for the supporting electrolyte alone; and (2) the organic compound has a free electron pair at a sulphur or nitrogen atom [4].

The procedure proposed for reducing the inhibition by surface-active substances is very simple: an organic substance which meets the requirements of the "cap-pair" effect is added to the sample before polarography. The results obtained by this procedure for the determination of zinc in the presence of Tween-80, a strong surface-active agent which acts similarly to various commercial detergents, are described on next page.

Experimental

Analytical-grade chemicals and twice-distilled water were used throughout. Solutions were deaerated with nitrogen. The electrodes used included the DME with a saturated calomel electrode and a mercury pool electrode. The square-wave polarograph was a Radelkis model OH-104.

Results and discussion

The effect of Tween-80 concentration on the height of the s.w. peak for 5×10^{-5} M zinc(II) in 1 M KCl is shown in Fig. 1 (curve a). As the Tween concentration increases, the height of the zinc peak decreases linearly, the peak is completely repressed by 0.0028% Tween. The introduction of thiourea, a substance which meets the requirements of the "cap-pair" principle in relation to zinc, diminishes this inhibition of the zinc peak, the effect depending on the concentration of thiourea. With thiourea concentrations of 1 g l^{-1}, there is initially considerable enhancement of the zinc peak (Fig. 1, curve b) but again the zinc peak disappears when 0.0028% Tween is present.

When the solution contains more thiourea (10 g l^{-1}) the heights of the zinc peaks increase further but the dependence of peak height on Tween concentration changes (Fig. 1, curve c). At Tween concentrations between 0 and 0.002%, there is a small drop in the zinc peak heights but this drop becomes much greater at higher Tween concentrations. The shape of curve (c) suggests that in the system KCl—Tween 80—thiourea at Tween concen-

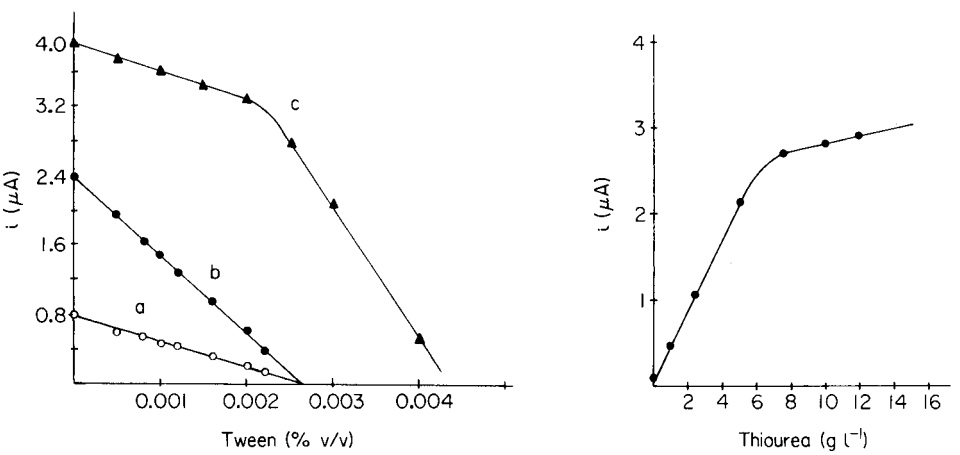

Fig. 1. The dependence of peak current for 5×10^{-5} M zinc(II) on Tween-80 concentration: (a) 1 M KCl; (b) 1 M KCl + 1 g l^{-1} thiourea; (c) 1 M KCl + 10 g l^{-1} thiourea.

Fig. 2. The dependence of the peak current for 5×10^{-5} M zinc(II) in 1 M KCl + 0.0025% Tween-80 on thiourea concentration.

trations of 0—0.002%, there is an adsorption balance, indicating the predominance of thiourea on the electrode surface, i.e., the "cap-pair" effect predominates. At higher Tween concentrations this effect decreases.

The effect of thiourea concentration on the peak height for 5×10^{-5} M zinc in 1 M KCl containing 0.002% (v/v) Tween 80 is shown in Fig. 2. As can be seen, the optimal thiourea concentration lies in the range 8—12 g l^{-1}.

The effectiveness of the proposed method is best illustrated by the calibration graphs for the determination of zinc in solutions containing Tween 80 (Fig. 3). The slope of the calibration plot for the range 5×10^{-6}—5×10^{-4} M zinc(II) in 1 M KCl (line a) is decreased about 3-fold by addition of 0.002% Tween to the supporting electrolyte (line b). Introduction of thiourea (10 g l^{-1}) to this solution causes a 16-fold increase in the slope (line c) compared with line (b). The addition of thiourea not only reduces the inhibition but also improves the analytical conditions. When 0.004% Tween is present the zinc peak is completely repressed, whereas addition of thiourea (10 g l^{-1}) restores the slope to a value close to that obtained with 1 M KCl alone in the supporting electrolyte (line d).

The determination of zinc by means of calibration graphs is possible only in solutions containing known amounts of Tween. Normally, sample solutions contain unknown concentrations of detergents and the application of this method would have to be preceded by determination of the detergent. However, the method of standard additions makes it possible to determine zinc in the presence of unknown Tween concentrations. Table 1 presents the results of such determinations in 1 M KCl solutions containing thiourea (10 g l^{-1}); good agreement between the actual and found contents of zinc was obtained.

The proposed method for determinations of zinc in the presence of Tween-80 should also be applicable for the determination of other depolarizers in the presence of various surface-active substances, given an appropriate organic substance which fulfils the conditions determined by the "cap-pair" principle.

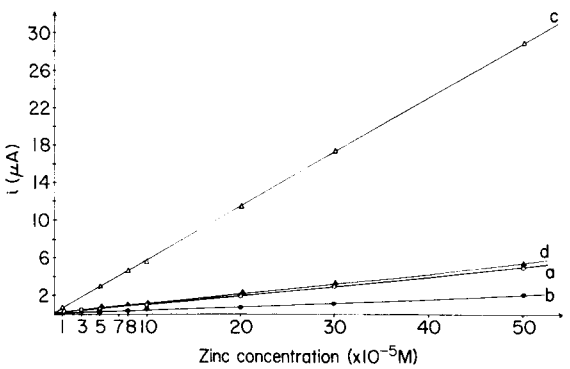

Fig. 3. Calibration curves for zinc: (a) 1 M KCl; (b) 1 M KCl + 0.002% Tween-80; (c) 1 M KCl + 0.002% Tween-80 + 10 g l^{-1} thiourea; (d) 1 M KCl + 0.004% Tween-80 + 10 g l^{-1} thiourea.

TABLE 1

S.w. polarographic determination of zinc(II) in 1 M KCl supporting electrolyte containing thiourea (10 g l^{-1}) in the presence of Tween-80 by the standard addition method

Tween-80 (% v/v)	Zinc concentration (M)		Tween-80 (% v/v)	Zinc concentration (M)	
	Present	Found		Present	Found
0.001	1.00×10^{-5}	0.94×10^{-5}	0.004	5.00×10^{-6}	4.00×10^{-6}
0.002	5.00×10^{-6}	4.80×10^{-6}	0.004	3.00×10^{-5}	2.80×10^{-5}
0.002	5.00×10^{-5}	5.00×10^{-5}	0.004	8.00×10^{-5}	8.12×10^{-5}
0.003	1.00×10^{-5}	0.97×10^{-5}	0.004	1.00×10^{-4}	1.00×10^{-4}
0.003	8.00×10^{-5}	7.80×10^{-5}			

REFERENCES

1 G. Dalmata, B. Nowicka and J. Saba, Dissertation, UMCS Poland, 1978.
2 K. Sykut, G. Dalmata, B. Nowicka and J. Saba., Ann. Univ. M. Curie Sklodowska, 33 (1978) 197.
3 K. Sykut, G. Dalmata, B. Nowicka and J. Saba, Biull. LTN, 20 (1978) 189.
4 K. Sykut, G. Dalmata, B. Nowicka and J. Saba, J. Electroanal. Chem., 90 (1978) 299.

Analytica Chimica Acta, 118 (1980) 373—376

Short Communication

DETERMINATION OF BENZHEXOL HYDROCHLORIDE IN TABLETS BY HIGH-PERFORMANCE LIQUID CHROMATOGRAPHY

C. P. LEUNG

Government Laboratory, Oil Street, North Point (Hong Kong)

(Received 16th December 1979)

Summary. Separation on a LiChrosorb C_2 reversed-phase column with methanolic ammonium dihydrogenphosphate as eluent provides a simple determination of benzhexol hydrochloride in tablets containing 2—5 mg of the drug. Common excipients do not interfere.

Benzhexol (trihexylphenidyl) hydrochloride is an anticholinergic agent used mainly in the treatment of Parkinsonism and commonly formulated in 2 mg or 5 mg tablets. The official methods of analysis laid down in the British and American Pharmacopoeias [1, 2] for the raw material employ non-aqueous titrimetry, and for tablets spectrophotometry with bromocresol purple. The latter method, although specific only for tertiary amines, works well for benzhexol hydrochloride tablets containing non-interfering excipients such as acacia, lactose, magnesium stearate and starch, but for tablets containing certain inorganic excipients, such as calcium dihydrogenphosphate, results tend to be low and irreproducible: the coloured complex is adsorbed on the inorganic phosphate and the colour intensity diminished.

Alternative procedures reported in the literature for the determination of benzhexol hydrochloride in tablets include potentiometric titration [3], fluorimetry [4] and gas chromatography [5]. The potentiometric method is not selective, the fluorimetric method is tedious, and the gas chromatographic method, although simple and sensitive, requires a column temperature of 245°C, close to the decomposition temperature (258.5°C) [6] for the compound.

High-performance liquid chromatography (h.p.l.c.) on a reversed-phase column with an alkaline eluent has been successfully applied to the determination of benzhexol hydrochloride in tablets in this laboratory. The method is selective and sensitive; common tablet excipients do not interfere. The validity of the method was demonstrated by comparison with the official colorimetric method and by recovery tests.

Experimental

Apparatus. The h.p.l.c. system (Altex Scientific) consisted of a constant flow pump operating at pressures up to 10,000 psi (Model 100A), a 20-μl constant-volume loop injector, a LiChrosorb C_2 10-μm microparticulate reversed-phase column, a variable-wavelength u.v. detector (Model 155, used with a Hitachi Model 100-30 spectrophotometer) and a strip-chart recorder (Rikadenki Model B-28B).

Chromatographic conditions and calibration. The eluent was a mixture of aqueous 0.1% (w/v) ammonium dihydrogenphosphate and methanol (1 : 3), pH 7.90, used at a flow rate of 2 ml min^{-1}. The detector wavelength was 220 nm (0.02 absorbance unit f.s.d.). Samples were injected into the 20-μl loop from a microsyringe. For calibration, a set of standards containing 0.02—0.08 mg ml^{-1} of benzhexol hydrochloride was prepared in methanol.

Assay of tablets. Weigh and powder 20 tablets. Dissolve as completely as possible (by heating or ultrasonic treatment) a quantity of powder equivalent to 4 mg of benzhexol hydrochloride in 100 ml of methanol. Centrifuge to obtain a clear supernatant liquid. Inject 20 μl of this solution into the h.p.l.c. system and measure the height of the peak with a retention time of 3.5 min.

Results and discussion

Benzhexol hydrochloride is the salt of a weakly basic tertiary amine. Under the conditions prescribed, it is eluted as a well-defined peak which is easily quantified by height or area measurements. When neutral aqueous methanol is used as eluent, the retention time is much longer and the broad peak shows tailing. Typical chromatograms are shown in Fig. 1.

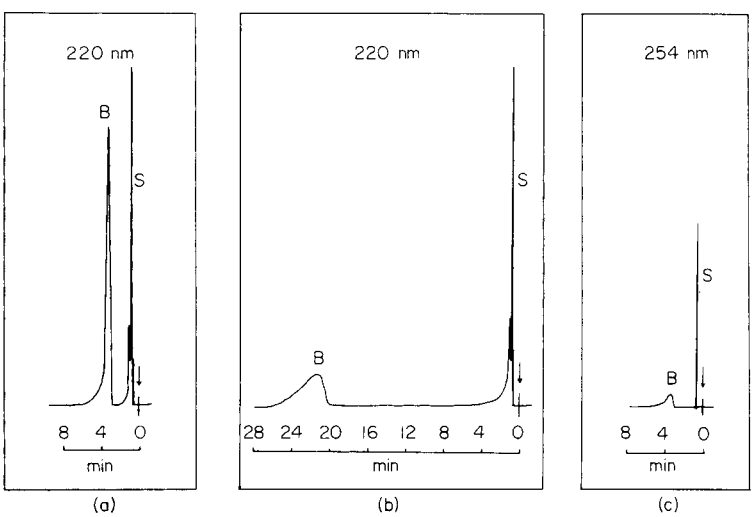

Fig. 1. Chromatograms for benzhexol hydrochloride: (a) 0.1% ammonium dihydrogenphosphate in water and methanol (1 : 3) as eluent with detection at 220 nm; (b) water—methanol (1 : 3) as eluent with detection at 220 nm; (c) as (a) with detection at 254 nm. S = solvent, B = benzhexol hydrochloride.

Benzhexol hydrochloride exhibits u.v. absorption maxima at 250, 256 and 262 nm in methanol, all of which show inadequate absorptivities; at 220 nm the absorptivity is about 20 times greater than that at 254 nm (Fig. 1a and c). Under the conditions used, the calibration graph was linear in the concentration range 0.4—1.6 μg of the drug in the aliquot injected.

Methanol was used to extract benzhexol hydrochloride from tablets. Ultrasonic treatment and warming were effective in assisting extraction. Common excipients were either insoluble in methanol or, if partly extracted, did not interfere with the h.p.l.c. determination. The chromatograms from the methanolic extracts were very similar to that shown in Fig. 1 (a).

Tests were carried out on four batches of 2-mg tablets and one batch of 5-mg tablets. The first three batches of 2-mg tablets contained the common excipients acacia, lactose, magnesium stearate and starch; in the fourth batch calcium dihydrogenphosphate replaced the lactose. For the first three batches and for the 5-mg tablets, results obtained by the h.p.l.c. method and by the official B.P. method of analysis were in good agreement (Table 1). For the tablets containing calcium dihydrogenphosphate (batch 4), only h.p.l.c. results are presented because the official method was found to be inapplicable.

Recovery experiments were carried out on two prepared mixtures each of which contained 10 mg of benzhexol hydrochloride. The first mixture contained acacia (50 mg), lactose (750 mg), magnesium stearate (100 mg), and starch (100 mg) to represent tablet excipients; in the second mixture calcium dihydrogenphosphate (750 mg) replaced lactose. Recoveries of 100.5 ± 1.5% and 99.0 ± 2.0%, respectively, were obtained for the two mixtures.

TABLE 1

Determination of benzhexol hydrochloride in tablets by h.p.l.c. and by the standard B.P. method

Batch no.	Labelled content (mg)	Percentage of labelled content found	
		H.p.l.c.[a]	B.P.
1	2	104.4 (±1.2)	103.0
2	2	93.2 (±0.7)	94.4
3	2	98.4 (±2.2)	97.4
4	2	94.0 (±1.0)	—
5	5	103.9 (±1.9)	103.0

[a] Average of 5 determinations; figures in brackets are standard deviations.

The author thanks Dr. A. J. Nutten, Government Chemist of Hong Kong, for permission to publish this paper.

REFERENCES

1 British Pharmacopoeia, H. M. Stationery Office, London, 1973, p. 49.
2 United States Pharmacopoeia, XIX, United States Pharmacopoeial Convention, Inc., 1975, p. 519.
3 L. G. Chatten and W. J. Racz, J. Pharm. Sci., 57 (1968) 137.
4 M. Gelbcke, J. Pharm. Belg., 31 (1976) 397.
5 D. J. Lovejoy, J. Chromatogr., 57 (1971) 137.
6 The Merck Index, 9th edition, Merck & Co., 1976, p. 1243.

Analytica Chimica Acta, 118 (1980) 377—380

Short Communication

A SIMPLE ACID DIGESTION METHOD FOR THE DETERMINATION OF TEN ELEMENTS IN AMBIENT AEROSOLS BY FLAME ATOMIC ABSORPTION SPECTROMETRY

THOMAS R. STOLZENBURG and ANDERS W. ANDREN*

Water Chemistry Program, University of Wisconsin, Madison, WI 53706 (U.S.A.)

(Received 25th January 1980)

Summary. A method is presented for multi-element determinations in ambient aerosols collected on Whatman 41 filter paper. Subsections of filters are exposed to vapor phase attack by nitric and hydrofluoric acids, and complete dissolution is accomplished by a mixture of nitric and perchloric acids at high temperatures in quartz tubes. The residue is taken up in dilute nitric acid and processed directly by standard additions with a flame atomic absorption spectrometer. The method was tested on NBS Coal Fly Ash, SRM 1633, and found to yield accurate results.

Multi-element determinations in aerosols collected on fiber filters are usually conducted by atomic absorption spectrometry or neutron activation [1—8]. Neutron activation, however, requires a reactor and expensive equipment. Atomic absorption can be performed either in the flame or the flameless mode. Most flameless techniques, following an acid digestion of aerosol particles, are exceedingly time-consuming and subject to chemical interferences. Residual perchloric acid or perchlorate compounds interfere with the atomic absorption signal of several elements, prohibiting accurate determinations [9, 10]. As an alternative, flame atomization is rapid, sensitive and relatively free from interferences. Required sample pre-treatment includes complete dissolution of the sample and filter matrix without introducing significant contamination.

In this study, 4—40 mg of aerosol particulate matter collected on 400 mg of cellulose is decomposed. Aerosol particles have an extremely high specific surface area, and are susceptible to vapor phase attack by hydrofluoric acid and nitric acids at ambient pressure. The method described by Feldman [11] is particularly suited for decomposing both the organic and inorganic components of an aerosol sample.

To digest the cellulose matrix completely, perchloric acid was selected since it is one of the most powerful oxidizing agents. Perchloric acid can be used safely in combination with nitric acid or by pretreating organic matrices with nitric acid [12]. The final solution is amenable to direct aspiration into a flame atomic absorption spectrometer (a.a.s.). Chemical interferences may become important when much larger sample masses are digested. Armannsson [13] needed solvent extraction to separate several metal ions from the interfering elements after dissolving 1000 mg of USGS rock reference sample with perchloric acid.

Experimental

Samples were collected at a constant flow rate of 0.85 m^3 min^{-1} for 48- or 72-h periods with a GCA/Precision Scientific high-volume sampler. Gravimetric determinations were conducted after the method of Strand et al. [14]. Approximately one-tenth of the collected surface of a 20 × 25 cm Whatman 41 filter paper is cut out with scissors. The sample section consists of 4 circles resulting from scoring a filter folded in quarters with a stainless steel die.

Tests showed that collected material is distributed unevenly on the filter. Up to 15—20% variation in the concentration of an element can be observed on different portions of the filter. Similar results were reported by Hoffman [15]. To counteract collection uniformity deviations, subsections are cut from the same central location on each filter sample.

The resulting circles are placed in a 50-ml teflon beaker. The beaker is set on a platform inside a 3.8-l polypropylene jar lying on its side. The jar contains a 50-ml pool of a (3 + 2) mixture of nitric and hydrofluoric acids. Heating is accomplished by placing the jar on its side in a 100°C sand bath overnight. The jar lid is loosely fitted to avoid pressure buildup.

The dry, brittle filters are then transferred to a flat-bottomed quartz tube (3 cm i.d. × 8.5 cm) using plastic forceps. A mixture of 3 ml of nitric acid and 2 ml of perchloric acid is pipetted into the tube. Small amounts of water are used to rinse any residue from the beaker into the tube.

The suspension is heated at a hot-plate temperature of 200°C until the remaining liquid is colorless. The plate temperature is then increased to 330°C to take the sample to dryness. Certain heavy metal perchlorates are susceptible to explosive decomposition. Use of a safety shield and ventilation in a fume hood is advised. The residue should not be exposed to an open flame or shock. When the residue has cooled, 500 μl of nitric acid and a small amount of water are added to the residue and heated to boiling. Essentially, all visible particulate matter is dissolved by this last step. After cooling, the sample is diluted to 25 ml in a polypropylene volumetric flask and transferred to a 30-ml screw-top polyethylene jar. The final acid concentration is assumed to be 2% nitric acid. All measurements were conducted on a Perkin-Elmer Model 603 a.a.s. with standard addition.

To check recoveries, measured quantities of NBS Coal Fly Ash (SRM 1633) were treated identically. For major elements, 10-mg amounts of fly ash yielded measurable concentrations. Up to 100 mg of fly ash was needed for trace element determinations. It was found that no more than 125 mg of fly ash can be completely decomposed using the acid amounts listed [9].

For all elements except aluminum, the sample solution was aspirated into the air—acetylene flame of a 4-in. single-slot burner head. Aluminum was atomized with a nitrous oxide—acetylene flame using a compatible 2-in. slot burner head. Broadband absorption was measured with a deuterium arc at the wavelengths of all elements considered for both the fly ash standards and aerosol samples.

Results and discussion

The results for fly ash are presented in Table 1. The excellent elemental recoveries obtained for SRM 1633 indicate that this method is relatively free from chemical interference.

Several fly ash and aerosol samples were tested for the degree of ionization error when determining the alkali metals. In every case, ionization control increased the measured concentration by less than 10%. Consequently, all samples were measured without adding an excess of an easily ionizable element. Measurements with the deuterium arc at each elemental wavelength showed that broadband absorption contributed less than 5% of the total absorbance signal in all cases tested. Accordingly, routine determinations were conducted without background correction.

Since coal fly ash is considered one of the most refractory components of ambient aerosols, complete elemental recoveries from fly ash suggest that this procedure yields accurate results for ambient aerosols. Table 2 lists the ranges of elemental particulate concentrations found at a residential sampling site near Milwaukee, WI [9]. All measured values represent the integrated

TABLE 1

Mean recoveries and standard deviations of Coal Fly Ash (SRM 1633). All values are given in $\mu g\ g^{-1}$ except where indicated.

Element	NBS	Ondov et al. [16]	This study
Al(%)	—	12.7 ± 0.5	14 ± 1
Ca(%)	—	4.7 ± 0.6	4.9 ± 0.2
Cu	128 ± 5	—	130 ± 5
Fe(%)	—	6.2 ± 0.3	6.8 ± 0.2
K(%)	1.72[a]	1.61 ± 0.15	1.60 ± 0.12
Mg(%)	—	1.8 ± 0.4	1.45 ± 0.05
Mn	493 ± 7	496 ± 19	530 ± 30
Na	—	3200 ± 400	3290 ± 110
Pb	70 ± 4	75 ± 5	77 ± 6
Zn	210 ± 20	216 ± 25	208 ± 9.5

[a]Not certified.

TABLE 2

Concentration ranges for 10 elements on aerosol particulate matter collected during 18 sampling periods over one year at a residential site near Milwaukee, WI

Element	Concentration range ($mg\ g^{-1}$)	Element	Concentration range ($mg\ g^{-1}$)	Element	Concentration range ($mg\ g^{-1}$)
Al	8.47—49.3	K	5.25—11.7	Na	2.96—34.9
Ca	19.8—52.5	Mg	8.12—35.5	Pb	2.01—24.7
Cu	0.150—1.74	Mn	0.413—1.99	Zn	0.439—3.51
Fe	12.5—42.1				

concentration over a 48- or 72-h sampling period. This method can be recommended for routine multi-element determinations in aerosols. Sophisticated sampling, digestion, or analytical equipment is not needed.

This work was supported in part by US EPA Grant No. R803971020 and U.S. Sea Grant.

REFERENCES

1 R. J. Thompson, G. B. Morgan and L. J. Purdue, At. Absorpt. Newsl., 9 (1970) 53.
2 T. Y. Kometani, J. L. Bove, B. Nathanson, S. Siebenberg and M. Magyar, Environ. Sci. Technol., 6 (1972) 617.
3 J. Y. Hwang, Anal. Chem., 44 (1972) 20A.
4 L. E. Ranweiler and J. L. Moyers, Environ. Sci. Technol., 8 (1974) 152.
5 B. C. Begnoche and T. H. Risby, Anal. Chem., 47 (1975) 1041.
6 R. Dams, K. A. Rahn, J. A. Robbins, G. D. Nifong and J. W. Winchester, Proceedings of the 2nd Int. Clean Air Congr., (1971) 509.
7 E. S. Gladney, W. H. Zoller, A. G. Jones and G. E. Gordon, Environ. Sci. Technol., 8 (1974) 551.
8 L. C. Bate, S. E. Lindberg and A. W. Andren, J. Radioanal. Chem., 32 (1976) 125.
9 T. R. Stolzenburg, Ph.D. Thesis, UW-Madison, (1979).
10 C. R. Parker, Technical Topics, Varian Techtron, August 1974.
11 C. Feldman, Anal. Chem., 49 (1977) 825.
12 A. A. Schilt, Perchloric Acid and Perchlorates, G. Frederick Smith Chemical Co., Columbus, OH, 1979, p. 156.
13 H. Armannsson, Anal. Chim. Acta, 88 (1977) 89.
14 J. Strand, T. Stolzenburg and A. W. Andren, Atmos. Environ., 12 (1978) 2027.
15 E. J. Hoffman and R. A. Duce, J. Geophys. Res., 79 (1974) 4474.
16 J. M. Ondov, W. H. Zoller, I. Olmez, N. K. Aras, G. E. Gordon, L. A. Rancitelli, K. H. Abel, R. H. Filby, K. R. Shah and R. C. Ragaini, Anal. Chem., 47 (1975) 1102.

Analytica Chimica Acta, 118 (1980) 381—383

Short Communication

DETERMINATION OF MERCURY IN ENVIRONMENTAL STANDARD REFERENCE MATERIALS BY PYROLYSIS

R. DUMAREY, R. HEINDRYCKX and R. DAMS*

Institute for Nuclear Sciences, Rijksuniversiteit Gent, Proeftuinstraat 86, B-9000 Gent (Belgium)

(Received 1st March 1980)

Summary. A cold-vapour method is described for the determination of mercury in reference materials by pyrolysis and a two-stage amalgamation on gold. Interfering pyrolysis products are eliminated by a combination of a catalytic converter and two absorbers for organic substances. The sensitivity of the method is 5 ppb for a 20-mg sample. The reproducibility depends on the homogeneity of the materials.

The two most widely used techniques for the determination of mercury in environmental samples are cold-vapour atomic absorption spectrometry (a.a.s.) [1] and destructive neutron activation analysis (n.a.a.) [2]. In both cases, wet digestion of the sample can cause serious contamination because of large reagent blanks. Losses of mercury from solution and during irradiation are well known. The digestion procedure as well as the chemical separations involved in n.a.a. are very cumbersome.

Recently, a modified a.a.s. technique was applied for the determination of total volatile [3] and total particulate [4] mercury in air; nearly the same procedure can be used for the determination of mercury in various other materials. The mercury is released from the sample by pyrolysis, purified from interfering substances and collected on a two-stage gold absorber system, being released later for the cold-vapour a.a.s. measurement. This method has the advantage of being very simple and rapid compared with the above-mentioned techniques. Sample inhomogeneity or high organic content in some cases can be a limiting factor.

Experimental

Pyrolysis. About 10—20 mg of undried material is weighed on a quartz-fibre filter (Gelman, 25-mm diameter), which has been pre-heated at 200°C for 1 h to reduce the blank. Then the filter is folded and placed inside a quartz tube. This tube is heated at 800°C with a Ni—Cr wire for 3 min under nitrogen and the released mercury is collected on a gold-coated sand absorber. Interfering organic products are removed by using a heated silver wool plug as catalyic converter followed by two absorbents for organic substances, i.e. silica gel and alumina. Moisture can be eliminated by a magnesium perchlorate absorber kept at room temperature. A detailed description of this pyrolysis section and procedure has been given previously [4].

For final calculation of the concentration, the results obtained are corrected for the moisture content of the sample.

Determination. After pyrolysis, the mercury-loaded gold absorber is connected to a second permanent absorber. The two absorbers are consecutively desorbed and the released mercury enters the optical cell of a modified Coleman MAS-50 spectrometer with nitrogen as carrier gas. Output signals are fed to a recorder and an integrator for peak-area measurements. These area data are used for further calculations.

Calibration is done by injecting known volumes of mercury-saturated air from a gas-tight syringe as described previously [3].

One measurement takes about 10 min, weighing and pyrolysis included. For best accuracy, it is desirable to do at least 5 determinations for each material.

Results and discussion

The efficiency of the purification section depends on the content of organic substances in the material to be analysed. Especially for biological samples, it is desirable to improve the absorption capacity by a fivefold increase in the purification stage. Reduction of the sample weight can cause irreproducible results because of inhomogeneity of the material. For other reference materials such as coal, ashes and rocks, the same purification system may be used as for the determination of particulate mercury in air [4].

The absorption capacity of the purification section is limited. Therefore, after 5—10 determinations, the stage is heated at 800°C under oxygen for 5 min to remove residual organic substances. Afterwards, the heated line is purged with nitrogen for another 5 min to free it from oxygen.

The sensitivity of the method is 0.1 ng mercury. This is equivalent to a concentration of 5 ppb for a 20-mg sample. The reproducibility is largely determined by the homogeneity of the materials. For most of them, homogeneity is only guaranteed above 250—500 mg. This may explain the higher relative standard deviation (% r.s.d.) values for some of the results listed in Tables 1 and 2.

Table 1 gives the results for two certified reference materials. The certified values are the average of both a.a.s. and n.a.a. results. In Table 2 are listed the results for seven BCR uncertified materials. Samples 1 and 2 are water plants; sample 3 consists of olive-tree leaves. In each case, 5 determinations were done on about 20 mg of material.

TABLE 1

Analysis of certified standard reference materials

Sample	Hg found (ppm)	R.s.d. (%)	Certified value (ppm)
NBS Coal SRM 1632	0.122 ± 0.029	24.0	0.12 ± 0.02
NBS Pine Needles SRM 1575	0.157 ± 0.018	11.5	0.15 ± 0.05

TABLE 2

Analysis of uncertified materials

Sample	Hg found (ppm)	R.s.d. (%)	Range found in other laboratories (ppm)
1. Lagarosiphon Major no. 60	0.33 ± 0.01	3.6	0.31—0.41
2. Platihypnidium Riparioides no. 61	0.20 ± 0.02	9.8	0.09—0.37
3. Olea Europaea no. 62	0.29 ± 0.04	13.1	0.25—0.53
4. Milk powder no. 63	0.008 ± 0.001	15.8	0.001—0.050
5. Fly ash no. 38	2.10 ± 0.03	1.4	2.0—2.2[a]
6. Coal no. 40	0.42 ± 0.02	4.2	0.38—0.87
7. Phosphate rock no. 32	0.015 ± 0.001	6.2	—

[a]Mean 2.11 ± 0.23.

One of the authors (R. Dumarey) is indebted to the Interuniversitair Instituut voor Kernwetenschappen — IIKW for financial support.

REFERENCES

1 A. M. Ure, Anal. Chim. Acta, 76 (1975) 1.
2 W. Zmyewska, J. Radioanal. Chem., 35 (1977) 389.
3 R. Dumarey, R. Heindryckx, R. Dams and J. Hoste, Anal. Chim. Acta, 107 (1979) 159.
4 R. Dumarey, R. Heindryckx and R. Dams, Anal. Chim. Acta, 116 (1980) 111.

Analytica Chimica Acta, 118 (1980) 385—396

Data Compilation

ELEMENTAL CONCENTRATIONS IN NBS BIOLOGICAL AND ENVIRONMENTAL STANDARD REFERENCE MATERIALS

ERNEST S. GLADNEY

University of California, Los Alamos Scientific Laboratory, P.O. Box 1663 Los Alamos, NM 87545 (U.S.A.)

(Received 4th January 1980)

SUMMARY

Elemental concentrations reported by 325 investigators in 16 NBS SRM's are summarized. Mean values, standard deviations and comparative data from NBS and other reviews are provided.

Inauguration of the National Bureau of Standards (NBS) program for biological and environmental Standard Reference Materials (SRM) with the certification of Orchard Leaves in 1972 marked the beginning of a period of rapid improvement in analytical capability for these complex matrices. This group of materials now includes 19 SRM's listed in Table 1, several of which are totally depleted (1630, 1643). The philosophy behind development and certification of SRM's as well as an NBS view on appropriate end uses of these materials has been described in a review by Uriano and Gravatt [1].

The accuracy and reliability of the certified values for these SRM's have proven to be excellent. A serious limitation of the program is the limited number of elements that NBS can afford to measure in each SRM. Numerous investigators have published data for elements that have either not been measured or have not been fully certified by NBS. Some of these data have been the subject of two recent articles including NBS SRM's 1571, 1577, 1632 and 1633 [2, 3]. The objects of the present compilation are to provide a more comprehensive coverage of the data for these four SRM's, and to include available data on twelve additional SRM's. Data from three of the SRM's shown in Table 1 (1631, 1634 and 1643), are not included because only very limited data are available on these three materials.

DATA COMPILATION

Fifteen major journals in analytical chemistry and geochemistry were exhaustively surveyed from 1972 to date, with less thorough coverage of books and reports. Some 325 different articles containing original data on

TABLE 1

National Bureau of Standards biological and environmental standard reference materials

SRM	Name	Certificate date
1567	Wheat Flour	1978
1568	Rice Flour	1978
1569	Brewers Yeast	1976
1570	Trace Elements in Spinach	1976
1571	Orchard Leaves	1972, 1976, 1977
1573	Tomato Leaves	1976
1575	Pine Needles	1976
1577	Bovine Liver	1972
1630	Mercury in Coal	1972
1631	Sulfur in Coal	1973, 1974
1632	Trace Elements in Coal	1974
1632a	Trace Elements in Coal (Bituminous)	1978
1633	Trace Elements in Coal Fly Ash	1975
1633a	Trace Elements in Coal Fly Ash	1979
1634	Trace Elements in Fuel Oil	1975, 1978
1635	Trace Elements in Coal (Subbituminous)	1978
1643	Trace Elements in Water	1977
1645	River Sediment	1978
1648	Urban Particulate Matter	1978

NBS SRM's were located. Initially, a mean and standard deviation were computed from all available data for a given element in an SRM. All data points outside three standard deviations from the mean were dropped and the mean and standard deviation recomputed.

These final means ± one standard deviation are reported in Tables 2—5 with an indication of the number of investigators reporting in parentheses. The summarized data are compared with NBS values and with those determined by Nadkarni and Morrison [2] and Becker et al. [3]. The detailed calculations including exactly which data were dropped, all individual data, uncertainties (where provided), and all individual references are available from the author upon request [4].

Mean values in Tables 2—5, which are based on fewer than three reports, do not include standard deviations. In a few instances, such values show three or more reports, but one or more of the reports included only upper-limit data for the elemental concentration, which have not been used in the computation of the mean (e.g., neodymium in SRM 1571). In some cases, the data reported had such a wide range as to render the mean ± one standard deviation value meaningless. Such cases are reported as ranges only (e.g., beryllium in SRM 1571). Additionally, there are a few elements where only upper-limit data have been reported and these are given as limit values in the Tables (e.g., erbium in SRM 1577).

ANALYTICAL METHODS USED

The distribution of individual data by analytical technique for each SRM is shown in Table 6. Neutron activation analysis (n.a.a.) includes thermal, epithermal, and capture γ-ray work, done by either instrumental or chemical separation methods. Photon activation analysis (p.a.a.) is shown in a separate category. Atomic absorption and atomic emission spectrometry (a.a.–a.e.s.) includes both flame and flameless methods. X-ray fluorescence (x.r.f.) covers both energy- and wavelength-dispersive procedures. Mass spectroscopy (m.s.) encompasses isotope dilution and spark-source techniques. The emission spectroscopy category (e.s.) includes all varieties of instruments, sources and data acquisition methods. Techniques reported as "other" include fluorimetry, electron spectroscopy for chemical analysis, gas chromatography coupled with mass spectroscopy, ion-selective electrodes, anodic stripping voltametry, charged particle activation, nuclear track, colorimetry, titration, combustion, spectrophotometry, delayed neutron assay, polarography, and ion chromatography. Also included under "other" are reports that used several measurement techniques, but did not specifically identify individual data by technique. For many of the more recently issued SRM's, there is a strong bias toward neutron activation data. Even among the older SRM's, neutron activation remains the predominant method reported. It is unfortunate that investigators employing methods other than activation are not more inclined to report data on SRM's, particularly for elements for which NBS has not provided certified values.

The mean elemental concentrations reported in this compilation represent a round-robin type approach, since no controls have been imposed upon the investigators. The limitations of such data must be recognized. Von Lehmden et al. [5], Flanagan [6, 7], Abbey [8], and Gladney et al. [9], have provided excellent insight into the problems associated with this approach. There is no substitute for careful certification of these SRM's by an agency of highest analytical reputation, such as NBS. Although compilation values have been reported for elements that NBS has certified, the NBS certified values must stand as the best data. In general, the two are in excellent agreement. For elements for which NBS has reported only uncertified values, the mean values from this study can add perspective to the accuracy of the NBS data, and perhaps provide some guide as to expected uncertainty in the value.

The principal value of this study is to provide a single collection of elemental data for uncertified species in these 16 SRM's. It is hoped that these data will stimulate additional research into technique improvement for environmental analysis as well as provide a guide as to where additional non-NBS SRM analyses should be directed.

TABLE 2

Elemental concentrations in two older NBS biological standard reference materials

Element	Units	NBS SRM 1571 Orchrad Leaves				NBS SRM 1577 Bovine Liver				
		This work[a]	NBS[b]	Nadkarni and Morrison [2]	Becker et al. [3]	This work[a]	NBS[b]	Nadkarni and Morrison [2] Table 2	Nadkarni and Morrison [2] Table 4	Becker et al. [3]
Ag	ppb	600 (1)				60 ± 20 (8)	60	63		60
Al	ppm	310 ± 100 (16)		410	400	30 ± 20 (9)		35.5	20.37	
As	ppm	11.5 ± 2.1 (56)	10 ± 2			0.053 ± 0.010 (28)	0.055	0.055	0.056	0.055
Au	ppb	1.8 ± 1.0 (6)		1.0		10 ± 15 (4)		30		
B	ppm	32 ± 4 (7)	33 ± 3			3.2 ± 0.9 (3)				
Ba	ppm	45 ± 8 (13)	44	46.3	45	0.1—123 (6)				
Be	ppb	7.5—110 (4)	27 ± 10			5 (2)				20
Bi	ppb	110 (1)	100	110	110	—				
Br	ppm	9.3 ± 1.2 (24)	10	9.14	10	8.7 ± 1.7 (17)		9.16	9.59	
C	%	46.3 ± 0.5 (4)				50.6 ± 1.1 (4)				
Ca	%	2.02 ± 0.09 (27)	2.09 ± 0.03			0.0116 ± 0.0018 (21)	0.0123	0.0124	0.0124	0.0123
Cd	ppb	122 ± 26 (27)	110 ± 10			276 ± 23 (33)	270 ± 40			
Ce	ppm	1.0 ± 0.1 (5)		1.0		0.046 (1)				
Cl	ppm	720 ± 50 (17)	690	721	750	2680 ± 160 (11)	2600	2640	2660	2610
Co	ppb	170 ± 90 (17)	200	170	200	240 ± 60 (22)	180	254	260	180
Cr	ppm	2.48 ± 0.34 (31)	2.6 ± 0.3			0.65 ± 0.73 (25)			0.05—1.6	0.2
Cs	ppb	32 ± 10 (4)		31		17 ± 7 (8)		19	15	13
Cu	ppm	11.7 ± 1.4 (55)	12 ± 1			189 ± 21 (46)	193 ± 10			
Dy	ppb	81 (3)				2.4 (1)				
Er	ppb	30 (1)				<0.5 (1)				
Eu	ppb	90 ± 110 (7)		26		0.2—3100 (3)				
F	ppm	4.3 (2)	4	4		—				
Fe	ppm	280 ± 50 (51)	300 ± 20			263 ± 13 (44)	270 ± 20			
Ga	ppb	88 ± 11 (5)	100	87		4—1100 (4)				
Gd	ppb	1.64—100 (2)				<1 (1)				
Ge	ppb	<400 (1)				<400 (1)				
H	%	5.9 ± 0.3 (3)				7.0 ± 0.2 (3)				
Hf	ppb	23 (1)				—		16		
Hg	ppb	158 ± 21 (29)	155 ± 15			17 ± 2 (23)	16 ± 2			
Ho	ppb	20 (1)				<0.9 (1)				
I	ppb	160 ± 50 (3)		170	200	190 (2)		180		200
In	ppb	1.5 ± 0.3 (3)		1.5		0.07 (3)				
Ir	ppb	15 (1)				—				
K	%	1.46 ± 0.06 (25)	1.47 ± 0.03			0.943 ± 0.099 (18)	0.97 ± 0.06			

La	ppm	1.2 ± 0.4 (11)		1.24		0.028 ± 0.023 (5)		0.016	0.02	
Li	ppm	5 ± 8 (3)	0.6		14	—				
Lu	ppb	6.1—10 (3)				<0.1 (1)				
Mg	ppm	6070 ± 580 (24)	6200 ± 200			587 ± 20 (16)	605	605	610	605
Mn	ppm	89 ± 5 (46)	91 ± 4			10.2 ± 0.9 (35)	10.3 ± 1.0			
Mo	ppm	1.4 ± 1.6 (10)	0.3 ± 0.1			3.1 ± 0.5 (18)	3.2	3.2	3.4	3.2
N	%	2.69 ± 0.05 (4)	2.76 ± 0.05			10.50 ± 0.22 (4)	10.6 ± 0.6			
Na	ppm	100 ± 40 (21)	82 ± 6			2440 ± 230 (15)	2430 ± 130			
Nd	ppb	400 (3)		300		170 (1)				
Ni	ppm	1.7 ± 1.0 (17)	1.3 ± 0.2			0.4 ± 0.4 (13)		0.23	0.27	
P	%	0.198 ± 0.019 (13)	0.21 ± 0.01			1.05 ± 0.16 (9)		1.36		
Pb	ppm	46 ± 4 (39)	45 ± 3			0.35 ± 0.06 (21)	0.34 ± 0.08			
Pr	ppb	60 (1)				4.6 (1)				
Pt	ppb	89—1200 (2)				—				
Rb	ppm	11.6 ± 1.2 (26)				19.5 ± 3.6 (24)	18.3 ± 1.0			
S	ppm	2080 ± 220 (5)	1900	1900		7100 ± 100 (3)				
Sb	ppm	3.0 ± 0.4 (22)	2.9 ± 0.3			0.005—0.070 (14)			0.005—0.06	
Sc	ppb	90 ± 60 (11)		68	40	1.0 ± 0.2 (8)		0.7	0.8	
Se	ppb	80 ± 9 (36)	80 ± 10			1080 ± 70 (54)	1100 ± 100			
Si	ppm	610 (2)		480		16.8 (2)		16.7		
Sm	ppb	110 ± 20 (6)		130		1.4 (2)				
Sn	ppm	0.3—4.1 (4)				0.016 (4)				
Sr	ppm	36 ± 4 (23)	37 ± 1	37.9	37	0.22 (4)	0.14	0.14	0.14	0.14
Ta	ppb	5 (1)				—				
Tb	ppb	1.2—80 (3)		17		<1.6 (1)				
Te	ppb	11 (1)	10		10	90 (1)				
Th	ppb	58 (3)	64 ± 6			<1000 (1)				
Ti	ppm	20 ± 20 (6)				2 (4)				
Tm	ppb	7 (2)				<0.3 (1)				
U	ppb	28 ± 3 (7)	29 ± 5			1.4 (4)	0.8	0.8		0.8
V	ppb	600 ± 150 (14)		610		33—600 (9)				
W	ppb	20 (2)				14 (2)		10		
Y	ppm	0.48 (2)				<1 (1)				
Yb	ppb	27 ± 11 (3)		30		0.5—830 (2)				
Zn	ppm	25 ± 3 (66)	25 ± 3			132 ± 10 (56)	130 ± 10			
Zr	ppm	2.0 ± 1.8 (4)				4 (2)				

[a]Numbers in parentheses refer to the number of individual values represented in the mean.
[b]NBS values with and without uncertainties are certified and uncertified, respectively, taken from the certificates of analysis.

TABLE 3

Elemental concentrations in six newer NBS biological standard reference materials

Element	Units	NBS SRM 1567 Wheat Flour		NBS SRM 1568 Rice Flour		NBS SRM 1569 Brewers Yeast	
		This work[a]	NBS[b]	This work[a]	NBS[b]	This work[a]	NBS[b]
Al	ppm					2300 ± 10	
As	ppb	5.4 ± 0.5	6	400 ± 10	410 ± 50		
B	ppm						
Ba	ppm						
Be	ppb						
Br	ppm	9.5 ± 1.5	9	1.23 ± 0.08	1	0.65 ± 0.03	
C	%						
Ca	%		0.019 ± 0.001		0.014 ± 0.002		
Cd	ppb		32 ± 7		29 ± 4		
Ce	ppm					2.3 ± 0.1	
Cl	ppm					460 ± 30	
Co	ppb	21 ± 4		18 ± 2	20 ± 1	260 ± 20	
Cr	ppm					1.8 ± 0.5[d]	2.12 ± 0.05
Cs	ppb						
Cu	ppm	2.0 ± 0.2	2.0 ± 0.3	2.2 ± 0.1	2.2 ± 0.3	11 ± 2	
Eu	ppb						
F	ppm						
Fe	ppm	17.2 ± 0.6	18.3 ± 1.0	8.85 ± 0.94	8.7 ± 0.6	707 ± 16	
Ga	ppb						
Gd	ppm					7.1 ± 0.5	
H	%						
Hf	ppb					130 ± 10	
Hg	ppb	1.0 ± 0.3	1.0 ± 0.8	6.4 ± 1.0	6.0 ± 0.7		
I	ppm						
In	ppb						
K	%	0.139 ± 0.004	0.136 ± 0.004	0.112 ± 0.002	0.112 ± 0.002	1.55 ± 0.05	
La	ppb						
Mg	ppm				1780 ± 100		
Mn	ppm	8.6 ± 0.4	8.5 ± 0.5	20.0 ± 0.7	20.1 ± 0.4	7.0 ± 0.8	
Mo	ppm		0.4		1.6		
N	%						
Na	ppm	10.4 ± 2.5	8.0 ± 1.5	6.9 ± 0.4	6.0 ± 1.5	510 ± 30	
Ni	ppm		0.18		0.16		
P	ppm						
Pb	ppm						
Rb	ppm	0.99 ± 0.16	1	7.27 ± 0.21	7	16 ± 1	
Sb	ppb	38 ± 1		5 ± 1		75 ± 5	
Sc	ppb					180 ± 10	
Se	ppm	1.12 ± 0.01	1.1 ± 0.2	0.42 ± 0.03	0.4 ± 0.1	0.92 ± 0.09	
Sn	ppm						
Sr	ppm						
Te	ppb		<2		<2		
Th	ppm					3.7 ± 0.2	
Ti	ppm					38 ± 2	
U	ppb					490 ± 20	
V	ppm					4.1 ± 0.1	
Zn	ppm	10.9 ± 0.6	10.6 ± 1.0	20.0 ± 0.7	19.4 ± 1.0	70 ± 2	

[a]All values from a single reference. [b]NBS values with and without uncertainties are certifie
the number of individual values represented in the mean. [d]Mean of data from four reference

NBS SRM 1570 Spinach		NBS SRM 1573 Tomato Leaves		NBS SRM 1575 Pine Needles	
This work[c]	NBS[b]	This work[c]	NBS[b]	This work[c]	NBS[b]
730 ± 220 (3)	870 ± 50	322—1225 (2)	1200	490 (2)	545 ± 30
140 (2)	150 ± 50	260 (1)	270 ± 50	200 (1)	210 ± 40
	30	33 (1)	30	17 (1)	9
13.1 (2)		56 ± 8 (3)		6.6 (2)	
<60 (1)					
46.8 ± 1.5 (3)	54	22.7 ± 2.3 (3)	26	6.9 ± 0.5 (3)	
40.82 (1)		37.92 (1)		51.6 ± 2.1 (3)	
1.52 ± 0.08 (3)	1.35 ± 0.03	2.96 ± 0.46 (3)	3.00 ± 0.03	0.43 (2)	0.41 ± 0.02
600 ± 300 (5)	1500		3	206 (1)	<500
			1.6		0.4
400 (2)		10800 ± 200 (3)		400 (2)	
000 ± 800 (4)	1500	490 ± 110 (3)	600	132 (2)	100
4.9 ± 0.6 (10)	4.6 ± 0.3	3.5 (2)	4.5 ± 0.5	2.4 (1)	2.6 ± 0.2
48 (1)		50 (2)		108 (2)	
11.5 ± 1.4 (5)	12 ± 2	13.6 ± 1.2 (5)	11 ± 1	3.9 (2)	3.0 ± 0.3
20 (2)	20	20 (2)	40	6.2 (2)	6
		5.0 (1)		3.7 (1)	
512 ± 38 (4)	550 ± 20	500 ± 120 (4)	690 ± 25	188 ± 14 (3)	200 ± 10
		69 (1)			
5.6 (2)		5.0 (2)		6.4 (2)	
34 (1)	30 ± 5	110 (2)	100	121 (1)	150 ± 50
1.1 (1)		0.35 (2)		0.15 (2)	
1.2 (1)					
3.58 ± 0.12 (4)	3.56 ± 0.03	4.36 ± 0.18 (5)	4.46 ± 0.03	0.390 ± 0.046 (3)	0.37 ± 0.02
320 (2)	370	500 (2)	900	140 (1)	200
8600 ± 1200 (4)		7100 (2)	7000	1400 (2)	
149 ± 27 (5)	165 ± 6	214 ± 13 (6)	238 ± 7	649 ± 22 (4)	675 ± 15
<5 (1)		0.62—8.8 (2)		2.5 (1)	
5.8 (2)	5.9	4.9 (2)	5.0	1.2 (2)	1.2
14400 ± 1200 (3)		534 ± 64 (4)		40 (2)	
5.3 (2)	6	1.2 (1)		2.2 (1)	3.5
5000 (2)	5500 ± 200	3340 ± 120 (3)	3400 ± 200	1200 (2)	1200 ± 200
1.17 ± 0.08 (4)	1.2 ± 0.2	6.07 (2)	6.3 ± 0.3	10.8 (2)	10.8 ± 0.5
10.8 (2)	12.1 ± 0.2	16.0 ± 0.8 (3)	16.5 ± 0.1	11.6 (2)	11.7 ± 0.1
38 (2)	40	40 (1)		180 (2)	200
165 (2)	160	170 ± 40 (3)	130	34 (2)	30
0.039 ± 0.015 (7)		0.060 ± 0.020 (3)		0.049± 0.004 (3)	
3.1 (1)					
	87 ± 2	50 ± 14 (3)	44.9 ± 0.3	7.5 (1)	4.8 ± 0.2
0.11 (1)	0.12 ± 0.03	0.19 (1)	0.17 ± 0.03	0.034 (1)	0.037±0.003
16.5 (1)		68 (1)			
	46 ± 9	50.2 (1)	61 ± 3	15.0 (1)	20 ± 4
1.27 ± 0.29 (4)		1.3 (2)		0.40 (2)	
57 ± 12 (7)	50 ± 2	61 ± 3 (3)	62 ± 6	61 ± 10 (3)	

uncertified, respectively, taken from the certificates of analysis. [c]Numbers in parentheses refer to

TABLE 4

Elemental concentrations in two older NBS environmental standard reference materials (ppm unless otherwise indicated)

Element	NBS SRM 1632: Coal			NBS SRM 1633: Coal Fly Ash		
	This work[a]	NBS[b]	Nadkarni and Morrison [2]	This work[a]	NBS[b]	Nadkarni and Morrison [2]
Ag	0.060 ± 0.015 (9)	≤0.1		0.25—1.3 (7)		
Al (%)	1.74 ± 0.13 (19)		1.81	12.5 ± 1.0 (22)		12.4
As	5.8 ± 0.6 (31)	5.9 ± 0.6		61 ± 5 (32)	61 ± 6	
Au (ppb)	0.85—200 (7)			2.7—1700 (5)		
B	40 ± 9 (3)			480 ± 40 (3)		
Ba	344 ± 33 (20)		333	2700 ± 170 (24)		2718
Be	1.4 ± 0.2 (4)	1.5		12 ± 1 (7)	12	
Bi	<1.5 (3)			<10 (3)		
Br	18.2 ± 2.1 (22)		18.0	8.6 ± 2.4 (18)		8.7
C (%)	71 ± 2 (3)			3.05 (1)		
Ca (%)	0.410 ± 0.046 (14)		0.40	4.6 ± 0.4 (25)		4.58
Cd	0.24 ± 0.06 (15)	0.19 ± 0.03		1.5 ± 0.2 (21)	1.45 ± 0.06	
Ce	21 ± 3 (17)		19.7	152 ± 11 (19)		146
Cl	880 ± 60 (19)		930	33 ± 13 (12)		20—58
Co	5.7 ± 0.5 (23)	6	5.9	40 ± 3 (27)	38	39.6
Cr	19.9 ± 1.7 (27)	20.2 ± 0.5		129 ± 11 (32)	131 ± 2	
Cs	1.6 ± 0.5 (20)		1.55	8.6 ± 1.8 (18)		8.7
Cu	17 ± 2 (14)	18 ± 2		127 ± 8 (20)	128 ± 5	
Dy	1.2 ± 0.3 (11)		0.85	8.8 ± 2.3 (8)		4.3—9.4
Er	<15 (1)			<100 (1)		
Eu	0.34 ± 0.05 (20)		0.32	2.6 ± 0.2 (15)		2.76
F	90 (2)			20 (1)		
Fe (%)	0.85 ± 0.07 (27)	0.87 ± 0.03		6.2 ± 0.4 (33)		6.27
Ga	6.0 ± 1.4 (11)			49 ± 14 (10)		
Gd	2.9 ± 1.2 (4)			11.2 (3)		
Ge	2.7—70 (3)			23 ± 4 (4)		
H (%)	4.23 ± 0.18 (3)			—		
Hf	0.98 ± 0.10 (17)		0.97	7.8 ± 1.1 (15)		8.4
Hg (ppb)	230 ± 250 (13)	120 ± 20		127—11000 (14)	140 ± 10	
Ho	0.24 (3)			1.94 (3)		
I	3.4 ± 1.2 (10)			2.7 ± 0.4 (6)		
In (ppb)	110 ± 90 (9)			240 ± 80 (9)		260
Ir	0.003—2.5 (4)			0.02—18.6 (4)		
K (%)	0.280 ± 0.012 (22)		0.284	1.70 ± 0.09 (27)	1.72	1.66
La	10.3 ± 1.2 (19)		10.7	79 ± 7 (20)		83
Li	24 (2)			110 (2)		
Lu	0.125 ± 0.017 (12)		0.127	1.5 ± 1.2 (12)		0.94
Mg (%)	0.180 ± 0.044 (16)		0.17	1.6 ± 0.3 (23)		1.63
Mn	42 ± 3 (26)	40 ± 3		492 ± 24 (35)	493 ± 7	
Mo	3.1 ± 1.3 (8)			29 ± 6 (10)		
N (%)	1.1 ± 0.2 (3)			—		
Na	376 ± 26 (22)		370	3200 ± 340 (25)		3200
Nb	<15 (1)			27 (3)		
Nd	9.2 ± 1.9 (6)			64 ± 8 (8)		63.4
Ni	15 ± 2 (17)	15 ± 1		98 ± 11 (22)	98 ± 3	
Os	<1 (1)			<4 (1)		
P	71 (1)			880—3000 (3)		
Pb	28 ± 5 (11)	30 ± 9		72 ± 5 (19)	70 ± 4	
Pd	<0.005 (1)			<0.002; <4 (2)		
Pr	<15 (1)			<100 (1)		
Pt	0.23 (3)			0.45—1.4 (3)		
Rb	21 ± 3 (22)		21.6	114 ± 10 (21)	112	117
Rh	<5 (1)			<4; <30 (2)		
Ru	0.018 (2)			0.2—3 (3)		

Table 4 (continued)

Element	NBS SRM 1632: Coal			NBS SRM 1633: Coal Fly Ash		
	This work[a]	NBS[b]	Nadkarni and Morrison [2]	This work[a]	NBS[b]	Nadkarni and Morrison [2]
S (%)	1.5 ± 0.4 (3)			0.39—0.90 (4)[c]		
Sb	3.6 ± 0.6 (22)		3.56	6.9 ± 0.4 (23)		6.87
Sc	3.79 ± 0.27 (21)		3.9	26 ± 2 (18)		25.2
Se	3.3 ± 0.3 (26)	2.9 ± 0.3		9.6 ± 0.8 (24)	9.4 ± 0.5	
Si (%)	2.8 ± 0.6 (3)	3.2		20.2 ± 2.5 (10)		
Sm	1.6 ± 0.2 (19)		1.7	12.4 ± 1.1 (17)		13.8
Sn	<10—125 (2)			9.4 ± 0.3 (7)		
Sr	145 ± 22 (22)		145	1380 ± 190 (26)	1380	1349
Ta	0.26 ± 0.07 (15)		0.24	2.2 ± 0.5 (15)		1.96
Tb	0.3 ± 0.1 (11)		0.25	2.1 ± 0.6 (12)		1.97
Te	0.80 (2)	<0.1		2.3—9.9 (4)		
Th	3.0 ± 0.7 (18)	3.0	3.1	25 ± 3 (15)	24	24.6
Ti	950 ± 120 (20)	800	960	7200 ± 720 (28)		7100
Tl	0.60 (2)	0.59 ± 0.03		4.1 ± 0.9 (4)	4	
Tm	0.30 (2)			1.3 (2)		
U	1.3 ± 0.2 (20)	1.4 ± 0.1		11.4 ± 1.4 (19)	11.6 ± 0.2	
V	35 ± 2 (20)	35 ± 3		216 ± 18 (27)	214 ± 8	
W	0.74 ± 0.07 (11)			5.5 ± 2.6 (11)		
Y	7.8 (2)			65 ± 3 (7)		
Yb	0.78 ± 0.13 (15)		0.84	6.4 ± 1.1 (14)		7.1
Zn	36 ± 3 (26)	37 ± 4		213 ± 13 (29)	210 ± 10	
Zr	36 ± 9 (7)			300 ± 75 (15)		303

[a]Numbers in parentheses refer to the number of individual values represented in the mean. [b]NBS values with and without uncertainties are certified and uncertified, respectively, taken from the certificates of analysis. [c]4200 ppm by prompt γ, 8400 ppm by x.r.f., two references each.

TABLE 5

Elemental concentrations in six newer NBS environmental standard reference materials (ppm

Element	NBS SRM 1630		NBS SRM 1632a		NBS SRM 1633a	
	This work[a]	NBS[b]	This work[a]	NBS[b]	This work[a]	NBS[b]
Ag			0.3 (1)			
Al(%)			2.97 ± 0.04 (3)	3.07	14.0 (1)	14
As			9.8 (2)	9.3 ± 1.0		145 ± 15
Au(ppb)			<50 (1)			
B			53 (2)		39.2 (1)	
Ba			130 (2)			1500
Br	37 (1)		43 ± 2 (3)			
C(%)			64 ± 6 (3)			
Ca			2300 ± 100 (3)		12900 (1)	11100 ± 100
Cd			0.21 (3)	0.17 ± 0.02	1.07 (1)	1.0 ± 0.
Ce			29 (2)	30		180
Cl			758 ± 50 (3)			
Co	3.7 (2)		7.0 (2)	6.8		46
Cr	7.1 (1)		35 (2)	34.4 ± 1.5		196 ± 6
Cs			2.0 (2)	2.4		11
Cu			15.9 (1)	16.5 ± 1.0		118 ± 3
Dy			2.2 (2)			
Eu			0.55 (2)	0.54		4
Fe(%)	0.50 (2)		1.13 ± 0.03 (3)	1.11 ± 0.02	9.7 (1)	9.40 ± 0
Ga	1.07 (1)		8.2 (2)	8.49		58
Gd			1.95 (2)		15.3 (1)	
H(%)			3.9 ± 0.3 (3)			
Hf			1.6 (2)	1.6		7.6
Hg	0.127 ± 0.014 (7)	0.13	0.117 (1)	0.13 ± 0.03		0.16 ± 0
I			1.8 (1)			
In(ppb)			38 (2)			
K			4100 ± 100 (3)		19700 (1)	18800 ± 600
La	4.0 (1)		16 (2)			
Li			36.2 (1)			
Lu(ppb)			200 (2)			
Mg			600—1300 (2)			4550 ± 100
Mn			31 ± 2 (3)	28 ± 2	190 (1)	190
Mo			<4 (1)			29
N(%)			1.27 ± 0.01 (3)			
Na	490 (1)		760 (2)		2100 (1)	1700 ± 100
Nd			12.0 (2)		65.6 (1)	
Ni			23 (2)	19.4 ± 1.0		127 ± 4
P			280 (1)		15000 (1)	
Pb			15 (2)	12.4 ± 0.6		72.4 ± 0.
Rb			30 (2)	31		131 ± 2
S(%)			1.45 ± 0.23 (3)	1.64	0.27 (1)	
Sb	1.7 (1)		0.70 (2)	0.58		7
Sc	1.4 (1)		6.5 (2)	6.3		40
Se	2.4 (2)		2.7 ± 0.3 (3)	2.6 ± 0.7		10.3 ± 0.
Si(%)			5.9 ± 0.2 (4)		22.2 (1)	22.8 ± 0.
Sm			2.3 ± 0.3 (3)		16.0 (1)	
Sr			88 (2)			830 ± 30
Ta			0.40 (2)			
Tb			0.34 (2)			
Th			4.5 (2)	4.5 ± 0.1		24.7 ± 0.
Ti			1650 ± 130 (3)	1750	8400 (1)	8000
U			1.2 ± 0.1 (3)	1.28 ± 0.02		10.2 ± 0.
V			44 (1)	44 ± 3	360 (1)	300
W	0.63 (1)		0.8 (2)			
Y			5.8 (1)			
Yb			1.1 (2)			
Zn			28 (2)	28 ± 2		220 ± 10
Zr			53 (1)			

[a]Numbers in parentheses refer to the number of individual values represented in the mean. [b]NI

unless otherwise indicated)

NBS SRM 1635		NBS SRM 1645		NBS SRM 1648	
This work[a]	NBS[b]	This work[a]	NBS[b]	This work[a]	NBS[b]
<0.6 (1)				6.4 (1)	6
0.32 ± 0.02 (3)	0.32		2.1	3.3 (1)	3.3
0.50 ± 0.18 (3)	0.42 ± 0.15		66	117 (2)	115 ± 10
<60 (1)					
105 (2)					
84 (2)				740 (1)	737
1.6 (2)				513 (2)	500
58 ± 4 (3)					
600 ± 200 (3)					
			29000	60000 (2)	
0.029 (2)	0.03 ± 0.01		10.2 ± 1.5	70 (1)	75 ± 7
3.2 (2)	3.6	614 (1)		54 (2)	55
26—120 (2)				4500 (1)	4500
0.67 (2)	0.65		8	17.6 (1)	18
	2.5 ± 0.3	32000 (1)	29600 ± 2800	421 (2)	403 ± 12
0.063 (2)				3.4 (1)	3
3.5 (2)	3.6 ± 0.3		109 ± 19	700 (1)	609 ± 27
0.28 (2)					
0.066 (2)	0.064	0.37 (1)		0.84 (2)	0.8
0.24 ± 0.03 (3)	0.239 ± 0.005		11.3 ± 1.2	3.93 ± 0.08 (3)	3.91 ± 0.10
1.1 (1)	1.05				
0.23 (2)					
4.13 ± 0.29 (3)					
0.32 (2)	0.29			4.2 (1)	4.4
			1.1 ± 0.5		
0.6 (1)				20 (1)	20
5 (2)				980 (1)	1000
95 ± 16 (3)			12000	10200 (2)	10000
1.9 (2)		8.2 (1)	9	41 (2)	42
1.46 (1)					
24 (2)				34 (1)	
980 (2)			24000	8300 (1)	8000
23 ± 1 (3)	21.4 ± 1.5		785 ± 97	830 (2)	860
<6 (1)					
1.1 ± 0.2 (3)			797 ± 48		
500 ± 280 (3)			5500	4300 (2)	4000
1.4 (1)		12.7 (1)			
1.4 (1)	1.74 ± 0.1	48 (2)	45.8 ± 2.9	83 (1)	82 ± 3
120 (1)			510 ± 14		
2.7 (1)	1.9 ± 0.2		714 ± 28	6780 (1)	6550 ± 80
0.8 (1)		39 (1)		53 (1)	
0.40 ± 0.13 (3)	0.33				
0.17 ± 0.06 (3)	0.14	42 (1)	51	46 (2)	45
0.68 (2)	0.63		2	6.7 (2)	7
0.92 ± 0.14 (4)	0.9 ± 0.3			27 (1)	24
0.64 ± 0.13 (4)		23.4 (1)	24	13.8 (2)	12.4 ± 0.2
0.25 ± 0.01 (3)				4.4 (2)	4.4
140 (2)				190 (1)	
0.053 (2)				8.2 (1)	
0.050 (1)		0.2 (1)			
0.58 (2)	0.62 ± 0.04		1.62 ± 0.22	7.4 (2)	7.4
210 ± 30 (3)	200			4300 (2)	4000
0.24 ± 0.04 (3)	0.24 ± 0.02	1.0 (2)	1.11 ± 0.05	5.42 (1)	5.5 ± 0.1
4.5 (1)	5.2 ± 0.5		23.5 ± 6.9	130 (1)	130
<0.6 (1)				4.8 (1)	4.8
0.16 (2)					
5.8 (2)	4.7 ± 0.5	1680 (1)	1720 ± 169	4680 (2)	4760 ± 140
16 (1)					

values with and without uncertainties are certified and uncertified, respectively.

TABLE 6

Distribution of individual data by technique (%)

SRM	Total no. of analyses	N.a.a.	A.a.-a.e.s.	X.r.f.	M.s.	P.a.a.	E.s.	Other
1567	13	100						
1568	13	100						
1569	26	96						4
1570	109	61	19			1	13	6
1571	899	45	22	14	3	6	5	5
1573	92	69	11		1	1	15	3
1575	74	64	10		1	1	19	5
1577	701	56	18	13	0.1	3	7	3
1630	21	70	20					10
1632	894	76	4	4	2	4	6	6
1632a	129	82	6	9				3
1633	996	61	8	12	1	10	7	1
1633a	16	100						
1635	114	85	4	7				4
1645	14	79				14		7
1648	59	68		20				2

I thank Verna Halloran and Mary Lou Keigher for their assistance with the preparation of this manuscript and R. A. Nadkarni for providing his detailed bibliography. This work was done under the auspices of the U.S. Department of Energy.

REFERENCES

1 G. A. Uriano and C. C. Gravatt, Crit. Rev. Anal. Chem., 6 (1977) 361.
2 R. A. Nadkarni and G. H. Morrison, J. Radioanal. Chem., 43 (1978) 347.
3 D. A. Becker, H. L. Rook and P. D. LaFleur, in S. Amiel (Ed.), Instrumental Neutron Activation Analysis, 1979, Chapter 5, in press.
4 E. S. Gladney, unpublished data, 1979.
5 D. J. von Lehmden, R. H. Jungers and R. E. Lee, Anal. Chem., 46 (1974) 239.
6 F. J. Flanagan, Geochim. Cosmochim. Acta, 38 (1974) 1731.
7 F. J. Flanagan, Geochim. Cosmochim. Acta, 39 (1975) 537.
8 S. Abbey, Geochim. Cosmochim. Acta, 39 (1975) 535.
9 E. S. Gladney, D. R. Perrin, J. W. Owens and D. Knab, Anal. Chem., 51 (1979) 1557.

ANALYTICA CHIMICA ACTA, Vol. 118 (1980)

AUTHOR INDEX

ACA announcements

ANNOUNCEMENTS OF MEETINGS

JOINT NL – UK SYMPOSIUM ON QUANTITATIVE ORGANIC ANALYSIS

The above symposium, organised by the Analytical Chemistry Section of the Royal Netherlands Chemical Society and the Analytical Division of the Chemical Society (London) will be held at Noordwijkerhout, The Netherlands, from 22 April to 24 April, 1981.

The Scientific programme will have plenary lectures to include the themes of: Analysis of Drugs and Drug Metabolites, Analysis of Polymers and/or Resins with possible attention to Additives, Aspects of Quantitative Analysis of Organic Vapours in Working and other Atmospheres, Functional Group Analysis and Chemical Derivatisation Methods, Modern Trends in Instrumentation in Quantitative Organic Analysis.

Anyone wishing to present a paper should send in details no later than 1 November, 1980 to: Dr. B. Griepink, Secretary of Analytical Chemistry Section of the Royal Netherlands Chemical Society, c/o Analytical Chemistry Laboratory, Croesestraat 77A, 3522 AD Utrecht, The Netherlands.

ANALYTIKTREFFEN 1980 – SCHWINGUNGSSPEKTROSKOPIE, 18–21 November, 1980, Neubrandenburg, D.D.R.

Die Sektion Chemie der Karl-Marx-Universität Leipzig veranstaltet gemeinsam mit der Chemischen Gesellschaft der Deutschen Demokratischen Republik vom 18–21 November 1980 in Neubrandenburg das Analytiktreffen 1980 zum Thema Schwingungsspektroskopie. Das Programm dieser Tagung mit internationaler Beteiligung besteht aus Plenar- und Hauptvorträgen (auf Einladung) und Posterbeiträgen zu folgenden Themenkreisen: Automatisierung der Analyse, Spektrenvorausberechnung, Beziehung zwischen Messgrösse und physikalischen Eigenschaften, Moderne Methoden, Untersuchungen an aggregierten Systemen (Festkörper, Hoch- und Biopolymere, Oberflächen).

Sekretär: Dr. sc. R. Salzer, Karl-Marx-Universität, Sektion Chemie, Linéstr. 2, 7010 Leipzig, D.D.R.

3. TAGUNG FESTKORPERANALYTIK, 23–27 Juni 1981 in Karl-Marx-Stadt

Die Chemische Gesellschaft der DDR führt gemeinsam mit der Sektion Chemie und Werkstofftechnik der Technischen Hochschule Karl-Marx-Stadt vom 23 bis 27 Juni 1981 in Karl-Marx-Stadt die 3. Tagung Festkorperanalytik mit internationaler Beteiligung durch. Es sind Plenar- und Diskussionsvorträge zu folgenden Themenschwerpunkten vorgesehen: Elementanalyse in und an Festkörpern, Strukturanalyse von Festkörpern und Festkörpergrenzflächen, und Bewertungskriterien und optimaler Einsatz von Analysenverfahren in der Festkörperanalytik. Zur Übernahme von Plenar- und Hauptvorträgen ergehen Einladungen. Für Diskussionsvorträge von 20 Minuten Dauer (einschliesslich Diskussionszeit) sowie für Posterbeiträge sind Anmeldungen bis spätestens 31 Oktober 1980 unter Beifügung eines offsetgerechten Kurzreferates an den Sekretär des Vorbereitungskomitees, Dr. K. Danzer, Technische Hochschule Karl-Marx-Stadt, Sektion Chemie und Werkstofftechnik, PSF 964, 9010 Karl-Marx-Stadt, D.D.R.

CALENDAR OF FORTHCOMING MEETINGS

Sep. 2–5, 1980 Prague, Czechoslovakia	**VII European Symposium on Connective Tissue Research** Contact: Dr. Z. Deyl, Physiological Institute Czechoslovak Academy of Sciences, 142 20 Budejovická 1083, Prague 4, Czechoslovakia.
Sep. 6–12, 1980 Liège, Belgium	**International Solvent Extraction Conference (ISEC '80)** Contact: Conference Secretariat ISEC '80, Department of Chemistry, University of Liège, Sart Tilman, B–4000 Liège, Belgium. (Further details published in Vol. 107)

Sep. 6–12, 1980 Bath, Great Britain	**IMLS Triennial Conference** Contact: K. Case, Area Central Laboratory, Royal United Hospital, Bath BA1 3NG, Great Britain.
Sep. 7–12, 1980 Florence, Italy	**IUPAC International Symposium on Macromolecules (Structural Order in Polymers)** Contact: Macro IUPAC 80, Fondazione Giovanni Lorenzini, Via Monte Napoleone 23, 20121 Milan, Italy.
Sep. 8–10, 1980 Oxford, Great Britain	**Photoelectrochemistry Discussion** Contact: Dr. M.D. Archer, Dept. of Physical Chemistry, Univ. of Cambridge, Lensfield Road, Cambridge, Great Britain.
Sep. 9–11, 1980 Eindhoven, The Netherlands	**2nd International Symposium on Isotachophoresis** Contact: ITP 80, Afd. Instrumentele Analyse, Technische Hogeschool Eindhoven, Postbus 513, 5600 MB Eindhoven, The Netherlands. (Further details published in Vol. 117)
Sept. 15–19, 1980 York, Great Britain	**10th European Solid State Device Research Conference** Contact: The Institute of Physics, 47 Belgrave Square, London SW7, Great Britain.
Sep. 16–19, 1980 Bratislava, Czechoslovakia	**6th International Symposium on Advances and Application of Chromatography in Industry** Contact: Dr. Ján Remeň, Analytical Section ČS VTS, pri n.p. Slovnaft, 82300 Bratislava, Czechoslovakia.
Sep. 17–18, 1980 Amsterdam, The Netherlands	**New Techniques in Analytical Chemistry** Contact: Robert S. First, Inc., 707 Westchester Avenue, White Plains, N.Y. 10604, U.S.A.
Sep. 22–26, 1980 Cannes, France	**8th International Vacuum Congress – 4th International Conference on Solid Surfaces – 3rd European Conference on Surface Science** Contact: Société Francaise du Vide, 19 Rue Renard, F–75004 Paris, France.
Sep. 22–26, 1980 Paris, France	**European Conference on Chemical Pathways in the Environment** Contact: Dr. C. Troyanowsky, Société de Chimie physique, 10, rue Vauquelin, F-75005 Paris, France. Tel. 707-54-48.
Sep. 23–25, 1980 Cardiff, Great Britain	**Chemical Society/Analytical Division – CS Autumn meeting: Trace and Ultratrace Analysis** Contact: The Secretary, Analytical Division, The Chemical Society, Burlington House, London W1V 0BN, Great Britain.
Sep. 24–28, 1980 Hamburg, F.R.G.	**EMBO-EMBL** **Workshop on X-ray and Neutron Scattering of Biological Structure** Contact: Prof. H. Stuhrmann, EMBL c/o DESY, Notkestrasse 85, D-2000 Hamburg 52, F.R.G.
Sep. 28–Oct. 3, 1980 Smolenice Castle, Czechoslovakia	**International Symposium on n.m.r. Spectroscopy** Contact: Ing. Igor Goljer, n.m.r. Laboratory, Faculty of Chemical Technology, Jánska 1, 880 37 Bratislava, Czechoslovakia. (Further details published in Vol. 117)

Sep. 28–Oct. 3, 1980 Philadelphia, Pa., U.S.A.	**7th Annual Meeting of Federation of Analytical Chemistry and Spectroscopy Societies (FACSS)** Contact: Mrs. J.G. Graselli, c/o Standard Oil Co., 4440 Warrensville Road, Cleveland, Ohio 44128, U.S.A.
Sep. 29–Oct. 3, 1980 York, Great Britain	**Modern Radiochemical Practice** Contact: The Secretary, Analytical Division, Chemical Society, Burlington House, London W1V 0BN, Great Britain.
Oct. 6–9, 1980 Houston, Texas, U.S.A.	**EXPOCHEM '80** Contact: Professor A. Zlatkis, Chemistry Department, University of Houston, Houston, Texas, 77004, U.S.A. Tel. (713) 749-2623. (Further details published in Vol. 116, No. 1)
Oct. 6–9, 1980 Houston, Texas, U.S.A.	**Chromatography '80 – 15th International Symposium on Advances in Chromatography** Contact: Professor A. Zlatkis, Chemistry Department, University of Houston, Houston, Texas 77004, U.S.A. Tel. (713) 749 2623. (Further details published in Vol. 115)
Oct. 7–9, 1980 Gatlinburg, Tenn., U.S.A.	**Analytical Chemistry in Environmental Regulation and Control** Contact: W.S. Lyon, Technical Program Chairman, Oak Ridge National Laboratory, P.O. Box 8, Oak Ridge, Tenn. 37830, U.S.A. Tel: (615) 574-4882. (Further details published in Vol. 117)
Oct. 9–15, 1980 Dusseldorf, West Germany	**INTERKAMA '80 – International Congress and Trade Fair for Instrumentation and Automation** Contact: German/American Chamber of Commerce, 666 Fifth Avenue, New York, NY 10019, U.S.A.
Oct. 15–17, 1980 Toyohashi, Japan	**Fifth International Conference on Computer in Chemical Research and Education (VICCCRE)** Contact: Prof. S. Sasaki, Toyohashi University of Technology, Tempaku, Toyohashi, Japan 440 (Further details published in Vol. 122, No. 2)
Oct. 16–17, 1980 Teddington, Middx., Great Britain	**Quantitative Surface Analysis** Contact: The Meetings Officer, The Institute of Physics, 47 Belgrave Square, London SW1X 8QZ, Great Britain.
Oct. 19–23, 1980 Washington, D.C., U.S.A.	**Annual Meeting of Assoc. of Official Analytical Chemists** Contact: K.M. Fominaya, Box 540, Benjamin Franklin Station, Washington, D.C. 20044, U.S.A.
Oct. 22–24, 1980 Rome, Italy	**Workshop on TCDD and Related Compounds** Contact: Prof. Dr. O. Hutzinger, University of Amsterdam, Nieuwe Achtergracht 166, Amsterdam, The Netherlands. (Further details published in Vol. 122, No. 1)
Oct. 26–29, 1980 Boston, Mass., U.S.A.	**10th Annual North American Thermal Analysis Society Meeting** Contact: Dr. R.C. Johnson, Du Pont Central Research and Development Dept., Experimental Station, Bldg. 228, Wilmington, Del. 19898, U.S.A.
Oct. 27–31, 1980 Endorf bei Rosenheim/ Bayern, F.R.G.	**EUCHEM – CONFERENCE: Die Darstellung logischer Strukturen in der Chemie durch Modelle und die Lösung chemischer Probleme mittels Computern** Contact: GDCh–Geschäftsstelle, P.O. Box 90 04 40, D–6000 Frankfurt/M 90, F.R.G. (Further details published in Vol. 122, No. 2)

Oct. 29–31, 1980 Milan, Italy	**New Trends in Antibiotics – Research and Therapy** Contact: Fondazione Giovanni Lorenzini, Via Monte Napoleone, 23, 20121 Milan, Italy. Tel: (02) 70 22 67 and 78 38 68
Nov. 11–15, 1980 Milan, Italy	**1st African and Mediterranean Congress of Clinical Chemistry and 6th Congress of the Italian Society of Clinical Biochemistry** Contact: 1st African and Mediterranean Congress of Clinical Chemistry, Via Keplero, 10-20124 Milan, Italy.
Nov. 18–21, 1980 Neubrandenburg, D.D.R.	**Analytiktreffen 1980 – Schwingungsspektroskopie** Contact: Dr. sc. R. Salzer, Karl–Marx–Universität, Sektion Chemie, Linéstr. 2, 7010 Leipzig, D.D.R.
Nov. 19–21, 1980 New York, N.Y., U.S.A.	**19th Eastern Analytical Symposium** Contact: Norman Gardner, Exposition Manager, 73 Ethel Street, Metuchen, N.J. 08840, U.S.A. Tel. (201) 548 7377.
Dec. 8–12, 1980 Porte de Versailles, Paris, France	**2ème Congrès de Chimie Analytique – 34ème Congrès du G.A.M.S.** Contact: Secrétriat du G.A.M.S. (Congrès), 88, Boulevard Malesherbes, 75008 Paris, France. (Further details published in Vol. 117)
Dec. 16–17, 1980 Brighton, Great Britain	**Chromatography, Equilibria and Kinetics** Contact: Mrs. Y.A. Fish, The Chemical Society, Burlington House, London W1V 0BN, Great Britain. Tel. 01-7349971.
Feb. 17–20, 1981 Vienna, Austria	**EURO FOOD CHEM I** Contact: Verein Osterreichischer Chemiker Dr. Werner Pfannhauser, FECS – WPFC – Secretary, Eschenbachgasse 9, A – 1010 Wien, Austria. Tel: 0 22 2/ 57 42 49
March 9–13, 1981 Atlantic City, U.S.A.	**1981 Pittsburgh Conference** Contact: John A. Queiser, Programme Chairman, 1981 Pittsburgh Conference, 2523 Greenboro Lane, Pittsburgh, PA 15220, U.S.A. Tel: 412 795–7110.
Apr. 13–16, 1981 Cardiff, Wales United Kingdom	**International Symposium on Electroanalysis in Clinical Environmental and Pharmaceutical Chemistry** Contact: Short Courses Section (Electroanalysis Symposium), UWIST, Cardiff CF1 3NU, Wales, United Kingdom. (Further details published in Vol. 116, No. 1
April 22–24, 1981 Noordwijkerhout, The Netherlands	**Joint NL – UK Symposium on Quantitative Organic Analysis** Contact: Dr. B. Griepink, Secretary of Analytical Chemistry Section of the Royal Netherlands Chemical Society, c/o Analytical Chemistry Laboratory, Croesestraat 77A, 3522 AD Utrecht, The Netherlands.
May 11–15, 1981 Avignon, France	**Vth International Symposium on Column Liquid Chromatography** Contact: Prof. G. Guiochon, Ecole Polytechnique, Laboratoire de Chimie Analytique Physique, Route de Saclay, 91128 Palaiseau Cedex, France. (Further details published in Vol. 118, No. 1)
May 20–22, 1981 Eger, Hungary	**Symposium on the Analysis of Steroids** Contact: Prof. S. Görög, c/o Hungarian Chemical Society, 1061 Budapest VI., Anker köz 1, Hungary.
June 1–5, 1981 Stresa, Lago Maggiore, Italy	**2nd European Symposium on Organic Chemistry** Contact: Prof. Giorgio Modena, Istituto di Chimica Organica, Via Marzolo, 1, 35100 Padova, Italy.

June 16–17, 1981 Venice, Italy	**1st International Symposium on Chromatography in Biochemistry, Medicine and Environmental Research** Contact: Dr. A. Frigerio, Italian Group for Mass Spectrometry in Biochemistry and Medicine, c/o Istituto di Ricerche Farmacologiche "Mario Negri", Via Eritrea 62, 20157 Milan, Italy. Tel: 35.54.546.
June 18–19, 1981 Venice, Italy	**8th International Symposium on Mass Spectrometry in Biochemistry, Medicine and Environmental Research** Contact: Dr. A. Frigerio, Italian Group for Mass Spectrometry in Biochemistry and Medicine, c/o Istituto di Ricerche Farmacologiche "Mario Negri" Via Eritrea 62 20157 Milan, Italy. Tel: 35.54.546.
June 22–26, 1981 Nijmegen, The Netherlands	**4th International Symposium on Affinity Chromatography and Related Techniques** Contact: Dr. T.C.J. Gribnau, Organon Scientific Development Group, P.O. Box 20, 5340 BH Oss, The Netherlands. (Further details published in Vol. 118, No. 1)
June 23–27, 1981 Karl–Marx–Stadt, D.D.R.	**Tagung Festkorperanalytik** Contact: Dr. K. Danzer, Technische Hochschule, Karl–Marx–Stadt, Sektion Chemie und Werkstofftechnik, PSF 964, 9010 Karl–Marx–Stadt, D.D.R.
July 6–9, 1981 Strasbourg, France	**27th IUPAC Symposium on Macromolecules** Contact: Secretariat, Macro 1981, Société de Chimie Industrielle, 28, rue Saint-Dominique, 75007 Paris, France.
Aug. 16–22, 1981 Vancouver, Canada	**28th Congress International Union of Pure and Applied Chemistry** Contact: Congress Secretariat, 28th IUPAC Congress, c/o The Chemical Institute of Canada, 151, Slater Street, Suite 906, Ottawa, Ontario, Canada K1P 5H3.
Aug. 23–28, 1981 University of Auckland, New Zealand	**Golden Jubilee Conference "Chemistry in the Service of Man"** Contact: Dr. D.J. McLennan, Chemistry Dept., Univ. of Auckland, Auckland, New Zealand.
Aug. 23–28, 1981 Espoo, Finland	**Euroanalysis IV – Triennal Conference of the Federation of European Chemical Societies** Contact: Professor L. Niinistoe, Department of Chemistry, Helsinki University of Technology, SF–02150 Espoo 15, Finland. (Further details published in Vol. 109, No. 1)
Aug. 23–28, 1981 Canberra, Australia	**Sixth Australian Symposium on Analytical Chemistry** Contact: Hon. Secretary, Miss B.J. Stevenson, P.O. Box 1397, Canberra City, A.C.T. 2601, Australia.
Aug. 30–Sep. 5, 1981 Vienna, Austria	**XI International Congress of Clinical Chemistry – IV European Congress of Clinical Chemistry** Contact: Congress Secretariat, Interconvention, P.O. Box 35, A-1095 Vienna, Austria. Tel. (0222) 42 13 52.
Sep. 1–4, 1981 Siofok, Hungary	**3rd Danube Symposium on Chromatography** Contact: Hungarian Chemical Society, H–1368 Budapest, P.O.B. 240, Hungary. Tel: Budapest 427–343. (Further details published in Vol. 115)

Sep. 4–8, 1981
Tokyo, Japan

9th International Conference on Atomic Spectroscopy and XXII Colloquium Spectroscopicum Internationale

Contact: The Japan Society for Analytical Chemistry, 9th ICAS/XXII CSI, Gotanda Sanhaitsu, 26-2 Nishigotanda 1-chome, Shinagawa-ku, Tokyo 141, Japan. (Further details published in Vol. 118, No. 1)

(continued from outside of cover)

CONTENTS

(continued on inside page of cover)

Printed in The Netherlands.